frontiers | Research Topics

Insights in coronary artery disease 2023

Edited by
Tommaso Gori, Giuseppe Ando', Felice Gragnano, Marco Zimarino, Toshiro Shinke, Viktor Kočka, Alberto Guido Pozzoli, Marco Giuseppe Del Buono, Javed Ahmed and Krishnaraj Rathod

Published in
Frontiers in Cardiovascular Medicine

ISSN 1664-8714
ISBN 978-2-8325-6391-5
DOI 10.3389/978-2-8325-6391-5

About Frontiers

Frontiers is more than just an open access publisher of scholarly articles: it is a pioneering approach to the world of academia, radically improving the way scholarly research is managed. The grand vision of Frontiers is a world where all people have an equal opportunity to seek, share and generate knowledge. Frontiers provides immediate and permanent online open access to all its publications, but this alone is not enough to realize our grand goals.

Frontiers journal series

The Frontiers journal series is a multi-tier and interdisciplinary set of open-access, online journals, promising a paradigm shift from the current review, selection and dissemination processes in academic publishing. All Frontiers journals are driven by researchers for researchers; therefore, they constitute a service to the scholarly community. At the same time, the *Frontiers journal series* operates on a revolutionary invention, the tiered publishing system, initially addressing specific communities of scholars, and gradually climbing up to broader public understanding, thus serving the interests of the lay society, too.

Dedication to quality

Each Frontiers article is a landmark of the highest quality, thanks to genuinely collaborative interactions between authors and review editors, who include some of the world's best academicians. Research must be certified by peers before entering a stream of knowledge that may eventually reach the public - and shape society; therefore, Frontiers only applies the most rigorous and unbiased reviews. Frontiers revolutionizes research publishing by freely delivering the most outstanding research, evaluated with no bias from both the academic and social point of view. By applying the most advanced information technologies, Frontiers is catapulting scholarly publishing into a new generation.

What are Frontiers Research Topics?

Frontiers Research Topics are very popular trademarks of the *Frontiers journals series*: they are collections of at least ten articles, all centered on a particular subject. With their unique mix of varied contributions from Original Research to Review Articles, Frontiers Research Topics unify the most influential researchers, the latest key findings and historical advances in a hot research area.

Find out more on how to host your own Frontiers Research Topic or contribute to one as an author by contacting the Frontiers editorial office: frontiersin.org/about/contact

Insights in coronary artery disease: 2023

Topic editors

Tommaso Gori — University Medical Centre, Johannes Gutenberg University Mainz, Germany

Giuseppe Ando' — University of Messina, Italy

Felice Gragnano — University of Campania Luigi Vanvitelli, Italy

Marco Zimarino — Asl Lanciano Vasto Chieti, Italy

Toshiro Shinke — Showa University, Japan

Viktor Kočka — Charles University, Czechia

Alberto Guido Pozzoli — Istituto Cardiocentro Ticino, Ospedale Regionale di Lugano, Switzerland

Marco Giuseppe Del Buono — Agostino Gemelli University Polyclinic (IRCCS), Italy

Javed Ahmed — Newcastle upon Tyne Hospitals NHS Foundation Trust, United Kingdom

Krishnaraj Rathod — Queen Mary University of London, United Kingdom

Citation

Gori, T., Ando', G., Gragnano, F., Zimarino, M., Shinke, T., Kočka, V., Pozzoli, A. G., Del Buono, M. G., Ahmed, J., Rathod, K., eds. (2025). *Insights in coronary artery disease: 2023*. Lausanne: Frontiers Media SA. doi: 10.3389/978-2-8325-6391-5

Table of contents

frontiers | Frontiers in Cardiovascular Medicine

TYPE Editorial
PUBLISHED 15 May 2025
DOI 10.3389/fcvm.2025.1619625

OPEN ACCESS

EDITED AND REVIEWED BY
Seokhun Yang,
Seoul National University Hospital, Republic of Korea

*CORRESPONDENCE
Giuseppe Ando'
giuseppe.ando@unime.it

RECEIVED 28 April 2025
ACCEPTED 01 May 2025
PUBLISHED 15 May 2025

CITATION
Ando' G, Gragnano F, Del Buono MG, Kočka V, Zimarino M, Shinke T, Rathod K, Ahmed J, Pozzoli AG and Gori T (2025) Editorial: Insights in coronary artery disease: 2023. Front. Cardiovasc. Med. 12:1619625. doi: 10.3389/fcvm.2025.1619625

Editorial: Insights in coronary artery disease: 2023

Giuseppe Ando'[1]*, Felice Gragnano[2], Marco Giuseppe Del Buono[3], Viktor Kočka[4], Marco Zimarino[5], Toshiro Shinke[6], Krishnaraj Rathod[7], Javed Ahmed[8], Alberto Guido Pozzoli[9] and Tommaso Gori[10]

[1]Department of Clinical and Experimental Medicine, University of Messina, Messina, Italy, [2]Department of Translational Medical Sciences, University of Campania "Luigi Vanvitelli", Caserta, Italy, [3]Department of Cardiology, Agostino Gemelli University Polyclinic (IRCCS), Rome, Italy, [4]Department of Cardiology, University Hospital Kralovske Vinohrady and Third Faculty of Medicine, Charles University, Prague, Czechia, [5]Department of Cardiology, ASL Lanciano Vasto Chieti, Chieti, Italy, [6]Division of Cardiology, Department of Medicine, Showa University School of Medicine, Tokyo, Japan, [7]Centre for Cardiovascular Medicine and Devices, Queen Mary University of London, London, United Kingdom, [8]Department of Cardiology, Newcastle upon Tyne Hospitals NHS Foundation Trust, Newcastle upon Tyne, United Kingdom, [9]Istituto Cardiocentro Ticino, Ospedale Regionale di Lugano, Lugano, Switzerland, [10]Zentrum für Kardiologie, University Medical Centre, Johannes Gutenberg University Mainz, Mainz, Germany

KEYWORDS

coronary artery disease, atherosclerosis, myocardial infarction, percutaneous coronar intervention, inflammation

Editorial on the Research Topic
Insights in coronary artery disease: 2023

Coronary artery disease (CAD) continues to pose a substantial global health burden, remaining one of the leading causes of death and disability across both developed and developing nations. Despite decades of progress in risk factor management (1), revascularization strategies (2), pharmacological treatments (3), and imaging technologies (4), significant challenges persist in achieving optimal prevention, diagnosis, and long-term outcomes. The Research Topic *"Insights in Coronary Artery Disease: 2023"*, hosted by *Frontiers in Cardiovascular Medicine*, presents a curated Research Topic of original research articles, reviews, and case reports that offer cutting-edge perspectives on various aspects of CAD—from interventional cardiology and intravascular imaging to digital modeling, inflammation, and even the gut-heart axis.

One of the central themes emerging from this Topic is the pursuit of better risk prediction and personalized care pathways for patients with CAD. Dai et al. developed and validated a user-friendly nomogram to predict the five-year risk of non-culprit lesion (NCL) revascularization in patients with ST-segment elevation myocardial infarction (STEMI) who had undergone primary percutaneous coronary intervention (PCI). Their model integrates clinical and laboratory variables such as age, body mass index, Killip class, and low-density lipoprotein cholesterol (LDL-C) levels to identify individuals at elevated long-term risk. The clinical relevance of this tool lies in its potential to inform more individualized surveillance, medical therapy intensification, and follow-up strategies tailored to residual risk—particularly important in the era of complete revascularization. Notably, prior studies (5) have also emphasized the prognostic value of non-culprit lesion assessment following STEMI, underscoring the need for refined risk stratification approaches.

Sex differences in outcomes following complex coronary interventions remain an area of growing interest (6). In a robust analysis from a nationwide Spanish registry,

Alperi et al. demonstrated that women undergoing complex PCI had a significantly higher risk of all-cause mortality and myocardial infarction compared to men. This disparity persisted despite adjustment for comorbidities and procedural complexity. Their findings underscore the need for continued investigation into sex-specific pathophysiology, differences in response to therapy, and underrepresentation of women in clinical trials—factors that may ultimately influence guideline recommendations and improve outcomes for female patients.

Technological advancements in stent platforms also feature prominently in this collection. The CAESAR registry, reported by Tarantini et al., evaluated the real-world performance of a novel ultrathin-strut, polymer-free sirolimus-eluting stent (Coroflex ISAR NEO) in an all-comers population with CAD. The results were encouraging, with low rates of target lesion revascularization and major adverse cardiac events at one year, confirming the safety and efficacy of this new-generation stent. These findings contribute to the growing body of evidence supporting polymer-free platforms, which may reduce chronic inflammation and improve endothelial healing.

Understanding the mechanistic basis of atherosclerosis progression and plaque rupture is key to preventing acute coronary syndromes. Bacigalupi et al. provided a comprehensive review on the role of biomechanical forces—particularly wall shear stress, axial plaque stress, and structural stress—in shaping plaque vulnerability. With the advent of high-resolution imaging and computational fluid dynamics (CFD), it is now possible to model these forces in patient-specific coronary geometries. This approach holds promise for identifying plaques at high risk of rupture before clinical events occur, thus enabling preemptive interventions.

In line with this, Lashgari et al. proposed the use of in silico 3D modeling as a novel adjunctive tool in the cardiac catheterization laboratory. They demonstrated how patient-specific coronary models, generated from angiographic data and processed using CFD, can provide functional insights beyond visual assessment. Such models may enhance diagnostic precision, especially for intermediate lesions where functional significance is uncertain. As digital health tools evolve, the integration of modeling and simulation into clinical workflows could revolutionize decision-making in interventional cardiology.

The inflammatory component of atherosclerosis remains a focal point for research, particularly as imaging tools allow for more nuanced plaque characterization. Los et al. reviewed current invasive coronary imaging techniques—such as intravascular ultrasound (IVUS), optical coherence tomography (OCT), and near-infrared spectroscopy (NIRS)—that can detect plaque features associated with inflammation and vulnerability. These modalities offer valuable prognostic information and may soon be integrated into risk algorithms to guide therapy beyond angiographic stenosis alone. Recent studies (7) have further highlighted the potential of imaging-derived inflammatory biomarkers to refine cardiovascular risk assessment and personalize therapeutic strategies.

The systemic nature of CAD, particularly in elderly patients, was addressed in a study by Xu et al., who evaluated the association between the Geriatric Nutritional Risk Index (GNRI) and the presence of sarcopenia, osteoporosis, and cognitive impairment in older adults with coronary disease. Their findings reinforce the importance of assessing frailty and nutritional status as part of a comprehensive management plan. As the population ages, addressing these geriatric syndromes in CAD patients is increasingly vital to improving quality of life and reducing rehospitalizations.

In an innovative study exploring the gut-heart axis, Hu et al. employed Mendelian randomization to investigate potential causal links between gut microbiota composition and coronary heart disease. Their analysis suggested that the presence of certain microbial genera—including *Bifidobacterium* and *Butyricicoccus*—may have protective or deleterious effects on CAD risk. While still exploratory, this line of research opens the door to microbiota-targeted preventive strategies and underscores the systemic and immunological dimensions of atherosclerosis.

Finally, Dall'Ara et al. presented a compelling case report of recurrent Takotsubo syndrome triggered by asymptomatic SARS-CoV-2 infection, adding to the evolving understanding of COVID-19's cardiovascular sequelae. The case highlights how viral infections, even in the absence of respiratory symptoms, can precipitate acute cardiac syndromes via neurohormonal (8) or inflammatory pathways. It also reinforces the importance of vigilance and multidisciplinary care in the post-COVID era.

In conclusion, the *Insights in Coronary Artery Disease: 2023* Research Topic underscores the significant breadth and depth of contemporary research in coronary artery disease, encompassing advancements in predictive modeling, stent technologies, digital innovation, and the understanding of biological, mechanical, and systemic contributors to disease progression.

The contributions assembled herein highlight the critical importance of interdisciplinary collaboration and the ongoing shift toward precision cardiovascular medicine. Collectively, these studies provide both a comprehensive resource and a strategic framework to guide future investigations, with the ultimate aim of improving clinical outcomes for patients with coronary artery disease.

It is our aspiration that this collection will serve as a valuable reference and a source of inspiration for researchers, clinicians, and trainees committed to advancing the field.

Author contributions

GA: Writing – review & editing, Writing – original draft. FG: Writing – original draft, Writing – review & editing. MD: Writing – review & editing. VK: Writing – review & editing. MZ: Writing – review & editing. TS: Writing – review & editing. KR: Writing – review & editing. JA: Writing – review & editing. AP: Writing – review & editing. TG: Writing – review & editing.

Conflict of interest

The authors declare that the research was conducted in the absence of any commercial or financial relationships that could be construed as a potential conflict of interest.

The author(s) declared that they were an editorial board member of Frontiers, at the time of submission. This had no impact on the peer review process and the final decision.

Generative AI statement

The author(s) declare that Generative AI was used in the creation of this manuscript. Generative AI (ChatGPT, OpenAI) was used to assist with language editing, structural refinement, and enhancement of clarity and formal tone in the preparation of this manuscript. The authors were solely responsible for the conception, content development, critical interpretation, and final approval of the manuscript.

Publisher's note

References

1. Gargiulo P, Basile C, Galasso G, Bellino M, D'Elia D, Patti G, et al. Strike early-strike strong lipid-lowering strategy with proprotein convertase subtilisin/kexin type 9 inhibitors in acute coronary syndrome patients: real-world evidence from the at-target-it registry. *Eur J Prev Cardiol.* (2024) 31(15):1806–16. doi: 10.1093/eurjpc/zwae170

2. Gragnano F, Branca M, Frigoli E, Leonardi S, Vranckx P, Di Maio D, et al. Access-site crossover in patients with acute coronary syndrome undergoing invasive management. *JACC Cardiovasc Interv.* (2021) 14(4):361–73. doi: 10.1016/j.jcin.2020.11.042

3. Gargiulo G, Carrara G, Frigoli E, Leonardi S, Vranckx P, Campo G, et al. Post-procedural bivalirudin infusion at full or low regimen in patients with acute coronary syndrome. *J Am Coll Cardiol.* (2019) 73(7):758–74. doi: 10.1016/j.jacc.2018.12.023

4. Buonpane A, Trimarchi G, Ciardetti M, Coceani MA, Alagna G, Benedetti G, et al. Optical coherence tomography in myocardial infarction management: enhancing precision in percutaneous coronary intervention. *J Clin Med.* (2024) 13(19):5791. doi: 10.3390/jcm13195791

5. Klancik V, Pesl L, Neuberg M, Tousek P, Kocka V. Long-term follow-up in patients with st-segment elevation myocardial infarction who underwent primary percutaneous coronary intervention. *Eur Heart J Suppl.* (2022) 24(Suppl B):B16–22. doi: 10.1093/eurheartjsupp/suac003

6. Calabro P, Niccoli G, Gragnano F, Grove EL, Vergallo R, Mikhailidis DP, et al. Are we ready for a gender-specific approach in interventional cardiology? *Int J Cardiol.* (2019) 286:226–33. doi: 10.1016/j.ijcard.2018.11.022

7. Cacciatore S, Andaloro S, Bernardi M, Oterino Manzanas A, Spadafora L, Figliozzi S, et al. Chronic inflammatory diseases and cardiovascular risk: current insights and future strategies for optimal management. *Int J Mol Sci.* (2025) 26(7):3071. doi: 10.3390/ijms26073071

8. Ando G, Trio O, de Gregorio C. Transient left ventricular dysfunction in patients with neurovascular events. *Acute Card Care.* (2010) 12(2):70–4. doi: 10.3109/17482941003732758

frontiers | Frontiers in Cardiovascular Medicine

TYPE Original Research
PUBLISHED 29 November 2023
DOI 10.3389/fcvm.2023.1275710

OPEN ACCESS

EDITED BY
Tommaso Gori,
Johannes Gutenberg University Mainz, Germany

REVIEWED BY
Long Jiang,
Second Affiliated Hospital of Nanchang University, China
Yasushi Ueki,
Shinshu University Hospital, Japan

*CORRESPONDENCE
Junhong Chen
cjh1029@sina.com
Tongda Xu
xyfyxys@163.com

†These authors have contributed equally to this work

RECEIVED 10 August 2023
ACCEPTED 13 November 2023
PUBLISHED 29 November 2023

CITATION
Dai F, Xu X, Zhou C, Li C, Tian Z, Wang Z, Yang S, Liao G, Shi X, Wang L, Li D, Hou X, Chen J and Xu T (2023) Development and validation of a nomogram to predict the five-year risk of revascularization for non-culprit lesion progression in STEMI patients after primary PCI. Front. Cardiovasc. Med. 10:1275710. doi: 10.3389/fcvm.2023.1275710

Development and validation of a nomogram to predict the five-year risk of revascularization for non-culprit lesion progression in STEMI patients after primary PCI

Feng Dai[1†], Xianzhi Xu[2†], Chunxue Zhou[1], Cheng Li[1], Zhaoxuan Tian[1], Zhaokai Wang[1], Shuping Yang[3], Gege Liao[1], Xiangxiang Shi[3], Lili Wang[1], Dongye Li[1], Xiancun Hou[4], Junhong Chen[1*] and Tongda Xu[1*]

[1]Department of Cardiology, The Affiliated Hospital of Xuzhou Medical University, Xuzhou, China, [2]Department of Oral Medicine, School of Stomatology, Xuzhou Medical University, Xuzhou, China, [3]Department of General Practice & Geriatrics, The Affiliated Hospital of Xuzhou Medical University, Xuzhou, China, [4]Department of Nuclear Medicine, The Affiliated Hospital of Xuzhou Medical University, Xuzhou, China

Background: Acute ST-segment elevation myocardial infarction (STEMI) patients after primary PCI were readmitted for revascularization due to non-culprit lesion (NCL) progression.

Objective: To develop and validate a nomogram that can accurately predict the likelihood of NCL progression revascularization in STEMI patients following primary PCI.

Methods: The study enrolled 1,612 STEMI patients after primary PCI in our hospital from June 2009 to June 2018. Patients were randomly divided into training and validation sets in a 7:3 ratio. The independent risk factors were determined by LASSO regression and multivariable logistic regression analysis. Multivariate logistic regression analysis was utilized to develop a nomogram, which was then evaluated for its performance using the concordance statistics, calibration plots, and decision curve analysis (DCA).

Results: The nomogram was composed of five predictors, including age (OR: 1.007 95% CI: 1.005–1.009, $P < 0.001$), body mass index (OR: 1.476, 95% CI: 1.363–1.600, $P < 0.001$), triglyceride and glucose index (OR: 1.050, 95% CI: 1.022–1.079, $P < 0.001$), Killip classification (OR: 1.594, 95% CI: 1.140–2.229, $P = 0.006$), and serum creatinine (OR: 1.007, 95% CI: 1.005–1.009, $P < 0.001$). Both the training and validation groups accurately predicted the occurrence of NCL progression revascularization (The area under the receiver operating characteristic curve values, 0.901 and 0.857). The calibration plots indicated an excellent agreement between prediction and observation in both sets. Furthermore, the DCA demonstrated that the model exhibited clinical efficacy.

Conclusion: A convenient and accurate nomogram was developed and validated for predicting the occurrence of NCL progression revascularization in STEMI patients after primary PCI.

KEYWORDS

non-culprit lesion, percutaneous coronary intervention, nomogram, ST-segment elevation myocardial infarction, primary PCI

Abbreviations

STEMI, ST-elevation myocardial infarction; PCI, percutaneous coronary intervention; NCL, non-culprit lesion; DCA, decision curve analysis; CAG, coronary angiography; BMI, body mass index; TyG, triglycerides and glucose index; SCr, serum creatinine; CKD, chronic kidney disease.

Introduction

Coronary artery disease causes 8.9 million patient deaths and 264 million workforce losses annually (1). Among the various manifestations of coronary artery disease, ST-elevation myocardial infarction (STEMI) is the most severe type characterized by rapid onset, progression, and high morbidity and mortality (2). Fortunately, the availability of thrombolytic therapy and primary percutaneous coronary intervention (PCI) has significantly improved STEMI patients' prognosis. Although the utilization of drug-eluting stents has contributed to reducing the occurrences of in-stent restenosis (3). Revascularization after PCI remains a common clinical problem. The rate of revascularization after PCI was 12% at 1 year, 15% at 2 years, 20% at 4 years, and 32.3% at 5 years (4, 5). The in-stent restenosis is not the sole cause of repeat revascularization. One study highlighted that non-culprit lesion (NCL) progression accounts for over half of all revascularizations (4). NCL progression refers to developing or worsening atherosclerotic lesions outside the culprit lesions that cause ischemia, angina, and myocardial infarction. Such progression can lead to recurrent ischemia, angina, myocardial infarction, or death. Nonetheless, not all non-culprit lesions necessitate revascularization. Hence, predicting the likelihood of revascularization for NCL progression in STEMI patients is crucial.

Several studies have examined risk factors associated with repeat revascularization, such as fasting glucose, peak cTnI levels, and complex lesions (6, 7). Compared to conventional statistical models, the nomogram provides several advantages such as validation of effectiveness, visual representation, and personalized risk assessment (8). The nomogram effectively quantifies risk factors and synthesizes them into a predictive score to inform clinical decisions.

However, there are no studies for developing and validating a nomogram specifically for NCL progression revascularization. The study aims to build and validate a nomogram to predict the likelihood of NCL progression revascularization in STEMI patients after complete revascularization.

In this retrospective study, a nomogram was established to screen high-risk groups based on our clinical results, which may provide guidance for clinicians and assesses STEMI patients' prognosis.

Study population

The study was conducted in accordance with the Declaration of Helsinki and approved by the Ethics Committee of the Affiliated Hospital of Xuzhou Medical University (XYFY2022-KL375-01). Since the study was retrospective, the committee waived the requirement for written informed consent. Personal private information was removed prior to the data is analyzed.

7,277 patients who underwent primary PCI for STEMI between 2009 and 2018 were initially screened in the affiliated hospital of Xuzhou medical university. Patients showing multivessel disease at the first CAG were included in the study only if NCL with diameter stenosis greater than 70% were treated. Secondly, 2,469 patients combined of at least one NCL (diameter stenosis between 50% and 70%) were readmitted to the hospital within 5 years after primary PCI for clinical symptoms such as chest pain and chest tightness. These patients underwent review coronary angiography (CAG). Finally, 1,612 patients were included in the study according to the exclusion and inclusion criteria.

Inclusion criteria: (1) diagnosis of acute ST-segment elevation myocardial infarction (9), (2) successful drug-eluting stent implantation procedure, (3) immediate complete revascularization or elective completion of complete revascularization within 2 months (10), (4) no in-hospital cardiovascular events such as cardiogenic shock, recurrent myocardial infarction, or death, (5) follow-up CAG within 5 years after the first PCI, (6) no anticoagulant or antiplatelet contraindications, (7) over 18 years old, (8). Combination of at least one NCL (diameter stenosis between 50% and 70%).

Exclusion criteria: (1) incomplete clinical data (n=576), (2) follow-up CAG showing in-stent restenosis or recommendation for coronary artery bypass graft (n=258), (3) severe hepatic insufficiency or renal insufficiency (n=23).

First PCI procedure

Patients undergoing the procedure were routinely administered stress dose medications (300 mg of aspirin, 600 mg of clopidogrel, or 180 mg of ticagrelor). To ensure proper anticoagulation, 3,000 IU of unfractionated heparin and 200 ug of nitroglycerin were administered prior to CAG. The administration of heparin was initiated at 100 IU/kg before the operation, with the option of adding 1,000 IU/h during the procedure. Additionally, intraoperative medications such as nitroprusside, nitroglycerin, tirofiban, and other drugs aimed at improving coronary ischemia were selectively administered based on the patient's condition.

Following the operation, medications were prescribed according to established guidelines. These included: (1) a dual antiplatelet regimen involving aspirin (100 mg once daily) combined with either clopidogrel (75 mg once daily) or ticagrelor (90 mg twice daily); (2) statin; (3) angiotensin converting enzyme inhibitor or angiotensin receptor blocker; and (4) beta-blocker.

Senior cardiologists performed both CAG and PCI procedures. Two skilled clinicians thoroughly analyzed all CAG images.

Clinical endpoints and definitions

The clinical endpoint was that STEMI patient readmitted with ischemic symptoms found to have NCL progression (diameter stenosis progresses from between 50%–70% to >70%) requiring revascularization within 5 years after PCI. NCL was defined as a vessel with stenosis between 50% and 70% at the first CAG (7). All patients underwent primary PCI of the culprit lesions successfully. Patients showing multivessel disease at the first CAG were included in the study only if they had completed complete revascularization or selective complete revascularization. Complete revascularization was defined as successful revascularization of all coronary artery lesions or segments ≥1.5 mm in diameter with

≥70% diameter stenosis regardless of their functional significance (11). Related definitions included the following: Calcified lesions were defined as the presence of moderate or severe calcification in the vessel wall (12); bifurcation lesions were defined as stenosis adjacent to and/or involving the opening of a major branch (13); ostial lesions were defined as lesions within 3 mm of the origin of the major coronary arteries (14); angular distortion lesions were defined as angles of at least one major branch of the coronary artery ≥45° along the direction of the main coronary artery (15).

Data collection

All patient clinical features (including demographics, previous history, laboratory indices, two-times coronary angiography images, and medication use at discharge) were collected. Each patient's blood was collected within 24 h of admission, and the central laboratory tested all laboratory parameters before operation. Data collection during PCI consisted of door-to-balloon time, calcified lesions, bifurcation lesions, open and angular distortion lesions, and culprit lesions. Echocardiography measures the left ventricular ejection fraction.

Data analysis

Categorical variables were displayed as counts and percentages and then compared using either the χ^2 or Fisher exact test. Meanwhile, continuous variables were presented as mean ± standard deviation. If the variables adhered to a normal distribution pattern, they were compared using the *t*-test. However, if the variables exhibited non-normal distribution, they were compared using the Mann–Whitney *U*-test. Univariate logistic regression was analyzed to filter significant variables in the training cohort. This part was done using SPSS version 25.0 (SPSS Inc., Chicago, IL, USA). LASSO regression was used to screen out non-zero coefficient characteristics, and multivariate logistic regression backward stepwise regression was used to analyze the independent predictors. The restricted cubic spline was performed to investigate the linear relationships between continuous variables and NCL progression revascularization. A nomogram was developed using variables with $P < 0.05$ based on the result of the multivariate logistic regression. The discrimination capability of the model was gauged by the concordance index, which is equal to the area under the receiver operating characteristics curve (AUC-ROC). This metric was used to assess the effectiveness of the nomogram's discrimination capacity. In order to determine the level of accuracy of the calibration, Hosmer-Lemeshow tests and calibration plots were carried out. Clinical efficacy was evaluated using decision curve analysis. The statistical threshold for determining significance was established at a level of $P < 0.05$ for the two-sided test. This part was analyzed using R Studio version 4.1.3 (https://cran.r-project.org).

Results

The study flow chart is shown in **Figure 1**. There are 1,612 STEMI patients were enrolled based on inclusion and exclusion criteria. Patients were randomly divided into training and validation sets in a 7:3 ratio. Among them, 14.8% (163/1,097) of patients in the training set underwent repeat PCI due to NCL progression, similar to 14.3% (74/515) of patients in the validation set. **Table 1** presents a comprehensive sight of the baseline characteristics of the two sets. **Table 2** displays the results of the univariate logistic regression. Univariate logistic regression analysis showed that the following factors were consistently associated with NCL revascularization in STEMI patients following primary PCI: age (OR: 1.09, 95% CI: 1.07–1.11, $P < 0.001$), body mass index (BMI) (OR: 1.55, 95% CI: 1.44–1.67, $P < 0.001$), triglyceride and glucose index (OR: 1.03, 95% CI: 1.01–1.05, $P = 0.005$), Killip classification (OR: 1.76, 95% CI: 1.31–2.35, $P < 0.001$), Hypertension (OR: 0.62, 95% CI: 0.44–0.86, $P = 0.005$), serum creatinine (SCr) (OR: 1.01, 95% CI: 1.00–1.01, $P < 0.001$), Lipoprotein-a (OR: 1.00, 95% CI: 1.00–1.00, $P < 0.001$), creatine kinase MB (OR: 1.00, 95% CI: 1.00–1.01, $P = 0.001$), total cholesterol (OR: 2.59, 95% CI: 2.18–3.08, $P < 0.001$). LASSO regression analysis showed that age, BMI, triglyceride and glucose index, Killip classification, and SCr were the more important predictors with non-zero coefficient, as shown in **Figure 2**. Multivariate logistic regression analysis identified in **Table 3** that age (OR: 1.007, 95% CI: 1.005–1.009, $P < 0.001$), BMI (OR: 1.476, 95% CI: 1.363–1.600, $P < 0.001$), triglyceride and glucose index (OR: 1.050, 95% CI: 1.022–1.079, $P < 0.001$), Killip classification (OR: 1.594, 95% CI: 1.140–2.229, $P = 0.006$), and SCr (OR: 1.007, 95% CI: 1.005–1.009, $P < 0.001$). A nomogram was built and displayed in **Figure 3**. A point value is projected at the top of the nomogram for each independent predictor. This process helps obtain a score ranging between 0 and 100. The scores of all variables are added to get a total score, which is projected down to a vertical line on the "Risk" line, indicating the risk of NCL revascularization. A higher overall score indicates a higher likelihood of NCL revascularization. Consequently, the model could visually predict the occurrence of NCL progression revascularization.

Validation of the nomogram

The AUC-ROC for the nomogram and validation sets (**Figures 4A,B**) was calculated to be 0.9014 (95% CI: 0.8795–0.9233) and 0.8574 (95% CI: 0.8103–0.9046), showing a good discrimination ability of the nomogram. The Hosmer-Lemeshow test produced χ^2 values of the nomogram (7.3528, $P = 0.4991$) and the validation group (2.961, $P = 0.9368$), respectively. These results attest to the model's excellent calibration capability. Additionally, the calibration curve demonstrates high consistency between the predicted and actual probabilities (**Figures 5A,B**).

The clinical effectiveness of the model was evaluated, which is depicted in **Figures 6A,B**. The horizontal line indicates a net benefit of 0, which occurs when no intervention is performed

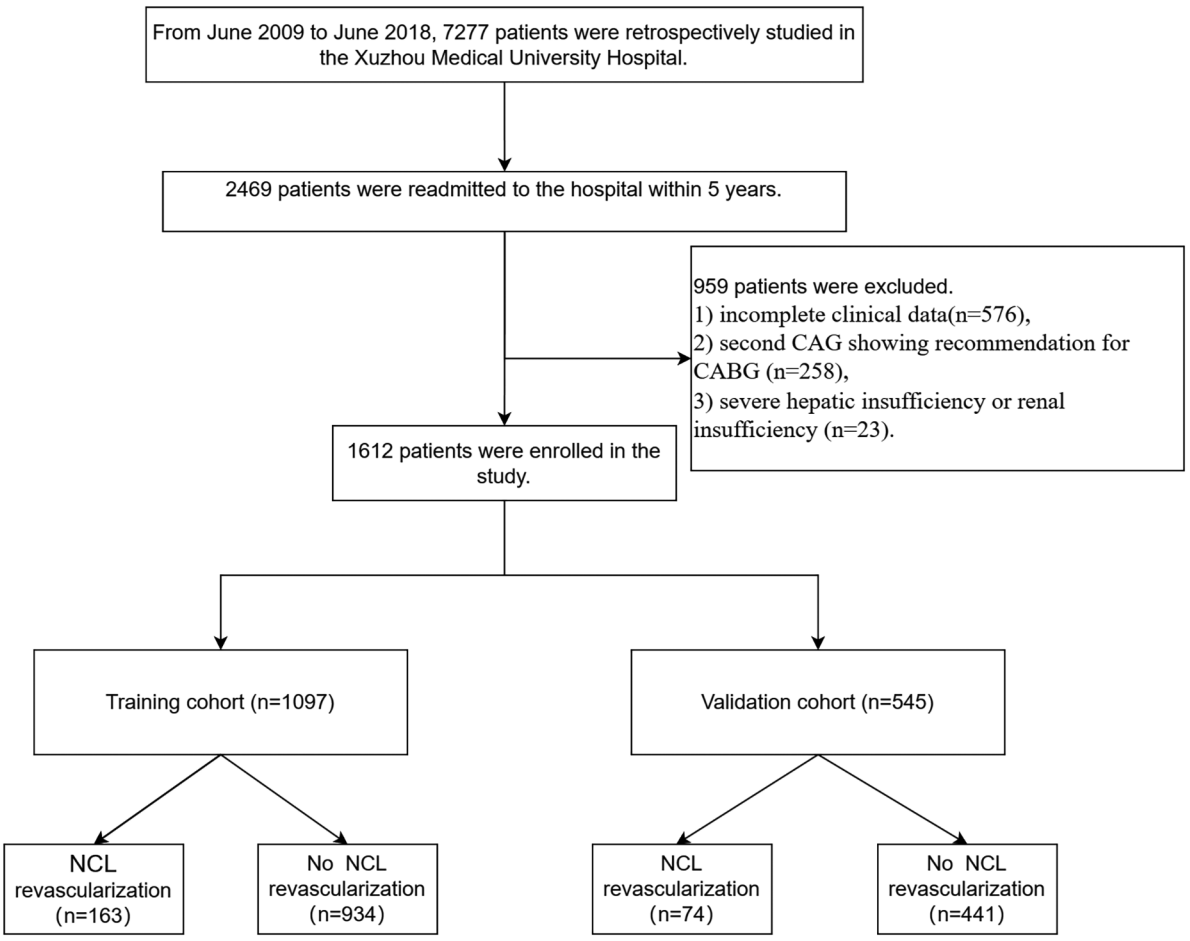

FIGURE 1
The study flowchart for developing and validating nomograms. CAG, coronary angiography; CABG, coronary artery bypass graft.

and all samples are negative (Pi < Pt). Conversely, the green line corresponds to a scenario where all interventions are applied, and all samples are positive. The DCA demonstrates that the nomogram can achieve a net benefit over a wide range of threshold probabilities, indicating our approach's clinical utility.

Discussion

With the aging of the population, there has been an annual increase in the incidence of acute ST-segment elevation myocardial infarction (STEMI). Fortunately, the prognosis for STEMI patients has improved with the widespread availability of percutaneous coronary intervention (PCI). Nevertheless, STEMI patients who have undergone PCI are still at risk of readmission due to in-stent restenosis or the non-culprit lesion (NCL) progression. The use of drug-eluting stents reduces incidences of in-stent restenosis as compared to bare metal stents. However, the application of drug-eluting stents has not demonstrated a commensurate improvement in the rate of revascularization. In two randomized controlled trials (16, 17), there was no difference between bare metal stent and drug-eluting stent applications for revascularization due to NCL progression in acute myocardial infarction (AMI) patients. Notably, numerous clinical trials (18–20) revealed that the rate of revascularization associated with NCL ranges from approximately 11.6%–19%, accounting for 42%–57% of all repeat procedures during the five years after PCI. It has been observed that while there have been several studies focusing on the progression of NCL, the repeated PCI for NCL progression has not received much attention. The study focuses on predicting repeat PCI due to NCL. One study of 480 patients identified fasting glucose and creatinine as independent risk factors for NCL progression (6), while another study of 492 patients suggested that several chronic stress and inflammation-related factors such as serum catecholamines, and C-reactive protein, as well as complex lesion rates, were related to the progression of NCL (7). We had a larger sample size ($n = 1{,}612$ vs. 480) and more complete clinical data (including angiographic, laboratory, and follow-up data) than previous studies, which increased the statistical power and generalizability of our results. Compared with traditional independent risk factors, nomograms could visualize the effect of predictors on NCL revascularization, which is a user-friendly tool to help clinicians and patients estimate the individualized risks and benefits of NCL PCI. Unlike

TABLE 1 Participant characteristics.

Variable	Cohort, No. (%)		*P*-value
	Training set, *N* = 1,097	Validation set, *N* = 515	
Intervals between coronary angiograms, months	41 (34, 47)	42 (35, 48)	0.342
Age, years	67 (57, 75)	66 (56, 75)	0.41
Sex, *n* (%)			0.968
Male	802 (73%)	377 (73%)	
Female	295 (27%)	138 (27%)	
Body mass index, kg/m2	25.64 (23.96, 27.42)	25.33 (23.80, 27.10)	0.057
Diabetes mellitus, *n* (%)			0.093
Yes	829 (76%)	369 (72%)	
No	268 (24%)	146 (28%)	
Hypertension, *n* (%)			0.361
Yes	555 (51%)	248 (48%)	
No	542 (49%)	267 (52%)	
Smoking status, *n* (%)			0.459
Yes	458 (42%)	205 (40%)	
No	639 (58%)	310 (60%)	
Alcohol drinking status, *n* (%)			0.954
Yes	146 (13%)	68 (13%)	
No	951 (87%)	447 (87%)	
Coronary heart disease, *n* (%)			0.184
Yes	34 (3%)	10 (2%)	
No	1,063 (97%)	505 (98%)	
Transient ischemic attack, *n* (%)			0.275
Yes	50 (5%)	30 (6%)	
No	1,047 (95%)	485 (94%)	
Aspirin, *n* (%)			1
Yes	1,097 (100%)	515 (100%)	
No	0 (0%)	0 (0%)	
Clopidogrel, *n* (%)			0.290
Yes	404 (37%)	175 (34%)	
No	693 (63%)	340 (66%)	
Ticagrelor, *n* (%)			0.510
Yes	671 (61%)	324 (63%)	
No	426 (39%)	191 (37%)	
Beta-blockers, *n* (%)			0.75
Yes	883 (80%)	418 (81%)	
No	214 (20%)	97 (19%)	
ACEI/ARB, *n* (%)			0.224
Yes	623 (57%)	309 (60%)	
No	474 (43%)	206 (40%)	
Calcium channel blockers, *n* (%)			0.467
Yes	139 (13%)	72 (14%)	
No	958 (87%)	443 (86%)	
Statins, *n* (%)			0.102
Yes	1,080 (98%)	512 (99%)	
No	17 (2%)	3 (1%)	
High intensity of statin, *n* (%)			0.657
Yes	401 (37%)	182 (35%)	
No	696 (63%)	333 (65%)	
Door-to-balloon time, min	295.24 ± 43.67	299.07 ± 69.13	0.177
Left ventricular ejection fraction, %	56 (50, 61)	55 (51, 60)	0.062
Creatine kinase MB, ng/ml	22 (5, 60)	24 (4, 97)	0.359
White blood cell, ×109/L	9.10 (7.40, 11.10)	9.10 (7.00, 11.30)	0.351
Neutrophile, $\times10^9$/L	6.81 (5.18, 8.72)	6.80 (6.34, 7.40)	0.236
Lymphocyte, $\times10^9$/L	1.50 (1.00, 2.00)	1.40 (1.00, 2.00)	0.172
High-sensitive C-reactive protein, mg/L	8 (3, 26)	5 (2, 31)	0.459
Fasting plasma glucose, mmol/L	5.5 (4.1, 7.4)	5.6 (3.6, 8.4)	0.998
Serum creatinine, umol/L	239 (69, 305)	228 (152, 287)	0.517
Serum uric acid, umol/L	308 (258, 355)	307 (302, 311)	0.656
Total cholesterol, mmol/L	1,007 (809, 1,169)	939 (544, 1,748)	0.221
Triglyceride, mmol/L	4.30 (3.73, 5.02)	4.27 (3.68, 4.97)	0.311
Triglyceride and glucose index	1.36 (0.98, 1.92)	1.30 (0.90, 1.94)	0.136
High-density lipoprotein cholesterol, mmol/L	1.03 ± 0.36	1.02 ± 0.29	0.588
Low Density Lipoprotein cholesterol, mmol/L	2.73 ± 0.88	2.68 ± 0.85	0.192
Low Density Lipoprotein cholesterol on re-admission, mmol/L	2.476 ± 0.85	2.43 ± 0.83	0.343
Lipoprotein-a, mg/L	2.66 (2.18, 3.21)	2.60 (2.14, 3.10)	0.101
Hypersensitive troponin T, ng/L	224 (152, 340)	223 (180, 299)	0.587
N-terminal pro-brain natriuretic peptide, pg/ml	673.43 ± 49.58	676.30 ± 49.42	0.277
Lactate dehydrogenase, U/L	300.19 ± 159.92	293.92 ± 152.84	0.449
Killip classification, *n* (%)			0.644
1	193 (18%)	92 (18%)	
2	722 (66%)	347 (67%)	
3	182 (17%)	76 (15%)	
Calcified lesions, *n* (%)			0.725
Yes	562 (51%)	259 (50%)	
No	535 (49%)	256 (50%)	
Bifurcation lesions, *n* (%)			0.402
Yes	202 (18%)	86 (17%)	
No	895 (82%)	429 (83%)	
Ostial lesions, *n* (%)			0.185
Yes	117 (11%)	44 (9%)	
No	980 (89%)	471 (91%)	
Angular distortion lesions, *n* (%)			0.756
Yes	44 (4%)	19 (4%)	
No	1,053 (96%)	496 (96%)	
Target left main, *n* (%)			0.335
Yes	2 (0%)	3 (1%)	
No	1,095 (100%)	512 (99%)	
Target left anterior descending, *n* (%)			0.245
Yes	283 (26%)	147 (29%)	
No	814 (74%)	368 (71%)	
Target left circumflex, *n* (%)			0.822
Yes	394 (36%)	182 (35%)	
No	703 (64%)	333 (65%)	

(*Continued*)

TABLE 1 Continued

Variable	Cohort, No. (%)		*P*-value
	Training set, *N* = 1,097	Validation set, *N* = 515	
Target right coronary artery, *n* (%)			0.11
Yes	352 (32%)	186 (36%)	
No	745 (68%)	329 (64%)	
Calcified lesions (NCL) *n* (%)			0.784
Yes	426 (39%)	196 (38%)	
No	671 (61%)	319 (62%)	
Bifurcation lesions (NCL), *n* (%)			0.739
Yes	224 (20%)	101 (20%)	
No	873 (80%)	414 (80%)	
Ostial lesions (NCL), *n* (%)			0.548
Yes	215 (20%)	108 (21%)	
No	882 (80%)	407 (79%)	
Angular distortion lesions (NCL), *n* (%)			0.948
Yes	232 (21%)	110 (21%)	
No	865 (79%)	405 (79%)	
NCL located on left anterior descending, *n* (%)			0.086
Yes	365 (33%)	149 (29%)	
No	732 (67%)	366 (71%)	
NCL located on left circumflex, *n* (%)			0.372
Yes	381 (35%)	191 (37%)	
No	716 (65%)	324 (63%)	
NCL located on right coronary artery, *n* (%)			0.361
Yes	347 (32%)	175 (34%)	
No	750 (68%)	340 (66%)	
Diameter stenosis, %	62.50 ± 6.98	61.98 ± 4.66	0.126
Lesion length, mm	13.77 ± 5.87	13.46 ± 5.84	0.324
Fractional flow reserve (FFR), *n* (%)			0.364
Yes	14 (1%)	9 (2%)	
NO	1,083 (99%)	506 (98%)	

ACEI, angiotensin converting enzyme inhibitor; ARB, angiotensin receptor inhibitor; NCL, non-culprit lesion.

previous studies that did not validate independent risk factors, we evaluated the validity of our model using ROC curve, calibration curve, and decision curve analyses both in the training and validation sets. The results showed that our model had good discrimination, calibration, and clinical utility. Therefore, the nomogram was useful and meaningful to predict NCL progression revascularization in STEMI patients who have undergone primary PCI.

To determine independent risk factors, a multivariate logistic regression analysis was performed. The variables analyzed included age, body mass index (BMI), triglycerides and glucose index (TyG), Killip classification, and serum creatinine (SCr). Furthermore, these five independent risk factors were integrated to build a nomogram to predict the revascularization for the progression of NCL in STEMI patients after PCI.

TABLE 2 Univariate logistic regression analysis in the training group.

Variables	OR (95% CI)	*P*-value
Intervals between coronary angiograms, months	0.99 (0.98–1.01)	0.333
Age, years	1.09 (1.07–1.11)	**<0.001**
Sex, male vs. female	1.20 (0.83–1.72)	0.323
Diabetes mellitus	1.22 (0.83–1.76)	0.307
Hypertension	0.62 (0.44–0.86)	**0.005**
Smoking status	1.09 (0.78–1.52)	0.612
Alcohol drinking status	1.22 (0.75–1.91)	0.409
Coronary heart disease	0.99 (0.33–2.38)	0.98
Transient ischemic attack	2.83 (1.02–11.73)	0.084
Aspirin, *n* (%)	1.00 (1.00–1.00)	1
Clopidogrel, *n* (%)	0.97 (0.69–1.37)	0.856
Ticagrelor, *n* (%)	1.11 (0.78–1.56)	0.566
Beta-blockers, *n* (%)	1.10 (0.72–1.65)	0.637
ACEI/ARB, *n* (%)	0.86 (0.63–1.22)	0.434
Calcium channel blockers, *n* (%)	0.86 (0.63–1.22)	0.174
Statins, *n* (%)	2.21 (0.52–9.43)	0.283
High intensity of statin, *n* (%)	0.89 (0.63–1.27)	0.528
Door-to-balloon time (D-to-B)	1.00 (1.00–1.00)	0.552
Left ventricular ejection fraction, (%)	0.99 (0.97–1.00)	0.148
Creatine kinase MB, ng/ml	1.00 (1.00–1.01)	**0.001**
White blood cell, $\times10^9$/L	0.97 (0.92–1.02)	0.282
Neutrophile, $\times10^9$/L	1.02 (0.97–1.08)	0.45
Lymphocyte, $\times10^9$/L	0.92 (0.75–1.12)	0.413
High-sensitive C-reactive protein (mg/L)	1.00 (0.99–1.01)	0.596
Fasting plasma glucose, mmol/L	0.94 (0.88–1.01)	0.083
Serum creatinine, umol/L	1.01 (1.00–1.01)	**<0.001**
Serum uric acid, umol/L	1.00 (1.00–1.00)	0.246
Total cholesterol, mmol/L	2.592 (2.18–3.08)	**<0.001**
Triglyceride, mmol/L	1.13 (0.99–1.27)	0.051
Triglycerides and glucose index	1.03 (1.01–1.05)	**0.005**
High density lipoprotein cholesterol, mmol/L	1.39 (0.90–2.10)	0.126
Low Density Lipoprotein cholesterol, mmol/L	0.88 (0.72–1.07)	0.202
Low Density Lipoprotein cholesterol on re-admission, mmol/L	1.06 (0.90–1.24)	0.488
Lipoprotein-a, mg/L	1.00 (1.00–1.00)	**<0.001**
Body mass index (kg/m^2)	1.55 (1.44–1.67)	**<0.001**
Hypersensitive troponin T, ng/L	1.00 (1.00–1.00)	0.872
Lactate dehydrogenase, U/L	0.99 (0.98–1.00)	0.01
N-terminal pro-brain natriuretic peptide, pg/ml	0.99 (0.99–1.00)	0.091
Killip classification	1.76 (1.31–2.35)	**<0.001**
Calcified lesions	0.99 (0.71–1.38)	0.932
Bifurcation lesions	0.77 (0.48–1.20)	0.273
Ostial lesions	1.21 (0.70–1.98)	0.473
Angular distortion lesions	1.73 (0.80–3.45)	0.139
Target left main	0.91 (0.27–3.18)	0.997
Target left anterior descending	1.12 (0.76–1.61)	0.567
Target left circumflex	0.84 (0.58–1.19)	0.327
Target right coronary artery	0.71 (0.51–1.01)	0.052
Calcified lesions (NCL)	1.25 (0.88–1.78)	0.204
Bifurcation lesions (NCL)	1.47 (0.99–2.17)	0.054
Ostial lesions (NCL)	1.27 (0.86–1.89)	0.230
Angular distortion lesions (NCL)	0.71 (0.45–1.10)	0.122
NCL located on left anterior descending	0.78 (0.55–1.10)	0.156
NCL located on left circumflex	1.07 (0.76–1.52)	0.696
NCL located on right coronary artery	1.18 (0.82–1.69)	0.384
Diameter stenosis, %	0.98 (0.96–1.00)	0.122
Lesion length, mm	1.00 (0.97–1.03)	0.824
Fractional flow reserve (FFR), *n* (%)	1.73 (0.47–6.36)	0.685

ACEI, angiotensin converting enzyme inhibitor; ARB, angiotensin receptor inhibitor; NCL, non-culprit lesion.
Bold values indicate significant $P < 0.05$.

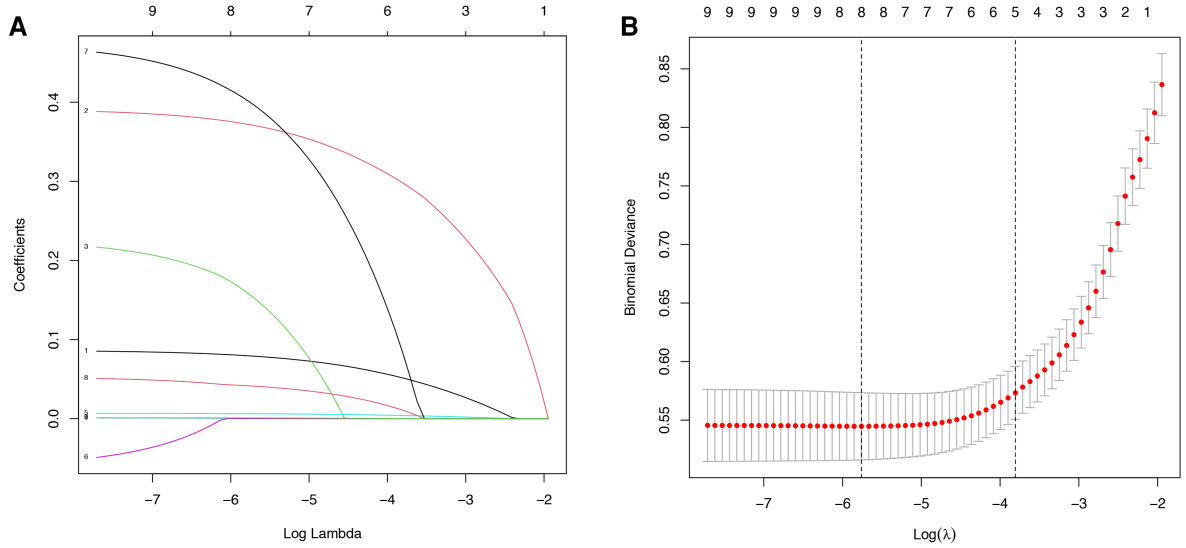

FIGURE 2
Variable screening based on lasso regression. (A) Characterization of the variation of variable coefficients; (B) The process of selecting the optimal value of the parameter λ in the Lasso regression model by the cross-validation method.

In the baseline characteristics, the population's age in the training and validation sets was 67 (57, 75) and 66 (56, 75) years. Notably, multivariate logistic regression results displayed that the likelihood of revascularization for NCL progression increased with advancing age. Based on statistical data, it is evident that the aging of the population has contributed to a steady rise in the occurrence of STEMI among older adults over the years. Currently, more than one-third of STEMI patients are over the age of 75 (21). In non-culprit lesions, plaque burden increases with age (22). Patients are mostly readmitted from acute coronary syndromes. In most acute coronary syndromes, thrombotic occlusion due to plaque rupture is considered a major pathological process (23). These plaques are generally characterized by a large plaque burden rich in lipid content. Unplanned revascularization is significantly more likely to occur in patients with large lipid plaques (24). The visceral and intramuscular fat ratio increases with age, reaching a peak between 60 and 75 years (25).

BMI is a valid indicator of obesity. According to the World Health Organization reported, worldwide obesity rates have almost tripled since 1975 (26). The risk ratios for repeat revascularization augment progressively with BMI increase, in other words, underweight patients have lower risk and severely obese patients possess higher risk (27). The mechanisms underlying the high risk of revascularization for NCL associated with high BMI are unclear. However, one potential explanation may be high BMI are associated with the impaired endothelium-dependent function of microvascular coronary arteries (28).

The TyG index is calculated from fasting triglycerides and blood glucose. A meta-analysis that included 5,731,29 patients showed that a higher TyG index may be independently associated with a higher incidence of atherosclerotic cardiovascular disease (29). TyG index is also a reliable alternative biomarker for assessing insulin resistance (30). Insulin resistance is a condition in which body tissues become resistant to insulin, leading to disturbances in lipid and glucose metabolism (31). These metabolic disturbances promote endothelial dysfunction, cardiovascular remodeling, oxidative stress, inflammatory factor release, and exacerbated blood pressure elevation, all of which may contribute to NCL revascularization after PCI (32, 33).

Killip classification is a simple clinical tool proposed by Killip et al. (34) in 1979 to quickly and effectively evaluate cardiac function. One study (35) found that Killip classification was associated with adverse cardiovascular events, including the progression of NCL. Another study (36) found that patients classified as a higher Killip classification tend to have more severe coronary artery injuries, which could eventually increase the likelihood of NCL progression. The coronary vascular endothelium in patients with a higher Killip classification is damaged by activation of the renin-angiotensin-aldosterone system and inflammatory storms (37, 38). These damages may be the cause of repeated PCI for NCL. Meanwhile, DeGeare et al. (39) reported that patients with high Killip classification were more susceptible to renal impairment after PCI. SCr can be a good indicator of kidney function. The prevalence of renal impairment increases with age. Severe renal impairment was reported that in 7% of patients aged 70%–80% and 11% of

TABLE 3 Multivariate logistic regression analysis in training group.

Variable	OR (95% CI)	*P*-value
Serum creatinine, umol/L	1.007 (1.005–1.009)	**<0.001**
Age, years	1.091 (1.067–1.115)	**<0.001**
Body mass index (kg/m^2)	1.476 (1.363–1.600)	**<0.001**
Triglyceride and glucose index	1.050 (1.022–1.079)	**<0.001**
Killip classification	1.594 (1.140–2.229)	**0.006**

Bold values indicate significant $P < 0.05$.

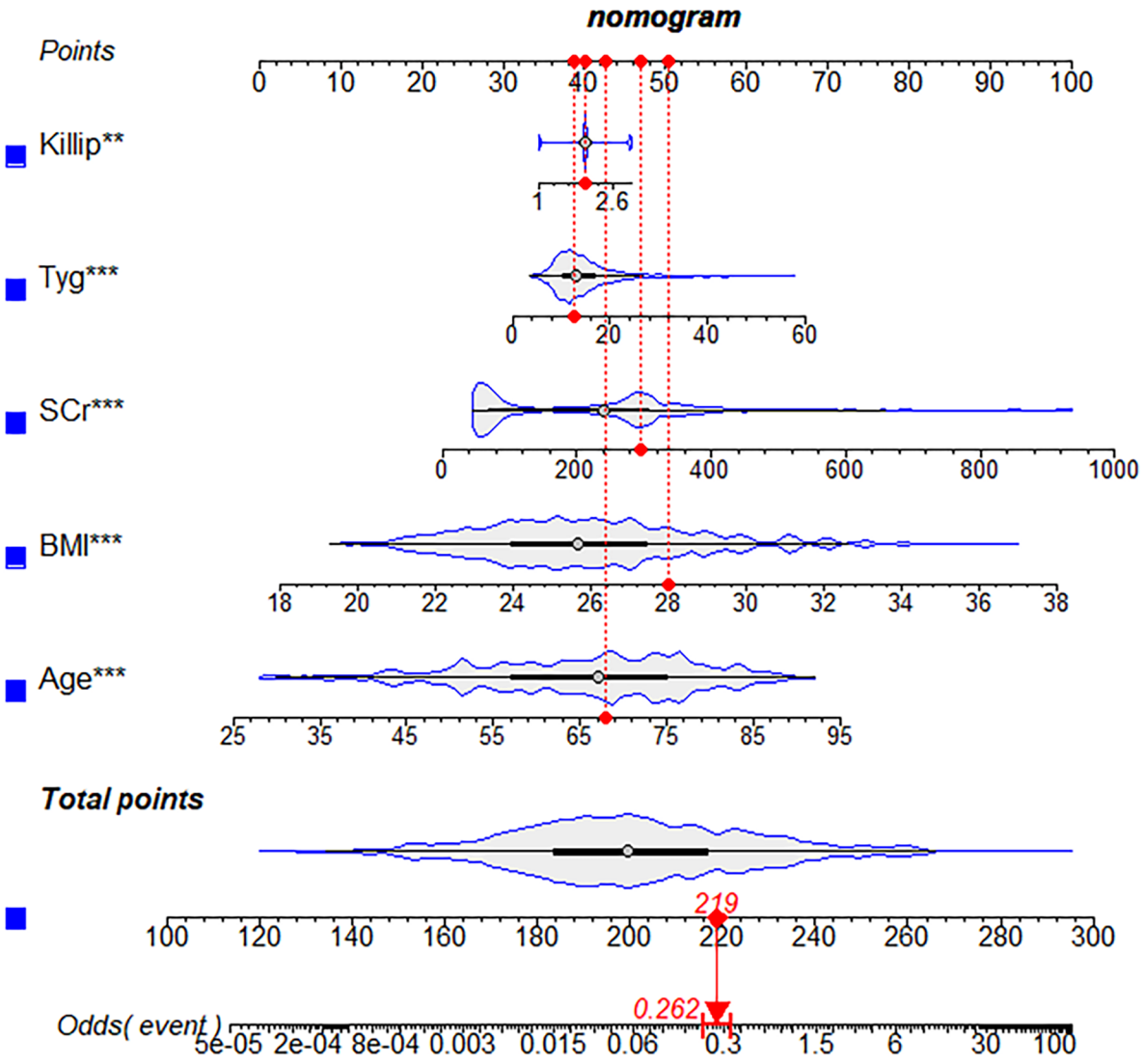

FIGURE 3
A nomogram for predicting the possibility of revascularization for non-culprit lesions progression. BMI, body mass index; SCr, serum creatinine.

patients aged 80 years or older (40). Miyagi et al. (41) found a significant correlation between an increased percentage of lipid volume and decreased percentage of fibrous volume in NCL of patients with renal insufficiency. Furthermore, Hayano et al. (42) found that moderate chronic kidney disease (CKD) patients had more lipid and less fibrous volume in NCL. It has also been found that after standard lipid-lowering therapy after PCI in patients with CKD), lipid plaque regression occurred in CKD stage 1–2, while lipid plaque increase occurred in CKD stage 3–5. Fibrous plaques were also increased in CKD stage 4–5. People with CKD frequently present with obesity, hyperlipidemia, hyperglycemia, and hypertension, all of which are risk factors that make them susceptible to atherosclerosis development. At the same time, chronic inflammation and stress can lead to maladaptive repair responses that destabilize plaque. Unstable coronary atheromatous plaque rupture often leads to downstream coronary artery obstruction (43). Besides, SCr concentrations are thought to be associated with oxidative stress, endothelial dysfunction, and more progressive atherosclerosis (44, 45). These biological abnormalities may also contribute to the risk of NCL revascularization.

Progression of NCL is responsible for more than half of the causes of revascularization after PCI in STEMI patients, but not all NCLs require revascularization. In this regard, identifying high-risk groups is critical. The nomogram in the study was constructed using 5 variables that were easy to obtain at the time of patient admission. The model can accurately and reliably assess the risk of NCL revascularization in STEMI patients after PCI. In clinical practice, clinicians can use the nomogram can be used to quantify the weighting of risk factors to obtain a total score based on the patient's condition. The total score could be used to locate the corresponding 5-year probability of NCL revascularization on the nomogram scale. Further, clinicians should use the probability of NCL revascularization to guide the

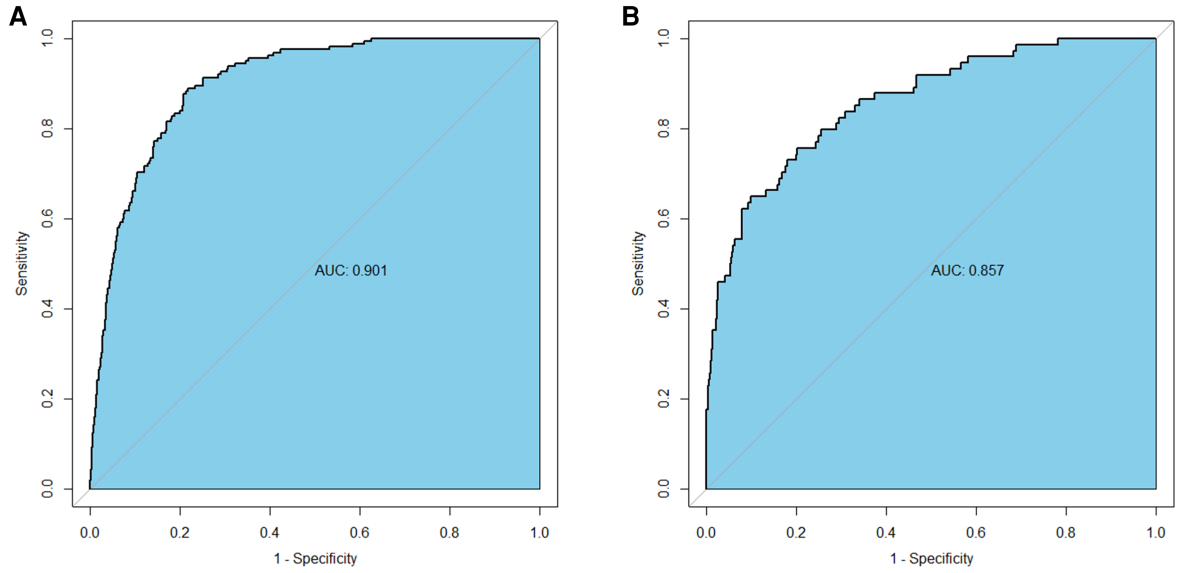

FIGURE 4
Receiver operating characteristics curve of the nomogram in the training group (A) and the validation group (B).

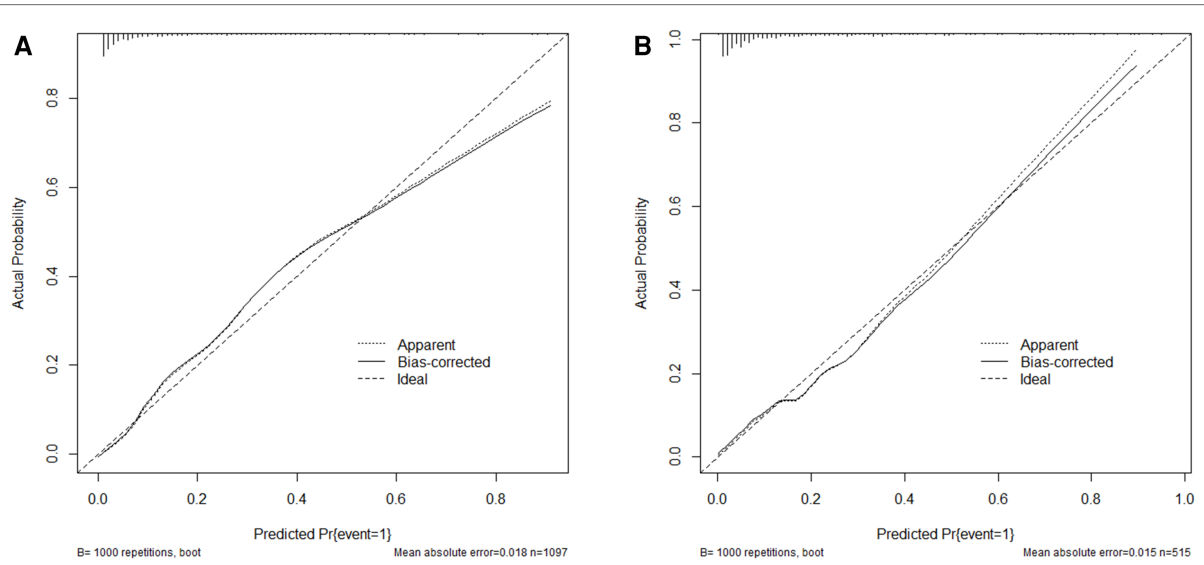

FIGURE 5
Calibration curve for the training group (A) and the validation group (B) the horizontal axis denotes the overall predicted probability of revascularization in STEMI patients after percutaneous coronary intervention due to non-culprit lesions, and the vertical axis displays the actual probability.

management of NCL in patients with STEMI. For example, if the probability is high (>50%), clinicians may choose to intensify medical treatment and follow-up of NCL to avoid possible intervention. If the probability is very low (<10%), it can reduce the patient's concern and psychological burden. If the probability is intermediate (10%–50%), clinicians can discuss the importance of medical therapy follow-up with patients, and make a joint decision based on the patient's preferences and clinical situation. Therefore, the tool is useful for clinicians to identify and target high-risk groups as early as possible.

Limitations

Limitations of the study should be acknowledged. Firstly, this is a retrospective study. Not all STEMI patients who received PCI at our hospital were included in the study, as some patients may choose to seek consultation elsewhere when NCL progression occurred again. This situation may have resulted in some bias in the study's findings. Secondly, although the study incorporated common clinical indicators, there were certain factors that were not taken into consideration. For instance, the research did not

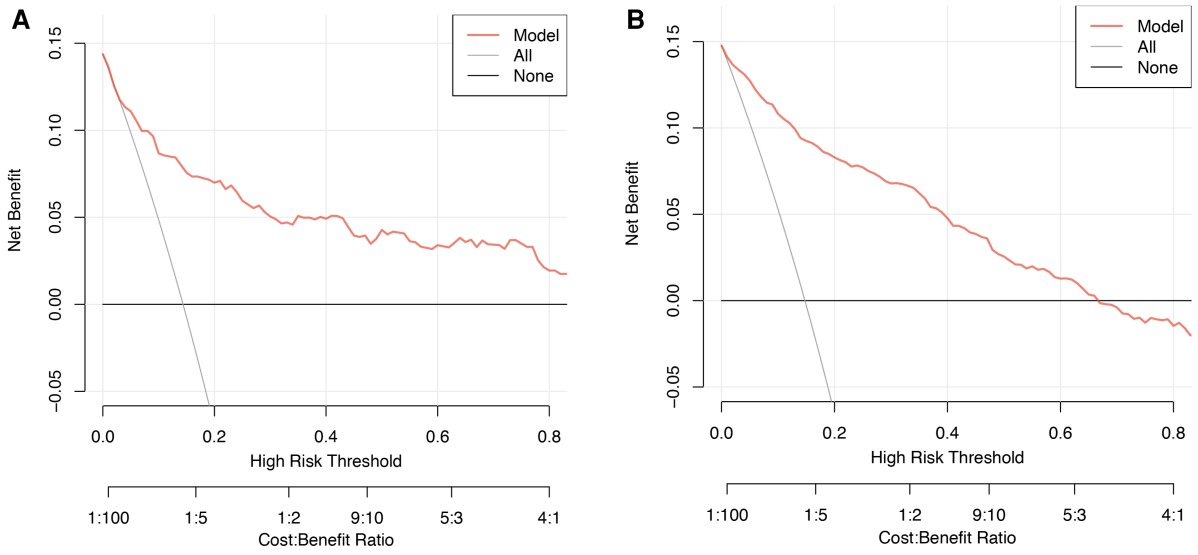

FIGURE 6
Decision curve analysis for the training group (A) and the validation group (B).

account for serum catecholamines, a risk factor for NCL progression. This omission may have implications for the interpretation of the study's findings. Thirdly, our study involved a retrospective analysis of readmitted patients who underwent NCL PCI. Therefore, our focus was on NCL revascularization as the primary endpoint, which is a common and clinically relevant outcome in patients with STEMI. Other endpoints, such as death, acute myocardial infarction, and culprit revascularization, were also important and could potentially impact the outcome of NCL PCI. However, we did not include them in this study. In terms of adjudicating endpoint events, we followed the definitions and methods documented in the hospital records. We acknowledge that this reliance on retrospective data may introduce inherent bias, a limitation inherent in this type of study. Fourthly, even when NCL progression occurs, patients do not tend to seek immediate medical care. Therefore, the time of readmission is not necessarily the time of NCL progression. We performed logistic regression rather than Cox regression for the detection of predictors of 5-year NCL-related revascularization because we were interested in the binary outcome of whether or not the revascularization occurred within 5 years, not in the time to revascularization. However, we also recognize that time to revascularization and revascularization should be considered together, but as a retrospective study, the absence of a rigorous follow-up mechanism is a major limitation. Finally, although the study had external validation, the data analyzed were collected from different periods within a single hospital. The nomogram's clinical value should be evaluated further using multicenter and larger sample sizes in future studies.

Conclusion

A convenient and accurate nomogram was developed and validated using five factors for predicting the revascularization due to NCL progression in STEMI patients after primary PCI. The nomogram enables clinicians to make appropriate disease management decisions by assessing the risk of NCL progression revascularization for STEMI patients after primary PCI.

Data availability statement

The raw data supporting the conclusions of this article will be made available by the authors, without undue reservation.

Ethics statement

The studies involving humans were approved by The Ethics Committee of the Affiliated Hospital of Xuzhou Medical University. The studies were conducted in accordance with the local legislation and institutional requirements. The ethics committee/institutional review board waived the requirement of written informed consent for participation from the participants or the participants' legal guardians/next of kin because the study was retrospective, thus the committee waived the requirement for written informed consent. Personal private information was removed prior to the data is analyzed.

Author contributions

FD: Conceptualization, Writing – original draft, Writing – review & editing, Methodology. XX: Writing – original draft, Writing – review & editing. CZ: Data curation, Writing – review & editing. CL: Data curation, Writing – review & editing. ZT: Data curation, Writing – review & editing. ZW: Visualization, Writing – review & editing. SY: Data curation, Writing – review

& editing, Supervision. GL: Writing – review & editing. XS: Writing – review & editing. LW: Writing – review & editing. DL: Writing – review & editing. XH: Writing – review & editing. JC: Funding acquisition, Project administration, Writing – review & editing. TX: Funding acquisition, Project administration, Writing – review & editing.

Funding

The author(s) declare financial support was received for the research, authorship, and/or publication of this article.

The study was funded by the Jiangsu Traditional Chinese Medicine Science and Technology Development Plan Project (Grant number: YB201988), Jiangsu Provincial Science and Technology Department Social Development Fund (Grant number: BE2019639), Jiangsu Provincial Health Commission Project Fund (Grant number: M2020015), Research and Practice Innovation Plan for Postgraduates in General Colleges and Universities in Jiangsu Province (Grant number: SJCX22_1267), and Xuzhou innovative plan to promote science technology (Grant number: KC21192).

Conflict of interest

The authors declare that the research was conducted in the absence of any commercial or financial relationships that could be construed as a potential conflict of interest.

Publisher's note

References

1. Ralapanawa U, Sivakanesan R. Epidemiology and the magnitude of coronary artery disease and acute coronary syndrome: a narrative review. *J Epidemiol Glob Health*. (2021) 11(2):169–77. doi: 10.2991/jegh.k.201217.001

2. Thrane PG, Olesen KKW, Thim T, Gyldenkerne C, Mortensen MB, Kristensen SD, et al. Mortality trends after primary percutaneous coronary intervention for ST-segment elevation myocardial infarction. *J Am Coll Cardiol*. (2023) 82 (10):999–1010. doi: 10.1016/j.jacc.2023.06.025

3. Ferenc M, Buettner HJ, Gick M, Comberg T, Rothe J, Khoury F, et al. Clinical outcome after percutaneous treatment of de novo coronary bifurcation lesions using first or second generation of drug-eluting stents. *Clin Res Cardiol*. (2016) 105 (3):230–8. doi: 10.1007/s00392-015-0911-7

4. Taniwaki M, Stefanini GG, Silber S, Richardt G, Vranckx P, Serruys PW, et al. 4-year clinical outcomes and predictors of repeat revascularization in patients treated with new-generation drug-eluting stents: a report from the RESOLUTE all-comers trial (A randomized comparison of a zotarolimus-eluting stent with an everolimus-eluting stent for percutaneous coronary intervention). *J Am Coll Cardiol*. (2014) 63(16):1617–25. doi: 10.1016/j.jacc.2013.12.036

5. Glaser R, Selzer F, Faxon DP, Laskey WK, Cohen HA, Slater J, et al. Clinical progression of incidental, asymptomatic lesions discovered during culprit vessel coronary intervention. *Circulation*. (2005) 111(2):143–9. doi: 10.1161/01.CIR.0000150335.01285.12

6. Wang J, Liu JH, Zhu XL, Zhang M, Wang SP, Zheng Z. Nonculprit lesion progression in patients with ST elevation myocardial infarction after primary percutaneous coronary intervention. *Int Heart J*. (2014) 55(1):48–52. doi: 10.1536/ihj.13-081

7. Wang J, Yan CY, Wang W, Wang TZ. The clinical prediction factors for non-culprit lesion progression in patients with acute ST elevation myocardial infarction after primary percutaneous coronary intervention. *BMC Cardiovasc Disord*. (2022) 22(1):529. doi: 10.1186/s12872-022-02974-2

8. Park SY. Nomogram: an analogue tool to deliver digital knowledge. *J Thorac Cardiovasc Surg*. (2018) 155(4):1793. doi: 10.1016/j.jtcvs.2017.12.107

9. Collet JP, Thiele H, Barbato E, Barthélémy O, Bauersachs J, Bhatt DL, et al. 2020 ESC guidelines for the management of acute coronary syndromes in patients presenting without persistent ST-segment elevation. *Eur Heart J*. (2021) 42 (14):1289–367. doi: 10.1093/eurheartj/ehaa575

10. Mehta SR, Wood DA, Storey RF, Mehran R, Bainey KR, Nguyen H, et al. Complete revascularization with multivessel PCI for myocardial infarction. *N Engl J Med*. (2019) 381(15):1411–21. doi: 10.1056/NEJMoa1907775

11. Gaba P, Gersh BJ, Ali ZA, Moses JW, Stone GW. Complete versus incomplete coronary revascularization: definitions, assessment and outcomes. *Nat Rev Cardiol*. (2021) 18(3):155–68. doi: 10.1038/s41569-020-00457-5

12. Shlofmitz RA, Galougahi KK, Jeremias A, Shlofmitz E, Thomas SV, Ali ZA. Calcium modification in percutaneous coronary interventions. *Interv Cardiol Clin*. (2022) 11(4):373–81. doi: 10.1016/j.iccl.2022.06.001

13. Medina A, de Lezo J S, Pan M. A new classification of coronary bifurcation lesions. *Rev Esp Cardiol*. (2006) 59(2):183. doi: 10.1157/13084649

14. Musallam A, Chezar-Azerrad C, Torguson R, Case BC, Yerasi C, Forrestal BJ, et al. Procedural outcomes of patients undergoing percutaneous coronary intervention for de novo lesions in the ostial and proximal left circumflex coronary artery. *Am J Cardiol*. (2020) 135:62–7. doi: 10.1016/j.amjcard.2020.08.014

15. Turgut O, Yilmaz A, Yalta K, Yilmaz BM, Ozyol A, Kendirlioglu O, et al. Tortuosity of coronary arteries: an indicator for impaired left ventricular relaxation? *Int J Cardiovasc Imaging*. (2007) 23(6):671–7. doi: 10.1007/s10554-006-9186-4

16. Leon MB, Allocco DJ, Dawkins KD, Baim DS. Late clinical events after drug-eluting stents: the interplay between stent-related and natural history-driven events. *JACC Cardiovasc Interv*. (2009) 2(6):504–12. doi: 10.1016/j.jcin.2009.04.004

17. Chacko R, Mulhearn M, Novack V, Novack L, Mauri L, Cohen SA, et al. Impact of target lesion and nontarget lesion cardiac events on 5-year clinical outcomes after sirolimus-eluting or bare-metal stenting. *JACC Cardiovasc Interv*. (2009) 2 (6):498–503. doi: 10.1016/j.jcin.2009.03.013

18. Gada H, Kirtane AJ, Newman W, Sanz M, Hermiller JB, Mahaffey KW, et al. 5-year Results of a randomized comparison of XIENCE V everolimus-eluting and TAXUS paclitaxel-eluting stents: final results from the SPIRIT III trial (clinical evaluation of the XIENCE V everolimus eluting coronary stent system in the treatment of patients with de novo native coronary artery lesions). *JACC Cardiovasc Interv*. (2013) 6(12):1263–6. doi: 10.1016/j.jcin.2013.07.009

19. Parodi G, Memisha G, Valenti R, Trapani M, Migliorini A, Santoro GM, et al. Five year outcome after primary coronary intervention for acute ST elevation myocardial infarction: results from a single centre experience. *Heart*. (2005) 91 (12):1541–4. doi: 10.1136/hrt.2004.054692

20. Stone GW, Maehara A, Lansky AJ, de Bruyne B, Cristea E, Mintz GS, et al. A prospective natural-history study of coronary atherosclerosis. *N Engl J Med*. (2011) 364(3):226–35. doi: 10.1056/NEJMoa1002358

21. Gabriel R, Alonso M, Reviriego B, Muñiz J, Vega S, López I, et al. Ten-year fatal and non-fatal myocardial infarction incidence in elderly populations in Spain: the EPICARDIAN cohort study. *BMC Public Health*. (2009) 9:360. doi: 10.1186/1471-2458-9-360

22. Schoenenberger AW, Urbanek N, Toggweiler S, Stuck AE, Resink TJ, Erne P. Ultrasound-assessed non-culprit and culprit coronary vessels differ by age and gender. *World J Cardiol*. (2013) 5(3):42–8. doi: 10.4330/wjc.v5.i3.42

23. Virmani R, Burke AP, Farb A, Kolodgie FD. Pathology of the vulnerable plaque. *J Am Coll Cardiol*. (2006) 47(8 Suppl):C13–8. doi: 10.1016/j.jacc.2005.10.065

24. Tashiro H, Tanaka A, Ishii H, Sakakibara K, Tobe A, Kataoka T, et al. Lipid-rich large plaques in a non-culprit left main coronary artery and long-term clinical outcomes. *Int J Cardiol*. (2020) 305:5–10. doi: 10.1016/j.ijcard.2020.01.072

25. Li CW, Yu K, Shyh-Chang N, Jiang Z, Liu T, Ma S, et al. Pathogenesis of sarcopenia and the relationship with fat mass: descriptive review. *J Cachexia Sarcopenia Muscle*. (2022) 13(2):781–94. doi: 10.1002/jcsm.12901

26. Boutari C, Mantzoros CS. A 2022 update on the epidemiology of obesity and a call to action: as its twin COVID-19 pandemic appears to be receding, the obesity and dysmetabolism pandemic continues to rage on. *Metabolism*. (2022) 92 (98):107–96. doi: 10.1016/j.metabol.2022.155217

27. Wang ZJ, Gao F, Cheng WJ, Yang Q, Zhou YJ. Body mass index and repeat revascularization after percutaneous coronary intervention: a meta-analysis. *Can J Cardiol*. (2015) 31(6):800–8. doi: 10.1016/j.cjca.2015.01.031

28. Koliaki C, Liatis S, Kokkinos A. Obesity and cardiovascular disease: revisiting an old relationship. *Metab Clin Exp*. (2019) 92:98–107. doi: 10.1016/j.metabol.2018.10.011

29. Ding X, Wang X, Wu J, Zhang M, Cui M. Triglyceride-glucose index and the incidence of atherosclerotic cardiovascular diseases: a meta-analysis of cohort studies. *Cardiovasc Diabetol*. (2021) 20(1):76. doi: 10.1186/s12933-021-01268-9

30. Sánchez-García A, Rodríguez-Gutiérrez R, Mancillas-Adame L, González-Nava V, Díaz González-Colmenero A, Solis RC, et al. Diagnostic accuracy of the triglyceride and glucose index for insulin resistance: a systematic review. *Int J Endocrinol*. (2020) 2020:4678526. doi: 10.1155/2020/4678526

31. Brown AE, Walker M. Genetics of insulin resistance and the metabolic syndrome. *Curr Cardiol Rep*. (2016) 18(8):75. doi: 10.1007/s11886-016-0755-4

32. Markus MRP, Rospleszcz S, Ittermann T, Baumeister SE, Schipf S, Siewert-Markus U, et al. Glucose and insulin levels are associated with arterial stiffness and concentric remodeling of the heart. *Cardiovasc Diabetol*. (2019) 18(1):145. doi: 10.1186/s12933-019-0948-4

33. Ormazabal V, Nair S, Elfeky O, Aguayo C, Salomon C, Zuñiga FA. Association between insulin resistance and the development of cardiovascular disease. *Cardiovasc Diabetol*. (2018) 17(1):122. doi: 10.1186/s12933-018-0762-4

34. Killip T 3rd, Kimball JT. Treatment of myocardial infarction in a coronary care unit. A two year experience with 250 patients. *Am J Cardiol*. (1967) 20(4):457–64. doi: 10.1016/0002-9149(67)90023-9

35. Li M, Wang X, Mi SH, Chi Z, Chen Q, Zhao X, et al. Short-term prognosis of fragmented QRS complex in patients with non-ST elevated acute myocardial infarction. *Chin Med J*. (2016) 129(5):518–22. doi: 10.4103/0366-6999.176989

36. Shiraishi J, Kohno Y, Sawada T, Takeda M, Arihara M, Hyogo M, et al. Predictors of in-hospital outcome after primary percutaneous coronary intervention for recurrent myocardial infarction. *Circ J*. (2008) 72(8):1225–9. doi: 10.1253/circj.72.1225

37. Bednár F, Widimský P, Groch L, Aschermann M, Zelízko M, Krupicka J. Acute myocardial infarction complicated by early onset of heart failure: safety and feasibility of interhospital transfer for coronary angioplasty. Subanalysis of Killip II-IV patients from the PRAGUE-1 study. *J Interv Cardiol*. (2003) 16(3):201–8. doi: 10.1034/j.1600-0854.2003.8047.x

38. Khot UN, Jia G, Moliterno DJ, Lincoff AM, Khot MB, Harrington RA, et al. Prognostic importance of physical examination for heart failure in non-ST-elevation acute coronary syndromes: the enduring value of Killip classification. *Jama*. (2003) 290(16):2174–81. doi: 10.1001/jama.290.16.2174

39. DeGeare VS, Boura JA, Grines LL, O'Neill WW, Grines CL. Predictive value of the Killip classification in patients undergoing primary percutaneous coronary intervention for acute myocardial infarction. *Am J Cardiol*. (2001) 87(9):1035–8. doi: 10.1016/S0002-9149(01)01457-6

40. Devlin G, Gore JM, Elliott J, Wijesinghe N, Eagle KA, Avezum A, et al. Management and 6-month outcomes in elderly and very elderly patients with high-risk non-ST-elevation acute coronary syndromes: the global registry of acute coronary events. *Eur Heart J*. (2008) 29(10):1275–82. doi: 10.1093/eurheartj/ehn124

41. Miyagi M, Ishii H, Murakami R, Isobe S, Hayashi M, Amano T, et al. Impact of renal function on coronary plaque composition. *Nephrol Dial Transplant*. (2010) 25 (1):175–81. doi: 10.1093/ndt/gfp423

42. Hayano S, Ichimiya S, Ishii H, Kanashiro M, Watanabe J, Kurebayashi N, et al. Relation between estimated glomerular filtration rate and composition of coronary arterial atherosclerotic plaques. *Am J Cardiol*. (2012) 109(8):1131–6. doi: 10.1016/j.amjcard.2011.11.052

43. Libby P, Buring JE, Badimon L, Hansson GK, Deanfield J, Bittencourt MS, et al. Atherosclerosis. *Nat Rev Dis Primers*. (2019) 5(1):56. doi: 10.1038/s41572-019-0106-z

44. Becker BN, Himmelfarb J, Henrich WL, Hakim RM. Reassessing the cardiac risk profile in chronic hemodialysis patients: a hypothesis on the role of oxidant stress and other non-traditional cardiac risk factors. *J Am Soc Nephrol*. (1997) 8(3):475–86. doi: 10.1681/ASN.V83475

45. Cauza E, Kletzmaier J, Bodlaj G, Dunky A, Herrmann W, Kostner K. Relationship of non-LDL-bound apo(a), urinary apo(a) fragments and plasma Lp(a) in patients with impaired renal function. *Nephrol Dial Transplant*. (2003) 18 (8):1568–72. doi: 10.1093/ndt/gfg181

frontiers | Frontiers in Cardiovascular Medicine

TYPE Original Research
PUBLISHED 08 January 2024
DOI 10.3389/fcvm.2023.1326091

OPEN ACCESS

EDITED BY
Marco Giuseppe Del Buono,
Agostino Gemelli University Polyclinic (IRCCS), Italy

REVIEWED BY
Rocco Vergallo,
University of Genoa, Italy
Dejan Orlic,
University of Belgrade, Serbia

*CORRESPONDENCE
Giuseppe Tarantini
✉ giuseppe.tarantini.1@unipd.it

†These authors have contributed equally to this work

RECEIVED 22 October 2023
ACCEPTED 11 December 2023
PUBLISHED 08 January 2024

CITATION
Tarantini G, Cardaioli F, De Iaco G, Tuccillo B, De Angelis MC, Mauro C, Boccalatte M, Trivisonno A, Ribichini F, Vadalà G, Caramanno G, Caruso M, Lombardi M, Fischetti D, Danesi A, Abbracciavento L, Lorenzoni G, Gregori D, Panza A, Nai Fovino L and Esposito G (2024) A more-Comers populAtion trEated with an ultrathin struts polimer-free Sirolimus stent: an Italian post-maRketing study (the CAESAR registry). Front. Cardiovasc. Med. 10:1326091. doi: 10.3389/fcvm.2023.1326091

A more-Comers populAtion trEated with an ultrathin struts polimer-free Sirolimus stent: an Italian post-maRketing study (the CAESAR registry)

Giuseppe Tarantini[1*†], Francesco Cardaioli[1†], Giuseppe De Iaco[2], Bernardino Tuccillo[3], Maria Carmen De Angelis[3], Ciro Mauro[4], Marco Boccalatte[5], Antonio Trivisonno[6], Flavio Ribichini[7], Giuseppe Vadalà[8], Giuseppe Caramanno[9], Marco Caruso[10], Mario Lombardi[11], Dionigi Fischetti[12], Alessandro Danesi[13], Leonardo Abbracciavento[14], Giulia Lorenzoni[15], Dario Gregori[15], Andrea Panza[1], Luca Nai Fovino[1] and Giovanni Esposito[16]

[1]Department of Cardiac, Thoracic, Vascular Sciences and Public Health, University of Padua, Padova, Italy, [2]Department of Cardiology, Hospital "Cardinal G. Panico", Tricase, Italy, [3]U.O.C. Cardiologia, P.O. Ospedale del Mare, Napoli, Italy, [4]Department of Cardiology, Hospital Cardarelli, Naples, Italy, [5]Interventional Cardiology Unit, Ospedale Santa Maria Delle Grazie Pozzuoli, Napoli, Italy, [6]Department of Cardiovascular Disease, "Antonio Cardarelli" Hospital, Campobasso, Italy, [7]Division of Cardiology, AOUI Verona, Verona, Italy, [8]Division of Cardiology, University Hospital Paolo Giaccone, Palermo, Italy, [9]Interventional Cardiology, San Giovanni di Dio Hospital, Agrigento, Italy, [10]Interventional Cardiology Unit, ARNAS Civico, G. Di Cristina Benfratelli, Palermo, Italy, [11]Interventional Cardiology Unit, A.O. Riuniti Villa Sofia-Cervello, Palermo, Italy, [12]Division of Cardiology, "V. Fazzi" Hospital, Lecce, Italy, [13]Division of Cardiology, S. Spirito Hospital, Rome, Italy, [14]Interventional Cardiology Unit, SS Annunziata Hospital, Taranto, Italy, [15]Unit of Biostatistics, Epidemiology and Public Health, University of Padova, Padova, Italy, [16]Division of Cardiology, Università Degli Studi di Napoli Federico II, Napoli, Italy

Introduction: The use of contemporary drug-eluting stents (DES) has significantly improved outcomes of patients with coronary artery disease (CAD) undergoing percutaneous coronary intervention (PCI). However, concerns exist regarding the long-term proinflammatory effects of durable polymer coatings used in most DES, potentially leading to long-term adverse events. First-generation polymer-free stent technologies, such as sirolimus- and probucol-eluting stents (PF-SES), have shown an excellent safety and efficacy profile. The aim of this study was to evaluate the safety and efficacy of the new ultrathin Coroflex ISAR NEO PF-SES, in a more-comers PCI population.
Methods: The CAESAR (a more-Comers populAtion trEated with an ultrathin struts polimer-free Sirolimus stent: An Italian post-maRketing study) registry is a multicenter, prospective study conducted in Italy, enrolling more-comers CAD patients undergoing PCI with the Coroflex ISAR NEO stent. Patients with

Abbreviations
ACS, acute coronary syndrome; BMS, bare-metal stents; CABG, coronary artery bypass grafts; CAD, coronary artery disease; CCS, chronic coronary syndrome; CIF, cumulative incidence functions; CS, cardiogenic shock; CTO, chronic total occlusion; DAPT, dual antiplatelet therapy; DES, drug-eluting stents; EP, endpoint; ISR, in-stent restenosis; LAD, left anterior descending coronary artery; LM, left main coronary artery; LVEF, left-ventricular ejection fraction; MACE, major adverse cardiovascular events; MI, myocardial infarction; MVD, multivessel disease; NYHA, New York Heart Association; OAC, oral anticoagulation; PCI, percutaneous coronary intervention; PF-SES, polymer-free sirolimus-eluting stents; PF, polymer-free; ST, stent thrombosis; TLR, target lesion revascularization; TVF, target vessel failure; TVR, target vessel revascularization.

10.3389/fcvm.2023.1326091

left main (LM) disease, cardiogenic shock (CS), or severely reduced left-ventricular ejection fraction (LVEF) were excluded. The primary endpoint was target-lesion revascularization (TLR) at 1 year.

Results: A total of 425 patients were enrolled at 13 centers (mean age 66.9 ± 11.6 years, Diabetes mellitus 29%, acute coronary syndrome 67%, chronic total occlusion 9%). Of these, 40.9% had multivessel disease (MVD) and in 3.3% cases, the target lesion was in-stent restenosis (ISR). Clinical device success was reached in 422 (99.6%) cases. At 1 year, only two (0.5%) subjects presented ischemia-driven TLR. The 1-year rates of target vessel revascularization and MACE were 0.5% and 5.1%, respectively. Major bleeding was observed in four (1.0%) patients.

Conclusion: In this multicenter, prospective registry, the use of a new ultrathin Coroflex ISAR NEO PF-SES in a more-comers PCI population showed good safety and efficacy at 1 year.

KEYWORDS

coronary artery disease, PCI, ultrathin struts, acute coronary syndrome (ACS), drug-eluting stent (DES)

Introduction

The development of contemporary drug-eluting stents (DES) has considerably improved clinical outcomes compared with both bare-metal stents (BMS) and earlier DES platform iterations (1–3). As a result, international guidelines now advocate the use of last-generation DES for patients with coronary artery disease (CAD) necessitating percutaneous coronary intervention (PCI) (4). However, concerns exist regarding the potential long-term pro-inflammatory effects of durable polymer coatings typically employed for drug release regulation of most contemporary DES, possibly leading to neo-atherosclerotic phenomena (2, 5, 6).

To overcome these drawbacks, polymer-free stent technologies have been implemented. A polymer-free stent eluting sirolimus and probucol (PF-SES) has been shown to be non-inferior to a new-generation polymer-based zotarolimus-eluting stent at long-term follow-up (2). In addition, sirolimus and probucol have been assessed on an ultrathin bare-metal platform, revealing favorable safety and efficacy profiles in a more-comers population (7). The Coroflex ISAR NEO (B. Braun, Melsungen, Germany) is the latest released ultrathin PF-SES platform, introducing a restyled design aimed at improving trackability and maximal stent expansion.

The aim of this study was to assess the safety and efficacy of the Coroflex ISAR NEO platform in a more-comers population including patients with *de novo* and restenotic lesions, both in native coronary arteries and coronary bypass grafts (CABG).

Methods

Study design and patient population

The CAESAR (a more-Comers populAtion trEated with an ultrathin strut polymer-free Sirolimus stent: An Italian post-maRketing study) registry is a prospective, national, multicenter, postmarket study enrolling patients with CAD undergoing PCI with the Coroflex ISAR NEO coronary stent at 13 Italian centers. According to the study protocol, we included patients ≥18 years of age with an acute coronary syndrome (ACS), chronic coronary syndrome (CCS), or objective proof of ischemia meeting the requirements for PCI (4). Either single- or multivessel stenting was allowed for treating *de novo* or restenotic lesions (reference diameters from 2.0 to 4.0 mm), both in native coronary arteries and CABG. Limited exclusion criteria were considered for the study [left main (LM) disease, cardiogenic shock (CS), severe calcified stenoses, and severely reduced left-ventricular ejection fraction (LVEF)], resulting in a more comprehensive cohort of PCI patients (more-comers). The complete study inclusion and exclusion criteria are provided in Table 1.

TABLE 1 Inclusion and exclusion criteria.

Inclusion criteria
– *De novo* and restenotic lesions in native coronary arteries and coronary bypass grafts with reference vessel diameter ≥2 and ≤4 mm, with suitable lesion length (target lesion lengths >34 mm need to be covered with at least 2 stents)
– Subjects ≥18 years of age
Exclusion criteria
– Intolerance to sirolimus and/or probucol
– Allergy to components of the coating
– Pregnancy and lactation
– Severely calcified stenosis
– Cardiogenic shock
– Hemorrhagic diathesis or another disorder such as gastrointestinal ulceration or cerebral circulatory disorders, which restrict the use of antiplatelet or anticoagulation therapy
– Planned surgery ≤6 months after myocardial revascularization
– Severe allergy to contrast media
– Patients with an ejection fraction of <30%
– Reference vessel diameter <2 and >4 mm
– Treatment of the left main stem
– Indication for bypass surgery
– Contraindication for whichever accompanying medication is necessary

Study device and procedure

The Coroflex ISAR NEO is the latest-generation PF-SES. Similarly to its predecessor (Coroflex ISAR), it is built on a premounted cobalt-chrome (Co-Cr) alloy ultrathin platform (7), while it presents a redesigned strut structure that enables greater stent expansion, maintaining at the same time good flexibility and radial force. The Coroflex ISAR NEO is available in 2.0 mm (55 µm thick) and 3.5 mm (65 µm thick) diameter sizes with a maximal expansion capability of up to 5.0 mm. Lesion pre-dilation was left to the discretion of the operators. The antiplatelet therapy after PCI had to follow the latest guidelines (4, 8–10). A dedicated electronic data capture system was used for data entry, and data accuracy was verified by the principal investigators at each center. Device success is defined as the successful delivery and deployment of the device and attainment of <50% diameter stenosis using only the study device. Procedural success was defined as a successful stent deployment with an antegrade thrombolysis in myocardial infarction (TIMI) grade 3 flow at the end of the procedure.

Study endpoints

The primary endpoint (EP) was target lesion revascularization (TLR) at 1 year defined as ischemia-driven revascularization of the target lesion (within the stent or the 5 mm borders adjacent to the stent). Secondary EPs were all-cause mortality, definite stent thrombosis (ST), bleeding events, major adverse cardiovascular events [MACE, a composite of all-cause and cardiac death, myocardial infarction (MI), and TLR], and target vessel failure [TVF, a composite of cardiac death, MI attributed to the target vessel, or target vessel revascularization (TVR)]. Myocardial infarctions were defined according to the fourth universal MI definition (11). The follow-up was prospectively performed at 30 days (±7 days) and 1 year (±30 days) with outpatient visits or telephone interviews. The definitions of individual endpoints can be found in the study protocol (Supplementary Appendix).

Statistical analysis

For the CAESAR study, the sample size calculation was based on the primary EP. The detailed description of the procedure regarding sample size calculation is reported in the Supplementary Material. Continuous variables are expressed as median [interquartile range (IQR)] and compared using the Mann–Whitney *U* test. Categorical variables are presented as counts (%) and were compared using the Chi-square test or Fisher's exact test. The Kaplan–Meier method was used to estimate survival and MACE-free survival at follow-up. Cumulative incidence functions (CIFs) were used to evaluate bleeding at follow-up accounting for competing risks. For all the analyses, a two-sided $p < 0.05$ was considered to be significant. The analyses were performed with the R software (R Foundation, Wien, Austria).

Results

Baseline clinical characteristics

Between August 2019 and March 2021, a total of 425 patients were enrolled in the CAESAR study at 13 centers. Detailed demographics and clinical characteristics are described in Table 2. In summary, patients were aged 66.9 ± 11.6 years and 75% were male. Diabetes mellitus was present in 29% of the patients (11% insulin-dependent). One-third of the study population had undergone previous percutaneous coronary artery revascularization. The median baseline LVEF was 55%. Clinical indications for PCI were ACS in 67% of the patients (>50% of the subjects were admitted because of acute MI), and 3% of them had a New York Heart Association (NYHA) Functional Class III–IV on admission.

TABLE 2 Baseline clinical characteristics.

Clinical characteristics	Overall population ($n = 425$)
Age (years)	66.96 (11.16)
Female gender	108 (25.4)
BMI (kg/m^2)	27.31 (24.9–29.4)
Hypercholesterolemia	382 (89.8)
Hypertension	351 (82.6)
Diabetes mellitus	124 (29.2)
IDDM	49 (39.5)
Dialysis	5 (1.2)
Smoking	
Current	118 (27.8)
Former	118 (27.8)
Previous MI	105 (24.7)
Atrial fibrillation	52 (12.1)
Previous coronary revasc.	125 (29.4)
LVEF	55 (45–60)
Previous stroke/TIA	12 (2.8)
COPD	30 (7.1)
Peripheral artery disease	55 (13.0)
Stress test	45 (10.6)
Clinical presentation	
Unstable angina	62 (14.6)
NSTEMI	109 (25.5)
STEMI	121 (28.5)
CCS	106 (25.0)
Other	27 (6.4)
NYHA class > 2	14 (3.3)
Angina	185 (43.5)
Angina class (CSS)	
1	40 (21.6)
2	90 (48.7)
3	55 (29.7)

Values are *n* (%), or median (range), as appropriate for categorical and continuous variables, respectively.
IDDM, insulin-dependent diabetes mellitus; COPD, chronic obstructive pulmonary disease; CAD, coronary artery disease; LVEF, left-ventricular ejection fraction; MI, myocardial infarction; PCI, percutaneous coronary intervention; TIA, transient ischemic attack; NSTEMI, non-ST-elevation myocardial infarction; STEMI, ST-elevation myocardial infarction; CCS, chronic coronary syndrome.

10.3389/fcvm.2023.1326091

Angiographic and procedural characteristics

Overall, 492 lesions were treated with 484 PF-SES. Angiographic and procedural characteristics are reported in Tables 3, 4. A total of 492 lesions were treated in 425 patients, with 174 (40.9%) patients presenting multivessel disease (MVD). Left anterior descending (LAD) was involved in 43% of the cases. In 16 (3.4%) cases, the target lesion resulted from in-stent restenosis (ISR), while three lesions were located on a previous CABG. Chronic total occlusion (CTO) represented 9% of the total treated lesions. Coronary stenting was performed through a radial approach in 92.9% of the cases, mostly by using a 6F guiding catheter (98.8%). Pre- and post-dilation were performed in 76% and 66% of the cases, respectively. Clinical device success was reached in 422 (99.6%) patients. In 10 cases, the use of an adjunctive different stent platform was considered necessary. No intraprocedural strokes or deaths were reported. Furthermore, there were no recorded cases of acute bleeding or thrombotic complications. Four (1%) periprocedural MI were reported. A P2Y12 pretreatment strategy was applied in 235 (55.4%) patients. In 10 (2.4%) cases, intraprocedural Cangrelor infusion was administered. The time prescription for dual antiplatelet therapy (DAPT) at discharge was 1–3 months for 55 (13%) patients (all with an indication for OAC), 6 months for 75 (17.6%) subjects, and ≥12 months for the rest of the study population (Supplementary Table S1). At 1-year follow-up, 53% of the patients were taking two antiplatelet drugs.

TABLE 3 Angiographic characteristics.

Angiographic characteristics	Total no. of patients ($n = 425$)
Multivessel disease	174 (40.9)
Total no. of lesions	($n = 492$)
Lesion location	
LAD	215 (43.7)
LCX	143 (29.0)
RCA	130 (26.4)
Grafts	4 (0.9)
Bifurcation	53 (10.8)
Calcification	112 (22.8)
Intracoronary thrombus	100 (20.3)
Lesion type	
A	63 (12.8)
B1	179 (36.4)
B2	150 (30.5)
C	100 (20.3)
Total occlusion	44 (8.9)
Restenosis	16 (3.4)
Ostial target	27 (5.5)
SVG involvement	3 (0.6)
Severe tortuosity	20 (4.1)

Values are *n* (%), or median (range), as appropriate for categorical and continuous variables, respectively.
LM, left main coronary artery; LAD, left anterior descending coronary artery; LCX, left circumflex coronary artery; RCA, right coronary artery; SVG, saphenous vein graft.

Outcomes

The rates of primary and secondary EP at different time points are provided in Table 5 and Supplementary Tables S2, S3. The 1-year follow-up was available for 410 (96.4%) patients. Only two (0.5%) subjects presented the primary EP, of those one was an early MI related to the target lesion, treated with PCI. Out of the 20 deaths (4.9%), one (5%) was cardiac in nature. The Kaplan–

TABLE 4 Procedural characteristics.

Procedural characteristics	Overall population ($n = 425$)
Vascular access	
Femoral	30 (7.1)
Radial	395 (92.9)
Guiding catheter	
6F	420 (98.8)
7F	5 (1.2)
N° of Coroflex ISAR/lesion	1.18 (0.32)
Lesion length (mm)	18.0 (9.0, 38.00)
Predilatation performed	323 (76.0)
Other DES	10 (2.4)
DEB	4 (0.9)
Two stent technique in bifurcation	9 (2.1)
Residual stenosis	
<40 (%)	402 (94.6)
41–69 (%)	21 (4.9)
>70%	2 (0.5)
Postdilatation performed	280 (66.0)
Final TIMI	
1	1 (0.2)
2	5 (1.2)
3	419 (98.6)
Clinical device success	422 (99.3)
Procedural success	425 (100.0)
Coronary perforation	0 (0.0)
Coronary dissection	4 (0.9)
Intraprocedural stroke	0 (0.0)
Intraprocedural death	0 (0.0)
Periporocedural MI	4 (1)
Use of IABP, ECMO, LVAD	
Planned	2 (0.5)
Unplanned	2 (0.5)
Bleeding complications	0 (0.0)
Acute intrastent thrombosis	0 (0.0)
Previous ASA treatment	337 (79.3)
P2Y12 pretreatment	235 (55.4)
Clopidogrel	72 (30.7)
Prasugrel	4 (1.7)
Ticagrelor	159 (67.6)
Chronic OAC treatment	94 (22.1)
GP IIb/IIIa inhibitor	37 (8.7)
Cangrelor	10 (2.4)

Values are *n* (%), or median (range), as appropriate for categorical and continuous variables, respectively.
DES, drug-eluting stent; DEB, drug-eluting balloon; MI, myocardial Infarction; IABP, intra-aortic balloon pump; ECMO, extra-corporeal membraneous oxygenation; LVAD, left ventricular assistance device; ASA, acetylsalicylic acid; PCI, percutaneous coronary intervention; OAC, oral anticoagulant.

10.3389/fcvm.2023.1326091

TABLE 5 One-year follow-up outcomes.

One-year follow-up outcomes	Overall population ($n = 410$)
TLR	2 (0.5)
PCI	2 (100.0)
Cumulative MACE	26 (6.1)
Death	20 (4.9)
Cardiac	1 (5.0)
Non-cardiac	19 (95.0)
TVR	2 (0.5)
PCI	2 (100.0)
MI	5 (1.1)
TVF	3 (0.7)
Stent thrombosis	0 (0.0)
Angina	8 (1.9)
Angina class (CSS)	
1	2 (25.0)
2	3 (37.5)
3	3 (37.5)
Stroke	1 (0.2)
Bleeding	4 (1.0)
BARC 2	3 (75.0)
BARC 3b	1 (25.0)

Values are *n* (%), or median (range), as appropriate for categorical and continuous variables, respectively.
ASA, acetylsalicylic acid; DAPT, dual antiplatelet therapy; MI, myocardial infarction; TLR, target lesion revascularization; TVR, target vessel revascularization; TVF, target vessel failure.

Meier curve for all-cause death is reported in Supplementary Figure S1. The 1-year rates of TVR and MACE were 0.5% (CI 0.1–0.9) and 6.1% (CI 4.6–7.2), respectively (Figure 1), while no ST was reported. Major bleeding was observed in four (1.0%) patients (Supplementary Figure S2).

Discussion

The CAESAR study was the first real-world registry to evaluate the performance of the new polymer-free, ultrathin, sirolimus- and probucol-eluting stent (Coroflex ISAR NEO) in a more-comers population.

The key findings of this study can be summarized as follows: (1) The Coroflex ISAR NEO stent demonstrated excellent procedural performance, with high rates of procedural and clinical success, (2) At 1-year follow-up, TLR, TVR, and ST rates were very low.

The advent of DES marked a pivotal step in preventing in-stent restenosis. However, early-generation DES demonstrated an increased risk of both late and very late stent thrombosis when compared with BMS (12, 13). This was likely attributable to compromised arterial healing subsequent to stent implantation, a consequence of inflammatory reaction associated with the polymer and endothelial cell dysfunction (14–16). In response, polymer-free (PF) stents were introduced to the market. The

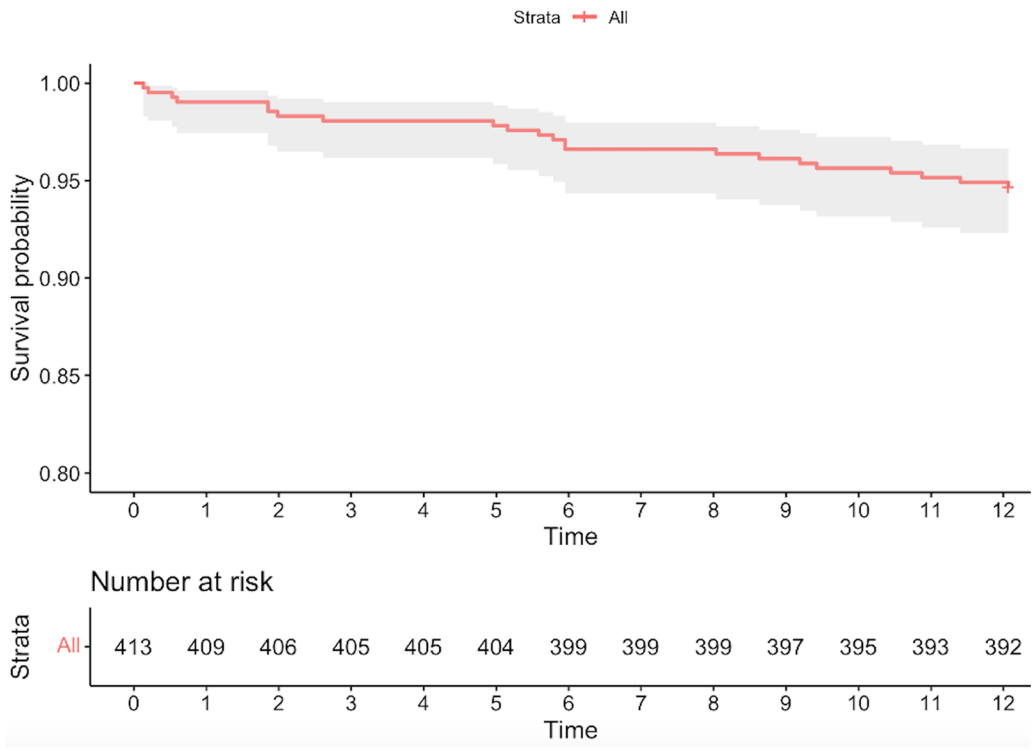

FIGURE 1
The Kaplan–Meier curve for MACE.

initial generations of PF stents displayed lower clinical effectiveness in comparison with the durable polymer DES, potentially owing to overly rapid drug elution without polymer control (17, 18). This challenge was effectively addressed in recent years by incorporating a secondary molecule to regulate drug release.

One such approach is the probucol- and sirolimus-coated polymer-free stents (19, 20). The first iteration exhibited favorable long-term (10-year) safety and efficacy when compared with high-performance durable polymer DES (2). The second generation of PF-SES (Coroflex ISAR), characterized by ultrathin struts (50/60 μm), was successfully tested in the international ISAR 2000 registry, demonstrating low event rates at 9-month follow-up in both CCS and ACS patients (7). Moreover, thanks to their ultrathin struts and the pro-reendothelializing effects of probucol, this type of device exhibited improved strut coverage at 3 months compared with a last-generation sirolimus-eluting stent with a bioresorbable degradable polymer (21).

The CAESAR registry was the first to evaluate the latest generation of PF-SES, the Coroflex ISAR NEO. In comparison with its predecessor, the new stent features a distinct structural backbone design that enhances visibility during the procedure and allows for broader expansion while maintaining radial stability, flexibility, strut thickness, and coating characteristics.

The device's procedural success reported in the present study was excellent, even in the presence of a high degree of target lesion complexity (>50% of patients presenting with type B2/C lesions, and almost 10% of treated lesions were CTOs), suggesting favorable stent performance in challenging anatomies as well. Regarding clinical outcomes, very low rates of adverse events were recorded during follow-up. Specifically, only two patients experienced the primary endpoint (TLR), and no case of stent thrombosis was reported. Comparing these findings with previous registries and trials involving PF-SES (as well as other platforms with ultrathin struts), the adverse stent-related event rate in this registry was notably lower (2, 7, 19, 22). This could be attributed to several factors, potentially synergistic: (1) the improved performance of the current device compared with its predecessors, (2) a relatively high 1-year mortality rate (especially due to non-cardiac causes), with death acting as a competing risk, and (3) the relatively small length of the treated lesions.

Nevertheless, the low rate of adverse events herein reported is reassuring in terms of the device's safety and efficacy profile. Furthermore, given the baseline high ischemic risk of the enrolled population (>50% of clinical presentations were ACS, and almost half of the enrolled patients had MVD), the limited number of ischemic events during follow-up is even more remarkable. The absence of mandatory angiographic follow-up might also explain the lower rates of TLR of the CAESAR study as compared with the previous trials [such as the ISAR-TEST 5 (7, 19)], potentially reducing the number of PCI indicated at angiographic follow-up.

Furthermore, it should be noted that, despite the baseline population's high ischemic risk (almost 70% of the cases were admitted because of unstable CAD), only 53% of the patients included in the study were prescribed a DAPT regimen at 12 months. Accordingly, the 1-year rate of major bleeding events was low and comparable with other previous registries (2, 7, 19, 22). Although the observational nature of the present analysis, along with its small sample size, does not allow for robust subanalysis on the impact of different DAPT regimens, the low event rates observed are encouraging.

The reported data must be viewed in light of the numerous inherent limitations of the study. Primarily, the potential sample size underestimation, combined with the less stringent data monitoring inherent to an observational study, might represent an adverse event under-reporting bias. As a consequence, the present results did not permit the execution of any subgroup analysis of those prespecified according to the study protocol. Secondly, the absence of a core laboratory for standardized assessment of baseline and procedural angiographies did not allow for a standardized angiogram evaluation. Similarly, the absence of an independent adjudication committee could have led to under-reported adverse event rates. Thirdly, the absence of angiographic follow-up and intravascular imaging data could have led to a reduced number of TLR reports and prevented a detailed struts coverage evaluation. Yet, indications of PCI for ISR in asymptomatic patients remain debatable. Furthermore, considering the relatively short follow-up period, very late stent thrombosis is not included as an endpoint in the current study and will be evaluated in subsequent analyses with a longer follow-up. Finally, it is important to note that the use of different DES platforms was necessary in 10 cases, potentially leading to biased outcomes. In conclusion, due to the specific inclusion and exclusion criteria and the utilization of a predetermined study platform, the findings from this analysis should not be generalized to more complex populations (e.g., severely calcified lesions or challenging anatomy) or to other devices, whether ultrathin or PF stents, which were not considered in this study.

Conclusions

The prospective CAESAR registry demonstrated the optimal safety and efficacy profile of the new-generation PF-SES Coroflex ISAR NEO in a more-comers population. This study contributes to the growing body of evidence supporting the use of PF-SES and showed promising results in terms of procedural success and low adverse event rates at 1-year follow-up. Further research is needed to confirm our results and explore the broader applicability of PF-SES in specific patient subsets, over an extended follow-up period.

Data availability statement

The original contributions presented in the study are included in the article and **Supplementary Material**. Further inquiries can be directed to the corresponding author.

Ethics statement

The studies involving humans were approved by UOSD Progetti e Ricerca Clinica, Azienda Ospedale-Università di Padova, Padua, Italy. The studies were conducted in accordance with the local legislation and institutional requirements. The participants provided their written informed consent to participate in this study. Written informed consent was obtained from the individual(s) for the publication of any potentially identifiable images or data included in this article.

Author contributions

GT: Project administration, Supervision, Writing – original draft, Writing – review and editing, Conceptualization, Data curation, Investigation, Methodology, Validation, Visualization. FC: Writing – original draft, Writing – review and editing, Conceptualization, Data curation, Formal Analysis, Investigation, Methodology, Supervision, Validation, Visualization. GI, BT, MA, CM, MB, AT, FR, GV, GC, MC, ML, DF, AD, and LA: Writing – review and editing, Writing – original draft. GL: Data curation, Formal Analysis, Methodology, Supervision, Writing – review & editing, Software, Validation, Writing – original draft. DG: Data curation, Formal Analysis, Methodology, Supervision, Writing – review & editing, Software, Validation, Writing – original draft. AP: Writing – review & editing, Data curation, Visualization, Writing – original draft. LN: Writing – original draft, Writing – review & editing, Conceptualization, Data curation, Formal Analysis, Investigation, Supervision, Visualization. GE: Writing – original draft, Writing – review & editing, Conceptualization, Data curation, Investigation, Methodology, Project administration, Supervision, Validation, Visualization.

Funding

The author(s) declare that no financial support was received for the research, authorship, and/or publication of this article.

Conflict of interest

The authors declare that the research was conducted in the absence of any commercial or financial relationships that could be construed as a potential conflict of interest.

The author(s) declared that they were an editorial board member of Frontiers, at the time of submission. This had no impact on the peer review process and the final decision.

Publisher's note

Supplementary material

The Supplementary Material for this article can be found online at: https://www.frontiersin.org/articles/10.3389/fcvm.2023.1326091/full#supplementary-material

References

1. Kaiser C, Galatius S, Erne P, Eberli F, Alber H, Rickli H, et al. Drug-eluting versus bare-metal stents in large coronary arteries. *N Engl J Med*. (2010) 363(24):2310–9. doi: 10.1056/NEJMoa1009406

2. Kufner S, Ernst M, Cassese S, Joner M, Mayer K, Colleran R, et al. 10-year outcomes from a randomized trial of polymer-free versus durable polymer drug-eluting coronary stents. *J Am Coll Cardiol*. (2020) 76(2):146–58. doi: 10.1016/j.jacc.2020.05.026

3. Tarantini G, Fovino LN, Varbella F, Trabattoni D, Caramanno G, Trani C, et al. A large, prospective, multicentre study of left main PCI using a latest-generation zotarolimus-eluting stent: the ROLEX study. *EuroIntervention*. (2023) 18(13):e1108–19. doi: 10.4244/EIJ-D-22-00454

4. Neumann F-J, Sousa-Uva M, Ahlsson A, Alfonso F, Banning AP, Benedetto U, et al. 2018 ESC/EACTS guidelines on myocardial revascularization. *Eur Heart J*. (2019) 40(2):87–165. doi: 10.1093/eurheartj/ehy394

5. Nakazawa G, Otsuka F, Nakano M, Vorpahl M, Yazdani SK, Ladich E, et al. The pathology of neoatherosclerosis in human coronary implants. *J Am Coll Cardiol*. (2011) 57(11):1314–22. doi: 10.1016/j.jacc.2011.01.011

6. Otsuka F, Byrne RA, Yahagi K, Mori H, Ladich E, Fowler DR, et al. Neoatherosclerosis: overview of histopathologic findings and implications for intravascular imaging assessment. *Eur Heart J*. (2015) 36(32):2147–59. doi: 10.1093/eurheartj/ehv205

7. Krackhardt F, Kočka V, Waliszewski MW, Utech A, Lustermann M, Hudec M, et al. Polymer-free sirolimus-eluting stents in a large-scale all-comers population. *Open Heart*. (2017) 4(2):e000592. doi: 10.1136/openhrt-2017-000592

8. Hindricks G, Potpara T, Dagres N, Arbelo E, Bax JJ, Blomström-Lundqvist C, et al. 2020 ESC guidelines for the diagnosis and management of atrial fibrillation developed in collaboration with the European Association for Cardio-Thoracic Surgery (EACTS). *Eur Heart J*. (2021) 42(5):373–498. doi: 10.1093/eurheartj/ehaa612

9. Arslan F, Damman P, Zwart B, Appelman Y, Voskuil M, Vos A de, et al. 2020 ESC guidelines on acute coronary syndrome without ST-segment elevation. *Neth Heart J*. (2021) 29(11):557–65. doi: 10.1007/s12471-021-01593-4

10. Tarantini G, Fovino LN, Tellaroli P, Chieffo A, Barioli A, Menozzi A, et al. Optimal duration of dual antiplatelet therapy after second-generation drug-eluting stent implantation in patients with diabetes: the SECURITY (Second-Generation Drug-Eluting Stent Implantation Followed by Six- Versus Twelve-Month Dual Antiplatelet Therapy)-diabetes substudy. *Int J Cardiol*. (2016) 207:168–76. doi: 10.1016/j.ijcard.2016.01.068

11. Thygesen K, Alpert JS, Jaffe AS, Chaitman BR, Bax JJ, Morrow DA, et al. Fourth universal definition of myocardial infarction (2018). *Eur Heart J*. (2019) 40(3):237–69. doi: 10.1093/eurheartj/ehy462

12. Serruys PW, Daemen J. Late stent thrombosis. *Circulation*. (2007) 115 (11):1433–9. doi: 10.1161/CIRCULATIONAHA.106.666826

13. Tada T, Byrne RA, Simunovic I, King LA, Cassese S, Joner M, et al. Risk of stent thrombosis among bare-metal stents, first-generation drug-eluting stents, and second-generation drug-eluting stents. *JACC Cardiovasc Interv*. (2013) 6(12):1267–74. doi: 10.1016/j.jcin.2013.06.015

14. Finn AV, Nakazawa G, Joner M, Kolodgie FD, Mont EK, Gold HK, Virmani R. Vascular responses to drug eluting stents. *Arterioscler Thromb Vasc Biol*. (2007) 27 (7):1500–10. doi: 10.1161/ATVBAHA.107.144220

15. Tarantini G, Cardaioli F. CHIP-PCI: ready for a prime time? *Catheter Cardiovasc Interv*. (2022) 100(5):721–2. doi: 10.1002/ccd.30466

16. Tarantini G, Cardaioli F. Coronary complete revascularization strategy: a puzzle still hard to complete. *Catheter Cardiovasc Interv*. (2022) 99(3):639–40. doi: 10.1002/ccd.30125

17. Mehilli J, Byrne RA, Wieczorek A, Iijima R, Schulz S, Bruskina O, et al. Randomized trial of three rapamycin-eluting stents with different coating strategies for the reduction of coronary restenosis. *Eur Heart J*. (2008) 29(16):1975–82. doi: 10.1093/eurheartj/ehn253

18. Gershlick A, Scheerder ID, Chevalier B, Stephens-Lloyd A, Camenzind E, Vrints C, et al. Inhibition of restenosis with a paclitaxel-eluting, polymer-free coronary stent. *Circulation*. (2004) 109(4):487–93. doi: 10.1161/01.CIR.0000109694.58299.A0

19. Massberg S, Byrne RA, Kastrati A, Schulz S, Pache J, Hausleiter J, et al. Polymer-free sirolimus- and probucol-eluting versus new generation zotarolimus-eluting stents in coronary artery disease. *Circulation*. (2011) 124(5):624–32. doi: 10.1161/CIRCULATIONAHA.111.026732

20. Kufner S, Sorges J, Mehilli J, Cassese S, Repp J, Wiebe J, et al. Randomized trial of polymer-free sirolimus- and probucol-eluting stents versus durable polymer zotarolimus-eluting stents. *JACC Cardiovasc Interv*. (2016) 9(8):784–92. doi: 10.1016/j.jcin.2016.01.009

21. Irurueta IO, Sucarrats SG, Molina JLB, Prado AP de, Massotti M, Ramírez MÁ C, et al. Can an ultrathin strut stent design and a polymer free, proendothelializing probucol matrix coating improve early strut healing? The FRIENDLY-OCT trial. An intra-patient randomized study with OCT, evaluating early strut coverage of a novel probucol coated polymer-free and ultra-thin strut sirolimus-eluting stent compared to a biodegradable polymer sirolimus-eluting stent. *Int J Cardiol*. (2022) 360:13–20. doi: 10.1016/j.ijcard.2022.04.043

22. Leschke M, Nhan VT, Waliszewski M, Palacios V, Horváth I, Ivanov VA, et al. The "all comer" coroflex please drug-eluting stent registry in Europe and Asia—an overall and transcontinental assessment of the 10-month major adverse cardiac events. *Indian Heart J*. (2012) 64(5):453–61. doi: 10.1016/j.ihj.2012.08.002

frontiers | Frontiers in Cardiovascular Medicine

TYPE Review
PUBLISHED 01 February 2024
DOI 10.3389/fcvm.2024.1352025

OPEN ACCESS

EDITED BY
Marco Zimarino,
Asl Lanciano Vasto Chieti, Italy

REVIEWED BY
Francesco Cardaioli,
University of Padua, Italy
Giulio Russo,
Policlinico Tor Vergata, Italy

*CORRESPONDENCE
Robert-Jan M. van Geuns
robertjan.vangeuns@radboudumc.nl

†These authors have contributed equally to this work and share last authorship

RECEIVED 07 December 2023
ACCEPTED 15 January 2024
PUBLISHED 01 February 2024

CITATION
Los J, Mensink FB, Mohammadnia N, Opstal TSJ, Damman P, Volleberg RHJA, Peeters DAM, van Royen N, Garcia-Garcia HM, Cornel JH, El Messaoudi S and van Geuns R-JM (2024) Invasive coronary imaging of inflammation to further characterize high-risk lesions: what options do we have? Front. Cardiovasc. Med. 11:1352025. doi: 10.3389/fcvm.2024.1352025

Invasive coronary imaging of inflammation to further characterize high-risk lesions: what options do we have?

Jonathan Los[1], Frans B. Mensink[1], Niekbachsh Mohammadnia[1], Tjerk S. J. Opstal[1,2], Peter Damman[1], Rick H. J. A. Volleberg[1], Denise A. M. Peeters[1], Niels van Royen[1], Hector M. Garcia-Garcia[3], Jan H. Cornel[1,2,4], Saloua El Messaoudi[1†] and Robert-Jan M. van Geuns[1*†]

[1]Department of Cardiology, Radboud University Medical Center, Nijmegen, Netherlands, [2]Department of Cardiology, Northwest Clinics, Alkmaar, Netherlands, [3]Department of Cardiology, MedStar Washington Hospital Center, Washington, DC, United States, [4]Dutch Network for Cardiovascular Research (WCN), Utrecht, Netherlands

Coronary atherosclerosis remains a leading cause of morbidity and mortality worldwide. The underlying pathophysiology includes a complex interplay of endothelial dysfunction, lipid accumulation and inflammatory pathways. Multiple structural and inflammatory features of the atherosclerotic lesions have become targets to identify high-risk lesions. Various intracoronary imaging devices have been developed to assess the morphological, biocompositional and molecular profile of the intracoronary atheromata. These techniques guide interventional and therapeutical management and allow the identification and stratification of atherosclerotic lesions. We sought to provide an overview of the inflammatory pathobiology of atherosclerosis, distinct high-risk plaque features and the ability to visualize this process with contemporary intracoronary imaging techniques.

KEYWORDS

atherosclerosis, inflammation, intravascular ultrasound, near-infrared spectroscopy, optical coherence tomography, near-infrared fluorescence imaging

1 Introduction

Atherosclerotic cardiovascular disease continues to be a major health burden worldwide (1). Ischemic heart disease is responsible for more than 15% of all global deaths (2, 3). The coronary vessel wall experiences accumulation of inflammatory cells, lipids, fibrous tissue and calcium leading to progressive narrowing of its lumen (4–6). Rupture of the fibrous cap or plaque erosion can trigger local thrombosis, which extends into the coronary lumen and subsequently impedes blood flow (7, 8). Plaque rupture is the most common

Abbreviations
PCSK9, proprotein convertase subtilisin kexin type 9; LDL, low-density-lipoprotein; NLRP3, NOD-, LRR- and pyrin domain-containing protein 3; IL, interleukin; TCFA, thin-cap fibroatheroma; ACS, acute coronary syndrome; CCS, chronic coronary syndrome; IVUS, intravascular ultrasound; VH-IVUS, virtual histology intravascular ultrasound; NIRS, near-infrared spectroscopy; LCBI, lipid core burden index; MACE, major adverse cardiovascular events; OCT, optical coherence tomography; μOCT, micro optical coherence tomography; NIRF, near-infrared fluorescence; ICG, indocyanine green; NIRAF, near-infrared autofluorescence.

mechanism of fatal acute myocardial infarction and sudden cardiac death (9). To reduce cardiovascular events, lipid-lowering- and plaque stabilization therapies, including statins and ezetimibe, have become cornerstones in treatment strategy. More recently, Proprotein Convertase Subtilisin Kexin type 9 (PCSK9) monoclonal antibodies have been added to the treatment possibilities (10, 11). Despite these intensive lipid-lowering treatments, residual risks persists. This most likely reflects mechanisms in the biology of atherosclerosis that are incompletely managed by controlling dyslipidemia, which includes the inflammatory response (12, 13). As exemplification, patients with target concentrations of low-density-lipoprotein (LDL) below 1.8 mmol/L and a high-sensitivity C-reactive protein (hsCRP) < 2 mg/L have the best clinical outcomes (14, 15). Furthermore, the anti-inflammatory drugs canakinumab and colchicine have demonstrated to reduce recurrent cardiovascular events (16, 17). Detection of coronary artery wall inflammation might identify which patients benefit from anti-inflammatory therapy (18).

Intracoronary imaging has greatly improved our understanding of the pathophysiology in atherosclerotic cardiovascular disease (19). Most articles discussing intracoronary imaging, focus on the structural characteristics of high-risk plaque. In addition to structural features, the present review aims to address the underlying inflammatory process and whether it is feasible to visualize markers of this process with current and future invasive *in vivo* imaging.

2 Inflammation in atherosclerosis

Atherosclerosis is initiated at the inner layer of the intima (Figure 1). LDL particles accumulate in the subendothelial space at sites with endothelial dysfunction and turbulent flow (20). Subsequently, LDL particles cluster and become oxidized by reactive oxygen species. Oxidized LDL increases local endothelial permeability (21). As a result, patrolling monocytes enter the subintimal space and differentiate into macrophages. These macrophages amass lipids through cholesterol uptake by scavenger receptors, leading to "foam cell" formation. Foam cells induce chemokine and cytokine production, which attracts new leukocytes (22). This positive feedback loop perpetuates and increases plaque formation. The accumulated inflammatory cells secrete a wide range of proteases. Cathepsins and matrix metalloproteinases are common, macrophage-derived, proteases within the atherosclerotic plaque. These proteases are involved in proteolysis of the extracellular matrix, lesion progression and plaque instability (23, 24).

In addition to inflammatory cells, vascular smooth muscle cells have shown to migrate into the intima (20). Upon exposure to lipids and cytokines, vascular smooth muscle cells transform into a proliferating cell type, expressing markers of macrophages (25). These macrophage-like cells can also take up lipids and may promote inflammation (20, 26).

Within the monocytes and macrophages, the NOD-, LRR- and pyrin domain-containing protein 3 (NLRP3) inflammasome pathway initiates cytokine production (27, 28). This protein complex is activated by cholesterol crystals (29, 30). Upon activation, Caspase 1 cleaves the inactive interleukin-1β (IL-1β) precursor. Thereafter, activated IL-1β is released into the circulation. IL-1β induces the inflammatory function of human endothelial cells and stimulates adhesion molecules that recruit leukocytes. IL-1β triggers the release of multiple cytokines, chemokines and other inflammatory mediators (31).

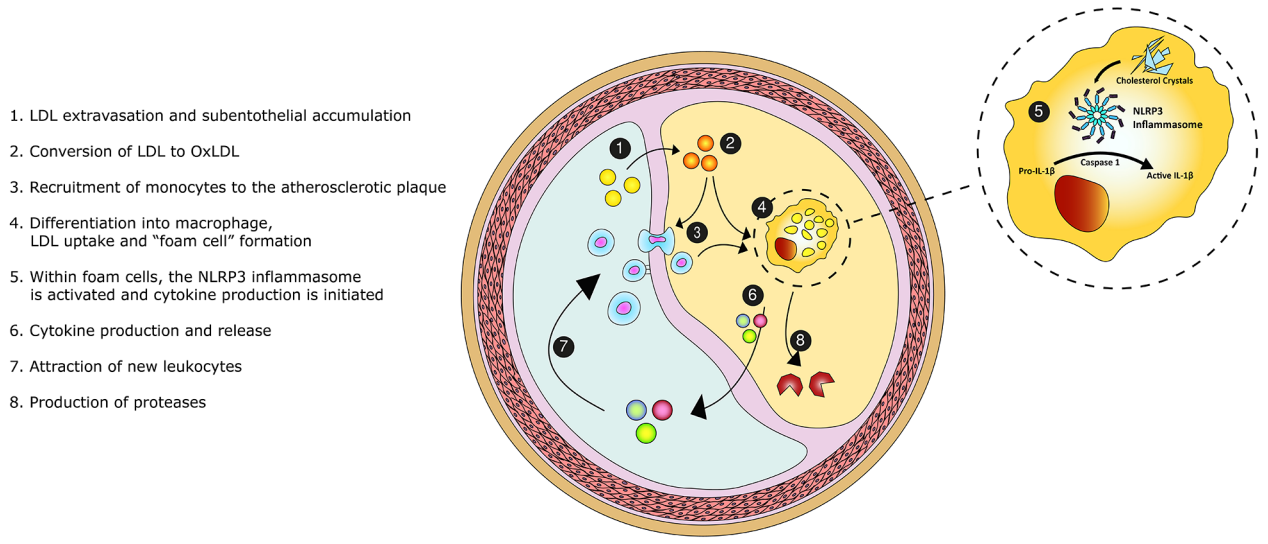

FIGURE 1
Graphical overview of the inflammatory pathobiology of atherosclerosis. Legend: Low-density-lipoprotein (LDL) enters the intimal space. The accumulated LDL particles become oxidized and promote the recruitment of monocytes. Monocytes transform into macrophages. Upon the scavenging of lipids, macrophage differentiate into foam cells. Within foam cells, the NOD-, LRR- and pyrin domain-containing protein 3 (NLRP3) inflammasome becomes activated and initiates cytokine en chemokine production, perpetuating the inflammatory process. Foam cells secrete proteases causing proteolysis of the extracellular matrix and destabilizing the atherosclerotic plaque.

For example, interleukin-6 is a downstream cytokine which induces the production of C-reactive protein (CRP) and fibrinogen, promoting thrombosis (28). Therefore, IL-1β is perceived to be the pivotal cytokine in the inflammatory cascade and a driver of atherosclerosis (32). Our understanding of atherosclerosis has thereby evolved to a complex, cholesterol crystal-induced, inflammation of the arterial wall.

3 Morphological features of high-risk plaque

Identification of high-risk lesions is of great importance, given that most atherosclerotic plaques responsible for acute coronary syndromes (ACS) are angiographically mild (33, 34). High-risk plaque refers to a lesion at high short-term risk of causing an acute clinical event (5). Lipid pools, cholesterol crystals, presence of macrophage, a large necrotic core, intraplaque hemorrhage and microcalcifications have been identified as hallmarks for high-risk lesions and represent markers of the underlying inflammatory driven process of atherosclerosis (35, 36). These hallmarks have become targets of intracoronary imaging techniques (Figure 2).

3.1 Lipid pools and cholesterol crystals

Plasma-derived lipids accumulate in the subintimal space in the initial phase of plaque formation (20). Lipid pools do not only initiate an inflammatory reaction, but also increase biomechanical stress (37). Liquid cholesterol in these pools crystalizes, leading to volume expansion (38). This volume increase destabilizes the atherosclerotic plaque. Moreover, cholesterol crystals can injure the arterial wall and disrupt the plaque (39).

Cholesterol crystals are found in ~39% of *de novo* culprit lesions of patients with either ACS or chronic coronary syndrome (CCS), and correlate with high-risk morphological features of culprit lesions (40). Cholesterol crystals are more often observed in culprit lesions in ST-elevation ACS patients compared to non-ST-elevation ACS patients, as is an increase in macrophage accumulation, spotty calcifications, mean lipid arc, thin-cap fibroatheromas (TCFAs) and thrombus (41). This supports the hypothesis that cholesterol crystals increase plaque vulnerability and trigger plaque rupture.

3.2 Macrophage and necrotic core

The necrotic core results from cell death and the inability to clear this debris. Macrophages play a major role in this process (42). Hypoxia, lipids and oxidative stress have shown to induce apoptosis in different cell types, including leukocytes and vascular smooth muscle cells (43). These signals trigger DNA fragmentation and expression of cell-surface markers that attract phagocytes (44). As macrophages are also the main phagocytes within the atherosclerotic plaque, effective clearance depends on neighboring cells. This process is called efferocytosis (45). There is no inflammatory reaction associated with apoptosis or efferocytosis, as cellular constituents are phagocytosed instead of released in the surroundings (44, 46). Within lipid-laden foam cells, intracellular cholesterol crystallizes and induces apoptosis (39). Efferocytosis becomes insufficient, which leads to a pool of dead macrophage forming a necrotic core.

A TCFA containing a large necrotic core, infiltrated by a high amount of macrophages is often displayed as "a classical example" of a lesion prone for rupture (47–49). The fibrous cap is defined as a distinctive layer of connective tissue overlying the necrotic core. It consists of smooth muscle cells in an extracellular matrix of collagen, proteoglycans and elastin. The media and adjacent adventitia may be infiltrated by varying degrees of lymphocytes,

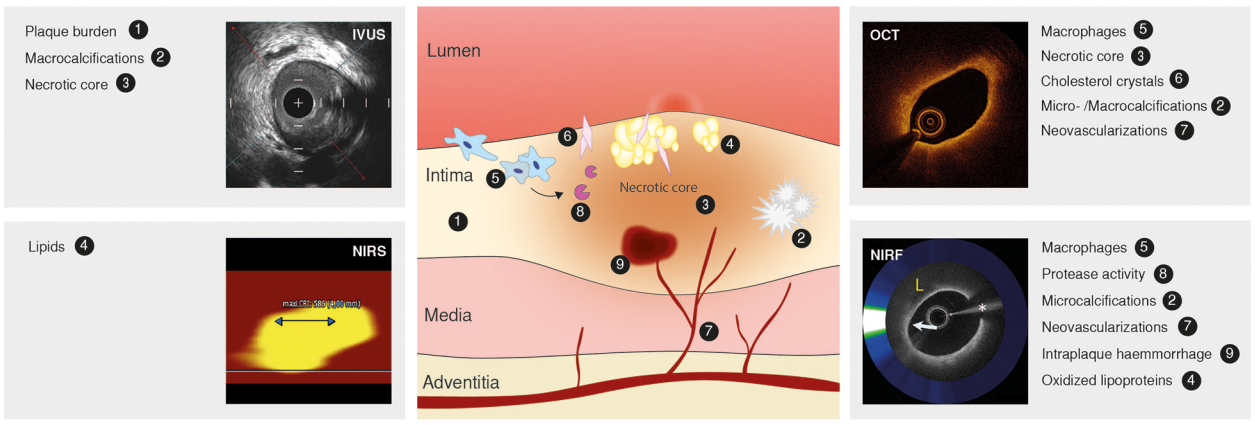

FIGURE 2
Atherosclerotic lesion, markers of inflammation and high-risk plaque and intravascular imaging techniques. Atherosclerotic lesion (middle) depicting the inflammatory pathobiology of atherosclerosis. Contemporary intracoronary imaging tools (intravascular ultrasound, IVUS; near-infrared spectroscopy, NIRS; optical coherence tomography, OCT; near-infrared fluorescence, NIRF) and their ability to display the process. Image of NIRF signal reused with permission from Ughi et al. (122).

macrophages and foam cells (50, 51). Historically, fibrous caps with a minimum thickness of <65 μm are considered to be thin, as histopathological analysis showed a cap thickness of <64 μm in 95% of arteries with ruptured plaque (49).

3.3 Plaque neovascularization and intraplaque hemorrhage

Neovascularization and intraplaque hemorrhage are common phenomenons within atherosclerotic plaques (52, 53). Neovessels are already established in the early phase of the atherosclerotic process and mainly originate from angiogenesis out of the vasa vasorum (53). Such neovessels are thin-walled, more fragile and may function as entrance for erythrocytes, lipids and inflammatory cells (35). As example, neovessel density is more prominent at sites infiltrated by macrophages and lymphocytes (53). Neovessels exhibit inadequate endothelial integrity, making them susceptible for microvascular leakage, which is thought to induce intraplaque hemorrhage (54). Accumulation of erythrocytes is associated with lesion instability and necrotic core expansion (52). Therefore, intraplaque hemorrhage may promote inflammation.

3.4 Microcalcifications

Atherosclerotic calcification is initiated within areas of inflammation (55). Serial *in vivo* imaging in apoE$^{-/-}$ mice showed that inflammation precedes osteogenic activity and that the initially formed crystals colocalize with macrophages (56). Proposed mechanisms of calcification include the nucleation of necrotic debris into calcium phosphate crystals, reduced activity of inhibitors of vascular calcification and transdifferentiation of intraplaque vascular smooth muscle cells and circulating hematopoietic stem cells into an osteo-, and chondrogenesis phenotype (55, 57). In turn, calcium phosphate crystals have shown to induce a pro-inflammatory response by macrophages (58). This suggests a positive feedback loop between inflammation and calcification. The calcium phosphate crystals congregate into microcalcifications. These microcalcifications, if present in the fibrous cap, may cause microfractures that could destabilize the atherosclerotic plaque (59). Therefore, presence of microcalcifications may refer to a more vulnerable phase in the progression of atherosclerotic plaque within regions of inflammation. Whereas increasing density is thought to reflect a stabilizing process (55).

4 Invasive imaging

4.1 Coronary angiography

Invasive coronary angiography has established itself as a reference standard for the assessment of coronary artery disease (60). It provides a two-dimensional representation of the coronary lumina, by injecting contrast media and performing different radiographic projections, with minimal information on the vessel wall. Coronary angiography is able to identify, albeit suboptimally, the presence of calcification and thrombus. Calcified lesions can be recognized as apparent radiopacities before contrast injection (61). Thrombus can be determined by contrast filling defects and intraluminal lucencies on the "luminogram" (62). The application of other intracoronary diagnostic tools offers the opportunity to look beyond luminal dimensions to identify previously indiscernible lesions.

Thermography was introduced in the early 2000s as an alternative tool to detect coronary artery wall inflammation (63). It was suggested that temperature heterogeneity could identify high-risk lesions. "Hot plaque", was supposed to reflect the higher metabolic rate of inflammatory cells. However, intracoronary thermography could not meet its expectations (63). In vivo experiments showed that intracoronary thermistors could not detect subtle changes in temperature during substantial influence of pressure, cardiac motion and coronary blood flow (64). Thereafter, it fell in oblivion. Notwithstanding, contemporary imaging techniques do have the ability to target inflammation.

4.2 Intravascular ultrasound (IVUS)

Novel high-definition IVUS may reach an axial resolution of approximately 40–60 μm using high-frequency ultrasound signals (60 MHz) (65). IVUS can differentiate between various plaque components, since calcified plaques are brighter with acoustic shadowing, while lipid-rich plaques appear less echo dense. Furthermore, IVUS can evaluate serial changes in coronary atheroma, to measure for example the effect of statins or PCSK9 inhibitors on atheroma volume (66–69). Using spectral analysis of the "backscattered" ultrasound signals, IVUS offers the opportunity to estimate plaque composition, so-called virtual histology IVUS (VH-IVUS). VH-IVUS has been used to differentiate fibrous plaque, fibrofatty plaque, necrotic core and calcium (Figure 3), which correlates with histologic samples (70). Moreover, serial changes in plaque morphology and pharmacological effects can be identified with VH-IVUS. For example, the "Integrated Biomarker and Imaging Study 2" (IBIS-2) trial showed that darapladib, a "lipoprotein-associated phospholipase A2 inhibitor", prevented necrotic core expansion after 12 months (71). However, not all studies could confirm the accuracy of VH-IVUS. Necrotic core determined by VH-IVUS did not correlate with histology within a porcine model (72). Therefore, concerns about the validity remain.

IVUS is less suited to detect microcytic or molecular factors of inflammation, such as macrophage accumulation or cholesterol crystals, owing to its relatively low resolution (73). However, high-risk plaque features detected by IVUS seem to be positively correlated with circulating inflammatory biomarkers, reflecting higher inflammatory activity (74–77). Within the "European Collaborative Project on Inflammation and Vascular Wall Remodeling in Atherosclerosis—Intravascular Ultrasound" (ATHEROREMO-IVUS) study, higher plaque burden and TCFA lesions were associated with higher levels of circulating tumor necrosis factor alpha and lower levels of circulating interleukin-10 (74). Furthermore, lesions with a plaque burden of ≥70% or

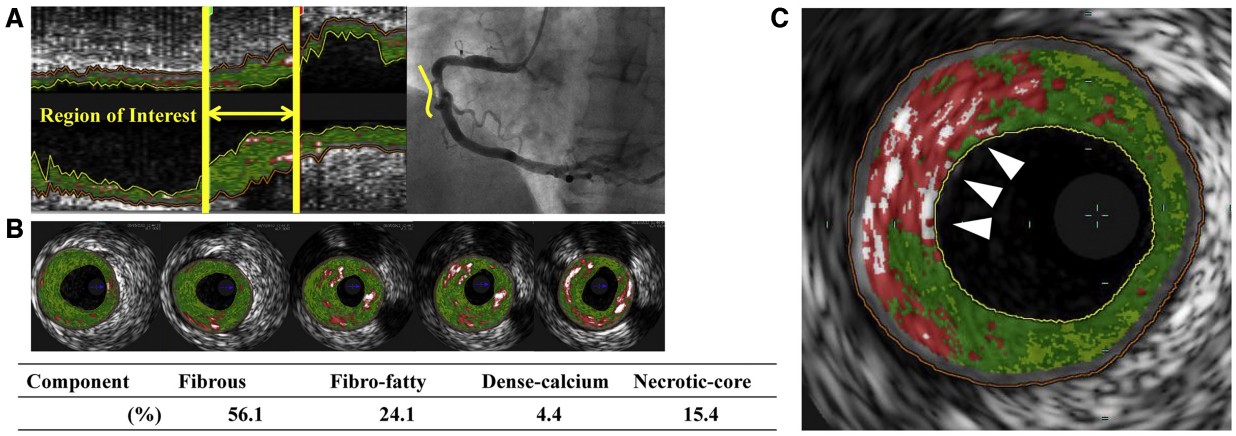

Component	Fibrous	Fibro-fatty	Dense-calcium	Necrotic-core
(%)	56.1	24.1	4.4	15.4

FIGURE 3
Virtual histology intravascular ultrasound (VH-IVUS) image of atherosclerotic plaque. Based on the reflected ultrasound signals, VH-IVUS automatically provides a colorized tissue map of plaque composition: fibrous (dark green), fibrofatty (light green), calcified (white) and necrotic core (red). (**A**) Longitudinal VH-IVUS image of an atherosclerotic lesion in the right coronary artery. (**B**) Cross-sectional images within the region of interest showing different tissue compositions. (**C**) A thin-cap fibroatheroma (TCFA), characterized as a necrotic-core rich lesion without a clear overlying fibrous cap (arrows). Reused with permission from Kuroda et al. (126).

TCFA were independently associated with higher rate of major adverse cardiac events within the same study (78).

In addition to tissue characterization, mechanical stress can affect coronary arteries (79). It is feasible that plaque rupture occurs at a location subject to higher mechanical stress. Mechanical strain refers to the tensile stress caused by the pulsatile intravascular blood pressure, whereas wall shear stress results from the tangential component of shearing deformation from blood flow (79). Mechanical strain can be assessed by using the displacement of radiofrequent IVUS signals at two different intracoronary pressures. This technique is called palpography (80). Patients presenting with ACS have more high strain spots than patients with CCS (80). Furthermore, the number of high strain spots seemed positively correlated with levels of hsCRP (80). Another *in vivo* study using Yucatan minipigs showed that regions with high strain levels were associated with presence of macrophage (81). However, within "The Providing Regional Observations to Study Predictors of Events in the Coronary Tree" (PROSPECT) trial, no difference was found in strain values between thin- and thick-cap fibroatheroma. They could not confirm the correlation between high strain spots and hsCRP in humans (82). Therefore, the diagnostic value of palpography remains uncertain.

Although smaller in magnitude than mechanical strain, wall shear stress is receiving increasing attention because of its biomechanical relevance. Low wall shear stress acts as a pro-inflammatory and pro-atherogenic stimulus on endothelial cells (79). A three-dimensional reconstruction of the coronary artery lumen is required, which also can be obtained using coronary angiography in combination with IVUS or optical coherence tomography (OCT). Thereafter, wall shear stress maps can be constructed using coronary geometries and computational fluid dynamics calculations (79). Unfortunately, results from *in vivo* studies on the correlation of wall shear stress and plaque progression remain scarce and conflicting. Both low and high wall shear stress have been associated with atherosclerosis and inflammation (79). Therefore, more clinical studies are needed to explore its use.

4.3 Near-infrared spectroscopy (NIRS)

IVUS can be combined with near-infrared spectroscopy (NIRS), which projects near-infrared light on the coronary wall, after which the reflected light is analyzed. Since cholesterol has unique features in the wavelength region, NIRS can be applied to characterize lipid-rich plaque, expressed by the lipid core burden index (LCBI) (83, 84). This index is calculated as the number of pixels with a probability of lipid core plaque > 0.6 divided by the total number of pixels and multiplied by 1,000. The $MaxLCBI_{4mm}$ is often used to detect the presence of a large lipid pool, which is the maximum LCBI value for any 4-mm segment (85). The PROSPECT II study showed that highly lipidic lesions with a $MaxLCBI_{4mm} \geq 324.7$ were independently associated with future cardiac events (86). Moreover, risk of non-culprit major adverse cardiovascular events (MACE) increased significantly for each 100-unit increase in $MaxLCBI_{4mm}$ in the "Lipid Rich Plaque" (LRP) study (87). NIRS confirms the crucial role lipids fulfil in the development of cardiovascular events and NIRS can be used to assess response to medical therapy, primarily lipid-lowering therapies (88). However, NIRS is unable to identify crystallization of cholesterol and lacks the ability to differentiate between inflamed or non-inflamed lesions. Furthermore, no association between LCBI and inflammatory biomarkers have been found so far (89).

A novel OCT-NIRS catheter is being developed to provide simultaneous microstructural and compositional imaging (Figure 4) (90). The superior resolution and characteristics of OCT could overcome some limitations inherent to IVUS imaging, as discussed in the next paragraph. A first-in-human study using OCT-NIRS is ongoing (NCT05241665).

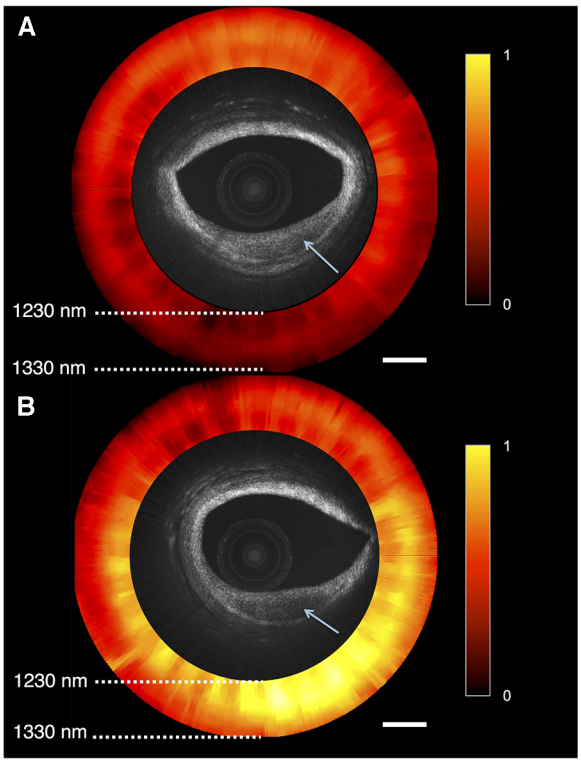

FIGURE 4
Optical coherence tomography near-infrared spectroscopy (OCT-NIRS) of cadaver coronary artery. Combinded OCT and NIRS (red and yellow circle) imaging of 2 lesions of cadaver coronary artery, showing reduced backscattering (arrows). (A) Lesion with low amounts of lipids, compatible with fibrotic tissue, as it is is shown in red. (B) Lipid-rich plaque displayed as yellow area. Reprinted with permission from Hoang et al. (90) © The Optical Society.

4.4 Optical coherence tomography (OCT)

OCT can provide microstructural images up to a maximal axial resolution of 10 μm at the cost of penetration depth, compared with IVUS (1–2 mm vs. 10 mm). The high resolution not only enables more detailed visualization of calcified nodules, thrombi, TCFAs, plaque erosions and ruptures, but also cholesterol crystal accumulation, macrophages and microvessels (Figure 5) (91, 92).

Macrophages scatter light efficiently, which creates signal-rich regions called bright spots with a cast shadow behind (93). (Figure 5A) While OCT has not been proven to distinguish between active and inactive macrophages (94), bright spots do have a strong correlation with inflammation measured by hsCRP (95). Bright spot density is significantly higher in lipid plaques compared to fibrous plaques and plaques with TCFA show a trend toward higher bright spot density (95). Moreover, bright spot density is also significantly higher in plaques with rupture than those without (95). These findings imply the ability of OCT to provide an overall estimate of macrophage accumulation. Furthermore, presence of OCT-defined macrophage accumulation is associated with adverse clinical outcome. In the "Relationship Between OCT Coronary Plaque Morphology and Clinical Outcome" (CLIMA) study, presence of macrophage accumulation in native left anterior descending coronary artery was associated with more clinical events, especially in the copresence of other high-risk plaque features including a thin fibrous cap and a large lipid arc (96).

Cholesterol crystals appear as thin, linear structures with high signal intensity, often localized nearby lipid-rich plaque (Figure 5C). It is suggested that needle-shaped cholesterol crystals could perforate the fibrous cap, causing plaque instability (93).

Intraplaque neovessels can be identified as well delineated signal-poor voids, which can be followed in consecutive frames (Figure 5D) (93). An ex vivo OCT study showed that coronary atherosclerotic plaques with neovessels were accompanied with greater luminal narrowing (97). Subsequent neovessel rupture could induce intraplaque hemorrhage. However, studies about neovessels and neovessel rupture on OCT imaging remain scarce.

OCT is the only imaging modality with sufficient spatial resolution to adequately measure fibrous cap thickness (Figure 5B). Numerous prospective and retrospective studies have demonstrated an association between OCT-identified TCFA and clinical outcome, whether or not in combination with other features of plaque instability (96, 98). The fibrous cap thickness cutoff to define TCFA differs between studies, as it has been suggested that the 65 um cutoff obtained in histopathological studies should be enlarged to adjust for potential tissue shrinkage during histopathological tissue processing (93). Nevertheless, Jiang et al. found a similar optimal cutoff of 66.7 um to distinguish lesions at higher risk of causing events (98). In this study, 883 patients were included, all 3 main epicardial vessels were scanned and follow-up lasted up to 4 years. OCT can differentiate whether ACS arises from rupture of the fibrous cap or endothelial injury with an intact fibrous cap, i.e. plaque erosion. These distinct patterns might have different underlying pathobiologies. The presence of OCT-identified culprit plaque rupture is associated with lower levels of T-cells but higher levels of effector molecules involved in the innate immune response compared to ACS with intact fibrous caps (99). This may indicate that the adaptive immune system plays an important role in inducing endothelial erosion. In proteomics analysis, patients with ruptured plaques also had a higher inflammatory response and more MACE during 2 years of follow-up (100).

OCT allows to evaluate change in high-risk plaque characteristics (101). The "High-Resolution Assessment of Coronary Plaques in a Global Evolocumab Randomized Study" (HUYGENS) showed that intensive lipid-lowering therapy with high-dose statins and evolocumab increased minimum fibrous cap thickness and decreased the macrophage index on serial OCT. The combination of statin and evolocumab resulted in more favorable changes than statin therapy alone (102).

4.4.1 Micro optical coherence tomography (μOCT)

In 2011, micro-OCT (μOCT) was introduced to improve the resolution of OCT imaging systems to achieve an axial resolution of 1–2 μm, which is another ten-fold improvement (103). Therefore, μOCT is capable of visualizing independent cells and subcellular features. Moreover, μOCT is able to differentiate between multiple inflammatory cells, including leukocytes, monocytes and macrophages.

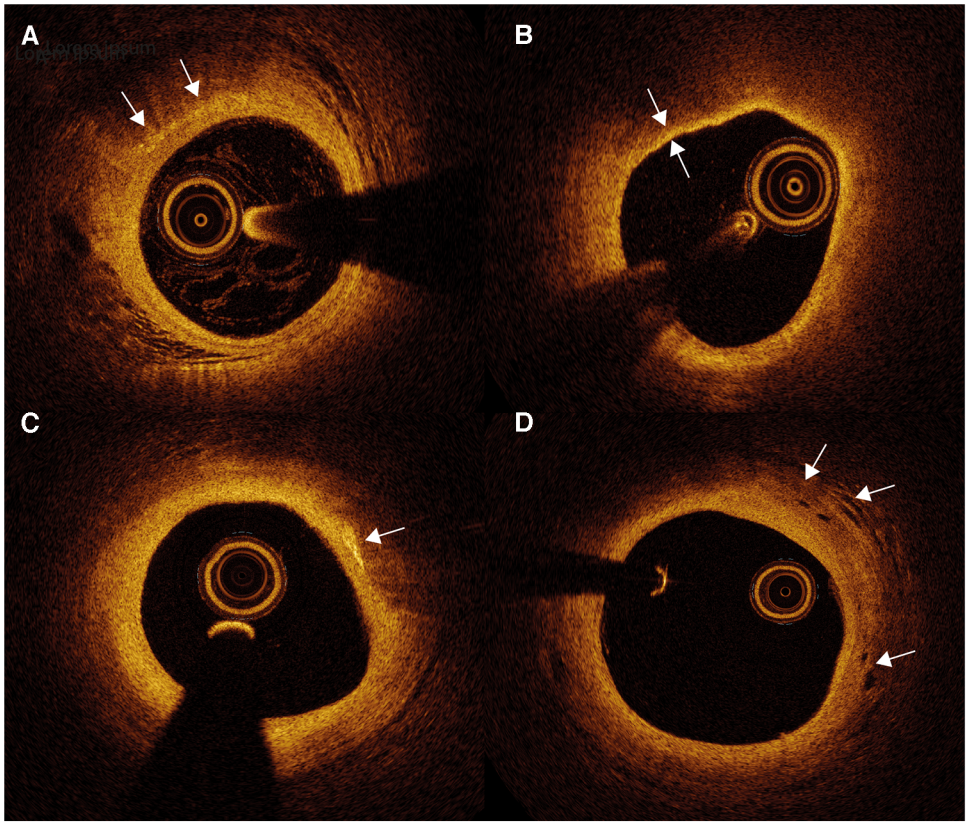

FIGURE 5
Optical coherence tomography (OCT) images of atherosclerotic plaque and inflammation markers. (**A**) Macrophages appear as signal-rich bright spots with a signal-poor region below (arrows). (**B**) Thin-cap fibroatheroma are identified as an atherosclerotic plaque covered by a fibrous cap of <65 µm (between arrows). (**C**) Cholesterol crystals appear as thin and linear structures with high signal intensity (arrow), often localized nearby lipid-rich plaque. (**D**) Intraplaque neovessels can be identified as well delineated signal-poor voids (arrows).

An intravascular µOCT catheter suitable for *in vivo* imaging was recently introduced. This device is able to display a wide range of cells and subcellular structures, including leukocytes, macrophages, smooth muscle cells, cholesterol crystals and platelets within rabbit aortae *in vivo* and human cadaver coronary arteries (104). To acquire high-resolution images, current µOCT imaging systems emit light with 800 nm wavelength. The use of a shorter wavelength compared to standard OCT might be at the expense of penetration depth, which is already a disadvantage compared to IVUS (105). Nevertheless, µOCT has the potential to visualize local inflammatory processes *in vivo* such as leukocyte adhesion, foam cell formation or inflammatory cells surrounding cholesterol crystals on microscopic level. More clinical studies are needed to explore further utilities.

4.5 Near-infrared fluorescence (NIRF)

Near-infrared fluorescence (NIRF) imaging is an emerging technique, allowing the visualization of molecular processes within the atherosclerotic plaque. It uses imaging agents which bind to specific targets, including protease activity, LDL, fibrin deposition and microcalcifications (106–108). These imaging agents consist of an fluorochrome, conjugated to an antibody, molecule or peptide. After injection, a NIRF-catheter is advanced within the coronary artery. A continuous wave laser diode emits excitational light within a 650 to 950 nm window (NIR spectral region) to stimulate the fluorophores. The subsequent fluorescence emission is collected and filtered within the NIRF-catheter (109).

Protease-activatable fluorophores have been developed to visualize enzymatic activity. At baseline, fluorophores emittance is quenched, but increases significantly after cleavage (110). Enzymatically active cathepsins, detected by NIRF, seem to colocalize with cathepsins and macrophages on immunohistochemistry in animal and human atheromata (107, 111, 112). Matrix metalloproteinase-specific fluorophores have shown similar results on NIRF imaging (113, 114). Indocyanine green (ICG) is an imaging agent, which can directly visualize macrophages. After injection, ICG is internalized by macrophages and foam cells by binding to albumin or LDL (108). In a recent study, the ICG NIRF signal, measured in freshly isolated carotid plaques, was highest in the most stenotic area. Subsequent histopathological analyses established that ICG targeted endothelial abnormalities, such as disrupted fibrous caps

and areas of neovascularization. ICG concentrated on zones of plaque lipids, macrophages and intraplaque hemorrhage (115). Furthermore, fluorophores have been developed to target fibrin deposition, activated factor XIIIa or thrombin activity to assess thrombosis. Validation of these fluorophores mostly rely on non-invasive NIRF imaging techniques (116–118). However, intravascular NIRF has been able to detect fibrin deposition overlying stent struts in rabbits (119).

Hybridization of intravascular molecular and structural imaging could potentially allow further study of the pathophysiological mechanisms of arterial plaques (120, 121). Both NIRF-OCT and NIRF-IVUS are being developed. The dual-of modality OCT and NIRF, can detect fluorescence from naturally occurring molecules, called near-infrared autofluorescence (NIRAF). NIRAF is elevated in advanced necrotic core-containing lesions and is associated with a high-risk morphological plaque phenotype (Figure 6) (122, 123). Interestingly, NIRAF elevation is specific to plaques with macrophage accumulations, as shown by OCT (122). However, the converse is not true, since many areas with elevated macrophage accumulation on OCT were NIRAF negative. This could be explained by low sensitivity/high specificity of NIRAF to macrophage accumulation, or by the concept of different macrophage phenotypes. The underlying molecular and chemical mechanisms that produce NIRAF are not yet fully understood.

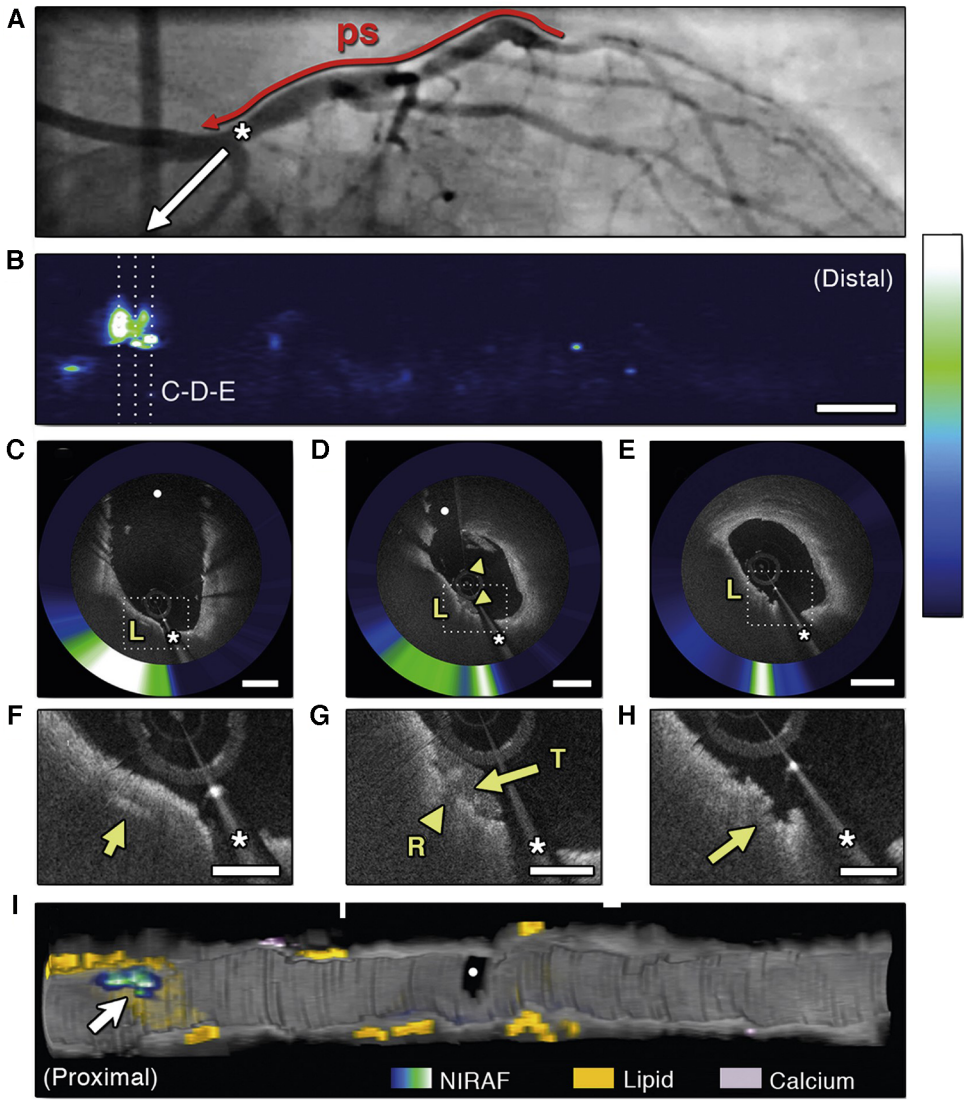

FIGURE 6
Optical coherence tomography near-infrared autofluorescence (OCT-NIRAF) imaging of a ruptured thin-cap fibroatheroma. (**A**) Coronary angiography of the left circumflex coronary artery. (**B**) 2-dimensional map of NIRAF signal. (**C–E**) Cross sectional OCT—NIRAF images showing a rupture of a thin fibrous cap covered with a small thrombus. The rupture site shows high NIRAF. (**F,G**) Magnified views revealing a cholesterol crystal (**F**, arrow), thrombus (**G**, arrows) and the rupture site (**H**, arrow). All colocalized with elevated NIRAF. (**I**) 3-dimensional rendered map demonstrating that the high NIRAF signal appears within regions containing high amount of lipids (arrow). The asterisk (*) corresponds with catheter artefact. L, lipid; R, rupture site; T, thrombus. Reused with permission from Ughi et al. (122).

TABLE 1 Characteristics of the imaging modalities and their ability to display high-risk features and inflammation markers.

	(VH) IVUS	NIRS	(μ)OCT	NIRF
Technique	Ultrasound	Near-infrared	Infrared	Near-infrared
Requiring blood removal	–	–	+	–
Axial resolution	up to 40–60 μm (HD IVUS)	NA	10 μm (OCT), 1–2 mm (μOCT)	NA
Penetration depth	10 mm	<3 mm	1–2 mm	3 mm
Quantification of plaque burden	+++	–	+	–
Lipids	++	+++	++	+++
Cholesterol crystals	–	–	+	–
Macrophage	–	–	++ (quantification, plus differentiation for μOCT)	+++ (activity)
Necrotic core	+	–	++	–
Detection of TCFA (<65 μm)	+	–	+++	–
Neovessels	–	–	+	+
Intraplaque hemorrhage	–	–	–	+
Microcalcifications	+	–	++	+++
Suitable (clinical) settings for use	– Assessment of vessel- and lumen dimensions, plaque morphology and aorto-ostial junction – Identification of high-risk lesions based on high plaque burden and small minimum lumen area – Guidance of percutaneous coronary intervention	– Detection of lipid-rich plaque – Combined with IVUS with similar indications	– Detailed assessment of plaque morphology and lumen dimensions – Detection of thrombus, plaque rupture and plaque erosion in unclear ACS mechanism – Identification of high-risk lesions based on TCFA – Guidance of percutaneous coronary intervention	– Detection of specific target molecules – Combined with OCT with similar indications

(VH) IVUS, (virtual histology) intravascular ultrasound; NIRS, near-infrared spectroscopy; (μ)OCT, (micro) optical coherence tomography; NIRF, near-infrared fluorescence. –, not possible; +,adequate; ++, good; +++, excellent; NA, not applicable; TCFA, thin-cap fibroatheroma; HD, high-definition; ACS, acute coronary syndrome.

5 Discussion

Atherosclerotic cardiovascular disease is a complex chronic inflammatory and fibroproliferative process fueled by atherogenic lipoproteins. This implies the requirement of precise diagnostic tools and targeted treatment strategies (124). Systemic inflammation has emerged as a therapeutic target to reduce cardiovascular events (16, 17). Intracoronary imaging allows the judgement of disease state of atheromata and identification of high-risk lesions. Given the inherent characteristics of different imaging modalities, they all facilitate distinctive insights in the inflammatory pathobiology of atherosclerosis (Table 1). IVUS gives a good "overview" of plaque burden and plaque composition. A higher plaque burden is associated with elevated systemic inflammation, reflected by increased pro-inflammatory biomarkers. However, it is unable to directly visualize the inflammatory process. NIRS provides a chemical analysis of the arterial wall but lacks the ability to detect inflammatory markers or cholesterol crystals. OCT is able to detect and measure TCFA, macrophages, neovessels and cholesterol crystals. Moreover, additional increase of resolution with μOCT allows further detection of individual cells and subcellular substances. NIRF imaging displays molecular- and inflammatory activity by targeting specific molecules, thereby allowing detection of early- and advanced stages of atherosclerosis.

Lesions with high-risk features on intracoronary imaging have shown to be predictive of MACE (125). However, current positive predictive value is still moderate. Novel hybrid modalities, in particular NIRF-OCT, could provide complementary morphological and functional imaging, further improving the diagnostic performance and prognostic stratification. In the near future, they may identify high-risk lesions of clinical value to revascularize or optimize medical therapy. For the moment, invasive imaging mainly has clinical indications (Table 1), but they can simultaneously identify more specific inflammatory characteristics, which strengthens the case for inflammation-targeted therapies. Moreover, hallmarks of inflammation and high-risk plaque are useful surrogate endpoints to assess the potency of medical therapy.

6 Conclusion

Contemporary and future intracoronary imaging techniques allow the identification of inflammatory markers within atherosclerotic plaque. They assess the biochemical composition and the underlying pathophysiology. Furthermore, they serve as a mechanism to evaluate drug efficacy. Conscientious implementation may allow the development of patient tailored treatment strategies and improve patient outcome.

Author contributions

JL: Writing – original draft, Writing – review & editing. FM: Writing – review & editing. NM: Writing – review & editing. TO: Writing – review & editing. PD: Writing – review & editing. RV: Writing – review & editing. DP: Writing – review & editing. NvR: Writing – review & editing. HG-G: Writing –

review & editing. JC: Writing – review & editing. SEM: Writing – review & editing. R-JvG: Writing – review & editing.

Funding

The author(s) declare that no financial support was received for the research, authorship, and/or publication of this article.

Conflict of interest

PD: received research grants and speaker fees from Abbott Vascular; research grants, speaker fees and consultancy fees from Philips; and research grants from AstraZeneca. NvR: research grants from Abbott, Philpis, Biotronik and Medtronic. Speaker fee: Abbott, Bayer, Rainmed, Microport. HG-G: receives consulting fees from Boston Scientific, Abbott and institutional grants from Phillips, Biotronik, Abbott, MedAlliance, Corflow, Chiesi and Medis. JC: Advisory board Amgen en Novo Nordisk. Received research grants from ZonMw. R-JvG: reported grants and personal fees from Boston Scientific, grants and personal fees from Abbott Vascular, grants and personal fees from Astra Zeneca, grants and personal fees from Amgen, grants from InfraRedx.

The other authors declare that the research was conducted in the absence of any commercial or financial relationships that could be construed as a potential conflict of interest.

Publisher's note

References

1. Vasan RS, Enserro DM, Xanthakis V, Beiser AS, Seshadri S. Temporal trends in the remaining lifetime risk of cardiovascular disease among middle-aged adults across 6 decades: the framingham study. *Circulation*. (2022) 145(17):1324–38. doi: 10.1161/CIRCULATIONAHA.121.057889

2. Roth GA, Huffman MD, Moran AE, Feigin V, Mensah GA, Naghavi M, et al. Global and regional patterns in cardiovascular mortality from 1990 to 2013. *Circulation*. (2015) 132(17):1667–78. doi: 10.1161/CIRCULATIONAHA.114.008720

3. Global, regional, and national age-sex specific all-cause and cause-specific mortality for 240 causes of death, 1990–2013: a systematic analysis for the global burden of disease study 2013. *Lancet*. (2015) 385(9963):117–71. doi: 10.1016/S0140-6736(14)61682-2

4. Weber C, Noels H. Atherosclerosis: current pathogenesis and therapeutic options. *Nat Med*. (2011) 17(11):1410–22. doi: 10.1038/nm.2538

5. Naghavi M, Libby P, Falk E, Casscells SW, Litovsky S, Rumberger J, et al. From vulnerable plaque to vulnerable patient: a call for new definitions and risk assessment strategies: part I. *Circulation*. (2003) 108(14):1664–72. doi: 10.1161/01.CIR.0000087480.94275.97

6. Falk E. Pathogenesis of atherosclerosis. *J Am Coll Cardiol*. (2006) 47(8 Suppl): C7–12. doi: 10.1016/j.jacc.2005.09.068

7. Libby P, Ridker PM, Hansson GK. Progress and challenges in translating the biology of atherosclerosis. *Nature*. (2011) 473(7347):317–25. doi: 10.1038/nature10146

8. Prati F, Uemura S, Souteyrand G, Virmani R, Motreff P, Di Vito L, et al. OCT-based diagnosis and management of STEMI associated with intact fibrous cap. *JACC Cardiovasc Imaging*. (2013) 6(3):283–7. doi: 10.1016/j.jcmg.2012.12.007

9. Fuster V, Moreno PR, Fayad ZA, Corti R, Badimon JJ. Atherothrombosis and high-risk plaque: part I: evolving concepts. *J Am Coll Cardiol*. (2005) 46(6):937–54. doi: 10.1016/j.jacc.2005.03.074

10. Navarese EP, Robinson JG, Kowalewski M, Kolodziejczak M, Andreotti F, Bliden K, et al. Association between baseline LDL-C level and total and cardiovascular mortality after LDL-C lowering: a systematic review and meta-analysis. *JAMA*. (2018) 319(15):1566–79. doi: 10.1001/jama.2018.2525

11. Ference BA, Cannon CP, Landmesser U, Lüscher TF, Catapano AL, Ray KK. Reduction of low density lipoprotein-cholesterol and cardiovascular events with proprotein convertase subtilisin-kexin type 9 (PCSK9) inhibitors and statins: an analysis of FOURIER, SPIRE, and the cholesterol treatment trialists collaboration. *Eur Heart J*. (2018) 39(27):2540–5. doi: 10.1093/eurheartj/ehx450

12. Ridker PM. Residual inflammatory risk: addressing the obverse side of the atherosclerosis prevention coin. *Eur Heart J*. (2016) 37(22):1720–2. doi: 10.1093/eurheartj/ehw024

13. Mohammadnia N, Opstal TSJ, El Messaoudi S, Bax WA, Cornel JH. An update on inflammation in atherosclerosis: how to effectively treat residual risk. *Clin Ther*. (2023) 45(11):1055–9. doi: 10.1016/j.clinthera.2023.08.016

14. Ridker PM, Danielson E, Fonseca FA, Genest J, Gotto AM Jr., Kastelein JJ, et al. Reduction in C-reactive protein and LDL cholesterol and cardiovascular event rates after initiation of rosuvastatin: a prospective study of the JUPITER trial. *Lancet*. (2009) 373(9670):1175–82. doi: 10.1016/S0140-6736(09)60447-5

15. Ridker PM, Cannon CP, Morrow D, Rifai N, Rose LM, McCabe CH, et al. C-reactive protein levels and outcomes after statin therapy. *N Engl J Med*. (2005) 352 (1):20–8. doi: 10.1056/NEJMoa042378

16. Ridker PM, Everett BM, Thuren T, MacFadyen JG, Chang WH, Ballantyne C, et al. Antiinflammatory therapy with canakinumab for atherosclerotic disease. *N Engl J Med*. (2017) 377(12):1119–31. doi: 10.1056/NEJMoa1707914

17. Nidorf SM, Fiolet ATL, Mosterd A, Eikelboom JW, Schut A, Opstal TSJ, et al. Colchicine in patients with chronic coronary disease. *N Engl J Med*. (2020) 383 (19):1838–47. doi: 10.1056/NEJMoa2021372

18. Biasucci LM, Pedicino D, Liuzzo G. Promises and challenges of targeting inflammation to treat cardiovascular disease: the post-CANTOS era. *Eur Heart J*. (2020) 41(23):2164–7. doi: 10.1093/eurheartj/ehz586

19. Mintz GS. Clinical utility of intravascular imaging and physiology in coronary artery disease. *J Am Coll Cardiol*. (2014) 64(2):207–22. doi: 10.1016/j.jacc.2014.01.015

20. Raggi P, Genest J, Giles JT, Rayner KJ, Dwivedi G, Beanlands RS, et al. Role of inflammation in the pathogenesis of atherosclerosis and therapeutic interventions. *Atherosclerosis*. (2018) 276:98–108. doi: 10.1016/j.atherosclerosis.2018.07.014

21. Mundi S, Massaro M, Scoditti E, Carluccio MA, van Hinsbergh VWM, Iruela-Arispe ML, et al. Endothelial permeability, LDL deposition, and cardiovascular risk factors-a review. *Cardiovasc Res*. (2018) 114(1):35–52. doi: 10.1093/cvr/cvx226

22. Kim KW, Ivanov S, Williams JW. Monocyte recruitment, specification, and function in atherosclerosis. *Cells*. (2020) 10(1). doi: 10.3390/cells10010015

23. Johnson JL. Metalloproteinases in atherosclerosis. *Eur J Pharmacol*. (2017) 816:93–106. doi: 10.1016/j.ejphar.2017.09.007

24. Newby AC. Dual role of matrix metalloproteinases (matrixins) in intimal thickening and atherosclerotic plaque rupture. *Physiol Rev*. (2005) 85(1):1–31. doi: 10.1152/physrev.00048.2003

25. Shankman LS, Gomez D, Cherepanova OA, Salmon M, Alencar GF, Haskins RM, et al. KLF4-dependent Phenotypic modulation of smooth muscle cells has a key role in atherosclerotic plaque pathogenesis. *Nat Med*. (2015) 21(6):628–37. doi: 10.1038/nm.3866

26. Bennett MR, Sinha S, Owens GK. Vascular smooth muscle cells in atherosclerosis. *Circ Res*. (2016) 118(4):692–702. doi: 10.1161/CIRCRESAHA.115.306361

27. Dinarello CA, Simon A, van der Meer JW. Treating inflammation by blocking interleukin-1 in a broad spectrum of diseases. *Nat Rev Drug Discov*. (2012) 11 (8):633–52. doi: 10.1038/nrd3800

28. Ridker PM. From C-reactive protein to interleukin-6 to interleukin-1: moving upstream to identify novel targets for atheroprotection. *Circ Res*. (2016) 118 (1):145–56. doi: 10.1161/CIRCRESAHA.115.306656

29. Duewell P, Kono H, Rayner KJ, Sirois CM, Vladimer G, Bauernfeind FG, et al. NLRP3 Inflammasomes are required for atherogenesis and activated by cholesterol crystals. *Nature*. (2010) 464(7293):1357–61. doi: 10.1038/nature08938

30. Rajamäki K, Lappalainen J, Oörni K, Välimäki E, Matikainen S, Kovanen PT, et al. Cholesterol crystals activate the NLRP3 inflammasome in human macrophages: a novel link between cholesterol metabolism and inflammation. *PLoS One*. (2010) 5(7):e11765. doi: 10.1371/journal.pone.0011765

31. Bevilacqua MP, Pober JS, Wheeler ME, Cotran RS, Gimbrone MA Jr. Interleukin 1 acts on cultured human vascular endothelium to increase the adhesion of polymorphonuclear leukocytes, monocytes, and related leukocyte cell lines. *J Clin Invest*. (1985) 76(5):2003–11. doi: 10.1172/JCI112200

32. Dinarello CA. Interleukin-1 in the pathogenesis and treatment of inflammatory diseases. *Blood*. (2011) 117(14):3720–32. doi: 10.1182/blood-2010-07-273417

33. Glaser R, Selzer F, Faxon DP, Laskey WK, Cohen HA, Slater J, et al. Clinical progression of incidental, asymptomatic lesions discovered during culprit vessel coronary intervention. *Circulation*. (2005) 111(2):143–9. doi: 10.1161/01.CIR.0000150335.01285.12

34. Little WC, Constantinescu M, Applegate RJ, Kutcher MA, Burrows MT, Kahl FR, et al. Can coronary angiography predict the site of a subsequent myocardial infarction in patients with mild-to-moderate coronary artery disease? *Circulation*. (1988) 78(5 Pt 1):1157–66. doi: 10.1161/01.CIR.78.5.1157

35. Bentzon JF, Otsuka F, Virmani R, Falk E. Mechanisms of plaque formation and rupture. *Circ Res*. (2014) 114(12):1852–66. doi: 10.1161/CIRCRESAHA.114.302721

36. Stone GW, Maehara A, Lansky AJ, de Bruyne B, Cristea E, Mintz GS, et al. A prospective natural-history study of coronary atherosclerosis. *N Engl J Med*. (2011) 364(3):226–35. doi: 10.1056/NEJMoa1002358

37. Huang H, Virmani R, Younis H, Burke AP, Kamm RD, Lee RT. The impact of calcification on the biomechanical stability of atherosclerotic plaques. *Circulation*. (2001) 103(8):1051–6. doi: 10.1161/01.CIR.103.8.1051

38. Abela GS, Aziz K. Cholesterol crystals cause mechanical damage to biological membranes: a proposed mechanism of plaque rupture and erosion leading to arterial thrombosis. *Clin Cardiol*. (2005) 28(9):413–20. doi: 10.1002/clc.4960280906

39. Abela GS. Cholesterol crystals piercing the arterial plaque and intima trigger local and systemic inflammation. *J Clin Lipidol*. (2010) 4(3):156–64. doi: 10.1016/j.jacl.2010.03.003

40. Nishimura S, Ehara S, Hasegawa T, Matsumoto K, Yoshikawa J, Shimada K. Cholesterol crystal as a new feature of coronary vulnerable plaques: an optical coherence tomography study. *J Cardiol*. (2017) 69(1):253–9. doi: 10.1016/j.jjcc.2016.04.003

41. Dai J, Tian J, Hou J, Xing L, Liu S, Ma L, et al. Association between cholesterol crystals and culprit lesion vulnerability in patients with acute coronary syndrome: an optical coherence tomography study. *Atherosclerosis*. (2016) 247:111–7. doi: 10.1016/j.atherosclerosis.2016.02.010

42. Gonzalez L, Trigatti BL. Macrophage apoptosis and necrotic core development in atherosclerosis: a rapidly advancing field with clinical relevance to imaging and therapy. *Can J Cardiol*. (2017) 33(3):303–12. doi: 10.1016/j.cjca.2016.12.010

43. Van Vré EA, Ait-Oufella H, Tedgui A, Mallat Z. Apoptotic cell death and efferocytosis in atherosclerosis. *Arterioscler Thromb Vasc Biol*. (2012) 32(4):887–93. doi: 10.1161/ATVBAHA.111.224873

44. Elmore S. Apoptosis: a review of programmed cell death. *Toxicol Pathol*. (2007) 35(4):495–516. doi: 10.1080/01926230701320337

45. Tabas I, Bornfeldt KE. Macrophage phenotype and function in different stages of atherosclerosis. *Circ Res*. (2016) 118(4):653–67. doi: 10.1161/CIRCRESAHA.115.306256

46. Savill J, Fadok V. Corpse clearance defines the meaning of cell death. *Nature*. (2000) 407(6805):784–8. doi: 10.1038/35037722

47. Kolodgie FD, Burke AP, Farb A, Gold HK, Yuan J, Narula J, et al. The thin-cap fibroatheroma: a type of vulnerable plaque: the major precursor lesion to acute coronary syndromes. *Curr Opin Cardiol*. (2001) 16(5):285–92. doi: 10.1097/00001573-200109000-00006

48. Libby P. Molecular bases of the acute coronary syndromes. *Circulation*. (1995) 91(11):2844–50. doi: 10.1161/01.CIR.91.11.2844

49. Burke AP, Farb A, Malcom GT, Liang YH, Smialek J, Virmani R. Coronary risk factors and plaque morphology in men with coronary disease who died suddenly. *N Engl J Med*. (1997) 336(18):1276–82. doi: 10.1056/NEJM199705013361802

50. Virmani R, Kolodgie FD, Burke AP, Farb A, Schwartz SM. Lessons from sudden coronary death: a comprehensive morphological classification scheme for atherosclerotic lesions. *Arterioscler Thromb Vasc Biol*. (2000) 20(5):1262–75. doi: 10.1161/01.ATV.20.5.1262

51. Stary HC, Chandler AB, Dinsmore RE, Fuster V, Glagov S, Insull W Jr., et al. A definition of advanced types of atherosclerotic lesions and a histological classification of atherosclerosis. A report from the committee on vascular lesions of the council on arteriosclerosis, American heart association. *Circulation*. (1995) 92(5):1355–74. doi: 10.1161/01.CIR.92.5.1355

52. Kolodgie FD, Gold HK, Burke AP, Fowler DR, Kruth HS, Weber DK, et al. Intraplaque hemorrhage and progression of coronary atheroma. *N Engl J Med*. (2003) 349(24):2316–25. doi: 10.1056/NEJMoa035655

53. Kumamoto M, Nakashima Y, Sueishi K. Intimal neovascularization in human coronary atherosclerosis: its origin and pathophysiological significance. *Hum Pathol*. (1995) 26(4):450–6. doi: 10.1016/0046-8177(95)90148-5

54. Sluimer JC, Kolodgie FD, Bijnens AP, Maxfield K, Pacheco E, Kutys B, et al. Thin-walled microvessels in human coronary atherosclerotic plaques show incomplete endothelial junctions relevance of compromised structural integrity for intraplaque microvascular leakage. *J Am Coll Cardiol*. (2009) 53(17):1517–27. doi: 10.1016/j.jacc.2008.12.056

55. Nakahara T, Dweck MR, Narula N, Pisapia D, Narula J, Strauss HW. Coronary artery calcification: from mechanism to molecular imaging. *JACC Cardiovasc Imaging*. (2017) 10(5):582–93. doi: 10.1016/j.jcmg.2017.03.005

56. Aikawa E, Nahrendorf M, Figueiredo JL, Swirski FK, Shtatland T, Kohler RH, et al. Osteogenesis associates with inflammation in early-stage atherosclerosis evaluated by molecular imaging in vivo. *Circulation*. (2007) 116(24):2841–50. doi: 10.1161/CIRCULATIONAHA.107.732867

57. Leszczynska A, O'Doherty A, Farrell E, Pindjakova J, O'Brien FJ, O'Brien T, et al. Differentiation of vascular stem cells contributes to ectopic calcification of atherosclerotic plaque. *Stem Cells*. (2016) 34(4):913–23. doi: 10.1002/stem.2315

58. Nadra I, Mason JC, Philippidis P, Florey O, Smythe CD, McCarthy GM, et al. Proinflammatory activation of macrophages by basic calcium phosphate crystals via protein kinase C and MAP kinase pathways: a vicious cycle of inflammation and arterial calcification? *Circ Res*. (2005) 96(12):1248–56. doi: 10.1161/01.RES.0000171451.88616.c2

59. Vengrenyuk Y, Carlier S, Xanthos S, Cardoso L, Ganatos P, Virmani R, et al. A hypothesis for vulnerable plaque rupture due to stress-induced debonding around cellular microcalcifications in thin fibrous caps. *Proc Natl Acad Sci U S A*. (2006) 103(40):14678–83. doi: 10.1073/pnas.0606310103

60. Windecker S, Kolh P, Alfonso F, Collet JP, Cremer J, Falk V, et al. 2014 ESC/EACTS guidelines on myocardial revascularization: the task force on myocardial revascularization of the European society of cardiology (ESC) and the European association for cardio-thoracic surgery (EACTS)Developed with the special contribution of the European association of percutaneous cardiovascular interventions (EAPCI). *Eur Heart J*. (2014) 35(37):2541–619. doi: 10.1093/eurheartj/ehu278

61. Mintz GS, Popma JJ, Pichard AD, Kent KM, Satler LF, Chuang YC, et al. Patterns of calcification in coronary artery disease. A statistical analysis of intravascular ultrasound and coronary angiography in 1155 lesions. *Circulation*. (1995) 91(7):1959–65. doi: 10.1161/01.CIR.91.7.1959

62. Chan KH, Ng MK. Is there a role for coronary angiography in the early detection of the vulnerable plaque? *Int J Cardiol*. (2013) 164(3):262–6. doi: 10.1016/j.ijcard.2012.01.027

63. Nissen SE. Vulnerable plaque and Einstein's definition of insanity. *J Am Coll Cardiol*. (2020) 75(12):1383–5. doi: 10.1016/j.jacc.2020.01.043

64. Cuisset T, Beauloye C, Melikian N, Hamilos M, Sarma J, Sarno G, et al. In vitro and in vivo studies on thermistor-based intracoronary temperature measurements: effect of pressure and flow. *Catheter Cardiovasc Interv*. (2009) 73(2):224–30. doi: 10.1002/ccd.21780

65. Garcia-Guimaraes M, Antuña P, De la Cuerda F, Maruri-Sanchez R, Cuesta J, Bastante T, et al. High-definition IVUS versus OCT to assess coronary artery disease and results of stent implantation. *JACC Cardiovasc Imaging*. (2020) 13(2 Pt 1):519–21. doi: 10.1016/j.jcmg.2019.08.019

66. Nicholls SJ, Puri R, Anderson T, Ballantyne CM, Cho L, Kastelein JJP, et al. Effect of evolocumab on coronary plaque composition. *J Am Coll Cardiol*. (2018) 72(17):2012–21. doi: 10.1016/j.jacc.2018.06.078

67. Nissen SE, Tuzcu EM, Schoenhagen P, Brown BG, Ganz P, Vogel RA, et al. Effect of intensive compared with moderate lipid-lowering therapy on progression of coronary atherosclerosis: a randomized controlled trial. *JAMA*. (2004) 291(9):1071–80. doi: 10.1001/jama.291.9.1071

68. Nissen SE, Nicholls SJ, Sipahi I, Libby P, Raichlen JS, Ballantyne CM, et al. Effect of very high-intensity statin therapy on regression of coronary atherosclerosis: the ASTEROID trial. *JAMA*. (2006) 295(13):1556–65. doi: 10.1001/jama.295.13.jpc60002

69. Nicholls SJ, Ballantyne CM, Barter PJ, Chapman MJ, Erbel RM, Libby P, et al. Effect of two intensive statin regimens on progression of coronary disease. *N Engl J Med*. (2011) 365(22):2078–87. doi: 10.1056/NEJMoa1110874

70. Groves EM, Seto AH, Kern MJ. Invasive testing for coronary artery disease: FFR, IVUS, OCT, NIRS. *Heart Fail Clin*. (2016) 12(1):83–95. doi: 10.1016/j.hfc.2015.08.007

71. Serruys PW, García-García HM, Buszman P, Erne P, Verheye S, Aschermann M, et al. Effects of the direct lipoprotein-associated phospholipase A(2) inhibitor darapladib on human coronary atherosclerotic plaque. *Circulation*. (2008) 118(11):1172–82. doi: 10.1161/CIRCULATIONAHA.108.771899

72. Thim T, Hagensen MK, Wallace-Bradley D, Granada JF, Kaluza GL, Drouet L, et al. Unreliable assessment of necrotic core by virtual histology intravascular ultrasound in porcine coronary artery disease. *Circ Cardiovasc Imaging*. (2010) 3(4):384–91. doi: 10.1161/CIRCIMAGING.109.919357

73. Brown AJ, Obaid DR, Costopoulos C, Parker RA, Calvert PA, Teng Z, et al. Direct comparison of virtual-histology intravascular ultrasound and optical coherence tomography imaging for identification of thin-cap fibroatheroma. *Circ Cardiovasc Imaging*. (2015) 8(10):e003487. doi: 10.1161/CIRCIMAGING.115.003487

74. Battes LC, Cheng JM, Oemrawsingh RM, Boersma E, Garcia-Garcia HM, de Boer SP, et al. Circulating cytokines in relation to the extent and composition of coronary atherosclerosis: results from the ATHEROREMO-IVUS study. *Atherosclerosis*. (2014) 236(1):18–24. doi: 10.1016/j.atherosclerosis.2014.06.010

75. Sawada T, Shite J, Shinke T, Watanabe S, Otake H, Matsumoto D, et al. Relationship between high sensitive C-reactive protein and coronary plaque component in patients with acute coronary syndrome: virtual histology study. *J Cardiol*. (2006) 48(3):141–50. PMID: 17007239.

76. Koskinas KC, Zaugg S, Yamaji K, García-García HM, Taniwaki M, Klingenberg R, et al. Changes of coronary plaque composition correlate with C-reactive protein levels in patients with ST-elevation myocardial infarction following high-intensity statin therapy. *Atherosclerosis*. (2016) 247:154–60. doi: 10.1016/j.atherosclerosis.2016.02.015

77. Hong YJ, Jeong MH, Choi YH, Cho SH, Hwang SH, Ko JS, et al. Relation between high-sensitivity C-reactive protein and coronary plaque components in patients with acute coronary syndrome: virtual histology-intravascular ultrasound analysis. *Korean Circ J*. (2011) 41(8):440–6. doi: 10.4070/kcj.2011.41.8.440

78. Cheng JM, Garcia-Garcia HM, de Boer SP, Kardys I, Heo JH, Akkerhuis KM, et al. In vivo detection of high-risk coronary plaques by radiofrequency intravascular ultrasound and cardiovascular outcome: results of the ATHEROREMO-IVUS study. *Eur Heart J*. (2014) 35(10):639–47. doi: 10.1093/eurheartj/eht484

79. Gijsen F, Katagiri Y, Barlis P, Bourantas C, Collet C, Coskun U, et al. Expert recommendations on the assessment of wall shear stress in human coronary arteries: existing methodologies, technical considerations, and clinical applications. *Eur Heart J*. (2019) 40(41):3421–33. doi: 10.1093/eurheartj/ehz551

80. Schaar JA, Regar E, Mastik F, McFadden EP, Saia F, Disco C, et al. Incidence of high-strain patterns in human coronary arteries: assessment with three-dimensional intravascular palpography and correlation with clinical presentation. *Circulation*. (2004) 109(22):2716–9. doi: 10.1161/01.CIR.0000131887.65955.3B

81. de Korte CL, Sierevogel MJ, Mastik F, Strijder C, Schaar JA, Velema E, et al. Identification of atherosclerotic plaque components with intravascular ultrasound elastography in vivo: a Yucatan pig study. *Circulation*. (2002) 105(14):1627–30. doi: 10.1161/01.CIR.0000014988.66572.2E

82. Brugaletta S, Garcia-Garcia HM, Serruys PW, Maehara A, Farooq V, Mintz GS, et al. Relationship between palpography and virtual histology in patients with acute coronary syndromes. *JACC Cardiovasc Imaging*. (2012) 5(3 Suppl):S19–27. doi: 10.1016/j.jcmg.2011.02.026

83. Gardner CM, Tan H, Hull EL, Lisauskas JB, Sum ST, Meese TM, et al. Detection of lipid core coronary plaques in autopsy specimens with a novel catheter-based near-infrared spectroscopy system. *JACC Cardiovasc Imaging*. (2008) 1(5):638–48. doi: 10.1016/j.jcmg.2008.06.001

84. Caplan JD, Waxman S, Nesto RW, Muller JE. Near-infrared spectroscopy for the detection of vulnerable coronary artery plaques. *J Am Coll Cardiol*. (2006) 47(8 Suppl):C92–6. doi: 10.1016/j.jacc.2005.12.045

85. Goldstein JA, Maini B, Dixon SR, Brilakis ES, Grines CL, Rizik DG, et al. Detection of lipid-core plaques by intracoronary near-infrared spectroscopy identifies high risk of periprocedural myocardial infarction. *Circ Cardiovasc Interv*. (2011) 4(5):429–37. doi: 10.1161/CIRCINTERVENTIONS.111.963264

86. Erlinge D, Maehara A, Ben-Yehuda O, Bøtker HE, Maeng M, Kjøller-Hansen L, et al. Identification of vulnerable plaques and patients by intracoronary near-infrared spectroscopy and ultrasound (PROSPECT II): a prospective natural history study. *Lancet*. (2021) 397(10278):985–95. doi: 10.1016/S0140-6736(21)00249-X

87. Waksman R, Di Mario C, Torguson R, Ali ZA, Singh V, Skinner WH, et al. Identification of patients and plaques vulnerable to future coronary events with near-infrared spectroscopy intravascular ultrasound imaging: a prospective, cohort study. *Lancet*. (2019) 394(10209):1629–37. doi: 10.1016/S0140-6736(19)31794-5

88. Kini AS, Baber U, Kovacic JC, Limaye A, Ali ZA, Sweeny J, et al. Changes in plaque lipid content after short-term intensive versus standard statin therapy: the YELLOW trial (reduction in yellow plaque by aggressive lipid-lowering therapy). *J Am Coll Cardiol*. (2013) 62(1):21–9. doi: 10.1016/j.jacc.2013.03.058

89. Anroedh SS, Akkerhuis KM, Oemrawsingh RM, Garcia-Garcia HM, Brankovic M, Regar E, et al. Associations of 26 circulating inflammatory and renal biomarkers with near-infrared spectroscopy and long-term cardiovascular outcome in patients undergoing coronary angiography (ATHEROREMO-NIRS substudy). *Curr Atheroscler Rep*. (2018) 20(10):52. doi: 10.1007/s11883-018-0752-8

90. Fard AM, Vacas-Jacques P, Hamidi E, Wang H, Carruth RW, Gardecki JA, et al. Optical coherence tomography–near infrared spectroscopy system and catheter for intravascular imaging. *Opt Express*. (2013) 21(25):30849–58. doi: 10.1364/OE.21.030849

91. Hoang V, Grounds J, Pham D, Virani S, Hamzeh I, Qureshi AM, et al. The role of intracoronary plaque imaging with intravascular ultrasound, optical coherence tomography, and near-infrared spectroscopy in patients with coronary artery disease. *Curr Atheroscler Rep*. (2016) 18(9):57. doi: 10.1007/s11883-016-0607-0

92. Tearney GJ, Regar E, Akasaka T, Adriaenssens T, Barlis P, Bezerra HG, et al. Consensus standards for acquisition, measurement, and reporting of intravascular optical coherence tomography studies: a report from the international working group for intravascular optical coherence tomography standardization and validation. *J Am Coll Cardiol*. (2012) 59(12):1058–72. doi: 10.1016/j.jacc.2011.09.079

93. Araki M, Park SJ, Dauerman HL, Uemura S, Kim JS, Di Mario C, et al. Optical coherence tomography in coronary atherosclerosis assessment and intervention. *Nat Rev Cardiol*. (2022) 19(10):684–703. doi: 10.1038/s41569-022-00687-9

94. Phipps JE, Vela D, Hoyt T, Halaney DL, Mancuso JJ, Buja LM, et al. Macrophages and intravascular OCT bright spots: a quantitative study. *JACC Cardiovasc Imaging*. (2015) 8(1):63–72. doi: 10.1016/j.jcmg.2014.07.027

95. Minami Y, Phipps JE, Hoyt T, Milner TE, Ong DS, Soeda T, et al. Clinical utility of quantitative bright spots analysis in patients with acute coronary syndrome: an optical coherence tomography study. *Int J Cardiovasc Imaging*. (2015) 31(8):1479–87. doi: 10.1007/s10554-015-0714-y

96. Prati F, Romagnoli E, Gatto L, La Manna A, Burzotta F, Ozaki Y, et al. Relationship between coronary plaque morphology of the left anterior descending artery and 12 months clinical outcome: the CLIMA study. *Eur Heart J*. (2020) 41(3):383–91. doi: 10.1093/eurheartj/ehz520

97. Kume T, Okura H, Yamada R, Koyama T, Fukuhara K, Kawamura A, et al. Detection of plaque neovascularization by optical coherence tomography: ex vivo feasibility study and in vivo observation in patients with angina pectoris. *J Invasive Cardiol*. (2016) 28(1):17–22. PMID: 26716590.

98. Jiang S, Fang C, Xu X, Xing L, Sun S, Peng C, et al. Identification of high-risk coronary lesions by 3-vessel optical coherence tomography. *J Am Coll Cardiol*. (2023) 81(13):1217–30. doi: 10.1016/j.jacc.2023.01.030

99. Leistner DM, Kränkel N, Meteva D, Abdelwahed YS, Seppelt C, Stähli BE, et al. Differential immunological signature at the culprit site distinguishes acute coronary syndrome with intact from acute coronary syndrome with ruptured fibrous cap: results from the prospective translational OPTICO-ACS study. *Eur Heart J*. (2020) 41(37):3549–60. doi: 10.1093/eurheartj/ehaa703

100. Gerhardt T, Seppelt C, Abdelwahed YS, Meteva D, Wolfram C, Stapmanns P, et al. Culprit plaque morphology determines inflammatory risk and clinical outcomes in acute coronary syndrome. *Eur Heart J*. (2023) 44(38):3911–25. doi: 10.1093/eurheartj/ehad334

101. Komukai K, Kubo T, Kitabata H, Matsuo Y, Ozaki Y, Takarada S, et al. Effect of atorvastatin therapy on fibrous cap thickness in coronary atherosclerotic plaque as assessed by optical coherence tomography: the EASY-FIT study. *J Am Coll Cardiol*. (2014) 64(21):2207–17. doi: 10.1016/j.jacc.2014.08.045

102. Nicholls SJ, Kataoka Y, Nissen SE, Prati F, Windecker S, Puri R, et al. Effect of evolocumab on coronary plaque phenotype and burden in statin-treated patients following myocardial infarction. *JACC Cardiovasc Imaging*. (2022) 15(7):1308–21. doi: 10.1016/j.jcmg.2022.03.002

103. Liu L, Gardecki JA, Nadkarni SK, Toussaint JD, Yagi Y, Bouma BE, et al. Imaging the subcellular structure of human coronary atherosclerosis using micro-optical coherence tomography. *Nat Med*. (2011) 17(8):1010–4. doi: 10.1038/nm.2409

104. Yin B, Piao Z, Nishimiya K, Hyun C, Gardecki JA, Mauskapf A, et al. 3D cellular-resolution imaging in arteries using few-mode interferometry. *Light Sci Appl*. (2019) 8:104. doi: 10.1038/s41377-019-0211-5

105. Nishimiya K, Tearney G. Micro optical coherence tomography for coronary imaging. *Front Cardiovasc Med*. (2021) 8:613400. doi: 10.3389/fcvm.2021.613400

106. Khraishah H, Jaffer FA. Intravascular molecular imaging: near-infrared fluorescence as a new frontier. *Front Cardiovasc Med*. (2020) 7:587100. doi: 10.3389/fcvm.2020.587100

107. Jaffer FA, Kim DE, Quinti L, Tung CH, Aikawa E, Pande AN, et al. Optical visualization of cathepsin K activity in atherosclerosis with a novel, protease-activatable fluorescence sensor. *Circulation*. (2007) 115(17):2292–8. doi: 10.1161/CIRCULATIONAHA.106.660340

108. Vinegoni C, Botnaru I, Aikawa E, Calfon MA, Iwamoto Y, Folco EJ, et al. Indocyanine green enables near-infrared fluorescence imaging of lipid-rich, inflamed atherosclerotic plaques. *Sci Transl Med*. (2011) 3(84):84ra45. doi: 10.1126/scitranslmed.3001577

109. Calfon MA, Vinegoni C, Ntziachristos V, Jaffer FA. Intravascular near-infrared fluorescence molecular imaging of atherosclerosis: toward coronary arterial visualization of biologically high-risk plaques. *J Biomed Opt*. (2010) 15(1):011107. doi: 10.1117/1.3280282

110. Jaffer FA, Weissleder R. Seeing within: molecular imaging of the cardiovascular system. *Circ Res*. (2004) 94(4):433–45. doi: 10.1161/01.RES.0000119321.18573.5A

111. Chen J, Tung CH, Mahmood U, Ntziachristos V, Gyurko R, Fishman MC, et al. In vivo imaging of proteolytic activity in atherosclerosis. *Circulation*. (2002) 105(23):2766–71. doi: 10.1161/01.CIR.0000017860.20619.23

112. Jaffer FA, Vinegoni C, John MC, Aikawa E, Gold HK, Finn AV, et al. Real-time catheter molecular sensing of inflammation in proteolytically active atherosclerosis. *Circulation*. (2008) 118(18):1802–9. doi: 10.1161/CIRCULATIONAHA.108.785881

113. Deguchi JO, Aikawa M, Tung CH, Aikawa E, Kim DE, Ntziachristos V, et al. Inflammation in atherosclerosis: visualizing matrix metalloproteinase action in

macrophages in vivo. *Circulation*. (2006) 114(1):55–62. doi: 10.1161/CIRCULATIONAHA.106.619056

114. Wallis de Vries BM, Hillebrands JL, van Dam GM, Tio RA, de Jong JS, Slart RH, et al. Images in cardiovascular medicine. Multispectral near-infrared fluorescence molecular imaging of matrix metalloproteinases in a human carotid plaque using a matrix-degrading metalloproteinase-sensitive activatable fluorescent probe. *Circulation*. (2009) 119(20):e534–6. doi: 10.1161/CIRCULATIONAHA.108.821389

115. Verjans JW, Osborn EA, Ughi GJ, Calfon Press MA, Hamidi E, Antoniadis AP, et al. Targeted near-infrared fluorescence imaging of atherosclerosis: clinical and intracoronary evaluation of indocyanine green. *JACC Cardiovasc Imaging*. (2016) 9 (9):1087–95. doi: 10.1016/j.jcmg.2016.01.034

116. McCarthy JR, Patel P, Botnaru I, Haghayeghi P, Weissleder R, Jaffer FA. Multimodal nanoagents for the detection of intravascular thrombi. *Bioconjug Chem*. (2009) 20(6):1251–5. doi: 10.1021/bc9001163

117. Hara T, Bhayana B, Thompson B, Kessinger CW, Khatri A, McCarthy JR, et al. Molecular imaging of fibrin deposition in deep vein thrombosis using fibrin-targeted near-infrared fluorescence. *JACC Cardiovasc Imaging*. (2012) 5(6):607–15. doi: 10.1016/j.jcmg.2012.01.017

118. Tung CH, Gerszten RE, Jaffer FA, Weissleder R. A novel near-infrared fluorescence sensor for detection of thrombin activation in blood. *Chembiochem*. (2002) 3(2–3):207–11. doi: 10.1002/1439-7633(20020301)3:2/3<207::AID-CBIC207>3.0.CO;2-B

119. Hara T, Ughi GJ, McCarthy JR, Erdem SS, Mauskapf A, Lyon SC, et al. Intravascular fibrin molecular imaging improves the detection of unhealed stents assessed by optical coherence tomography in vivo. *Eur Heart J*. (2017) 38 (6):447–55. doi: 10.1038/nm.2555

120. Yoo H, Kim JW, Shishkov M, Namati E, Morse T, Shubochkin R, et al. Intra-arterial catheter for simultaneous microstructural and molecular imaging in vivo. *Nat Med*. (2011) 17(12):1680–4. doi: 10.1038/nm.2555

121. Bourantas CV, Jaffer FA, Gijsen FJ, van Soest G, Madden SP, Courtney BK, et al. Hybrid intravascular imaging: recent advances, technical considerations, and current applications in the study of plaque pathophysiology. *Eur Heart J*. (2017) 38 (6):400–12. doi: 10.1093/eurheartj/ehw097

122. Ughi GJ, Wang H, Gerbaud E, Gardecki JA, Fard AM, Hamidi E, et al. Clinical characterization of coronary atherosclerosis with dual-modality OCT and near-infrared autofluorescence imaging. *JACC Cardiovasc Imaging*. (2016) 9(11):1304–14. doi: 10.1016/j.jcmg.2015.11.020

123. Wang H, Gardecki JA, Ughi GJ, Jacques PV, Hamidi E, Tearney GJ. Ex vivo catheter-based imaging of coronary atherosclerosis using multimodality OCT and NIRAF excited at 633 nm. *Biomed Opt Express*. (2015) 6(4):1363–75. doi: 10.1364/BOE.6.001363

124. Knuuti J, Wijns W, Saraste A, Capodanno D, Barbato E, Funck-Brentano C, et al. 2019 ESC guidelines for the diagnosis and management of chronic coronary syndromes. *Eur Heart J*. (2020) 41(3):407–77. doi: 10.1093/eurheartj/ehz425

125. Gallone G, Bellettini M, Gatti M, Tore D, Bruno F, Scudeler L, et al. Coronary plaque characteristics associated with major adverse cardiovascular events in atherosclerotic patients and lesions: a systematic review and meta-analysis. *JACC Cardiovasc Imaging*. (2023) 16(12):1584–1604. doi: 10.1016/j.jcmg.2023.08.006

126. Kuroda M, Shinke T, Sakaguchi K, Otake H, Takaya T, Hirota Y, et al. Effect of daily glucose fluctuation on coronary plaque vulnerability in patients pre-treated with lipid-lowering therapy: a prospective observational study. *JACC Cardiovasc Interv*. (2015) 8(6):800–11. doi: 10.1016/j.jcin.2014.11.025

frontiers | Frontiers in Cardiovascular Medicine

TYPE Original Research
PUBLISHED 01 February 2024
DOI 10.3389/fcvm.2023.1335572

OPEN ACCESS

EDITED BY
Tommaso Gori,
University Medical Centre, Johannes Gutenberg University Mainz, Germany

REVIEWED BY
Simone Brogi,
University of Pisa, Italy
Cláudio Lera Orsatti,
University of Western São Paulo, Brazil

*CORRESPONDENCE
Shan Zhang
✉ zs648368310@outlook.com

RECEIVED 09 November 2023
ACCEPTED 26 December 2023
PUBLISHED 01 February 2024

CITATION
Xu X, Li D and Zhang S (2024) Retrospective study for correlation analysis of nutritional status with osteoporosis, sarcopenia and cognitive impairment in elderly patients with coronary heart disease.
Front. Cardiovasc. Med. 10:1335572.
doi: 10.3389/fcvm.2023.1335572

Retrospective study for correlation analysis of nutritional status with osteoporosis, sarcopenia and cognitive impairment in elderly patients with coronary heart disease

Xiao Xu, Daohong Li and Shan Zhang*

Department of Geriatric, Suzhou Ninth People's Hospital, Suzhou, Jiangsu, China

Coronary heart disease (CHD) is an abbreviation of coronary atherosclerotic heart disease, which remains challenging for diagnosis and treatment. Current study aims to explore the correlation between geriatric nutritional risk index (GNRI) and osteoporosis, sarcopenia, cognitive dysfunction in elderly patients with CHD, and to analyze the clinical diagnostic value of GNRI in the above complications. A total of 92 elderly patients with CHD treated in Suzhou Ninth People's Hospital from January 2020 to October 2023 were retrospectively collected as the experimental group, and 68 non-CHD subjects matched for sex and age in the same period of physical examination were randomly selected as the control group. Osteoporosis, sarcopenia and cognitive dysfunction were analyzed in all patients, and the correlation between GNRI and these indices in different populations was analyzed by Spearman's rank correlation. The diagnostic efficacy of GNRI in osteoporosis, sarcopenia, and cognitive impairment was analyzed by ROC curves. There was no significant difference in age, sex distribution, body mass index (BMI) and serum biological indexes between the elderly patients with CHD and the control group (all $P > 0.05$). Correlation analysis showed that GNRI level was positively correlated with bone mineral content (BMC), bone mineral density (BMD) T value and osteocalcin (OCN) (All $r > 0$, $P < 0.05$). In addition, GNRI levels were positively correlated with skeletal muscle mass (ASMI), grip strength and calf circumference (CC) (All $r > 0$, $P < 0.05$). However, there was no significant correlation between GNRI levels and cognitive dysfunction-related indicators ($P > 0.05$). In the elderly and elderly with CHD, the diagnostic AUC of GNRI was 0.875 and 0.862 in osteoporosis, and 0.912 and 0.932 in sarcopenia, respectively. The level of GNRI is significantly correlated with osteoporosis and sarcopenia. GNRI level, as an auxiliary diagnostic tool in elderly patients with CHD, exerts important clinical significance for early detection of the risk of complications, such as osteoporosis and sarcopenia.

KEYWORDS

coronary heart disease, nutritional risk index for the elderly, osteoporosis, sarcopenia, cognitive impairment

1 Introduction

Coronary heart disease (CHD) is an abbreviation of coronary atherosclerotic heart disease, which is a heart disease caused by stenosis, spasm and even occlusion of the vascular lumen due to atherosclerotic lesions of coronary arteries, resulting in myocardial ischemia, hypoxia or necrosis (1). In recent years, the incidence of CHD has increased year by year, seriously endangering human health (2). Elderly patients with CHD are in a state of cardiac insufficiency for a long time, physiology and metabolism are affected to some extent, and are prone to malnutrition (3). Malnutrition is a common comorbidity in elderly patients, particularly in the elderly population, with adverse effects on the short- and long-term prognosis of patients (4). Nutritional status is affected in many ways, and poor nutritional status can exacerbate the severity of the disease in patients (5). Malnutrition and CHD interact to affect patient outcomes (5). Studies evaluating the nutritional status of patients have shown that elderly patients with poor nutritional status are higher than those with normal nutritional status in terms of infection incidence, case fatality, length of stay and medical costs (6).

Malnutrition in elderly patients with CHD predisposes to other complications (6). Osteoporosis is more common in the elderly, characterized by increased bone fragility and decreased bone mineral density (7). The etiology of osteoporosis is complex, among which malnutrition is an important cause, while the elderly are more prone to malnutrition due to physiological decline, poor dietary compliance and many underlying diseases (8). In addition, malnutrition is extremely common in elderly patients, mainly manifested by loss of muscle content and thus predisposes to the development of sarcopenia (9). Sarcopenia is the most common health problem in the elderly population and is one of the important causes leading to falls, fractures and decreased cardiopulmonary function in the elderly (9). Since the onset of sarcopenia is insidious and there are no obvious clinical symptoms in the early stage, most patients with sarcopenia are not actively diagnosed and treated (10). Early screening for sarcopenia and timely intervention are beneficial to improve clinical outcomes in elderly patients with CHD (11). In addition, sarcopenia may be related to cardiac function in patients, and chronic heart failure is a risk factor for the development of sarcopenia (12). Furthermore, CHD is tightly associated with the development of cognitive impairment, with an average 45% increased the risks of cognitive impairment or dementia in patients with CHD (13, 14). Studies by Greaves et al. showed that approximately 40% of patients with CHD undergoing cardiac bypass surgery were diagnosed with cognitive impairment within 1–5 years after surgery (15). Cognitive impairment occurred in 42.4% of patients with stable CHD after 4 years of follow-up (16).

Analyzing the correlation between malnutrition and osteoporosis, sarcopenia, cognitive impairment in elderly patients with CHD is helpful to intervene pertinently and reduce the occurrence and development of the above complications in elderly patients with CHD. However, studies on malnutrition in elderly patients with CHD have focused on patients with diabetes mellitus, lung infection, tumor, or perioperative period (17, 18), and studies on nutritional status in elderly patients with osteoporosis, sarcopenia, and cognitive impairment are lacking.

In this study, we try to analyze the relationship between nutritional status and osteoporosis, sarcopenia and cognitive dysfunction in elderly patients with CHD. At the same time, the predictive value of nutritional status on complications, such as osteoporosis, sarcopenia and cognitive impairment in elderly patients with CHD, was also explored in order to provide theoretical basis for early intervention.

2 Data and methods

2.1 Clinical data

A total of 92 elderly patients with CHD treated in Suzhou Ninth People's Hospital from January 2020 to October 2023 were retrospectively collected as the experimental group, and 68 non-CHD subjects matched for sex and age in the same period of physical examination were randomly selected as the control group (Figure 1).

Inclusion criteria of case group: (1) Age ≥60 years old; (2) The patients met the diagnostic criteria of CHD and were diagnosed as CHD by coronary angiography; (3) The clinical data of the patients are complete; (4) Sign the informed consent form.

Inclusion criteria of control group: (1) Age ≥60 years old; (2) Patients did not meet the diagnostic criteria of CHD; (3) The clinical data of the patients are complete; (4) Sign the informed consent form.

Exclusion criteria: (1) Atrial fibrillation, supraventricular tachycardia, pacemaker pacing rhythm; (2) Patients with autoimmune diseases and severe acute and chronic infectious diseases; (3) Patients with malignant tumors and hematological diseases; (4) End-stage elderly patients who have received radiotherapy, chemotherapy and hormone therapy; (5) Endocrine diseases such as hypothyroidism and hyperthyroidism, long-term use of glucocorticoids or surgery may affect bone mineral density; (6) Patients with routine anti-osteoporosis treatment.

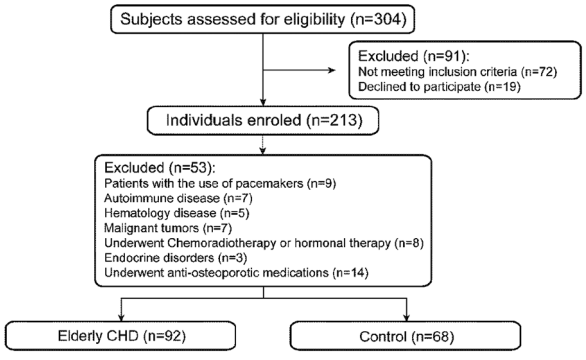

FIGURE 1
Flow diagram illustrating selection of study participants.

2.2 Methods

2.2.1 Examination of general clinical data

General data such as sex, age and blood pressure of the two groups were collected. Height and weight were measured and BMI was calculated. Venous blood samples were collected overnight for more than 10 h, and metabolic parameters including fasting blood glucose level (FBGL), total cholesterol (TC), triglyceride (TG), high density lipoprotein cholesterol (HDL-C), low density lipoprotein cholesterol (LDL-C) and serum albumin were measured by Siemens ADVIA 2400 automatic biochemical analyzer.

2.2.2 Bone metabolism parameters

BMC and BMD T value were measured with Lunar-DPX-MD DXA from GE company. The T value of BMD of L1-L4 vertebrae in each patient was measured in anteroposterior position. According to WHO diagnostic criteria, osteoporosis is diagnosed if the T value of bone mineral density is ≤−2.5 SD (19). The serum OCN levels were measured by enzyme-linked immunosorbent assay (ELISA) method. The parameters of bone metabolism, including procollagen of type I N-propeptide (P1NP), β-isomerized C-terminal telopeptides (β-CTX), 25-hydroxyvitamin D (25-OH-D) and parathyroid hormone (PTH), were measured by Swiss Roche electrochemiluminescence analyzer Cobas e602.Geriatric Nutritional Risk Index (GNRI) = 1.489 × serum albumin + 41.7 × (body weight/ideal body weight). Male ideal weight = 0.75 × height-62.5, female ideal weight = 0.6 × height-40.

2.2.3 Examination of metabolic parameters in sarcopenia

Skeletal muscle mass (ASM) and percent total body fat (TBF%) of the extremities were measured using GE Lunar-DPX-MD DXA. Skeletal muscle mass index (ASMI) of extremities = ASM/Height^2. Grip strength and gait speed were used to measure muscle strength and area-provided energy, respectively. Grip strength was tested by grip strength meter CamryEH101. All subjects underwent a 6-m reentrant movement measurement of gait speed. The calf circumference (CC) was measured with an inelastic band at a resolution of 1 mm, measured by researchers trained in standardized measurements. Waist to hip ratio (WHR) = waist/hip circumference.

2.2.4 Cognitive function test

The subjects' overall cognitive function was assessed using the Mini-Mental State Examination (MMSE) and Montreal Cognitive Assessment Scale (MoCA). The MMSE and MoCA scale assessments were completed by two deputy chief physicians. The MMSE scores included language, calculation, visuospatial, place orientation, time orientation, attention, immediate memory, delayed memory and so on, with a total of 30 items, with a total score of 30. The score was positively correlated with the level of cognitive status, and MMSE <27 was judged as cognitive impairment. The MoCA scale included 8 cognitive assessments of visuospatial executive ability, naming, memory, attention, language fluency, abstract thinking, delayed memory, orientation and so on, with a total of 30 points. The score was positively correlated with the level of cognitive status, and MoCA <27 was judged as cognitive impairment.

2.3 Statistical analysis

The data were analyzed by SPSS 27.0 software. The measurement data of normal distribution are expressed as x ± s, and the data of normal distribution are expressed as medians (first quartile, third quartile). Independent sample *t*-test was used for comparison between the two groups. Counting data were expressed by number and percentage, and $\chi 2$ test was used for comparison between the two groups. Correlation analysis was performed by Spearman rank correlation. Diagnostic power analysis was performed by ROC curves. $P < 0.05$ was statistically significant.

3 Results

3.1 Analysis of general data of elderly patients with CHD

According to the inclusion and exclusion criteria, 92 elderly patients with CHD and 68 controls were included in this study. There were 38 males and 54 females in the elderly patients with CHD, while 33 males and 35 females in the control group. There was no significant difference in the sex ratio between the two groups ($P > 0.05$). The results showed that systolic blood pressure (SBP), diastolic blood pressure (DBP) and fasting blood glucose level (FBGL) were non-normal distribution, and other data obeyed normal distribution. Mann–Whitney *U* rank sum test (statistic is Z) or independent sample t test (statistic is t) will be performed for measurement data, and the results are shown in Table 1. The height and weight of the elderly patients with CHD were significantly lower than those of the control group (all $P < 0.01$). In addition, there were no significant differences in age, BMI, blood pressure,

TABLE 1 Comparison of general data between elderly patients with CHD and control subjects.

Characteristic	Elderly CHD group ($n = 92$)	Control group ($n = 68$)	t/Z	*P*
Sex (male/female)	38/54	33/35	0.909	0.363
Age	71.71 ± 7.37	70.04 ± 4.57	1.755	0.081
Height	162.25 ± 7.10	166.72 ± 5.70	−4.412	<0.001
Body weight	57.18 ± 9.62	61.13 ± 5.52	−3.273	0.001
BMI	21.68 ± 3.17	22.01 ± 1.97	−0.813	0.448
Systolic blood pressure	116.00 (105.25, 129.00)	116.00 (103.00, 130.75)	−0.116	0.908
Diastolic blood pressure	74.00 (68.00, 82.00)	77.00 (68.25, 84.75)	−0.884	0.377
TG (mmol/L)	1.54 ± 0.69	1.76 ± 0.70	−1.977	0.050
TC (mmol/L)	4.41 ± 1.23	4.24 ± 1.14	0.893	0.373
HDL-C (mmol/L)	1.20 ± 0.21	1.22 ± 0.23	−0.481	0.632
LDL-C (mmol/L)	2.53 ± 0.80	2.48 ± 0.70	0.414	0.679
Serum albumin (g/L)	32.95 ± 5.38	32.66 ± 6.53	0.304	0.762
FBGL (mmol/L)	5.40 (5.10, 5.80)	5.50 (5.00, 6.08)	−0.832	0.406

lipid-related indexes, serum albumin level and FBGL between the elderly patients with CHD and the control group (all $P > 0.05$).

3.2 Relationship between nutritional status and osteoporosis in elderly patients with CHD

Spearman rank correlation was used to analyze the correlation between GNRI and different osteoporosis-related indexes. As shown in Table 2, GNRI in the total population was positively correlated with BMC, BMD T value, OCN and P1NP (All $r > 0$, $P < 0.05$), and negatively correlated with β-CTX and PTH (All $r < 0$, $P < 0.05$). Similarly, GNRI was positively correlated with BMC, BMD T value, OCN and P1NP (All $r > 0$, $P < 0.05$), but negatively correlated with β-CTX and PTH (All $r < 0$, $P < 0.01$).In addition, GNRI did not show significant correlations with P1NP or β-CTX in the control population (both $P > 0.05$). These results collectively suggested that the nutritional status was significantly correlated with the related indexes of osteoporosis.

3.3 Relationship between nutritional status and sarcopenia in elderly patients with CHD

Spearman rank correlation was used to analyze the correlation between GNRI and different sarcopenia-related indicators. As shown in Table 3, there was a significant positive correlation between GNRI and ASMI, grip strength and CC in the total population (All $r > 0$, $P < 0.05$), but not with gait speed, WHR and TBF% (All $P > 0.05$). In addition, GNRI was positively correlated with grip strength, gait speed and CC (All $r > 0$, $P < 0.05$), but not with ASMI, WHR and TBF% (All $P > 0.05$). Interestingly, in the control population, GNRI showed a significant positive correlation only with ASMI ($r > 0$, $P < 0.05$), but not with other sarcopenia-related indicators (all $P > 0.05$).

3.4 Relationship between nutritional status and cognitive impairment in elderly patients with CHD

Spearman's rank correlation was used to analyze the correlation between GNRI and different cognitive function-related indicators. As shown in Table 4, there was no significant correlation between GNRI and MMSE or Mo CA in the total population (All $P > 0.05$). Interestingly, there was a significant negative correlation between GNRI and Mo CA in the control population ($r < 0$, $P < 0.05$), possibly related to the small sample size. In addition, there was no significant correlation between GNRI and MMSE or MoCA scores in elderly patients with CHD (All $P > 0.05$).

TABLE 2 Correlation analysis between GNRI and osteoporosis-related indicators.

Variables	Total population		Elderly CHD group		Control group	
	r	*P*	*r*	*P*	*r*	*P*
BMC	0.421	<0.001	0.435	<0.001	0.409	<0.001
BMD T value	0.475	<0.001	0.439	<0.001	0.554	<0.001
OCN	0.503	<0.001	0.559	<0.001	0.420	<0.001
P1NP	0.170	0.031	0.268	0.010	0.009	0.944
β-CTX	−0.172	0.029	−0.307	0.003	0.037	0.762
25-OH-D	0.012	0.885	0.043	0.683	−0.036	0.770
PTH	−0.347	<0.001	−0.341	<0.001	−0.353	0.003

TABLE 3 Correlation between GNRI and sarcopenia.

Variables	Total population		Elderly CHD group		Control group	
	r	*P*	*r*	*P*	*r*	*P*
ASMI	0.234	0.003	0.203	0.052	0.275	0.023
Grip strength	0.231	0.003	0.227	0.030	0.236	0.053
Gait speed	0.147	0.063	0.268	0.010	−0.052	0.671
CC	0.181	0.022	0.312	0.002	0.018	0.885
WHR	−0.003	0.972	−0.008	0.938	0.010	0.937
TBF%	0.071	0.374	−0.018	0.865	0.190	0.122

3.5 Predictive value of GNRI in osteoporosis, sarcopenia or cognitive impairment in elderly patients with CHD

The diagnostic efficacy of nutritional status in osteoporosis, sarcopenia, or cognitive impairment was analyzed by ROC curves in the total population and in the elderly with CHD.As shown in Figure 2 and Table 5, the diagnostic AUCs of GNRI for osteoporosis and sarcopenia in the total population were 0.875 and 0.912, respectively. In addition, the diagnostic sensitivity was 82.5% and 88.6%, and the diagnostic specificity was 79.4% and 88.8%, respectively. Similarly, GNRI showed high diagnostic AUC, sensitivity, and specificity in both osteoporosis and sarcopenia in the elderly population with CHD. In particular, when the Youden index was 0.890, the sensitivity of GNRI in the diagnosis of sarcopenia reached 100%. These results collectively suggested that GNRI has the potential to be an early diagnostic modality for osteoporosis and sarcopenia. In addition, the AUCs of GNRI in the diagnosis of cognitive impairment were only 0.562 and 0.583 in the total population and in the elderly population with CHD, respectively, indicating that the nutritional status of patients has no potential diagnostic value for cognitive impairment.

4 Discussion

CHD is a heart disease caused by a variety of factors leading to atherosclerosis of coronary arteries, leading to stenosis or even

TABLE 4 Correlation analysis between GNRI and different cognitive function-related indicators.

Variables	Total population		Elderly CHD group		Control group	
	r	*P*	*r*	*P*	*r*	*P*
MMSE	−0.048	0.547	−0.021	0.843	−0.118	0.337
MoCA	0.028	0.722	0.081	0.443	−0.240	0.048

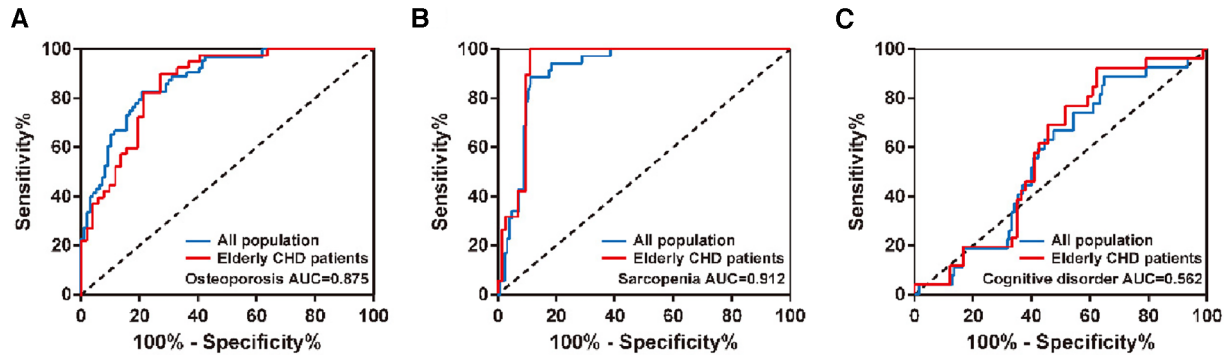

FIGURE 2
ROC curves of GNRI in the diagnosis of (A) osteoporosis, (B) sarcopenia, or (C) cognitive impairment in different populations.

occlusion of the vascular lumen, followed by myocardial hypoxia, ischemia or necrosis (2). In recent years, the incidence of cardiovascular diseases is still rising sharply, about 2.5% worldwide. Nine billion people suffer from cardiovascular disease, 1.1 million of whom are patients with CHD (20). With the development of medical level and improvement of surgical technical concept, the mortality and complication rate of CHD in the elderly have been greatly reduced, but risk factors need to be strictly controlled to improve the prognosis (21). The poor nutritional status of elderly patients with CHD is related to aging, cardiac insufficiency, malabsorption of nutrients due to gastrointestinal congestion, multiple concomitant underlying diseases and polypharmacy (22). In recent years, more studies have shown that nutritional status is associated with the prognosis of CHD (23). In addition, malnutrition is prone to the occurrence of various prognostic complications, such as osteoporosis, sarcopenia and cognitive impairment. The GNRI is a nutritional assessment index based on serum albumin and BMI. GNRIs are primarily used to assess the risk of complications associated with malnutrition in the elderly population (24). Unlike other nutritional indicators, GNRI is obtained by calculation of albumin, height, and weight, is easy to perform, is less affected by subjective factors, and has good inter-rater agreement (25). GNRI was first proposed by BOWEN et al. in 2005 to predict malnutrition-related complications (pressure ulcers and infections) and mortality in hospitalized elderly patients (26).

Therefore, the purpose of this study was to investigate the correlation between GNRI and osteoporosis, sarcopenia, cognitive dysfunction in elderly patients with CHD, and to analyze the diagnostic efficacy of GNRI in osteoporosis, sarcopenia and cognitive dysfunction by ROC curve.

A total of 92 elderly patients with CHD and 68 control patients were included in this study. Firstly, the clinical data of the two groups were analyzed. There was no significant difference in age distribution and sex composition between the elderly patients with CHD and the control group ($P > 0.05$). In addition, the height and weight of the elderly patients with CHD were significantly lower than those of the control group (both $P < 0.01$), but the BMI level was not significantly different between the two groups ($P > 0.05$). In addition, there were no significant differences in age, BMI, blood pressure, lipid-related indexes, serum albumin level and FBGL between the elderly patients with CHD and the control group (all $P > 0.05$). There was no significant difference in the general clinical data between the elderly patients with CHD and the control group, indicating the feasibility of the study. Therefore, we further analyzed the association of GNRI with osteoporosis, sarcopenia, and cognitive impairment in different populations.

Due to the decline of body function, poor digestive and absorption function, the incidence of malnutrition is high. Malnutrition can lead to insufficient absorption of trace elements such as calcium, phosphorus, zinc, magnesium, copper, imbalance of bone metabolism, and lead to osteoporosis. The results of Spearman's rank correlation analysis showed that GNRI was positively correlated with BMC, BMD T value, OCN and P1NP, but negatively correlated with β-CTX and PTH, suggesting that the nutritional status of the elderly population was significantly correlated with the occurrence and development of osteoporosis. In recent years, many studies have found a close

TABLE 5 Diagnostic efficacy of GNRI in osteoporosis, sarcopenia, or cognitive impairment.

Population	Indication	AUC (95% CI)	Youden index	Sensitivity (%)	Specificity (%)	*P* value
Total population	Osteoporosis	0.875 (0.823, 0.928)	0.619	82.5	79.4	<0.001
	Sarcopenia	0.912 (0.866, 0.957)	0.774	88.6	88.8	<0.001
	Cognitive disorder	0.562 (0.457, 0.667)	0.242	88.9	35.3	0.311
Elderly CHD patients	Osteoporosis	0.862 (0.788, 0.935)	0.631	90.0	73.1	<0.001
	Sarcopenia	0.932 (0.880, 0.983)	0.890	100.0	89.0	<0.001
	Cognitive disorder	0.583 (0.464, 0.702)	0.302	92.3	37.9	0.218

relationship between CHD and osteoporosis (27, 28). Samelson et al. have shown a higher incidence of CHD in women with low bone mineral density (28). Marcovitz et al. used coronary angiography to evaluate the degree of coronary stenosis in 209 patients. Current results showed that osteoporosis or osteopenia were independent risk factors for CHD in the elderly population, and the highest relative risk of osteoporosis was found in multivariate analysis of traditional risk factors of osteoporosis and CHD (e.g., diabetes mellitus, hypertension, smoking, hyperlipidemia, family history of cardiovascular disease, etc.) (27, 28). In this study, both GNRI and osteoporosis-related indicators in the elderly population with CHD showed significant correlations, consistent with previous findings (27, 28).

Previous studies have confirmed that nutritional factors are closely related to osteoporosis, as well as nutrition-related diseases such as sarcopenia, and that sarcopenia and osteoporosis share many of the same pathogenesis (29, 30). In addition, studies have shown that nutrient deficiency and malnutrition are also important risk factors for sarcopenia, such as vitamin D, vitamin A and mineral deficiencies (31). In this study, GNRI was positively correlated with ASMI, grip strength, CC and other sarcopenia-related indicators in the total population, suggesting that the nutritional status of the elderly population is significantly correlated with the occurrence of sarcopenia. Because elderly people are also at high risk for cardiovascular disease, comorbidities of sarcopenia and cardiovascular disease are common. Sarcopenia is an important complication of abnormal cardiac functions, which in turn can accelerate the occurrence of sarcopenia (32). Sarcopenia has been shown to be an independent predictor of decreased cardiac function in patients with chronic heart failure (33). Chronic heart failure can contribute to the development of sarcopenia through a variety of pathophysiological mechanisms, including malnutrition and inflammation (34). The results of Spearman's rank correlation analysis showed that GNRI was significantly correlated with sarcopenia-related indexes such as grip strength, gait speed and CC in elderly patients with CHD. We hypothesize that as nutritional risk increases in patients with CHD, heart failure progresses and cardiac function further declines, and skeletal muscle mass progresses to sarcopenia. The occurrence of sarcopenia may be due to decreased muscle strength and affect motor function, resulting in dyspnea and decreased cardiac function, further exacerbating heart failure.

There are few studies on the association between nutritional status and cognitive impairment. Some studies have suggested that nutritional status predicts mortality and the probability of complications in patients with mild cognitive impairment (35, 36). In addition, some studies have shown a 23% risk of malnutrition in patients with mild cognitive impairment (35). At the same time, malnutrition can also promote negative emotions, exacerbate their cognitive impairment and reduce their quality of life (36). However, the results of this study showed no significant correlation between GNRI and cognitive function-related measures in the elderly or elderly with CHD, suggesting no potential link between nutritional status and the development of cognitive dysfunctions in patients.

GNRI was associated with osteoporosis and sarcopenia. Thus, osteoporosis and sarcopenia can be predicted by GNRI. Therefore, we analyzed the diagnostic efficacy of GNRI for osteoporosis, sarcopenia, and cognitive impairment in different populations by ROC curves. GNRI predicted the largest area under the ROC curve for sarcopenia, both in the elderly and in the elderly with CHD. In addition, the sensitivity of GNRI in the diagnosis of sarcopenia reached 100% in elderly patients with CHD, indicating that there were no missed cases. In addition, GNRI also showed high diagnostic efficacy for osteoporosis in different populations. From the point of view of human anatomy, skeleton and muscle are adjacent. Common factors regulating osteoporosis and sarcopenia include nutritional factors, genetic factors, endocrine factors and disease factors, and they have closely related signaling pathways and common targets. This may also account for the similar diagnostic efficacy of GNRI in osteoporosis and sarcopenia. In addition, the low AUC of GNRI in the diagnosis of cognitive impairment in different populations suggests that the nutritional status of patients has no potential diagnostic value for cognitive impairment.

The study has the following limitations: (1) This study is a single-center, retrospective, observational study, which is limited to some extent by the clinical data of patients, and inaccurate description will interfere with the results. For the inaccurate data recorded, it may lead to the deviation of one item in CHD group or control group, further resulting in the difference of this indicator or inaccurate correlation analysis results; (2) The sample size is relatively small, and there is some bias in the process of retrospective data collection; (3) At present, there are few reports on this topic, so it is difficult to compare with other studies of the same type and analyze the similarities and differences between different studies.

In conclusion, the nutritional status in elderly patients with CHD is significantly associated with the development of osteoporosis and sarcopenia, with higher nutritional risk as well as the higher risk indicators-related to osteoporosis and sarcopenia. GNRI can be used as an early diagnostic modality for the complications of osteoporosis and sarcopenia in elderly patients with CHD, and has important significance in improving the clinical prognosis of CHD and preventing the occurrence of osteoporosis and sarcopenia.

Data availability statement

The raw data supporting the conclusions of this article will be made available by the authors, without undue reservation.

Ethics statement

The research related to human use has been complied with all the relevant national regulations, institutional policies and in accordance with the tenets of the Helsinki Declaration, and has been approved by the ethnical committee of Suzhou Ninth People's Hospital with approval No. KYLW2023-046-01.

Author contributions

XX: Conceptualization, Data curation, Formal Analysis, Investigation, Methodology, Writing – original draft, Writing – review & editing. DL: Project administration, Validation, Writing – original draft, Writing – review & editing. SZ: Resources, Supervision, Writing – original draft, Writing – review & editing.

Funding

The authors declare financial support was received for the research, authorship, and/or publication of this article.

This work was supported by Clinical Technology Application Research Project Construction Unit (project number LD2021030).

Conflict of interest

The authors declare that the research was conducted in the absence of any commercial or financial relationships that could be construed as a potential conflict of interest.

Publisher's note

References

1. Menotti A, Puddu PE, Kromhout D, Kafatos A, Tolonen H. Coronary heart disease mortality trends during 50 years as explained by risk factor changes: the European cohorts of the seven countries study. *Eur J Prev Cardiol*. (2020) 27 (9):988–98. doi: 10.1177/2047487318821250

2. Moerschel KS, De Bacquer D, De Backer G, Wood D, Kotseva K, Wellmann J, et al. Assessing the probability of risk factor control in patients with coronary heart disease: results from the ESC-EORP EUROASPIRE V survey. *Eur J Prev Cardiol*. (2022) 29(10):1465–75. doi: 10.1093/eurjpc/zwac079

3. Liu J, Huang Z, Huang H, He Y, Yu Y, Chen G, et al. Malnutrition in patients with coronary artery disease: prevalence and mortality in a 46,485 Chinese cohort study. *Nutr Metab Cardiovasc Dis*. (2022) 32(5):1186–94. doi: 10.1016/j.numecd.2021.12.023

4. Houston M. The role of noninvasive cardiovascular testing, applied clinical nutrition and nutritional supplements in the prevention and treatment of coronary heart disease. *Ther Adv Cardiovasc Dis*. (2018) 12(3):85–108. doi: 10.1177/1753944717743920

5. Eilat-Adar S, Goldbourt U. Nutritional recommendations for preventing coronary heart disease in women: evidence concerning whole foods and supplements. *Nutr Metab Cardiovasc Dis*. (2010) 20(6):459–66. doi: 10.1016/j.numecd.2010.01.011

6. Marshall S, Bauer J, Isenring E. The consequences of malnutrition following discharge from rehabilitation to the community: a systematic review of current evidence in older adults. *J Hum Nutr Diet*. (2014) 27(2):133–41. doi: 10.1111/jhn.12167

7. Miller PD. Management of severe osteoporosis. *Expert Opin Pharmacother*. (2016) 17(4):473–88. doi: 10.1517/14656566.2016.1124856

8. Aspray TJ, Hill TR. Osteoporosis and the ageing skeleton. *Subcell Biochem*. (2019) 91:453–76. doi: 10.1007/978-981-13-3681-2_16

9. Inoue T, Maeda K, Nagano A, Shimizu A, Ueshima J, Murotani K, et al. Undernutrition, sarcopenia, and frailty in fragility hip fracture: advanced strategies for improving clinical outcomes. *Nutrients*. (2020) 12(12):3743. doi: 10.3390/nu12123743

10. Petermann-Rocha F, Balntzi V, Gray SR, Lara J, Ho FK, Pell JP, et al. Global prevalence of sarcopenia and severe sarcopenia: a systematic review and meta-analysis. *J Cachexia Sarcopenia Muscle*. (2022) 13(1):86–99. doi: 10.1002/jcsm.12783

11. Hurst C, Robinson SM, Witham MD, Dodds RM, Granic A, Buckland C, et al. Resistance exercise as a treatment for sarcopenia: prescription and delivery. *Age Ageing*. (2022) 51(2):afac003. doi: 10.1093/ageing/afac003

12. Curcio F, Testa G, Liguori I, Papillo M, Flocco V, Panicara V, et al. Sarcopenia and heart failure. *Nutrients*. (2020) 12(1):211. doi: 10.3390/nu12010211

13. Kasprzak D, Rzeźniczak J, Ganowicz T, Łuczak T, Słomczyński M, Hiczkiewicz J, et al. A review of acute coronary syndrome and its potential impact on cognitive function. *Glob Heart*. (2021) 16(1):53. doi: 10.5334/gh.934

14. Deckers K, Schievink SHJ, Rodriquez MMF, van Oostenbrugge RJ, van Boxtel MPJ, Verhey FRJ, et al. Coronary heart disease and risk for cognitive impairment or dementia: systematic review and meta-analysis. *PLoS One*. (2017) 12(9): e0184244. doi: 10.1371/journal.pone.0184244

15. Greaves D, Psaltis PJ, Ross TJ, Davis D, Smith AE, Boord MS, et al. Cognitive outcomes following coronary artery bypass grafting: a systematic review and meta-analysis of 91,829 patients. *Int J Cardiol*. (2019) 289:43–9. doi: 10.1016/j.ijcard.2019.04.065

16. Stewart RAH, Held C, Krug-Gourley S, Waterworth D, Stebbins A, Chiswell K, et al. Cardiovascular and lifestyle risk factors and cognitive function in patients with stable coronary heart disease. *J Am Heart Assoc*. (2019) 8(7):e010641. doi: 10.1161/JAHA.118.010641

17. Kose E, Wakabayashi H, Yasuno N. Polypharmacy and malnutrition management of elderly perioperative patients with cancer: a systematic review. *Nutrients*. (2021) 13(6):1961. doi: 10.3390/nu13061961

18. Gaman MA, Cozma MA, Dobrica EC, Bacalbasa N, Bratu OG, Diaconu CC. Dyslipidemia: a trigger for coronary heart disease in Romanian patients with diabetes. *Metabolites*. (2020) 10(5):195. doi: 10.3390/metabo10050195

19. Organization WH. *Who Scientific Group on the Assessment of Osteoporosis at Primary Health Care Level*. Geneva: WHO Press, World Health Organization (2004). Available online at: http://www.associazionemediciendocrinologi.it/materiali/linee_guida/download_file_824230695.pdf (accessed June 06, 2023).

20. Lin C. Early diagnosis and treatment of coronary heart disease with image features of optical coherence tomography under adaptive segmentation algorithm. *Comput Math Methods Med*. (2022) 2022:1261259. doi: 10.1155/2022/1261259

21. Pagliaro BR, Cannata F, Stefanini GG, Bolognese L. Myocardial ischemia and coronary disease in heart failure. *Heart Fail Rev*. (2020) 25(1):53–65. doi: 10.1007/s10741-019-09831-z

22. Hirose S, Matsue Y, Kamiya K, Kagiyama N, Hiki M, Dotare T, et al. Prevalence and prognostic implications of malnutrition as defined by GLIM criteria in elderly patients with heart failure. *Clin Nutr*. (2021) 40(6):4334–40. doi: 10.1016/j.clnu.2021.01.014

23. Billingsley HE, Hummel SL, Carbone S. The role of diet and nutrition in heart failure: a state-of-the-art narrative review. *Prog Cardiovasc Dis*. (2020) 63(5):538–51. doi: 10.1016/j.pcad.2020.08.004

24. Bouillanne O, Morineau G, Dupont C, Coulombel I, Vincent JP, Nicolis I, et al. Geriatric nutritional risk index: a new index for evaluating at-risk elderly medical patients. *Am J Clin Nutr*. (2005) 82(4):777–83. doi: 10.1093/ajcn/82.4.777

25. Dent E, Hoogendijk EO, Visvanathan R, Wright ORL. Malnutrition screening and assessment in hospitalised older people: a review. *J Nutr Health Aging*. (2019) 23(5):431–41. doi: 10.1007/s12603-019-1176-z

26. Bowen RES, Graetz TJ, Emmert DA, Avidan MS. Statistics of heart failure and mechanical circulatory support in 2020. *Ann Transl Med*. (2020) 8(13):827. doi: 10.21037/atm-20-1127

27. Marcovitz PA, Tran HH, Franklin BA, O'Neill WW, Yerkey M, Boura J, et al. Usefulness of bone mineral density to predict significant coronary artery disease. *Am J Cardiol*. (2005) 96(8):1059–63. doi: 10.1016/j.amjcard.2005.06.034

28. Samelson EJ, Kiel DP, Broe KE, Zhang Y, Cupples LA, Hannan MT, et al. Metacarpal cortical area and risk of coronary heart disease: the framingham study. *Am J Epidemiol*. (2004) 159(6):589–95. doi: 10.1093/aje/kwh080

29. Duque PG. Sarcopenia and osteoporotic fractures. *Clin Rev Bone Miner Metab*. (2016) 14(1):38–44. doi: 10.1007/s12018-016-9204-6

30. Daly RM, Duckham RL, Gianoudis J. Evidence for an interaction between exercise and nutrition for improving bone and muscle health. *Curr Osteoporos Rep*. (2014) 12(2):219–26. doi: 10.1007/s11914-014-0207-2

31. Rossi AP, Micciolo R, Rubele S, Fantin F, Caliari C, Zoico E, et al. Assessing the risk of sarcopenia in the elderly: the mini sarcopenia risk assessment (MSRA) questionnaire. *J Nutr Health Aging*. (2017) 21(6):743–9. doi: 10.1007/s12603-017-0921-4

32. Konishi M, Kagiyama N, Kamiya K, Saito H, Saito K, Ogasahara Y, et al. Impact of sarcopenia on prognosis in patients with heart failure with reduced and preserved ejection fraction. *Eur J Prev Cardiol*. (2021) 28(9):1022–9. doi: 10.1093/eurjpc/zwaa117

33. Springer J, Springer JI, Anker SD. Muscle wasting and sarcopenia in heart failure and beyond: update 2017. *ESC heart Failure*. (2017) 4(4):492–8. doi: 10.1002/ehf2.12237

34. Lena A, Anker MS, Springer J. Muscle wasting and sarcopenia in heart failure-the current state of science. *Int J Mol Sci*. (2020) 21(18):6549. doi: 10.3390/ijms21186549

35. Gómez-Gómez ME, Zapico SC. Frailty, cognitive decline, neurodegenerative diseases and nutrition interventions. *Int J Mol Sci*. (2019) 20(11):2842. doi: 10.3390/ijms20112842

36. Taylor MK, Swerdlow RH, Sullivan DK. Dietary neuroketotherapeutics for Alzheimer's disease: an evidence update and the potential role for diet quality. *Nutrients*. (2019) 11(8):1910. doi: 10.3390/nu11081910

frontiers | Frontiers in Cardiovascular Medicine

TYPE Original Research
PUBLISHED 25 March 2024
DOI 10.3389/fcvm.2024.1273666

OPEN ACCESS

EDITED BY
Tommaso Gori,
University Medical Centre, Johannes Gutenberg University Mainz, Germany

REVIEWED BY
Lovel Giunio,
University of Split, Croatia
Xingyu He,
University of Cincinnati, United States

*CORRESPONDENCE
Ming Yan
✉ cnming.yan@hotmail.com
Hong-chao Feng
✉ hcfeng@gzu.edu.cn

†These authors have contributed equally to this work

RECEIVED 07 August 2023
ACCEPTED 12 March 2024
PUBLISHED 25 March 2024

CITATION
Hu X-z, Fu L-l, Ye B, Ao M, Yan M and Feng H-c (2024) Gut microbiota and risk of coronary heart disease: a two-sample Mendelian randomization study.
Front. Cardiovasc. Med. 11:1273666.
doi: 10.3389/fcvm.2024.1273666

Gut microbiota and risk of coronary heart disease: a two-sample Mendelian randomization study

Xiang-zhi Hu[1†], Ling-ling Fu[2†], Bin Ye[2], Man Ao[2], Ming Yan[2,3*] and Hong-chao Feng[2*]

[1]Medical College, Guizhou University, Guiyang, China, [2]Department of Oral and Maxillofacial Surgery, Guiyang Hospital of Stomatology, Guiyang, China, [3]Department of Oral and Maxillofacial Surgery, University Medical Center Hamburg-Eppendorf, Hamburg, Germany

Background: The relationship between gut microbiota composition and coronary heart disease (CHD) has been recently reported in several observational studies. However, the causal effect of gut microbiota on coronary heart disease is uncharted.
Objective: This study attempted to investigate the effect of gut microbiota on coronary heart disease by Mendelian randomization (MR) analysis.
Methods: Through the two-sample MR method, single-nucleotide polymorphisms relevant to gut microbiota were selected as instrument variables to evaluate the causal association between gut microbiota and the risk of CHD.
Results: According to the selection criteria of the inverse variance-weighted average method, Class Actinobacteria, Class Lentisphaeria, Family Clostridiales vadinBB60group, Genus *Clostridium innocuum* group, Genus *Bifidobacterium*, Genus *Butyricicoccus*, Genus *Oxalobacter*, Genus *Turicibacter*, and Order Victivallales, presented a suggestive association with coronary heart disease.
Conclusion: This two-sample Mendelian randomization study found that gut microbiota was causally associated with coronary heart disease. Further randomized controlled trials are needed to clarify the protective effect of probiotics on coronary heart disease and their specific protective mechanisms.

KEYWORDS

coronary heart disease, gut microbiota, causal inference, Mendelian randomization study, inverse variance-weighted

1 Introduction

The gut bacteria present in human intestines are a large population of bacteria that constitute the largest microbiota in the body (1). The human intestine contains at least 1,000 species of bacteria, with a total of more than 100 million bacteria, forming a complex group (2). The genes encoding these microbes are at least one billion times larger than the human genome.

Many scholars have done many profound studies on the physiological processes of gut bacteria in humans, and since the discovery of gut flora (3), it has been acknowledged that the gut bacteria flora play an important role in regulating the nervous system and metabolism and immunity, and a delicate balance is maintained between them and humans (4).

Coronary heart disease (CHD) is damage to the myocardium caused by an imbalance between the blood supply to the coronary arteries and the demand on the myocardium due to functional or organic pathology, also known as ischemic heart disease (5). The most common cause of coronary heart disease is atherosclerosis, which accounts for about 90% of cases and is a chronic, progressive inflammatory disease that occurs in the vascular system. Atheromatous plaques in the coronary arteries gradually increase in size and cause. The main mechanism of coronary heart disease is the blockage of blood flow or the exposure of endothelial collagen fibers as a result of plaque rupture, leading to thrombosis. This is regulated by a combination of inflammatory factors and metabolic substances (6).

In healthy people, the gut microbiome is made up mostly of good bacteria, with few bad ones. These two bacterial types are in homeostasis to maintain a healthy state of the host (7). Previous studies have shown that imbalances in the gut microbiome are strongly associated with infectious and inflammatory and metabolic diseases (8). The imbalance of gut microbiota leads to the disorder of bacterial structure and the destruction of basic metabolic processes of the host, which may be closely related to the occurrence of cardiovascular diseases such as coronary heart disease, hypertension, and heart failure (9).

Studies have shown that gut bacteria are associated with many other risk factors for coronary heart disease, such as obesity, diabetes, high blood cholesterol, and high blood pressure (10). The gut microbiome has been observed to play an important role in coronary heart disease. Karlsson (11) found that the number of *Collinsella* bacteria increased in patients with coronary heart disease compared with healthy people, while the count of *Rothia* and *Eubacterium* spp. bacteria decreased. Emoto et al. (12) found that a significant increase in the number of mature lactic acid bacteria and a significant decrease in the number of bacteriophages (*Bifidobacterium* and *Prevotella*) were found in patients with coronary artery disease (13). Furthermore, there was a significant increase in the proportion of the thick-walled phylum/bacteroidetes (14). The proportion of lactobacilli in the gut microbiota of patients with coronary artery disease who did not use antibiotics was significantly higher and the proportion of *Bacillus mimicus* was significantly lower (15).

Figure 1 shows an overview flow diagram of the Mendelian randomization (MR) hypothesis. This study used MR to explore the causal association between gut microbiota and coronary heart disease (16). In MR, the causal relationship between exposure and disease outcomes is estimated through instrumental variables (IV) used to construct genotypes (17). The random distribution of genotypes is designed according to Mendelian laws of inheritance. If the genotype determines the phenotype, then the genotype is associated with the disease through the phenotype, so the genotype can be used as an instrumental variable to infer the association between the phenotype and the disease. It uses genetic variants strongly associated with exposure factors as instrumental variables to assess the causal relationship between exposure factors and outcomes. There are three hypotheses of Mendelian randomization: (1) Association hypothesis: single-nucleotide polymorphisms (SNPs) are strongly correlated with exposure factors; (2) Independence hypothesis: SNPs are independent from confounders; (3) Exclusivity hypothesis: SNPs can only have an effect on outcomes through exposure factors. For studying the causal relationship between gut microbiota and diseases (including metabolic diseases), MR has been widely used for studying autoimmune diseases and rheumatoid arthritis (18). A genome-wide association study (GWAS) summary from the MiBioGen and MR-Base consortiums was used in this study, and coronary heart disease and gut microbiota were evaluated using MR analysis of two samples (19).

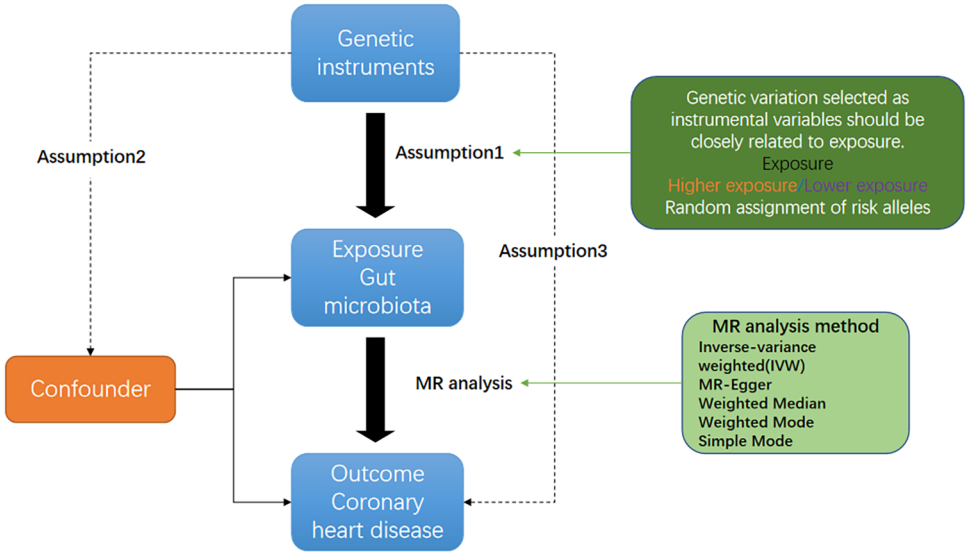

FIGURE 1
Three corresponding principal assumptions in this two-sample Mendelian randomization study.

2 Methods

2.1 Data sources

The MiBioGen consortium conducted the largest genome-wide meta-analysis to date for gut microbiota composition to identify genetic variants. The study included 18,340 individuals from 24 cohorts from the USA, Canada, Israel, Germany, Denmark, the Netherlands, Belgium, Sweden, Finland, and the UK (20). To identify host genetic variants associated with the abundance levels of bacterial taxa, a microbiota quantitative trait loci mapping analysis was performed. The study identified 131 genera with a mean abundance greater than 1%, including 12 genera that were unknown. Therefore, 119 genus-level taxa were included in the current study for analysis. CHD in this study was defined as heart disease involving plaque buildup in the heart arteries (atherosclerosis) and reduced blood flow to the heart muscle, resulting in myocardial ischemia, hypoxia, or necrosis. Summary statistics for CHD were developed using the GWAS summary dataset for CHD obtained from the IEU Open GWAS project (ieu-a-7) (21). A total of 184,305 adult subjects and 123,504 controls participated in this GWAS. Sex, age, first 10 principal components, and genotyping batch were corrected during the analysis (22).

2.2 Instrumental variable

The screening of IVs in MR studies is consistent with the aforementioned three core hypotheses of MR: (1) Association hypothesis: SNPs are strongly correlated with exposure factors, with F-value > 10 as the closely related criterion; (2) Independence hypothesis: SNPs are independent from confounders. (3) Exclusivity hypothesis: SNPs can only have an effect on outcomes through exposure factors. IVs were selected based on the following criteria: (1) Statistically significant SNPs in each genus ($P < 1.0 \times 10^{-5}$) are considered potential IVs; (2) A reference panel of European samples was used to calculate linkage disequilibrium (LD) between SNPs in the 1000 Genomes project, and among those SNPs that had $R^2 < 0.001$ (clumping window size = 10,000 kb), only the SNPs with the lowest P-values were retained; (3) SNPs with minor allele frequency (MAF) ≤0.01 were removed; and (4) Allele frequency information was used to determine forward strand alleles when palindromic SNPs existed (23). Basic information on the instrumental variables is in the Supplementary material S1 (Basic information on instrumental variables).

2.3 Statistical analysis

To verify whether there was a correlation between exposure to gut microbiota and the outcome CHD, MR analysis was conducted using five methods such as the inverse variance-weighted average method (IVW) (23), the weighted median method (24). MR-Egger regression analysis (25), and weighted mode. In addition, Cochran's IVW Q was utilized to quantify the heterogeneity of IVs (26). Further, to identify potentially heterogeneous SNPs, a "leave-one-out" analysis was performed by ignoring each tool for analyzing SNPs in turn (27).

All statistical analyses were performed using R version 4.2.1. MR analyses were performed using the TwosampleMR (version 0.5.6), MR-PRESSO (version 1.0), and q-value R packages (28).

3 Results

3.1 SNP selection

According to the IVs screening criteria, 128, 235, 294, 516, 1761SNPs associated with the intestinal microbiome were identified at the phylum, class, order, family, and genus levels. After a series of quality control, a total of 2,906 IVs were determined.

The F statistics of IVs were all >10, indicating that there was no evidence of weak instrument bias. According to the third hypothesis of Mendelian randomization, IVs must pass the exposure to affect the outcome. If the IVs can directly affect the result without exposure, then the idea of Mendelian randomization is violated, that is, the test results have horizontal pleiotropy. Therefore, the main premise of causality inference using Mendelian randomization is that there is no horizontal pleiotropy. We used the MR-PRESSO method to examine horizontal pleiotropy (MR-PRESSO global test $p > 0.05$; Supplementary File: res_presso).

Bacterial genera containing multiple SNPs were tested using four MR methods to account for multiple test corrections in the set of SNPs used as IV that are smaller than the genome-wide statistical significance threshold (1×10^{-5}). According to the selection criteria for IVs, a total of 2,458 SNPs were used as IVs for 211 bacterial genera.

For all instrumental variables, their F statistics are all greater than 10, and all weak instrumental variables were excluded (Supplementary File: res_data).

As presented in Table 1, nine bacterial genera were found to be associated with CHD in IVW. Among them, Class Actinobacteria, Genus *Clostridium innocuum* group, Genus *Bifidobacterium*, Genus *Oxalobacter*, and Genus *Turicibacter*, show by analysis of the results that they are related to coronary heart disease (OR > 1); however, MR analysis results of Class Lentisphaeria, Family Clostridiales vadinBB60 group, Genus *Butyricicoccus*, and Order Victivallales reflect potential protection from CHD.

Cochran's IVW Q test exhibited no heterogeneity in these IVs (Supplementary File: res_hete).

Potential outliers were present in the IV of *Clostridium innocuum* group, *Oxalobacter*, and *Turicibacter* in visual tests on scatter plots and retention plots. MR-PRESSO analysis further, however, did not find any significant outliers. Thus, there was not enough evidence to show a pleiotropic relationship between these bacteria and CHD level.

Figure 2 shows the causal association between gut microbiota and CHD. The correlation between gut microbiota and CHD was visualized in a scatter plot. In this plot, each black dot represented an SNP. With the correlation between SNP and

TABLE 1 Causal effects of gut microbiota on CHD.

Bacterial taxa (exposure)	Number of SNPs	MR method	*P*-value	OR	95% CI
Class Actinobacteria	22	MR-Egger	0.91	0.99	0.82–1.19
		Weighted median	0.02	1.12	1.02–1.24
		Inverse variance-weighted	0.04	1.08	1.00–1.16
		Simple mode	0.11	1.17	0.97–1.41
		Weighted mode	0.07	1.16	0.99–1.35
Class Lentisphaeria	8	MR-Egger	0.30	0.87	0.69–1.11
		Weighted median	0.18	0.94	0.86–1.03
		Inverse variance-weighted	0.02	0.92	0.87–0.99
		Simple mode	0.45	0.94	0.83–1.08
		Weighted mode	0.53	0.95	0.83–1.10
Family Clostridiales vadinBB60 group	15	MR-Egger	0.18	0.86	0.71–1.06
		Weighted median	0.07	0.91	0.83–1.01
		Inverse variance-weighted	0.02	0.92	0.86–0.99
		Simple mode	0.28	0.91	0.78–1.07
		Weighted mode	0.21	0.90	0.78–1.05
Genus *Clostridium innocuum* group	9	MR-Egger	0.62	1.09	0.77–1.57
		Weighted median	0.53	1.02	0.94–1.12
		Inverse variance-weighted	0.02	1.07	1.01–1.15
		Simple mode	0.61	1.03	0.91–1.18
		Weighted mode	0.62	1.03	0.91–1.18
Genus *Bifidobacterium*	20	MR-Egger	0.41	1.09	0.88–1.37
		Weighted median	0.01	1.13	1.03–1.24
		Inverse variance-weighted	0.03	1.07	1.01–1.16
		Simple mode	0.23	1.11	0.94–1.32
		Weighted mode	0.09	1.12	0.99–1.28
Genus *Butyricicoccus*	8	MR-Egger	0.07	0.82	0.68–0.99
		Weighted median	0.06	0.87	0.75–1.01
		Inverse variance-weighted	0.01	0.87	0.79–0.97
		Simple mode	0.10	0.81	0.66–1.01
		Weighted mode	0.08	0.85	0.74–1.00
Genus *Oxalobacter*	11	MR-Egger	0.19	1.20	0.93–1.56
		Weighted median	0.02	1.08	1.01–1.17
		Inverse variance-weighted	0.01	1.08	1.03–1.15
		Simple mode	0.06	1.11	1.01–1.24
		Weighted mode	0.07	1.11	1.00–1.23
Genus *Turicibacter*	10	MR-Egger	0.82	1.04	0.73–1.50
		Weighted median	0.14	1.08	0.97–1.22
		Inverse variance-weighted	0.01	1.12	1.03–1.23
		Simple mode	0.62	1.05	0.86–1.29
		Weighted mode	0.56	1.05	0.88–1.26
Order Victivallales	8	MR-Egger	0.30	0.87	0.69–1.11
		Weighted median	0.16	0.94	0.86–1.03
		Inverse variance-weighted	0.02	0.92	0.87–0.99
		Simple mode	0.48	0.94	0.82–1.09
		Weighted mode	0.53	0.95	0.83–1.10

OR, odds ratio; CI, confidence interval.

exposure taken as the *X* axis, and the correlation between SNP and outcome taken as the *Y* axis, the slope of the drawn line marked the potential causal correlation of each method.

It was observed that Class Lentisphaeria, Family Clostridiales vadinBB60 group, Genus *Butyricicoccus*, and Order Victivallales could inhibit the occurrence of CHD, exerting a protective effect, while Class Actinobacteria, Genus *Clostridium innocuum* group, and Genus *Bifidobacterium*, Genus *Oxalobacter*, and Genus *Turicibacter* were positively correlated with the occurrence of CHD.

Figure 3 shows the causal association between Actinobacteria, *Bifidobacterium*, and CHD. The leave-one-out analysis showed no significant difference in the causal association between the aforementioned nine bacterial genera and CHD. After eliminating each SNP as an IV one by one, the overall trend did not change significantly, that is, no SNP was found with a great impact on the outcome among IVs. Visualizations of other bacteria are shown in the Supplementary material S2 (Visualizations of leave-one-out results).

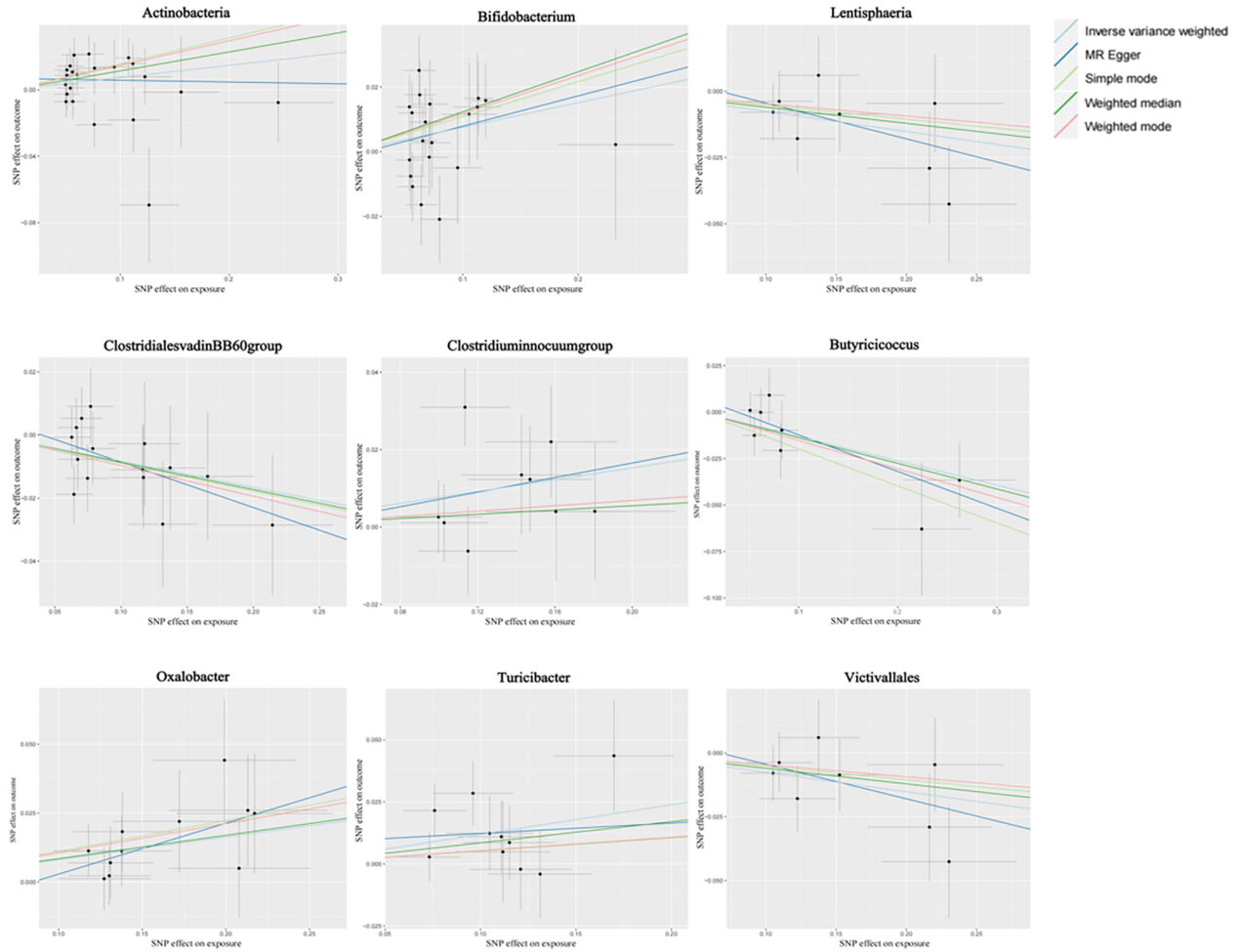

FIGURE 2
Causal effects of gut microbiota on CHD outcomes.

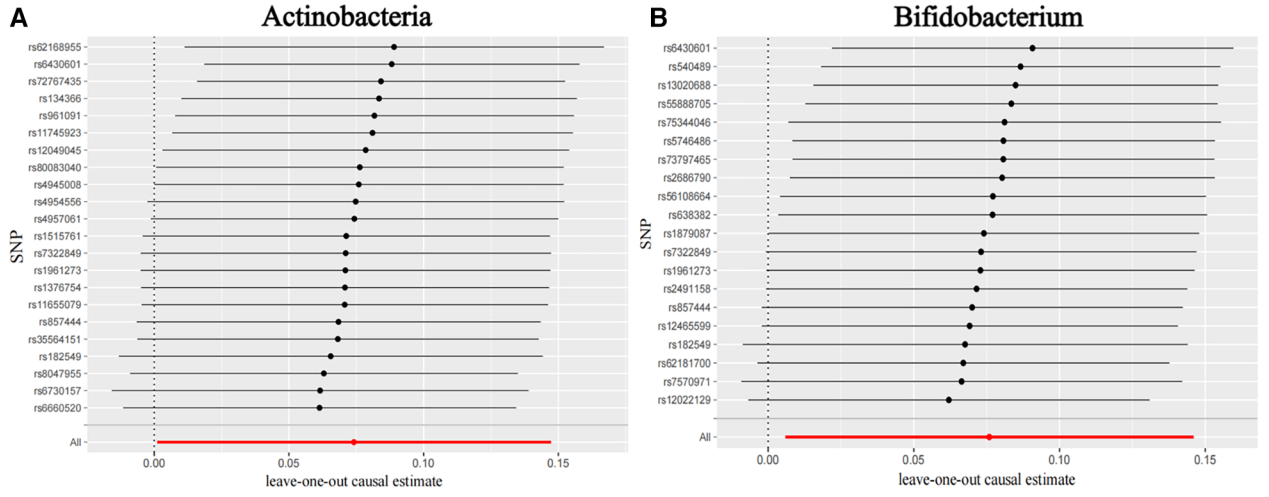

FIGURE 3
Leave-one-out plots for the causal association between gut microbiota and CHD. (**A**) Actinobacteria and (**B**) *Bifidobacterium*.

4 Discussion

In this study, pooled statistics for gut microbiome from the largest GWAS meta-analysis conducted by the MiBioGen consortium and pooled statistics for coronary heart disease from the GWAS pooled dataset were used (29).

The gut microbiome is a complex and dynamic collection of ecological microbial communities colonized in the human gut. These bacteria play a vital role in the homeostasis of the digestive system and the health of the host, with a variety of metabolic, immune, and protective functions (30). System development and the function of gut bacteria stabilize and increase in diversity as age grows. Based on more than 450,000 European integrated genetic data (31), we have identified a number of genetic predispositions in the gut microbiome that are causally associated with CHD. We also identified that some may be a potential risk factor for CHD gut microbiota. These results may be designed to reduce the risk of coronary heart disease by public health interventions, hence they have enlightenment significance.

In this study, the GWAS summary statistics of intestinal bacteria from MiBioGen Alliance and the GWAS summary statistics of coronary heart disease from MR-Base were used to conduct MR analysis on the two samples to study the causal relationship between gut microbiota and CHD. In this study, five species of bacteria (Class Actinobacteria, Genus *Clostridium innocuum* group, Genus *Bifidobacterium*, Genus *Oxalobacter*, Genus *Turicibacter*) have shown potential role in CHD, and four kinds of bacteria (Class Lentisphaeria, Family Clostridiales vadinBB60 group, Genus *Butyricicoccus*, Order Victivallales) have shown protective effect on CHD.

Through its metabolites, the gut microbiome is involved in mediating basic metabolic processes, such as cholesterol metabolism, uric acid metabolism, oxidative stress, and inflammatory response, which can lead to atherosclerosis and coronary heart disease.

Many observational studies have reported a link between gut microbiota and coronary heart disease. *Bifidobacterium* is one of the most prominent probiotics, which is generally considered safe and friendly bacteria (32). However, in our study, it was positively associated with coronary heart disease, which we believe may be due to the following reasons. First, the GWAS data of gut microbiota we used remained at the genus level, and the specific data of *Bifidobacterium* species have not been counted, so detailed GWAS data of different species of *Bifidobacterium* are needed to conduct further MR research. Secondly, with the deepening of research on *Bifidobacterium*, the types of *Bifidobacterium* found are also gradually increasing. In the latest study, the *Bifidobacterium* obtained based on 16S rDNA sequencing technology was divided into 34 different species, including *Bifidobacterium adolescium*, *Bifidobacterium keratobium*, and *Bifidobacterium animalis* (33). The roles and benefits of some *Bifidobacterium* species have been found, including immune regulation, promoting tolerance, and playing a protective role in cardiovascular diseases. However, the effects and mechanisms of most *Bifidobacterium* species on CHD have not been clearly explored, which requires further experiments.

The gut microbiota produces a variety of metabolites that have different roles in blood pressure regulation, and beneficial metabolites include short-chain fatty acids (SCFAs) and vitamins. Short-chain fatty acids are thought to be beneficial for lowering blood pressure primarily through their vascular relaxation and anti-inflammatory effects, in contrast to another metabolite produced by the gut microbiome, trimethylamine N-oxide (TMAO), which is positively associated with high blood pressure (34). TMAO has pro-atherogenic and pro-thrombotic effects, so the gut microbiome produces different metabolites that have different effects on the risk of CHD. Short-chain fatty acids can improve its control, while TMAO is harmful.

The gut microbiota may also influence blood lipids, one of the risk factors for cardiovascular disease. Through metabolites, the broken-chain fatty acids are produced by a variety of gut bacteria, which are important metabolites for protecting against dyslipidemia. The physiological and metabolic activities of the gut microbiota are critical for regulating and maintaining balanced lipid metabolism in humans. *Firmicutes* and *Bacteroides* are the main bacterial groups that affect the changes of blood lipids. Lipid metabolites of the gut microbiota (such as choline, TMAO, and betaine) promote atherosclerosis and increase the risk of cardiovascular disease. Gut microbiota affects the conversion of serum triglycerides and high-density lipoprotein cholesterol. Three mechanisms are likely to cause dyslipidemia. First, the gut flora produces bile salt hydroxylase, which converts bound bile acids into secondary free bile acids. Secondary free bile acids can regulate liver and lipid metabolism through G protein-coupled receptors, and gut microbiota disorders can lead to abnormal bile acid secretion, resulting in dyslipidemia. Second, the gut flora converts choline and carnitine from the host to trimethylamine (TMA), and TMA is converted to TMAO in the liver (35). TMAO can cause dyslipidemia and atherosclerotic plaque by affecting cholesterol transport and metabolism and bile acid levels. Third, SCFAs can inhibit the activity of liver fat synthetase and regulate the distribution of cholesterol in the blood and liver, thus playing a role in reducing serum 3-acylglycerol and cholesterol levels. In addition, patients with dyslipidemia often exhibit high levels of TMAO, which reduces HDL-C levels and hence increases the risk of CHD (36). TMAO can also induce overreaction of platelets and is therefore a risk factor for atherosclerosis. The interaction between TMAO and platelets may promote platelet hyperreactivity and enhance thrombosis *in vivo* by altering platelet-dependent calcium signaling. Platelet hyperreactivity has been reported as a risk factor for cardiovascular events. Recent evidence suggests that TMAO can quickly send signals to cells within minutes. In endothelial or smooth muscle cells, TMAO rapidly induces mitogen-activated protein kinases and NF-κB activation, and causes downstream upregulation of adhesion molecules. Increased TMAO levels were also associated with increased phosphorylation of the SMAD-3 protein. SMAD-3 is a key signal in the transforming growth factor beta (TGF-β) pathway. In animal models, TMAO promotes vascular inflammation and induces aortic endothelial cell activation and upregulation of adhesion proteins. These effects are key mechanisms of acute coronary syndrome. Gut microbiota may also contribute to coronary heart

disease through the role of uric acid in serum uric acid level, which may be an independent risk factor for coronary heart disease. Uric acid has oxidizing properties in the body. Elevated blood uric acid levels lead to increased oxygen free radicals in blood uric acid, oxidative stress, vascular endothelial dysfunction, inflammatory responses, and the development of atherosclerosis (37).

In short, intestinal microbiota and its metabolites have a close influence on the risk of coronary heart disease. The disturbance of intestinal microbiota will lead to the disturbance of its metabolites, and then lead to a series of risk factors related to coronary heart disease, such as hypertension, hyperlipidemia, and diabetes. As a result, the combination of systemic and local diseases leads to the occurrence of coronary heart disease.

There are some limitations to our study. First, MR must follow three strict core assumptions, namely, correlation, independence, and exclusion constraints. Nevertheless, we employed a careful study design to avoid any violation of these assumptions. Secondly, the GWAS data of intestinal flora used in our study only reached the genus level, but did not reach the more detailed species level, which also has a certain impact on our study. The impact of specific intestinal bacteria on coronary heart disease needs further experimental verification or more detailed species-level data analysis. Finally, to minimize the effect of racial differences, we only used GWAS data from individuals of European descent for the MR analysis. Therefore, the generalization of our findings to other populations deserves further exploration and verification. In addition, while the MR analysis provides valuable insights into etiology, it is important to note that our findings should be validated through rigorous randomized controlled trials and basic research before being applied to the clinic.

5 Conclusion

This study presents multiple benefits. Specifically, it employed MR analysis to establish a causal relationship between gut microbiota and CHD, thereby mitigating the influence of confounding variables and reversing the direction of causality in causal inference. The genetic variation in the gut microbiota was obtained from the most extensive GWAS meta-analysis, ensuring the robustness of the MR analysis. In addition, cross-sectional polymorphisms were identified and eliminated through the utilization of MR-PRESSO and MR-Egger regression intercept term tests. A two-sample MR design with non-overlapping exposure and outcome summary level data was used to avoid bias. We identified nine different species of gut bacteria with potential causal relationship to CHD, but due to the limitations of gut flora database and CHD data, further studies or observational experiments are needed to confirm.

Data availability statement

The original contributions presented in the study are included in the article/**Supplementary Material**, further inquiries can be directed to the corresponding authors.

Ethics statement

Ethical approval was not required for the study involving humans in accordance with the local legislation and institutional requirements. Written informed consent to participate in this study was not required from the participants or the participants' legal guardians/next of kin in accordance with the national legislation and the institutional requirements.

Author contributions

XH: Conceptualization, Writing – original draft. LF: Writing – review & editing. BY: Formal Analysis, Methodology, Writing – review & editing. MA: Data curation, Investigation, Writing – review & editing. MY: Conceptualization, Writing – review & editing. HF: Formal Analysis, Funding acquisition, Project administration, Writing – review & editing.

Funding

The authors declare financial support was received for the research, authorship, and/or publication of this article.

This work was supported by a grant from the Guizhou Provincial Health Commission (gzwkj2022-431). MY was supported by the Merit Scholarship of Hamburg University for International Students (No. 7238065).

Conflict of interest

The authors declare that the research was conducted in the absence of any commercial or financial relationships that could be construed as a potential conflict of interest.

Publisher's note

Supplementary material

The Supplementary Material for this article can be found online at: https://www.frontiersin.org/articles/10.3389/fcvm.2024.1273666/full#supplementary-material.

References

1. Zeng Y, Cao S, Yang H. Roles of gut microbiome in epilepsy risk: a Mendelian randomization study. *Front Microbiol*. (2023) 14:1115014. doi: 10.3389/fmicb.2023.1115014

2. Fändriks L. Roles of the gut in the metabolic syndrome: an overview. *J Intern Med*. (2017) 281(4):319–36. doi: 10.1111/joim.12584

3. Sanz Y, Santacruz A, Gauffin P. Gut microbiota in obesity and metabolic disorders. *Proc Nutr Soc*. (2010) 69(3):434–41. doi: 10.1017/S0029665110001813

4. Diamant M, Blaak EE, de Vos WM. Do nutrient-gut-microbiota interactions play a role in human obesity, insulin resistance and type 2 diabetes? *Obes Rev*. (2011) 12 (4):272–81. doi: 10.1111/j.1467-789X.2010.00797.x

5. Shaya GE, Leucker TM, Jones SR, Martin SS, Toth PP. Coronary heart disease risk: low-density lipoprotein and beyond. *Trends Cardiovasc Med*. (2022) 32 (4):181–94. doi: 10.1016/j.tcm.2021.04.002

6. Di Angelantonio E, Thompson A, Wensley F, Danesh J. Coronary heart disease. *IARC Sci Publ*. (2011) (163):363–86. PMID: 22997872.

7. Kootte RS, Vrieze A, Holleman F, Dallinga-Thie GM, Zoetendal EG, de Vos WM, et al. The therapeutic potential of manipulating gut microbiota in obesity and type 2 diabetes mellitus. *Diabetes Obes Metab*. (2012) 14(2):112–20. doi: 10.1111/j.1463-1326.2011.01483.x

8. Esteve E, Ricart W, Fernández-Real JM. Gut microbiota interactions with obesity, insulin resistance and type 2 diabetes: did gut microbiote co-evolve with insulin resistance? *Curr Opin Clin Nutr Metab Care*. (2011) 14(5):483–90. doi: 10.1097/MCO.0b013e328348c06d

9. Liu H, Zhuang J, Tang P, Li J, Xiong X, Deng H. The role of the gut microbiota in coronary heart disease. *Curr Atheroscler Rep*. (2020) 22(12):77. doi: 10.1007/s11883-020-00892-2

10. Avolio E, Gualtieri P, Romano L, Pecorella C, Ferraro S, Palma G, et al. Obesity and body composition in man and woman: associated diseases and the new role of gut microbiota. *Curr Med Chem*. (2020) 27(2):216–29. doi: 10.2174/0929867326666190326113607

11. Karlsson FH, Fåk F, Nookaew I, Tremaroli V, Fagerberg B, Petranovic D, et al. Symptomatic atherosclerosis is associated with an altered gut metagenome. *Nat Commun*. (2012) 3:1245. doi: 10.1038/ncomms2266

12. Emoto T, Yamashita T, Kobayashi T, Sasaki N, Hirota Y, Hayashi T, et al. Characterization of gut microbiota profiles in coronary artery disease patients using data mining analysis of terminal restriction fragment length polymorphism: gut microbiota could be a diagnostic marker of coronary artery disease. *Heart Vessels*. (2017) 32(1):39–46. doi: 10.1007/s00380-016-0841-y

13. Emoto T, Yamashita T, Sasaki N, Hirota Y, Hayashi T, So A, et al. Analysis of gut microbiota in coronary artery disease patients: a possible link between gut microbiota and coronary artery disease. *J Atheroscler Thromb*. (2016) 23(8):908–21. doi: 10.5551/jat.32672

14. Yamashita T, Emoto T, Sasaki N, Hirata KI. Gut microbiota and coronary artery disease. *Int Heart J*. (2016) 57(6):663–71. doi: 10.1536/ihj.16-414

15. Zhu Q, Gao R, Zhang Y, Pan D, Zhu Y, Zhang X, et al. Dysbiosis signatures of gut microbiota in coronary artery disease. *Physiol Genomics*. (2018) 50(10):893–903. doi: 10.1152/physiolgenomics.00070.2018

16. Li N, Wang Y, Wei P, Min Y, Yu M, Zhou G, et al. Causal effects of specific gut microbiota on chronic kidney diseases and renal function—a two-sample Mendelian randomization study. *Nutrients*. (2023) 15(2):360. doi: 10.3390/nu15020360

17. Mazidi M, Shekoohi N, Covic A, Mikhailidis DP, Banach M. Adverse impact of *Desulfovibrio* spp. and beneficial role of *Anaerostipes* spp. on renal function: insights from a Mendelian randomization analysis. *Nutrients*. (2020) 12(8):2216. doi: 10.3390/nu12082216

18. Mazidi M, Dehghan A, Banach M, On Behalf Of The Lipid And Blood Pressure Meta-Analysis Collaboration Lbpmc Group And The International Lipid Expert Panel Ilep. Genetically higher level of mannose has no impact on cardiometabolic risk factors: insight from Mendelian randomization. *Nutrients*. (2021) 13(8):2563. doi: 10.3390/nu13082563

19. Kintu C, Soremekun O, Kamiza AB, Kalungi A, Mayanja R, Kalyesubula R, et al. The causal effects of lipid traits on kidney function in Africans: bidirectional and multivariable Mendelian-randomization study. *EBioMedicine*. (2023) 90:104537. doi: 10.1016/j.ebiom.2023.104537

20. Kurilshikov A, Medina-Gomez C, Bacigalupe R, Radjabzadeh D, Wang J, Demirkan A, et al. Large-scale association analyses identify host factors influencing human gut microbiome composition. *Nat Genet*. (2021) 53(2):156–65. doi: 10.1038/s41588-020-00763-1

21. Hemani G, Zheng J, Elsworth B, Wade KH, Haberland V, Baird D, et al. The MR-Base platform supports systematic causal inference across the human phenome. *eLife*. (2018) 7:e34408. doi: 10.7554/eLife.34408

22. Ren Z, Simons PIHG, Wesselius A, Stehouwer CDA, Brouwers MCGJ. Relationship between NAFLD and coronary artery disease: a Mendelian randomization study. *Hepatology*. (2023) 77(1):230–8. doi: 10.1002/hep.32534

23. Burgess S, Dudbridge F, Thompson SG. Combining information on multiple instrumental variables in Mendelian randomization: comparison of allele score and summarized data methods. *Stat Med*. (2016) 35(11):1880–906. doi: 10.1002/sim.6835

24. Pierce BL, Burgess S. Efficient design for Mendelian randomization studies: subsample and 2-sample instrumental variable estimators. *Am J Epidemiol*. (2013) 178(7):1177–84. doi: 10.1093/aje/kwt084

25. Burgess S, Small DS, Thompson SG. A review of instrumental variable estimators for Mendelian randomization. *Stat Methods Med Res*. (2017) 26 (5):2333–55. doi: 10.1177/0962280215597579

26. Yang Y, Xian W, Wu D, Huo Z, Hong S, Li Y, et al. The role of obesity, type 2 diabetes, and metabolic factors in gout: a Mendelian randomization study. *Front Endocrinol (Lausanne)*. (2022) 13:917056. doi: 10.3389/fendo.2022.917056

27. Xu H, Jin C, Guan Q. Causal effects of overall and abdominal obesity on insulin resistance and the risk of type 2 diabetes mellitus: a two-sample Mendelian randomization study. *Front Genet*. (2020) 11:603. doi: 10.3389/fgene.2020.00603

28. Lee Y, Kim YA, Seo JH. Causal association of obesity and dyslipidemia with type 2 diabetes: a two-sample Mendelian randomization study. *Genes (Basel)*. (2022) 13(12):2407. doi: 10.3390/genes13122407

29. Ni JJ, Li XS, Zhang H, Xu Q, Wei XT, Feng GJ, et al. Mendelian randomization study of causal link from gut microbiota to colorectal cancer. *BMC Cancer*. (2022) 22 (1):1371. doi: 10.1186/s12885-022-10483-w

30. O'Hara AM, Shanahan F. The gut flora as a forgotten organ. *EMBO Rep*. (2006) 7(7):688–93. doi: 10.1038/sj.embor.7400731

31. Xiang K, Wang P, Xu Z, Hu YQ, He YS, Chen Y, et al. Causal effects of gut microbiome on systemic lupus erythematosus: a two-sample Mendelian randomization study. *Front Immunol*. (2021) 12:667097. doi: 10.3389/fimmu.2021.667097

32. Shanahan F. The gut microbiota-a clinical perspective on lessons learned. *Nat Rev Gastroenterol Hepatol*. (2012) 9(10):609–14. doi: 10.1038/nrgastro.2012.145

33. Gavzy SJ, Kensiski A, Lee ZL, Mongodin EF, Ma B, Bromberg JS. *Bifidobacterium* mechanisms of immune modulation and tolerance. *Gut Microbes*. (2023) 15(2):2291164. doi: 10.1080/19490976.2023.2291164

34. Fennema D, Phillips IR, Shephard EA. Trimethylamine and trimethylamine N-oxide, a flavin-containing monooxygenase 3 (FMO3)-mediated host-microbiome metabolic axis implicated in health and disease. *Drug Metab Dispos*. (2016) 44 (11):1839–50. doi: 10.1124/dmd.116.070615

35. Belkaid Y, Hand TW. Role of the microbiota in immunity and inflammation. *Cell*. (2014) 157(1):121–41. doi: 10.1016/j.cell.2014.03.011

36. Yoo JY, Sniffen S, McGill Percy KC, Pallaval VB, Chidipi B. Gut dysbiosis and immune system in atherosclerotic cardiovascular disease (ACVD). *Microorganisms*. (2022) 10(1):108. doi: 10.3390/microorganisms10010108

37. Wang Q, Guo M, Liu Y, Xu M, Shi L, Li X, et al. *Bifidobacterium breve* and *Bifidobacterium longum* attenuate choline-induced plasma trimethylamine N-oxide production by modulating gut microbiota in mice. *Nutrients*. (2022) 14(6):1222. doi: 10.3390/nu14061222

frontiers | Frontiers in Cardiovascular Medicine

TYPE Case Report
PUBLISHED 24 May 2024
DOI 10.3389/fcvm.2024.1418316

OPEN ACCESS

EDITED BY
Tommaso Gori,
Johannes Gutenberg University Mainz, Germany

REVIEWED BY
Niya Mileva,
Aleksandrovska University Hospital, Bulgaria
Giulia Iannaccone,
Catholic University of the Sacred Heart, Italy

*CORRESPONDENCE
Gianni Dall'Ara
dallara.gianni@gmail.com

RECEIVED 16 April 2024
ACCEPTED 15 May 2024
PUBLISHED 24 May 2024

CITATION
Dall'Ara G, Compagnone M, Carletti R, Piciucchi S, Gardini E and Galvani M (2024) Case Report: Asymptomatic SARS-COV2 infection triggering recurrent Takotsubo syndrome.
Front. Cardiovasc. Med. 11:1418316.
doi: 10.3389/fcvm.2024.1418316

Case Report: Asymptomatic SARS-COV2 infection triggering recurrent Takotsubo syndrome

Gianni Dall'Ara[1,2]*, Miriam Compagnone[2], Roberto Carletti[2], Sara Piciucchi[3], Elisa Gardini[2] and Marcello Galvani[1,2,4]

[1]Department of Medical and Surgical Sciences (DIMEC), University of Bologna, Forlì Campus, Forlì, Italy, [2]Cardiology Unit, Morgagni-Pierantoni Hospital, Forlì, Italy, [3]Department of Radiology, Morgagni-Pierantoni Hospital, Forlì, Italy, [4]Cardiovascular Research Unit, Myriam Zito Sacco Heart Foundation, Forlì, Italy

Takotsubo syndrome (TTS) is a rare disease mimicking acute coronary syndrome, often triggered by physical or emotional stress, and characterized by transient left ventricular dysfunction. Recurrences are described in about 5% of cases and may have different clinical and imaging patterns. In the present report, SARS-COV-2 infection, even in the absence of symptoms and overt emotional stress, seems correlated with recurrence of TTS, due to the absence of other recognized triggers. The hypothesis is that in predisposed patients, events like catecholamine-induced myocyte injury, direct viral damage, cytokine storm, immune-mediated damage, and procoagulant state, all possibly induced by the infection, may elicit endothelial dysfunction as substrate for TTS onset.

KEYWORDS

Takotsubo, stress cardiomyopathy, apical ballooning syndrome, recurrence, COVID, SARS-CoV-2

Introduction

The coronavirus disease-2019 (COVID-19) is mainly a respiratory syndrome with variable severity, but with documented evidence of potential cardiovascular involvement, such as myocarditis, pericarditis, thromboembolism, arrhythmias, Kawasaki's disease, acute coronary syndrome (ACS), and Takotsubo syndrome (TTS). Patients hospitalized for COVID-19 complicated by myocardial injury, identified as an increase in markers of myocardial cell necrosis, have a higher risk of in-hospital mortality (1). TTS, also known as stress cardiomyopathy, is a rare syndrome with well-known clinical manifestations most of the times mimicking, in its early phase, an ACS. Indeed, chest discomfort, ST-T changes on electrocardiogram (ECG), and plasmatic troponin elevation are often reported. TTS is responsible for 1%–2% of hospital admissions with suspected ACS. It is typically characterized by transient left ventricular dysfunction not associated with coronary artery obstruction or extending beyond a coronary distribution. A physical or emotional stress, often part of the medical history, is known to trigger the disease. However, there are few certainties about the pathophysiological mechanisms underlying the syndrome (2).

Case description

The patient is a 74-year-old woman with type 2 diabetes mellitus, hypercholesterolaemia, mild overweight (25.7 Kg/m^2), and a remote undocumented history of myocardial infarction in the infero-lateral wall treated by intravenous fibrinolysis. Back then, no coronary artery disease

was found at angiography. More recently, in 2021, she was admitted to hospital with a diagnosis of TTS. In that case, she complained of new onset chest pain following an argument on the phone. The 12-lead ECG showed negative T-waves in the infero-lateral leads (Figure 1A). The coronary angiography documented tortuous epicardial coronary arteries, free from significant lesions, with diffuse slow flow (Figures 2A,B). Hyperkinesia of the basal segments, akinesia of the middle and apical segments, and ejection fraction (EF) of 35% were seen at left ventriculography (Figures 2C, D). White blood cell count was 6,690/mmc (URL 10,000/mmc), peak plasma level of high-sensitive troponin-T was 216 ng/L (female gender URL <10), whereas urinary metanephrines were within normal limits. On day 5, a cardiac magnetic resonance (CMR) confirmed the diagnosis (Figures 3A–E) showing in addition the presence of a small intraventricular thrombotic formation (15 × 8 mm) for which oral anticoagulant therapy was given. Discharge therapy included an angiotensin-converting enzyme (ACE) inhibitor. Oral beta blocker was not prescribed in consideration of the occurrence of significant bradycardia on that drug. The clinical course was uncomplicated and, 6 months after the event, a planned CMR found complete functional recovery of the left ventricle, oedema reduction, disappearance of the intraventricular thrombus, subendocardial late gadolinium-enhancement (LGE) at the basal inferolateral wall level (Figures 3F–J) as a result of remote necrosis. Oral anticoagulation was stopped.

In early 2023, the patient arrived at the Emergency Room complaining of fatigue and chest pain. Since the ECG showed slight QRS widening, left anterior hemiblock, and ST-segment elevation in the lateral leads (Figure 1B), the patient underwent an immediate invasive angiography, which excluded again the presence of coronary artery stenosis and showed the apical ballooning pattern of the left ventricle, as in the previous episode (Figures 2E–H). The diagnosis was recurrent TTS. Research of obvious physical or emotional stress was negative. The only relevant finding was a positive routine swab test for severe acute respiratory syndrome coronavirus-2 (SARS-COV-2), in the absence of fever or respiratory symptoms. The hospital stay was prolonged due to transient QT-segment elongation, but no complications occurred. In consideration of the paucity of data about TTS relapse, the patient performed a third CMR. The imaging pattern was similar to that observed 2 years before: extended akinesia at the level of the middle and apical segments, which appeared diffusely oedematous in the STIR sequences; stable subendocardial LGE with ischemic pattern

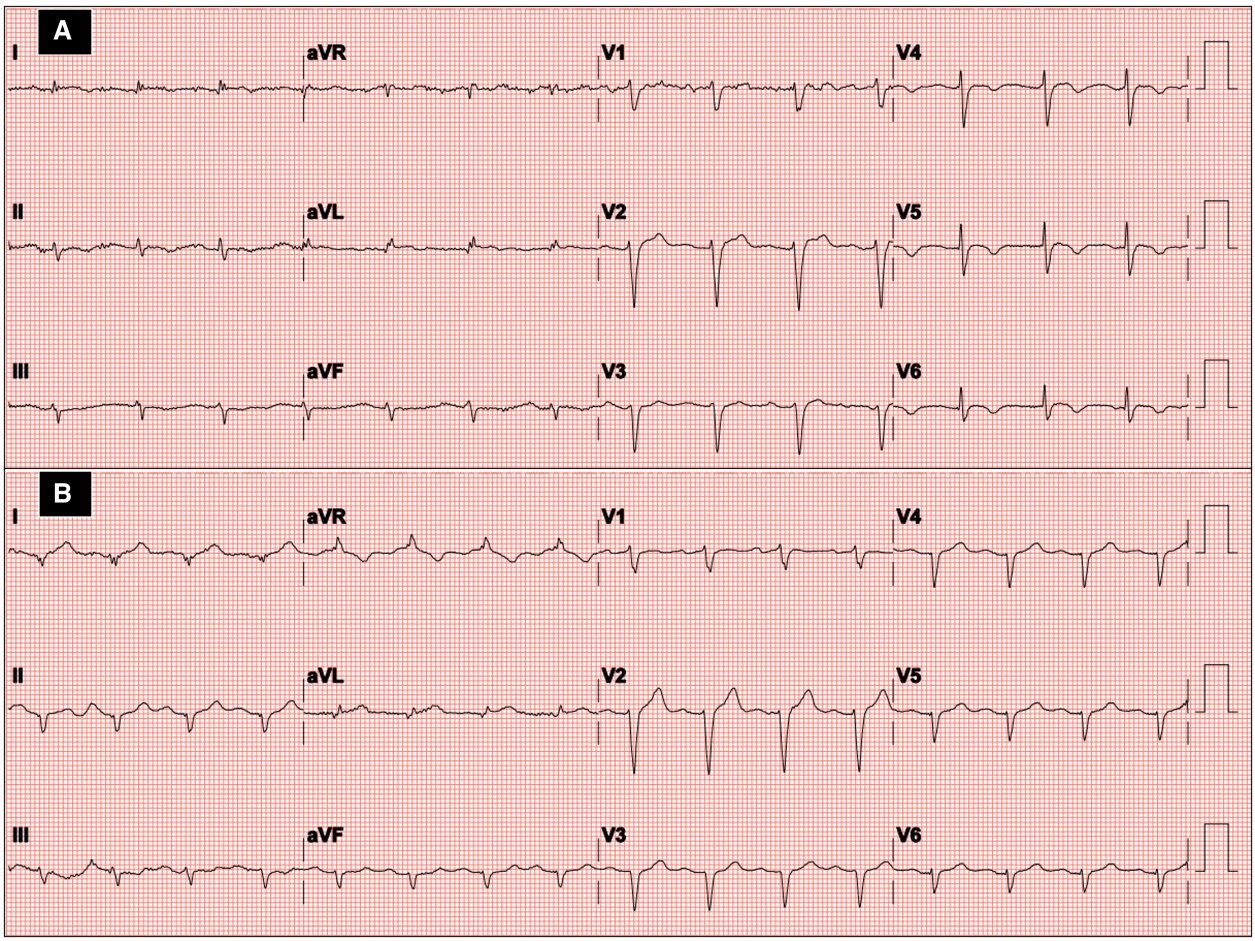

FIGURE 1
Twelve-lead ECG at hospital admission in the first episode (A) and recurrence of Takotsubo syndrome (B).

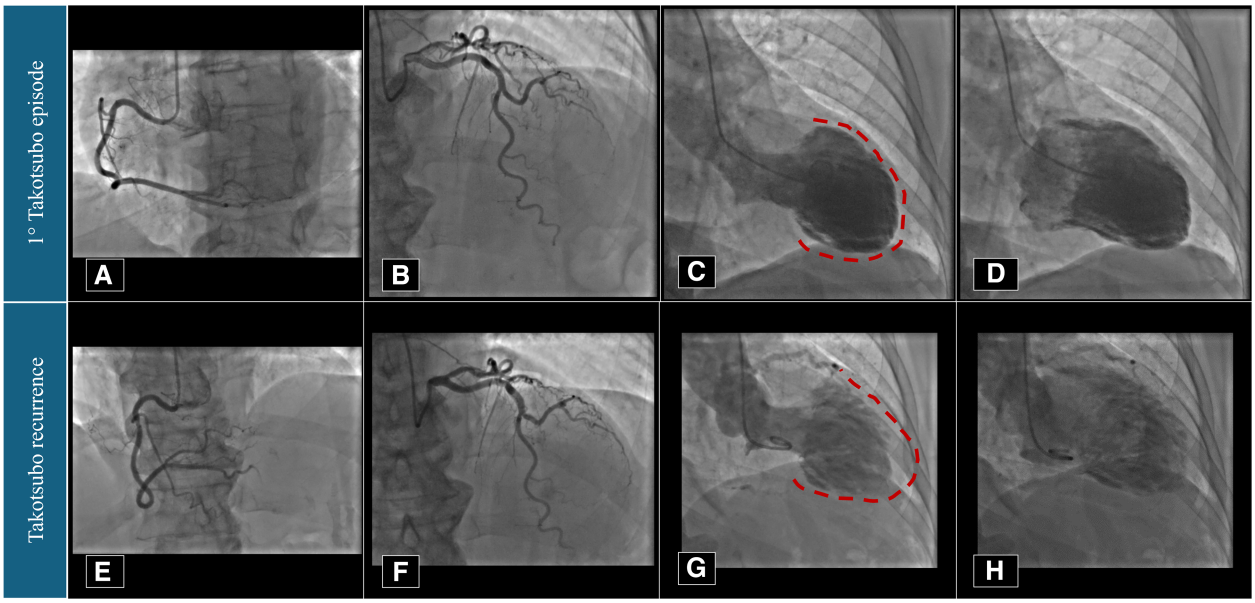

FIGURE 2
Coronary angiography and left ventriculography imaging performed in 2021 (A–D) and 2023 (E–H). Red dotted lines underline the apical akinesia during left ventricular systole.

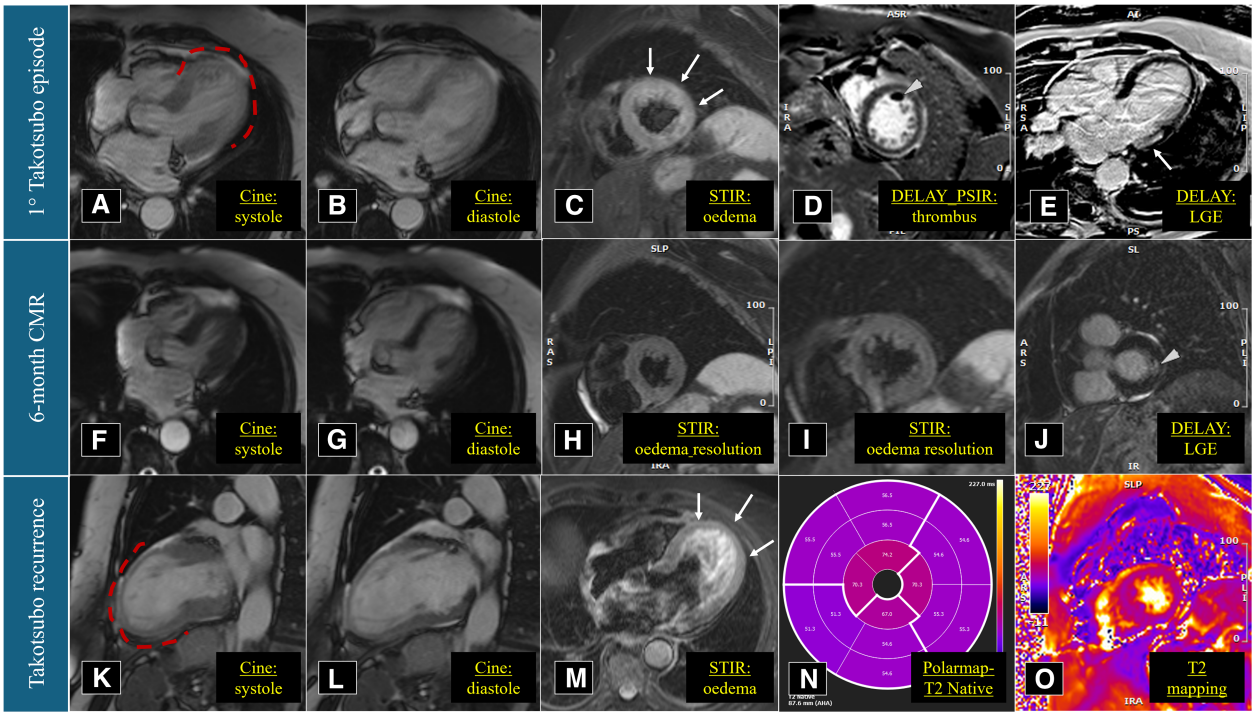

FIGURE 3
Cardiac magnetic resonance imaging performed in March 2021 (A–E), September 2021 (F–J), and March 2023 (K–O). Red dotted lines underline the apical akinesia during left ventricular systole.

at the basal infero-lateral wall (Figures 3K–O). We repeated the urinary metanephrine assay which demonstrated a slight, but not significant, increase in normetanephrine. WBC count was 5,450/mmc (URL 10,000/mmc), plasmatic interleukin-6 title was 44.7 pg/ml (URL < 5.9), while high-sensitive troponin-T peak was 386 ng/L (female gender URL <10).

Low dose of bisoprolol was added to therapy before discharge. At 1-month follow-up, a trans-thoracic echocardiography showed

the left ventricle with normal size, complete recovery of the systolic function (EF 64%), mild diastolic dysfunction. The patient had no further clinical events at 1-year.

Discussion

TTS is one of the possible cardiovascular complications of COVID-19, characterized by myocardial injury, left ventricular dysfunction, and clinical features of heart failure or ACS. In these patients, TTS may typically manifest as chest pain (38%) associated with respiratory symptoms, but in few cases with cardiac symptoms only (7.7%). Cardiac troponins are often elevated (>80%) and, notably, in-hospital mortality is high (18%–19%) (3, 4).

We reported a case of TTS recurrence in a 74-year-old lady, without a clear physical or emotional stress, but silent SARS-COV-2 infection with elevated inflammation markers. Noteworthy, recurrence is a rare circumstance for this uncommon disease. Singh et al. reported an annual recurrence rate of approximately 1.5%. It is estimated that 2%–5% of patients discharged to home may be affected by a second or more episodes of TTS in a 6-year period (5). Lau et al. observed a median time to recurrence of 2.87 years (6). In our patient, in line with previous data, in spite of differences in term of presence of a stressor, clinical presentation, and ECG alterations, the second episode presented with the same angiographic and CMR pattern (Table 1) (7). This can raise the hypothesis that the underlying myocardial injury may be similar despite possible different triggers. Indeed, the incidence of TTS during the COVID-19 pandemic increased likely due to the intense emotional stress caused by fear of getting seriously ill, fear for loved ones, changes to lifestyle habits including unemployment, economic crisis, and social distancing (8). On the other hand, in COVID-19 patients, irrespective of the severity of the clinical manifestation, several conditions which may favour TTS onset can occur: like catecholamine-induced myocyte injury and neurogenic myocardial stunning, cytokine storm, immune-mediated damage, direct viral myocyte injury, procoagulant state, microvascular coronary impairment due to endothelial injury, and vasospasm (9, 10). The hypothesis is that SARS-COV-2 infection, even asymptomatic, may precipitate TTS onset in predisposed patients, where endothelial dysfunction plays a pivotal role as cause of microvascular impairment (11). The existence of an individual susceptibility can likely manifest itself with episodes of relapse many years apart, in a different social and emotional context, with a different trigger event or in its absence (12). Interestingly, cases of TTS associated with Influenza A and B infection are reported (13).

TTS incidence is higher in postmenopausal women and its recurrence is similarly observed more frequently in the female gender. Conversely, several studies report a slightly higher incidence of SARS-COV-2 infection related TTS cases in males (14). Our patient was not taking a beta-blocker at the time of TTS recurrence. Some observational data found a protective effect of this therapy, but controversy exist about the efficacy of both beta-blockers and ACE-inhibitors administration (6, 15, 16). In consideration of the possible TTS onset without clinical suspicion of COVID-19 disease, its incidence in this setting may be underestimated. Therefore, the diagnosis can be missed or misdiagnosed as ACS or viral myocarditis (17).

TABLE 1 Timeline.

Sequence of events	1st episode of Takotsubo syndrome	Recurrence of Takotsubo syndrome
Presentation	Chest pain	Fatigue and chest pain
ECG	Negative T-waves in infero-lateral leads	ST-segment elevation in the lateral leads
Possible trigger	Argument on the phone	Asymptomatic SARS-COV-2 infection
Angiography	• No coronary stenosis, but slow flow • Left ventricle apical ballooning	• No coronary stenosis, but slow flow • Left ventricle apical ballooning
CMR	Hypokinesia of the mid-apical segments, with myocardial oedema	Akinesia of the mid-apical segments, with myocardial oedema
Outcome	Complete recovery	Complete recovery

Conclusion

SARS-COV-2 infection, irrespective of symptoms, is correlated with a higher risk of TTS and its recurrence.

Data availability statement

The raw data supporting the conclusions of this article will be made available by the authors, without undue reservation.

Ethics statement

The studies involving humans were approved by Comitato Etico Della Romagna CEROM. The studies were conducted in accordance with the local legislation and institutional requirements. The participants provided their written informed consent to participate in this study. Written informed consent was obtained from the individual(s) for the publication of any potentially identifiable images or data included in this article.

Author contributions

GD: Conceptualization, Writing – original draft, Writing – review & editing. MC: Data curation, Investigation, Writing – original draft. RC: Data curation, Writing – review & editing. SP: Data curation, Writing – review & editing. EG: Data curation, Writing – review & editing. MG: Conceptualization, Funding acquisition, Supervision, Writing – review & editing.

Funding

The author(s) declare financial support was received for the research, authorship, and/or publication of this article.

The study was supported by Fondazione Cardiologica M. Zito Sacco.

Conflict of interest

The authors declare the research was conducted in the absence of any commercial or financial relationships that could be construed as a potential conflict of interest.

Publisher's note

References

1. Bonow RO, Fonarow GC, O'Gara PT, Yancy CW. Association of coronavirus disease 2019 (COVID-19) with myocardial injury and mortality. *JAMA Cardiol.* (2020) 5(7):751–3. doi: 10.1001/jamacardio.2020.1105

2. Ghadri JR, Wittstein IS, Prasad A, Sharkey S, Dote K, Akashi YJ, et al. International expert consensus document on Takotsubo syndrome (part I): clinical characteristics, diagnostic criteria, and pathophysiology. *Eur Heart J.* (2018) 39 (22):2032–46. doi: 10.1093/eurheartj/ehy076

3. John K, Lal A, Mishra A. A review of the presentation and outcome of Takotsubo cardiomyopathy in COVID-19. *Monaldi Arch Chest Dis.* (2021) 91(3):1710. doi: 10.4081/monaldi.2021.1710

4. José SG, Carrizales-Sepúlveda EF, Vera-Pineda R, Morales-Rendón EJ, de Jesús Ortiz-Corona J, Flores-Ramírez R. Takotsubo cardiomyopathy and COVID-19: a case report and literature review. *Curr Cardiol Rev.* (2023) 19(2):e180822207660. doi: 10.2174/1573403X18666220818155039

5. Singh K, Carson K, Usmani Z, Sawhney G, Shah R, Horowitz J. Systematic review and meta-analysis of incidence and correlates of recurrence of Takotsubo cardiomyopathy. *Int J Cardiol.* (2014) 174(3):696–701. doi: 10.1016/j.ijcard.2014.04.221

6. Lau C, Chiu S, Nayak R, Lin B, Lee MS. Survival and risk of recurrence of Takotsubo syndrome. *Heart.* (2021) 107(14):1160–6. doi: 10.1136/heartjnl-2020-318028

7. Kato K, Di Vece D, Cammann VL, Micek J, Szawan KA, Bacchi B, et al. Takotsubo recurrence: morphological types and triggers and identification of risk factors. *J Am Coll Cardiol.* (2019) 73(8):982–4. doi: 10.1016/j.jacc.2018.12.033

8. Jabri A, Kalra A, Kumar A, Alameh A, Adroja S, Bashir H, et al. Incidence of stress cardiomyopathy during the coronavirus disease 2019 pandemic. *JAMA Netw Open.* (2020) 3(7):e2014780. doi: 10.1001/jamanetworkopen.2020.14780

9. Crea F, Iannaccone G, La Vecchia G, Montone RA. An update on the mechanisms of Takotsubo syndrome: "at the end an acute coronary syndrome.". *J Mol Cell Cardiol.* (2024) 191:1–6. doi: 10.1016/j.yjmcc.2024.04.009

10. Dong F, Yin L, Sisakian H, Hakobyan T, Jeong LS, Joshi H, et al. Takotsubo syndrome is a coronary microvascular disease: experimental evidence. *Eur Heart J.* (2023) 44(24):2244–53. doi: 10.1093/eurheartj/ehad274

11. Angelini P. Transient Takotsubo syndrome and its recurrence: why does it happen, why does it end, and why does it rarely reappear? *Int J Cardiol.* (2021) 330:142–4. doi: 10.1016/j.ijcard.2021.02.033

12. Iannaccone G, Montone RA, Del Buono MG, Meucci MC, Rinaldi R, Gurgoglione FL, et al. Recurrent asymptomatic takotsubo syndrome after 20 years: are we looking at the tip of the iceberg only? *Future Cardiol.* (2021) 17(2):309–14. doi: 10.2217/fca-2020-0043

13. Lozano A, Bastante T, Salamanca J, Aguilar R, Montes de Oca R, Rodríguez D, et al. Tako-tsubo cardiomyopathy triggered by influenza A virus infection. *Int J Cardiol.* (2014) 174(2):e52–53. doi: 10.1016/j.ijcard.2014.04.033

14. Giustino G, Croft LB, Oates CP, Rahman K, Lerakis S, Reddy VY, et al. Takotsubo cardiomyopathy in COVID-19. *J Am Coll Cardiol.* (2020) 76(5):628–9. doi: 10.1016/j.jacc.2020.05.068

15. Templin C, Ghadri JR, Diekmann J, Napp LC, Bataiosu DR, Jaguszewski M, et al. Clinical features and outcomes of Takotsubo (stress) cardiomyopathy. *N Engl J Med.* (2015) 373(10):929–38. doi: 10.1056/NEJMoa1406761

16. Santoro F, Sharkey S, Citro R, Miura T, Arcari L, Urbano-Moral JA, et al. Beta-blockers and renin-angiotensin system inhibitors for Takotsubo syndrome recurrence: a network meta-analysis. *Heart.* (2024) 110(7):476–81. doi: 10.1136/heartjnl-2023-322980

17. Sala S, Peretto G, Gramegna M, Palmisano A, Villatore A, Vignale D, et al. Acute myocarditis presenting as a reverse Tako-tsubo syndrome in a patient with SARS-CoV-2 respiratory infection. *Eur Heart J.* (2020) 41(19):1861–2. doi: 10.1093/eurheartj/ehaa286

frontiers | Frontiers in Cardiovascular Medicine

TYPE Review
PUBLISHED 05 July 2024
DOI 10.3389/fcvm.2024.1398290

OPEN ACCESS

EDITED BY
Tommaso Gori,
Johannes Gutenberg University Mainz, Germany

REVIEWED BY
João Silva Marques,
Centro Hospitalar Universitário Lisboa Norte (CHULN), Portugal
Steffen Daub,
University Medical Center of the Johannes Gutenberg University, Germany

*CORRESPONDENCE
Abhirup Banerjee
✉ abhirup.banerjee@eng.ox.ac.uk

RECEIVED 09 March 2024
ACCEPTED 06 June 2024
PUBLISHED 05 July 2024

CITATION
Lashgari M, Choudhury RP and Banerjee A (2024) Patient-specific *in silico* 3D coronary model in cardiac catheterisation laboratories. Front. Cardiovasc. Med. 11:1398290. doi: 10.3389/fcvm.2024.1398290

Patient-specific *in silico* 3D coronary model in cardiac catheterisation laboratories

Mojtaba Lashgari[1], Robin P. Choudhury[2] and Abhirup Banerjee[1,2]*

[1]Institute of Biomedical Engineering, Department of Engineering Science, University of Oxford, Oxford, United Kingdom, [2]Division of Cardiovascular Medicine, Radcliffe Department of Medicine, University of Oxford, Oxford, United Kingdom

Coronary artery disease is caused by the buildup of atherosclerotic plaque in the coronary arteries, affecting the blood supply to the heart, one of the leading causes of death around the world. X-ray coronary angiography is the most common procedure for diagnosing coronary artery disease, which uses contrast material and x-rays to observe vascular lesions. With this type of procedure, blood flow in coronary arteries is viewed in real-time, making it possible to detect stenoses precisely and control percutaneous coronary interventions and stent insertions. Angiograms of coronary arteries are used to plan the necessary revascularisation procedures based on the calculation of occlusions and the affected segments. However, their interpretation in cardiac catheterisation laboratories presently relies on sequentially evaluating multiple 2D image projections, which limits measuring lesion severity, identifying the true shape of vessels, and analysing quantitative data. *In silico* modelling, which involves computational simulations of patient-specific data, can revolutionise interventional cardiology by providing valuable insights and optimising treatment methods. This paper explores the challenges and future directions associated with applying patient-specific *in silico* models in catheterisation laboratories. We discuss the implications of the lack of patient-specific *in silico* models and how their absence hinders the ability to accurately predict and assess the behaviour of individual patients during interventional procedures. Then, we introduce the different components of a typical patient-specific *in silico* model and explore the potential future directions to bridge this gap and promote the development and utilisation of patient-specific *in silico* models in the catheterisation laboratories.

KEYWORDS

x-ray coronary angiography, coronary artery disease, catheterisation laboratory, patient-specific model, *in silico* medicine, segmentation, 3D reconstruction, blood flow simulation

1 Introduction

Coronary artery disease (CAD) is a pathological process characterised by atherosclerotic plaque accumulation in the epicardial coronary arteries. There are several clinical manifestations of this disease, including chronic stable angina and acute coronary syndromes. According to the World Health Organisation's global health estimates and global burden of disease data (estimates for 2019), CAD is the most commonly diagnosed heart disease worldwide. It is estimated around 200 million people are living with CAD, and it kills an estimated 9 million people each year (1).

Investigation of CAD includes functional evaluations, such as stress echocardiography, perfusion stress magnetic resonance imaging, and nuclear scintigraphy in myocardial perfusion imaging. In addition, computed tomography coronary angiography and invasive x-ray angiography can be used to evaluate the coronary arteries directly. Invasive x-ray coronary angiography is particularly valuable in patients with more severe disease, informing treatment decisions including the possibility of revascularisation through percutaneous coronary intervention (PCI) or bypass surgery. Coronary angiography provides high-resolution images of the coronary arteries that are widely used for stent implantation. It is often augmented with additional techniques, such as pressure wire evaluation of fractional flow reserve (FFR), intravascular ultrasound (IVUS), and intravascular optical coherence tomography (IOCT).

Although x-ray angiography is one of the most invaluable tools, it does have some drawbacks. First of all, it is an invasive procedure with potential vascular injury, haemorrhage, and embolisation. Furthermore, this procedure involves the use of x-ray contrast media that can cause or exacerbate renal dysfunction and cause adverse allergic reactions. For example, the US National Cardiovascular Data Registry reported that 7.1% of patients undergoing elective and urgent coronary intervention experienced contrast-induced acute kidney injury (2). In addition, there are issues of ionising radiation exposure for both the patient and the operator (3). Finally, the interpretation of the angiographic images is partially subjective and is prone to misinterpretation or variable interpretation (4). It is estimated that 70% of treatment decisions still depend on the visual assessment of angiographic stenosis within clinical settings, which has limited accuracy (about 60%–65%) in predicting FFR < 0.80, as reported by Hae et al. (5).

To overcome such vagaries, additional physiological studies including FFR or intravascular imaging are often utilised. For example, Jones et al. (6)'s large observational study confirms that IVUS and IOCT-guided PCI reduces in-hospital major adverse cardiac event rates and improves long-term survival when compared with standard x-ray angiography-guided PCI. However, they are expensive and time-consuming (7).

Patient-specific *in silico* models have shown their capability to enhance qualitative assessment by introducing quantitative elements into the diagnostic, interventional, and prognostic processes in different cardiovascular diseases (8–10). With *in silico* techniques, coronary arteriography could be more accurately assessed in real-time, with fewer views, less radiation, less contrast, and easier administration, all of which would benefit clinical practice. Using artificial intelligence (AI)-assisted *in silico* models, cardiologists only need two series of x-ray angiography sequence to generate the 3D structure of a coronary arterial tree, as shown by (11), thus reducing the time of x-ray exposure and dye injection while providing an accurate quantitative assessment. Additionally, it offers the computation of haemodynamic metrics such as FFR non-invasively, through blood flow simulation over the 3D structure, using mechanistic (12, 13) or data-driven (14) approaches.

In this paper, we review the key components needed to create a patient-specific *in silico* coronary model, as shown in Figure 1. After acquiring comprehensive and high-quality x-ray angiography sequences of a patient, the coronary arteries can be segmented using automated approaches discussed in Section 2. Detailed anatomical 3D digital twins of the patient's coronary tree can then be generated using the techniques discussed in Section 3. In the next steps, the digital twins of coronary arteries can be used for blood flow simulations, detailed in Section 4, which can be applied for computions of quantitative haemodynamic metrics to detect coronary stenoses and assess their severity (Section 5). Finally, Section 6 comprehensively discusses how patient-specific *in silico* models can be utilised to optimise the patientcare pathway in the catheterisation laboratory (cath. lab.). The paper concludes in Section 7.

2 Coronary vessels segmentation

3D reconstruction of the coronary arteries, discussed in detail in Section 3, often relies on the back-projection model-based methods, which require accurate skeletal representation and radius of coronary arteries as the inputs. The skeleton and radius of the vessels are typically obtained by segmenting the blood vessels. This section provides a comprehensive overview of different coronary vessel segmentation methods used for this purpose.

2.1 Non-temporal methods

2.1.1 Traditional statistical and machine learning based

- **Image thresholding** is a simple image segmentation method in which grayscale images are turned into binary images by categorising each pixel according to its intensity level concerning a threshold value. To improve the result of image thresholding in x-ray angiography, the coronary vessels are usually enhanced by utilising different imaging filters (16–19).
- **Vessel tracking** is another form of segmentation that involves extracting a path along a vessel from a designated starting point (20). Some techniques focus on isolating individual paths with defined start and endpoints, while others can identify the entire vessel tree and adeptly manage vessel branching (21–25).
- **Edge detection** identifies and extracts a set of points representing changes in brightness on an image, commonly referred to as an edge contour, arising from variations in grayscale between vessels and the background (26–29).
- In **region growing** method, seed pixels are used to create regions, and neighbouring pixels meeting specific criteria are added to those regions (30). To improve the results of region growing for vessel segmentation, different approaches have been proposed such as incorporating directional information (31–33), integrating with different methods such as random forest (34), and variable searching method of the pixels (35).
- **Graph-cut** uses a graph model to represent the image, where nodes represent pixels and edges represent the relationships between pixels in a graph. It divides the image into segments based on certain criteria, such as colour or intensity, to find the

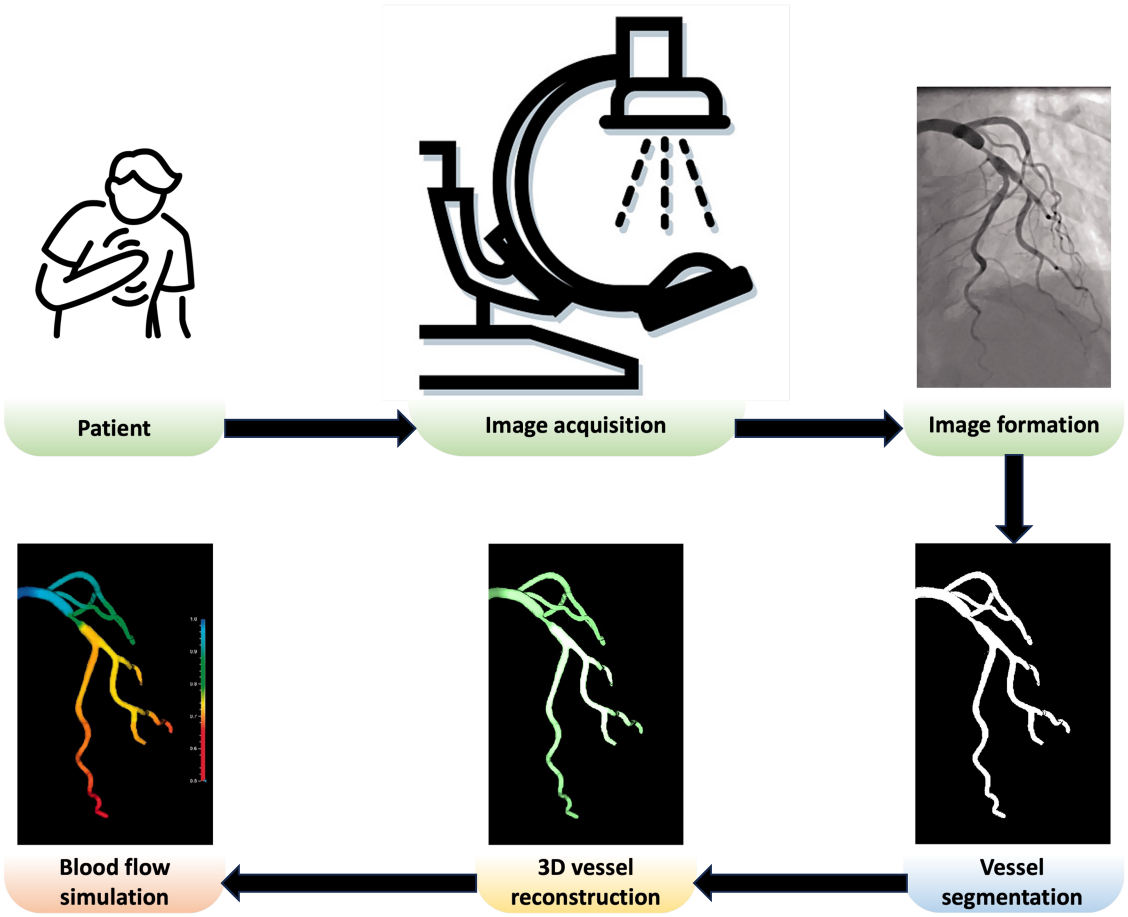

FIGURE 1
Overview of a patient-specific *in silico* model in the cath. lab. Adapted with permission from (15), © The Foundation Acta Radiologica 2021, https://doi.org/10.1177/0284185120983977.

optimal cut in the graph (36). Hernandez-Vela et al. (37), Sun et al. (38), Mabrouk et al. (39) developed automated multi-scale vessel extraction algorithms using the graph-cut method.

- **Fuzzy inference** uses the human-like reasoning style and offers potent and adaptable universal approximations, allowing interpretable IF-THEN rules (40). Sun et al. (41) used fuzzy mathematical morphology operations to extract coronary arteries, while Shoujun et al. (42) proposed a tracking approach that relied on both probabilistic vessel tracking and fuzzy structure pattern inference.
- In **deformable models**, a segmentation objective function (or energy function) is optimised through the calculus of variation. Image data constructs an energy function; minimising it yields segmentation results. These models use the original image for initial and boundary value problems. The contour, initially set as the desired region's boundary, evolves based on geometric image regions (43). Different variations of deformable models have been used for coronary vessels segmentation, such as parametric active contours (44, 45), geometric active contours (32, 46, 47), gradient vector flow active contour (48), region-based active contour (49), etc.
- Methods based on **machine learning** models leverage intricate algorithms and training on diverse datasets to enhance the ability to discern intricate coronary vessels structures from a complex background of x-ray angiography. The machine learning methods used for coronary vessels segmentation include marginal space learning paradigm and probabilistic boosting trees (50), random forest (51), robust principal component analysis (PCA) (52, 53), etc.

2.1.2 Neural network based

Neural networks, modelled after the human brain, consist of interconnected neurons organised into layers. During training, they adjust connection strengths between neurons to minimise prediction errors using a method called backpropagation. Once trained, neural networks make predictions by passing new data through the network based on learned patterns. Success depends on training data quality, network architecture, and parameter selection. Neural networks generally segment images by classifying pixels into specific categories, such as objects or boundaries. This process involves leveraging patterns and features within the image data to accurately delineate different regions. One of the oldest applications of neural networks for identifying

coronary vessels in x-ray angiograms was done by Sun (54), pioneering the use of neural networks in medical imaging for precise vessel localisation and analysis.

- **Convolutional neural networks** (CNNs), a type of deep learning model, have been employed for tasks of coronary vessels segmentation in multiple studies (55–58). CNNs, as shown in Figure 2A, utilise layers to learn hierarchical features through convolutional operations, pooling, and fully connected layers, enabling automatic and adaptive spatial feature learning from the input images.
- **Encoder-decoder**, illustrated in Figure 2B, is another type of deep learning neural network used for coronary vessel segmentation (59, 60). Encoding involves passing an image through a series of convolutional and pooling layers, e.g., Figure 2A. In these layers, spatial dimensions are downsampled while capturing the important features, thus extracting hierarchical features while condensing the input image. In the decoder, the spatial dimensions are gradually reconstructed using upsampling operations based on the feature map from the encoder.
- **U-Net** architecture, as shown in Figure 2C, is an example of encoder-decoder architecture designed to segment images. It was introduced by Ronneberger et al. (61) and has since become a popular and effective neural network used for coronary vessels segmentation (62–65). It is named after its distinct U-shaped structure and differs from other encoder-decoder networks because it uses skip connections to connect the corresponding layers of encoding and decoding, thus preserving fine-grained details during segmentation.
- **Adversarial learning** is another type of neural network applied for coronary vessels segmentation (66). This network involves training a model against adversarial examples generated to deceive the model. The model learns to be more robust by experiencing and adapting to these adversarial inputs. A popular branch of adversarial learning is generative adversarial networks (GANs), which have been used for vessel segmentation in x-ray angiography (67, 68). A GAN consists of two structures, a generator and a discriminator, as presented in Figure 2D. The generator generates data instances, while a discriminator evaluates them. Both are trained simultaneously, with the generator aiming to produce realistic data and the discriminator aiming to distinguish between the real and the generated data.
- **Attention mechanism** enables models to make predictions while focusing on specific details of coronary vessels in images (69). This mechanism is usually incorporated into various deep neural networks such as encoder-decoder (70), U-net (71), and adversarial network (66).
- **Ensemble deep learning** is intended to enhance the model's generalisation, robustness, and accuracy by leveraging the diversity of multiple models. To improve the overall performance of vessel segmentation, ensemble deep learning models combine vessel predictions from multiple individual neural network models such as combining style transfer with dense extreme inception network and convolution block attention (72), EfficientNet with U-Net (73), gradient-boosting decision trees with deep forest classifiers (74), ensemble encoder-decoder networks (75), U-Net with DenseNet-121 (76), and bi-directional ConvLSTM algorithm with U-Net and DenseNet models (77).

More recently, advanced deep learning architectures namely Nested U-Nets or UNet++ (78), graph neural network (79), etc. have been utilised for acheiving state-of-the-art performance for coronary vessels segmentation in x-ray angiography.

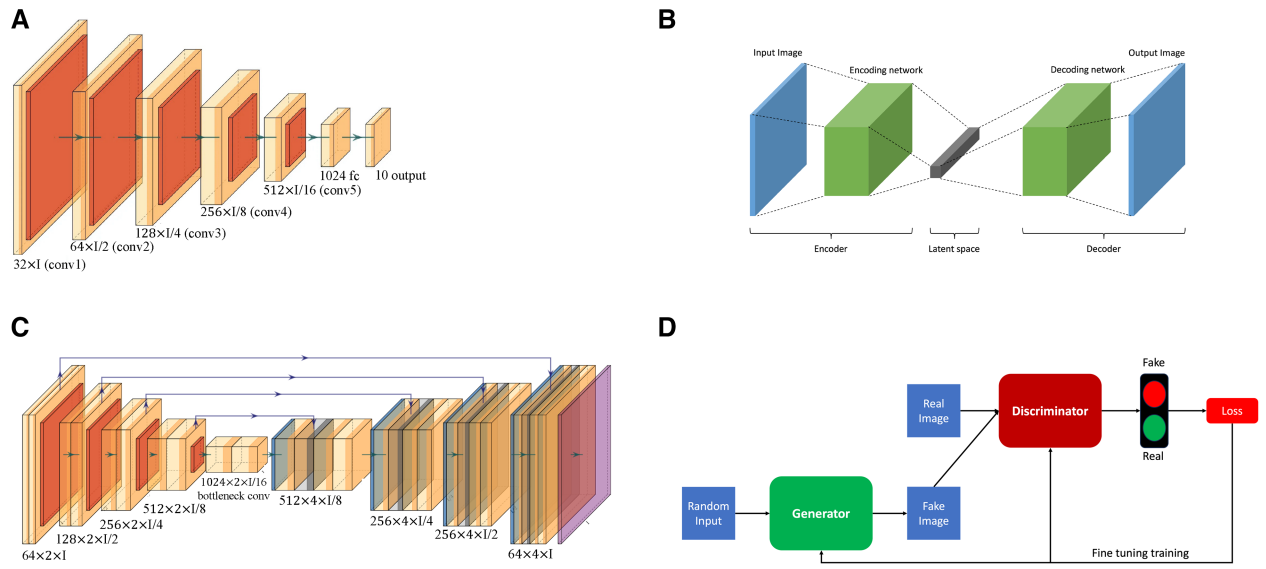

FIGURE 2
Overview of the basic neural network architectures used for coronary vessels segmentation: (**A**) Convolutional neural network (CNN); (**B**) Encoder-decoder; (**C**) U-Net; and (**D**) Generative adversarial network (GAN).

2.2 Temporal methods

All the methods discussed in the previous subsection used a single frame to segment the coronary vessels. Some studies in the literature also utilised multiple invasive coronary angiography (ICA) frames to capture temporal information for vessels segmentation. These studies aimed at mitigating noise and motion, enhancing overall contrast, and were robust to variations in image quality, illumination, and other artifacts. Temporal methods have been applied to improve segmentation quality over a variety of techniques, including vessel tracking (80), region growing (81), graph cut (82, 83), machine learning (84), as well as neural network approaches of CNN (85, 86), encoder-decoder (87), U-Net (88, 89), ensemble learning (90), etc.

3 3D reconstruction of coronary arteries from ICA images

A patient-specific model relies heavily on 3D geometry of the coronary vessels or the whole coronary arterial (CA) tree. This helps cardiologists and medical professionals better understand the anatomy, structure, and any potential abnormalities in the arteries during the intervention, and guide catheters and devices to the target area with greater accuracy. Additionally, the reconstructed 3D CA tree model allows for personalised treatment plans tailored to the specific anatomy of the patient through simulating different treatment scenarios, leading to optimised outcomes and reducing the risk of complications. However, creating an accurate 3D model of coronary arteries is a sensitive task and crucial to a successful intervention as well as a personalised treatment plan. For example, Solanki et al. (91) using arterial phantom models showed that minor reconstruction errors led to clinically significant inaccuracies in "virtual" fractional flow reserve (vFFR) computation.

Çimen et al. (92) reviewed the leading methods for reconstructing the 3D surface of coronary arteries using high-contrast x-ray angiography. In this section, we explain briefly the categories introduced by Çimen et al. (92) along with a brief review of the most recent 3D CA tree reconstruction approaches.

3.1 Back-projection based methods

Though several different approaches have been proposed for coronary artery reconstruction in the literature, back-projection based methods remain the most common. Back-projection methods fall into the model-based reconstruction categories, which aim to create a 3D/4D binary model of coronary arteries, typically comprising a centerline and sometimes the vessel surface. In back-projection modelling, the CA tree is constructed by projecting two-dimensional (2D) information derived from ECG-gated projection images. There are two types of methods: methods that rely on 2D feature matching and methods that use back-projection of vesselness responses (92).

Methods based on 2D feature matching, depicted in Figure 3A, begin by segmenting artery centerlines and identifying key structures such as bifurcations within projection images. Using epipolar geometry, correspondences between centerlines are established between different views, and computer vision algorithms are used to reconstruct 3D points representing the CA tree. The accuracy of these methods relies heavily on segmentation accuracy during centerlines extraction. Recently, Çimen et al. (92) represented 3D coronary artery centerlines as a mixture of Student's *t*-distributions and performed a maximum-likelihood estimation of model parameters using 2D x-ray image segmentation. Unberath et al. (93) enhanced reconstruction quality by effectively removing erroneously reconstructed points on the centerline. Vukicevic et al. (94) used a robust genetic algorithm optimiser to identify calibration parameters for x-ray

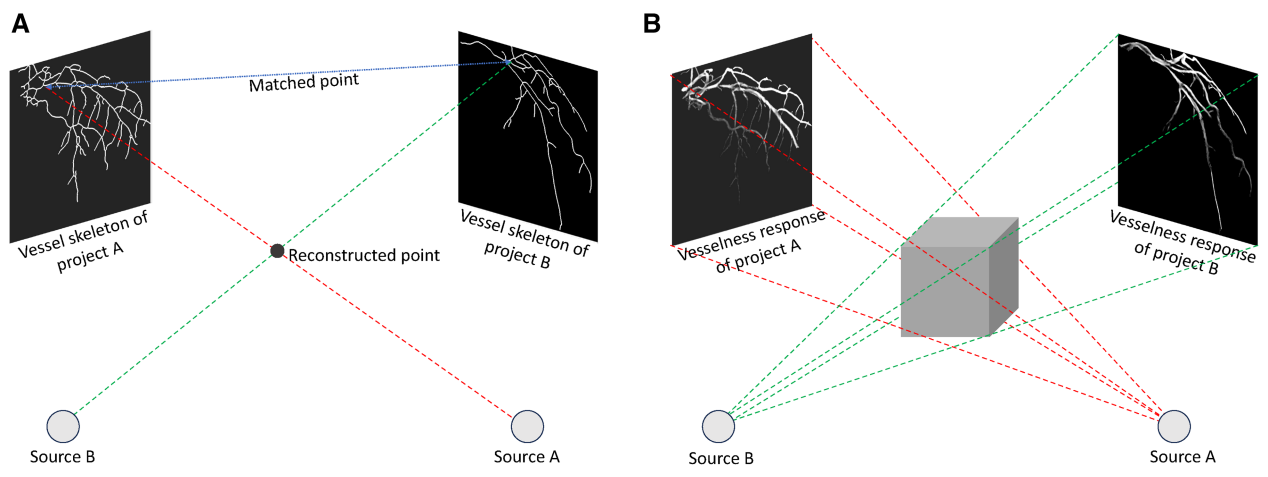

FIGURE 3
Back-projection methods to reconstruct 3D coronary arteries: (A) Techniques relying on 2D feature matching establish correspondences between centrelines in distinct 2D views and perform reconstruction through triangulation, (B) Approaches centered on the back-projection of vesselness response generate a 3D volumetric vesselness response from 2D vesselness responses for subsequent processing.

angiography views. A partial-matching approach was applied to establish correspondences between frames in x-ray acquisitions, and the same matching method was applied to reconstruct vessel centerlines efficiently. Galassi et al. (95) reconstructed the 3D centerlines by intersecting surfaces from matching branches from 2D views. Then, the 3D luminal contours were created by interpolating computed 3D boundary points with non-uniform rational basis splines. In another work, Banerjee et al. (11) first reduced angiographic motion artifacts for rigid and non-rigid motion (96, 97), and then used an innovative point-cloud based approach to 3D vessel centerline reconstruction by iteratively minimising reconstruction error. These methods are beneficial to non-calibrated systems since they can easily incorporate the estimation of geometry parameters that relate to the projection images used for reconstruction. The vascular start/end and bifurcation points, which are extracted during segmentation, are often used for this purpose. Although some works tried to match these corresponding points (98–103), most of the 3D reconstruction methods need clinicians to manually find these corresponding points in the projected images.

In contrast, in **methods based on back-projection of vesselness responses**, shown in Figure 3B, 2D projection images are used to calculate vesselness responses, such as binary segmentation (104), tubularity response (105), and distance map to centreline (106). These responses are then back-projected based on imaging geometry to generate 3D volumetric vesselness responses. Following this, coronary artery reconstruction is conducted using segmentation methods. One of the drawbacks of these methods is that they may require more rotational x-ray angiogrms in order to generate an accurate 3D reconstruction.

3.2 Forward-projection based methods

Another type of model-based reconstruction methods is forward-projection that employs 3D models that adapt to vessel structures in 2D x-ray projections. The forward-projection reconstruction often relies on 3D parametric active contour methods, where external and internal energy, computed from images, are used to adjust 3D active contours (107–109). In CA tree reconstruction, every artery branch has its active contour model, which presents a challenge in designing energy components. Cong et al. (107) compared common deformable model based methods, namely potential energy (110), gradient vector flow (111), and generalised gradient vector flow (112), on a series of experiments on phantom and clinical data.

3.3 Tomographic reconstruction

Tomographic reconstruction creates coronary artery volumes directly from x-ray coronary angiography images. As opposed to binary model based reconstruction, it provides information on x-ray absorption coefficients, as well. Due to the minimal knowledge they require about the CA trees, these methods accommodate atypical anatomies (e.g., collaterals, tortuous branches). As a result, they provide more detailed vessel surface information without any preprocessing or manual inputs (113–115).

The drawbacks of these methods are they assume pre-acquisition calibration of the x-ray imaging system and typically require more x-ray images with wider angular coverage than modelling based reconstructions. For coronary artery branches to be visible, these methods require precise isocentering and consistent injection of contrast. Moreover, they ignore the propagation of contrast agents over time, assuming constant contrast distribution over time. Finally, these approaches typically require more computational resources than model based reconstructions. Also, it is often necessary to hold breath during coronary angiography to minimise respiratory motion to reconstruct tomographic images (92).

3.4 3D+time (4D) model based reconstruction

Model based methods can be extended to 4D coronary artery reconstructions. The basic 4D strategy involves independent 3D reconstructions for each cardiac phase, which requires vessels segmentation for each phase. To avoid this, temporal constraints which penalise differences between adjacent phases have been utilised, and temporal correspondences have been established through branch or tree-matching algorithms (116–118).

4 Simulation

The final component for completing the patient-specific model in cath. lab. is to simulate hemodynamics in coronary arteries. The patient-specific model of blood flow in the coronary arteries using computed tomography has been well established due to fewer challenges in the creation of a 3D model of coronary arteries (12, 119). Some of the technological developments for blood flow simulation using computed tomography can be used directly over 3D vascular models from x-ray angiography, as these methods are often independent of imaging techniques. The following subsections describe the developments for coronary blood flow simulation.

4.1 *In silico* flow computation approaches

The Navier-Stokes equations are a set of partial differential equations that represent the physics of a fluid dynamic. However, they are complex partial differential equations, which are difficult to solve analytically and computationally expensive to simulate accurately. There are two distinct approaches of mechanistic modelling and data-driven modelling (Figure 4) to simulate blood flow based on the Navier-Stokes equations, each with its own set of characteristics and advantages.

4.1.1 Mechanistic approaches

This approach involves formulating mathematical equations that represent these processes. This approach is commonly used

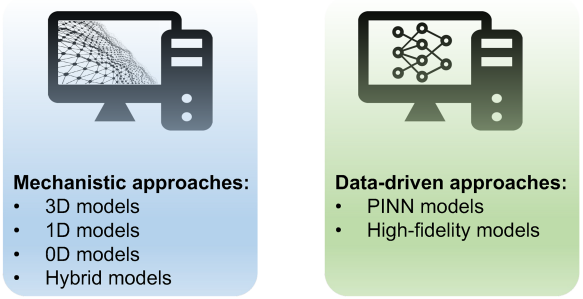

FIGURE 4
Overview of *in silico* flow computation approaches.

in fields where a deep understanding of the system is available, and where the goal is to gain insights into the underlying processes, optimise system performance, or test hypotheses. The mechanistic models to solve Navier–Stokes equations can be divided into four groups (12, 13).

(a) **3D models** use numerical methods such as finite elements to solve Navier–Stokes equations. Using this approach, circulation geometry can be accurately represented, 3D pulsatile flow (including turbulence) can be captured, and complex blood and vessel material models can be incorporated (120).

(b) **1D models** are created by averaging the Navier-Stokes equations over a vessel's cross-section. These models ignore non-axial velocity components, assume an axial velocity profile across locations of vessels, and maintain constant pressure across the vessel cross-section. However, these models are invalid near side branches, bifurcations, or diseased segments, especially for serial lesions or lesions at branches and bifurcations (120–123).

(c) The **0D model** or lumped parameter circulation model, developed by Sagawa et al. (124), consolidates spatially varying properties into discrete components. Considering the flow steady, axisymmetric, unidirectional, and vessel segments as circular cylinders, this model simplifies fluid resistance in vessels to a single resistive element. It often results in a high level of inaccuracy in blood flow in diseased coronary arteries, where no steady or unidirectional flow occurs or no axisymmetry or circular shape to vessel segments exist (122, 124–126).

(d) The **hybrid models** aim to reduce computational time while providing more accurate simulation results. It includes a combination of the different mechanistic approaches such as 0D and 1D models (123, 125) and 1D and 3D models (13, 127–129).

4.1.2 Data-driven approaches

Data-driven approaches extract patterns, relationships, or trends from observed data without explicitly considering underlying physical or mechanistic principles. The technique is often used for modelling complex, unknown, time-consuming, or difficult-to-model physical processes. There is, however, a lack of sufficient training data for data-driven methods (130). To address the lack of experimental data, two solutions exist: enhancing deep learning through physics-based losses, known as physics-informed neural networks (PINN) (131–134), or conducting high-fidelity *in silico* simulations to implicitly make the model sensitive to the underlying physics (135–139).

In the application of coronary blood flow using a large high-fidelity dataset, Itu et al. (140) introduced a machine learning model to predict fractional flow reserve (FFR), trained on a large database of synthetically generated coronary anatomies with flow parameters like velocity computed using the mechanistic approaches. Carson et al. (141) compared the performance of three AI models – feed-forward neural network (FFNN), long short-term memory, and multivariate polynomial regression, to measure FFR. Based on a 1D physics-based model, algorithms were trained and compared on a single vessel, multi-vessel network, as well as a virtual patient database, demonstrating the outperformance of a FFNN over two other methods in all cases. Gao et al. (142) proposed TreeVes-Net, a recurrent neural network (RNN) that captures geometric details for blood-related representation using a tree-structured representation encoder. This tree-structured RNN creates long-distance spatial dependencies, enhancing coronary flow modelling. Xie et al. (143) suggested a physics-informed graph neural network for FFR assessment, incorporating morphology and boundary conditions as inputs to learn conditioned features. In another work, Zhang et al. (144) proposed a PINN including a morphology feature encoder and an attention network to simulate the pressure and velocity along the centerline of the vessels based on the morphology features of coronary arteries.

4.2 *In silico* flow computation based on x-ray angiography images

Mechanistic model developed by Morris et al. (145), termed virtual FFR (vFFR), was one of the first to accurately predict coronary artery disease based on patients' FFR using only x-ray angiography images. The initial vFFR model necessitated over 24 hours of computation, employing a fully transient, 3D-0D coupled model. Faster methods were introduced in 2017 (146) and 2023 (147), yielding results in just 3 min and less than 30 s, respectively, while maintaining the accuracy of a full 3D model (148). Recently, more studies have been developed to provide angiography-derived FFR based on mechanistic modelling (149–156).

With **Data-driven models**, Zhao et al. (157), Xie et al. (143) proposed deep neural networks based on CNN and graph neural network to compute the FFR and coronary flow reserve (CFR), respectively.

5 Quantitative hemodynamic metrics for coronary artery assessment

Functional metrics for coronary lesion severity assessment can be established through the development of patient-specific *in silico*

models. Incorporating computational simulations with clinical data allows to gain a more detailed understanding of the complex dynamics inside coronary arteries, enabling better assessment metrics. According to several studies (158–161), quantitative measurements of arterial stenosis severity reduce unnecessary surgeries and cardiac events in patients with coronary artery disease. This section discusses the most important metrics used for this purpose.

(i) **Fractional flow reserve (FFR)** traditionally has been used for assessing the hemodynamics of coronary arteries. As part of the cardiac catheterisation procedure, a special wire is threaded through the coronary arteries, equipped with a pressure sensor. FFR is then calculated by comparing blood pressure before and after the stenosis as shown in Figure 5. Using this ratio, clinicians can determine how much blood flow to the heart has been impeded by the narrowing. FFR can provide valuable insights into whether coronary stenosis requires intervention, such as angioplasty or stent placement, or can be treated medically (162).

(ii) **Coronary flow reserve (CFR)** is another diagnostic metric in the decision-making process for coronary interventions. It is calculated by comparing coronary blood flow during maximal vasodilation and at rest. Three factors influence it: vascular resistance in the small and large coronary arteries, myocardial resistance, and factors that affect blood composition. CFR provides valuable information for evaluating coronary artery dilation ability and determining whether coronary interventions are necessary (163). By comparing the CFR of a stenotic coronary artery to a reference segment, such as a non-stenotic segment or one with minimal disease, relative CFR (rCFR) can be calculated. It is particularly useful when evaluating the functional implications of a coronary artery by comparing the blood flow through a particular stenosis to that of another less affected artery (158, 164, 165).

(iii) **Index of microcirculatory resistance (IMR)** was introduced in 2003, where a pressure wire uses its sensor as a thermistor and measures temperature. The tool functions as a thermometer and measures the mean transit time of room-temperature saline injected into a coronary artery using a thermodilution curve. As part of the test, pressure and temperature are measured in the heart's small vessels, both at rest and at maximum blood flow. It allows the clinician to determine how well blood flows in the heart's small vessels (166–168).

(iv) **Instantaneous wave-free ratio (iFR)** is a test using a special catheter to check the pressure in the heart's blood vessels. It looks at pressure during both the wave-free period and the entire cardiac cycle. This helps doctors see how a blockage affects blood flow. One of the advantages of iFR is that it doesn't need adenosine, a medicine used in other tests to stress the heart and check blood flow (169–171).

(v) **Resting full-cycle ratio (RFR)** is a new index that is used to evaluate the significance of coronary vessel lesions. In the cardiac cycle, it is defined as the lowest ratio of distal pressure to aortic pressure, measured at rest without the introduction of hyperemia (172–174).

Table 1 summarises the quantitative hemodynamic metrics for coronary artery assessment, along with the mathematical formula.

6 Discussion

The development of patient-specific models in the cath. lab. can enhance patient care and improve outcomes in various ways. A patient-specific model can provide detailed insight into

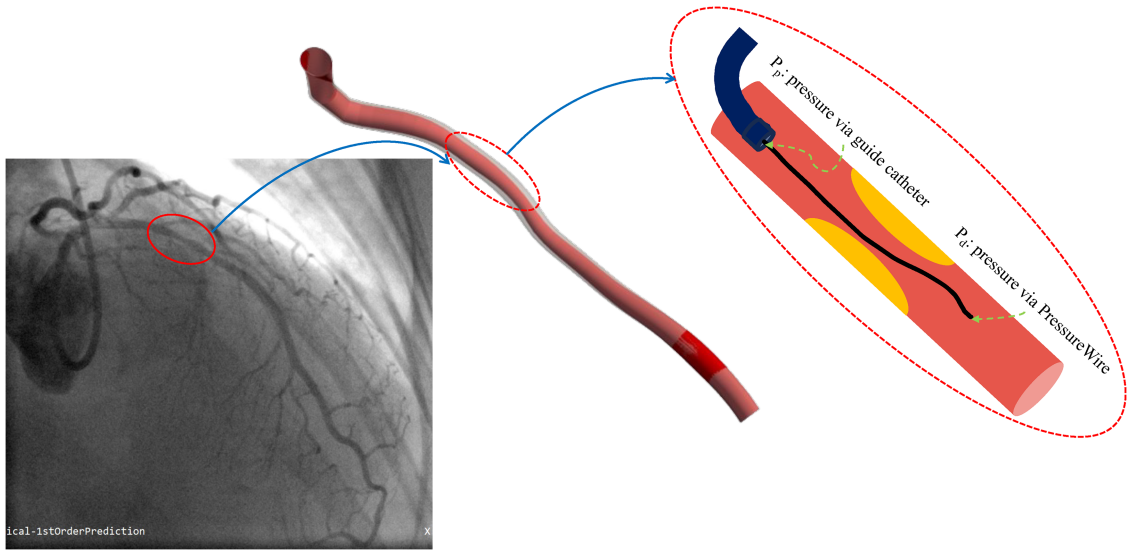

FIGURE 5
Measuring blood pressure before and after stenosis.

TABLE 1 Summary of quantitative hemodynamic metrics for coronary artery assessment.

Formula	Usage
$FFR = \frac{P_d}{P_p}$	To determine functional significance of a coronary stenosis (162).
$CFR = \frac{F_h}{F_r}$	To determine whether coronary arteries can dilate and accommodate increased blood flow (163).
$rCFR = \frac{CFR_{\text{Stenosis}}}{CFR_{\text{Reference}}}$	To evaluate the impact of a specific stenosis on blood flow compared with a healthier or less affected reference region (158).
$IMR = \frac{P_d}{T_{\text{mn}}}$	To provide information about the status of microcirculatory resistance.
$iFR = \frac{P_{d_{wave-free}}}{P_{a_{wave-free}}}$	Similar to FFR, without the need to administer a hyperemic agent, such as adenosine (169).
$RFR = \frac{P_d}{P_a}$	Similar to FFR, without the need to administer a hyperemic agent, such as adenosine (173).

P_d, pressure measured at the distal of a stenosis; P_p, pressure measured at the proximal of a stenosis; F_h, coronary blood flow during maximal hyperemia; F_r, coronary blood flow at rest; T_{mn}, mean transit time of a specific flow and temperature; $P_{d_{\text{wave-free}}}$, P_d measured at rest during a wave-free period; $P_{a_{\text{wave-free}}}$, P_a measured at rest during a wave-free period; P_a, aortic pressure.

the anatomy and pathology of a patient's vascular system. Clinicians can use this information to plan and customise cardiac interventions like angioplasty, stent placement, or other procedures. Furthermore, physicians can anticipate challenges by simulating procedures on patient-specific models before they are performed. In addition, patient-specific models help with the selection and size of medical devices, such as stents and catheters, based on accurate vessel dimensions and measurements. Additionally, patient-specific models enhance research by exploring new treatment strategies, testing innovative devices, and understanding underlying physiology.

As illustrated in Figure 1, a variety of medical image analysis methods should be employed to develop patient-specific models, including segmenting coronary arteries, reconstructing 3D geometry, and simulating blood flow to compute physiological biomarkers to detect and assess stenosis severity. There are potential sources of uncertainty in each stage of the modelling process, which can potentially propagate to the subsequent stages, resulting in an unreliable simulation result. For instance, Solanki et al. (91) demonstrated that the errors arising from the epipolar line projection method used to reconstruct 3D coronary anatomy from x-ray angiography images are small but result in clinically relevant errors in vFFR simulation, amounting to approximately 40% of the total error associated with vFFR. In the following paragraphs, we discuss the potential sources of uncertainty at each stage of the analysis.

Segmentation: According to Table 2, deep learning methods have significantly improved coronary vessels segmentation accuracy. However, there exist three potential challenges that limit the generalisation performance and result in discontinuity in segmented vessels. The first challenge is the imaging artifacts such as weak contrast between coronary arteries and the background, unknown vessel tree shape, and shadows of overlapping body structures. Secondly, due to the acquisition of a complex 3D structure in 2D projection planes, the coronary vessels overlap on x-ray angiography images, making segmentation and vessel delineation difficult, especially in regions where vessels are close together. Last but not least, the x-ray angiography captures contrast agents flowing through vessels during dynamic imaging. Hence, segmentation methods often face challenges with temporal changes and vessel appearance variations throughout the cardiac cycle. The recent advances in AI and deep learning have shown promising results in addressing some of these shortcomings, though they are often limited by the training datasets.

3D reconstruction: In recent years, 3D reconstruction methods for coronary arteries based on x-ray angiography have gone through significant advances, though they still face some challenges. First, the 3D surface reconstruction can be irregular due to non-orthogonal contours to the vessel centerline and difficulties defining its cross-sectional shape. The information available from 2D x-ray angiography projections is often limited, as they can only provide limited information at a finite number of projection planes and may not provide a complete representation of the vessel geometry. Secondly, movements in coronary arteries mainly due to cardiac and respiratory motions create difficulties in establishing correspondences between 2D segmented vessels and, as a result, affect the vessel centerlines reconstruction. Since correspondence is commonly based on epipolar constraints, significant vessels overlap and foreshortening may impact their performance.

The 3D vascular geometry can also be reconstructed using IVUS and IOCT, which are both intravascular imaging technologies to capture cross-sections of coronary arteries. In contrast to x-ray angiography, IVUS and IOCT images reveal external elastic membrane and plaque materials in addition to

TABLE 2 Summary of the best performance of different coronary vessels segmentation methods.

Study	Method	Dataset size	Dice	Sensitivity	Specificity	Precision	Accuracy
Felfelian et al. (17)	Thresholding	50 (Test)	72.79	74.92	98.32	–	97.09
Tsai et al. (24)	Tracking	20 (Test)	–	96.70	96.30	–	96.30
Mabrouk et al. (39)	Graph-cut	91 (Test)	75.60	76.60	–	77.60	–
Lv et al. (46)	Deformable model	4 (Test)	76.24	72.33	–	80.59	–
Jin et al. (52)	PCA	223 (Test)	76.97	71.25	83.95	–	–
Zhu et al. (58)	CNN	73 (Train), 36 (Test)	88.40	87.30	–	90.10	–
Iyer et al. (59)	Encoder-decoder	370 (Train), 92 (Test)	86.40	91.80	98.70	–	98.30
Yang et al. (64)	U-Net	2,642 (Train), 660 (Test)	89.60	89.30	–	90.60	–
Hamdi et al. (67)	GAN	100 (Train), 50 (Test)	81.18	81.09	98.11	81.26	96.55
Tao et al. (70)	Attention mechanism	104 (Train), 30 (Test)	–	87.70	97.89	–	97.29
Gao et al. (74)	Ensemble method	104 (Train), 26 (Test)	87.40	90.20	99.20	85.70	–

the coronary lumen. These approaches, however, are used to image a single branch of non-bifurcated vessels, and they considerably increase patient-care costs (175, 176). X-ray angiography, on the other hand, provides a very accurate image of the entire coronary arterial tree with minimal invasion, which makes it safer and more useful for automated 3D reconstruction of coronary vessels.

Blood flow simulation: The development of sophisticated computational fluid dynamics techniques has allowed researchers to model blood flow in complex coronary arteries with greater accuracy. There still exist some challenges and limitations. Limitations in segmenting small or terminal vessels limit coronary blood flow simulation in larger epicardial vessels. The boundary conditions at the outlet of the terminal vessel approximate downstream arterial circulation behaviour, and the lack of segmenting terminal vessels leads to a wrong boundary conditions assignment which invalidates assessment of the disease's impact on myocardial blood flow (177, 178). Gamage et al. (179) showed that side branches downstream of stenosis result in a lower FFR, while those upstream have minimal impact. Moreover, to estimate FFR accurately, side branches with a diameter greater than one-third of the main vessel diameter should be taken into account. In addition, it is crucial to consider patient-specific boundary conditions and the associated uncertainties. If the associated parameters of the 3D inflow velocity profile cannot be specified, the domain flow field can be significantly impacted (180). Further research should try to calculate patient-specific boundary conditions by estimating the blood velocity in coronary arteries using cine x-ray angiographic sequence (181).

7 Conclusion

While coronary angiography remains a vital diagnostic tool in the assessment of coronary artery disease, the limitations inherent in the current interpretation methods call for a paradigm shift. Patient-specific *in silico* models, with their ability to simulate and analyse individualised data, present a promising avenue for advancing interventional cardiology. By addressing the challenges highlighted in this paper and accordingly embracing these models in catheterisation laboratories, we can unlock the full potential of *in silico* modelling. The integration of patient-specific *in silico* models into routine practice has the potential to revolutionise treatment optimisation, providing clinicians with valuable insights and enhancing the precision of interventions. Future research and development efforts should focus on bridging the existing gap and promoting the widespread adoption of these models in the cath. lab. settings.

Author contributions

ML: Conceptualization, Investigation, Visualization, Writing – original draft, Writing – review & editing. RPC: Funding acquisition, Project administration, Resources, Supervision, Writing – review & editing. AB: Conceptualization, Funding acquisition, Investigation, Project administration, Resources, Supervision, Visualization, Writing – original draft, Writing – review & editing.

Funding

The authors declare financial support was received for the research, authorship, and/or publication of this article.

AB is a Royal Society University Research Fellow and is supported by the Royal Society Grant No. URF\R1\221314. The work of ML, RPC, and AB was supported by the British Heart Foundation (BHF) Project under Grant PG/20/21/35082. The work of RPC was supported in part by the BHF Centre of Research Excellence, Oxford and NIHR Oxford Biomedical Research Centre.

Acknowledgments

The authors acknowledge the use of the facilities and services of the Institute of Biomedical Engineering (IBME), Department of Engineering Science, University of Oxford.

Conflict of interest

The authors declare that the research was conducted in the absence of any commercial or financial relationships that could be construed as a potential conflict of interest.

Publisher's note

References

1. Knuuti J, Wijns W, Saraste A, Capodanno D, Barbato E, Funck-Brentano C, et al. 2019 ESC guidelines for the diagnosis and management of chronic coronary syndromes: the task force for the diagnosis and management of chronic coronary syndromes of the European Society of Cardiology (ESC). *Eur Heart J.* (2020) 41:407–77. doi: 10.1093/eurheartj/ehz425

2. Manda YR, Baradhi KM. Cardiac catheterization risks and complications. (2018).

3. Sdogkos E, Xanthopoulos A, Giamouzis G, Skoularigis J, Triposkiadis F, Vogiatzis I. Data from: Diagnosis of coronary artery disease: potential complications of imaging techniques. (2022).

4. Giacoppo D, Laudani C, Occhipinti G, Spagnolo M, Greco A, Rochira C, et al. Coronary angiography, intravascular ultrasound, and optical coherence tomography for guiding of percutaneous coronary intervention: a systematic review and network

meta-analysis. *Circulation*. (2024) 149:1065–86. doi: 10.1161/CIRCULATIONAHA.123.067583

5. Hae H, Kang S-J, Kim W-J, Choi S-Y, Lee J-G, Bae Y, et al. Machine learning assessment of myocardial ischemia using angiography: development and retrospective validation. *PLoS Med*. (2018) 15:e1002693. doi: 10.1371/journal.pmed.1002693

6. Jones DA, Rathod KS, Koganti S, Hamshere S, Astroulakis Z, Lim P, et al. Angiography alone versus angiography plus optical coherence tomography to guide percutaneous coronary intervention: outcomes from the pan-london pci cohort. *JACC: Cardiovasc Interv*. (2018) 11:1313–21. doi: 10.1016/j.jcin.2018.01.274

7. Gaede L, Möllmann H, Rudolph T, Rieber J, Boenner F, Tröbs M. Coronary angiography with pressure wire and fractional flow reserve. *Dtsch Arztebl Int*. (2019) 116:205–11. doi: 10.3238/arztebl.2019.0205

8. Corral-Acero J, Margara F, Marciniak M, Rodero C, Loncaric F, Feng Y, et al. The "digital twin" to enable the vision of precision cardiology. *Eur Heart J*. (2020) 41:4556–64. doi: 10.1093/eurheartj/ehaa159

9. Gray RA, Pathmanathan P. Patient-specific cardiovascular computational modeling: diversity of personalization and challenges. *J Cardiovasc Transl Res*. (2018) 11:80–8. doi: 10.1007/s12265-018-9792-2

10. Hokken TW, Ribeiro JM, De Jaegere PP, Van Mieghem NM. Precision medicine in interventional cardiology. *Interv Cardiol Rev*. (2020) 15. doi: 10.15420/icr.2019.23

11. Banerjee A, Galassi F, Zacur E, De Maria GL, Choudhury RP, Grau V. Point-cloud method for automated 3D coronary tree reconstruction from multiple non-simultaneous angiographic projections. *IEEE Trans Med Imaging*. (2019) 39:1278–90. doi: 10.1109/TMI.2019.2944092

12. Taylor CA, Petersen K, Xiao N, Sinclair M, Bai Y, Lynch SR, et al. Patient-specific modeling of blood flow in the coronary arteries. *Comput Methods Appl Mech Eng*. (2023) 14:116414. doi: 10.1016/j.cma.2023.116414

13. Yan Q, Xiao D, Jia Y, Ai D, Fan J, Song H, et al. A multi-dimensional CFD framework for fast patient-specific fractional flow reserve prediction. *Comput Biol Med*. (2024) 168:107718. doi: 10.1016/j.compbiomed.2023.107718

14. Schwarz EL, Pegolotti L, Pfaller MR, Marsden AL. Beyond CFD: emerging methodologies for predictive simulation in cardiovascular health and disease. *Biophys Rev*. (2023) 4:4. doi: 10.1063/5.0109400

15. Li Y, Qiu H, Hou Z, Zheng J, Li J, Yin Y, et al. Additional value of deep learning computed tomographic angiography-based fractional flow reserve in detecting coronary stenosis and predicting outcomes. *Acta Radiol*. (2022) 63:133–40. doi: 10.1177/0284185120983977

16. Cruz-Aceves I, Oloumi F, Rangayyan RM, Aviña-Cervantes JG, Hernandez-Aguirre A. Automatic segmentation of coronary arteries using Gabor filters and thresholding based on multiobjective optimization. *Biomed Signal Process Control*. (2016) 25:76–85. doi: 10.1016/j.bspc.2015.11.001

17. Felfelian B, Fazlali HR, Karimi N, Soroushmehr SMR, Samavi S, Nallamothu B, et al. Vessel segmentation in low contrast x-ray angiogram images. In: *2016 IEEE International Conference on Image Processing (ICIP)*. IEEE (2016). p. 375–9.

18. Kottke DP, Sun Y. Segmentation of coronary arteriograms by iterative ternary classification. *IEEE Trans Biomed Eng*. (1990) 37:778–85. doi: 10.1109/10.102793

19. Poli R, Valli G. An algorithm for real-time vessel enhancement and detection. *Comput Methods Programs Biomed*. (1997) 52:1–22. doi: 10.1016/S0169-2607(96)01773-7

20. Preim B, Botha CP. *Visual Computing for Medicine: Theory, Algorithms, and Applications*. Newnes (2013).

21. Ko C-C, Mao C-W, Sun Y-N, Chang S-H. A fully automated identification of coronary borders from the tree structure of coronary angiograms. *Int J Biomed Comput*. (1995) 39:193–208. doi: 10.1016/0020-7101(94)01067-B

22. Liu I, Sun Y. Recursive tracking of vascular networks in angiograms based on the detection-deletion scheme. *IEEE Trans Med Imaging*. (1993) 12:334–41. doi: 10.1109/42.232264

23. Sun Y. Automated identification of vessel contours in coronary arteriograms by an adaptive tracking algorithm. *IEEE Trans Med Imaging*. (1989) 8:78–88. doi: 10.1109/42.20365

24. Tsai Y-C, Lee H-J, Chen MY-C. Automatic segmentation of vessels from angiogram sequences using adaptive feature transformation. *Comput Biol Med*. (2015) 62:239–53. doi: 10.1016/j.compbiomed.2015.04.029

25. Yang G, Lv T, Shen Y, Li S, Yang J, Chen Y, et al. Vessel structure extraction using constrained minimal path propagation. *Artif Intell Med*. (2020) 105:101846. doi: 10.1016/j.artmed.2020.101846

26. Al-Fahoum A. Adaptive edge localisation approach for quantitative coronary analysis. *Med Biol Eng Comput*. (2003) 41:425–31. doi: 10.1007/BF02348085

27. Carballal A, Novoa FJ, Fernandez-Lozano C, García-Guimaraes M, Aldama-López G, Calviño-Santos R, et al. Automatic multiscale vascular image segmentation algorithm for coronary angiography. *Biomed Signal Process Control*. (2018) 46:1–9. doi: 10.1016/j.bspc.2018.06.007

28. Chen Z, Molloi S. Vascular tree object segmentation by deskeletonization of valley courses. *Comput Med Imaging Graph*. (2002) 26:419–28. doi: 10.1016/S0895-6111(02)00037-X

29. Li Z, Zhang Y, Gong H, Li W, Tang X. Automatic coronary artery segmentation based on multi-domains remapping and quantile regression in angiographies. *Comput Med Imaging Graph*. (2016) 54:55–66. doi: 10.1016/j.compmedimag.2016.08.006

30. Ikonomatakis N, Plataniotis K, Zervakis M, Venetsanopoulos A. Region growing and region merging image segmentation. In: *Proceedings of 13th International Conference on Digital Signal Processing*. IEEE (1997). Vol. 1. p. 299–302.

31. Kerkeni A, Benabdallah A, Manzanera A, Bedoui MH. A coronary artery segmentation method based on multiscale analysis and region growing. *Comput Med Imaging Graph*. (2016) 48:49–61. doi: 10.1016/j.compmedimag.2015.12.004

32. Wan T, Shang X, Yang W, Chen J, Li D, Qin Z. Automated coronary artery tree segmentation in x-ray angiography using improved Hessian based enhancement and statistical region merging. *Comput Methods Programs Biomed*. (2018) 157:179–90. doi: 10.1016/j.cmpb.2018.01.002

33. Wang S, Li B, Zhou S. A segmentation method of coronary angiograms based on multi-scale filtering and region-growing. In: *2012 International Conference on Biomedical Engineering and Biotechnology*. IEEE (2012). p. 678–81.

34. Rodrigues E, Rodrigues L, Lima J, Casanova D, Favarim F, Dosciatti E, et al. X-ray cardiac angiographic vessel segmentation based on pixel classification using machine learning and region growing. *Biomed Phys Eng Express*. (2021) 7:055026. doi: 10.1088/2057-1976/ac13ba

35. Ma G, Yang J, Zhao H. A coronary artery segmentation method based on region growing with variable sector search area. *Technol Health Care*. (2020) 28:463–72. doi: 10.3233/THC-209047

36. Peng B, Zhang L, Zhang D. A survey of graph theoretical approaches to image segmentation. *Pattern Recognit*. (2013) 46:1020–38. doi: 10.1016/j.patcog.2012.09.015

37. Hernandez-Vela A, Gatta C, Escalera S, Igual L, Martin-Yuste V, Sabate M, et al. Accurate coronary centerline extraction, caliber estimation, and catheter detection in angiographies. *IEEE Trans Inf Technol Biomed*. (2012) 16:1332–40. doi: 10.1109/TITB.2012.2220781

38. Sun S-Y, Wang P, Sun S, Chen T. Model-guided extraction of coronary vessel structures in 2D x-ray angiograms. In: *Medical Image Computing and Computer-Assisted Intervention–MICCAI 2014: 17th International Conference, Boston, MA, USA, September 14-18, 2014, Proceedings, Part II 17*. Springer (2014). p. 594–602.

39. Mabrouk S, Oueslati C, Ghorbel F. Multiscale graph cuts based method for coronary artery segmentation in angiograms. *IRBM*. (2017) 38:167–75. doi: 10.1016/j.irbm.2017.04.004

40. Kar S, Das S, Ghosh PK. Applications of neuro fuzzy systems: a brief review and future outline. *Appl Soft Comput*. (2014) 15:243–59. doi: 10.1016/j.asoc.2013.10.014

41. Sun K, Chen Z, Jiang S, Wang Y. Morphological multiscale enhancement, fuzzy filter and watershed for vascular tree extraction in angiogram. *J Med Syst*. (2011) 35:811–24. doi: 10.1007/s10916-010-9466-3

42. Shoujun Z, Jian Y, Yongtian W, Wufan C. Automatic segmentation of coronary angiograms based on fuzzy inferring and probabilistic tracking. *Biomed Eng Online*. (2010) 9:1–21. doi: 10.1186/1475-925X-9-40

43. Kumar A, Jain SK. Deformable models for image segmentation: a critical review of achievements and future challenges. *Comput Math Appl*. (2022) 119:288–311. doi: 10.1016/j.camwa.2022.05.034

44. Klein AK, Lee F, Amini AA. Quantitative coronary angiography with deformable spline models. *IEEE Trans Med Imaging*. (1997) 16:468–82. doi: 10.1109/42.640737

45. Taghizadeh Dehkordi M, Doost Hoseini AM, Sadri S, Soltanianzadeh H. Local feature fitting active contour for segmenting vessels in angiograms. *IET Computer Vision*. (2014) 8:161–70. doi: 10.1049/iet-cvi.2013.0083

46. Lv T, Yang G, Zhang Y, Yang J, Chen Y, Shu H, et al. Vessel segmentation using centerline constrained level set method. *Multimed Tools Appl*. (2019) 78:17051–75. doi: 10.1007/s11042-018-7087-x

47. Sun K, Chen Z, Jiang S. Local morphology fitting active contour for automatic vascular segmentation. *IEEE Trans Biomed Eng*. (2011) 59:464–73. doi: 10.1109/TBME.2011.2174362

48. Nirmala Devi S, Kumaravel N. Comparison of active contour models for image segmentation in x-ray coronary angiogram images. *J Med Eng Technol*. (2008) 32:408–18. doi: 10.1080/09687630801889440

49. Liu Y, Wan W, Zhang X, Liu S, Liu Y, Liu H, et al. Segmentation and automatic identification of vasculature in coronary angiograms. *Comput Math Methods Med*. (2021) 2021:2747274. doi: 10.1155/2021/2747274

50. Socher R, Barbu A, Comaniciu D. A learning based hierarchical model for vessel segmentation. In: *2008 5th IEEE International Symposium on Biomedical Imaging: From Nano to Macro*. IEEE (2008). p. 1055–8.

51. Gupta V, Kale A, Sundar H. A robust and accurate approach to automatic blood vessel detection and segmentation from angiography x-ray images using multistage random forests. In: Haynor DR, Ourselin S, editors. *Medical Imaging 2012: Computer-Aided Diagnosis*. SPIE (2012). Vol. 8315. p. 704–9

52. Jin M, Li R, Jiang J, Qin B. Extracting contrast-filled vessels in x-ray angiography by graduated RPCA with motion coherency constraint. *Pattern Recognit*. (2017) 63:653–66. doi: 10.1016/j.patcog.2016.09.042

53. Qin B, Jin M, Hao D, Lv Y, Liu Q, Zhu Y, et al. Accurate vessel extraction via tensor completion of background layer in x-ray coronary angiograms. *Pattern Recognit*. (2019) 87:38–54. doi: 10.1016/j.patcog.2018.09.015

54. Sun Y. Back-propagation network and its configuration for blood vessel detection in angiograms. *IEEE Trans Neural Netw*. (1995) 6:64–72. doi: 10.1109/72.363449

55. Nasr-Esfahani E, Karimi N, Jafari MH, Soroushmehr SMR, Samavi S, Nallamothu B, et al. Segmentation of vessels in angiograms using convolutional neural networks. *Biomed Signal Process Control*. (2018) 40:240–51. doi: 10.1016/j.bspc.2017.09.012

56. Zhang H, Gao Z, Zhang D, Hau WK, Zhang H. Progressive perception learning for main coronary segmentation in x-ray angiography. *IEEE Trans Med Imaging*. (2022) 42:864–79. doi: 10.1109/TMI.2022.3219126

57. Zhang J, Wang G, Xie H, Zhang S, Huang N, Zhang S, et al. Weakly supervised vessel segmentation in x-ray angiograms by self-paced learning from noisy labels with suggestive annotation. *Neurocomputing*. (2020) 417:114–27. doi: 10.1016/j.neucom.2020.06.122

58. Zhu X, Cheng Z, Wang S, Chen X, Lu G. Coronary angiography image segmentation based on PSPNet. *Comput Methods Programs Biomed*. (2021) 200:105897. doi: 10.1016/j.cmpb.2020.105897

59. Iyer K, Najarian CP, Fattah AA, Arthurs CJ, Soroushmehr SR, Subban V, et al. Angionet: a convolutional neural network for vessel segmentation in x-ray angiography. *Sci Rep*. (2021) 11:18066. doi: 10.1038/s41598-021-97355-8

60. Jun TJ, Kweon J, Kim Y-H, Kim D. T-net: nested encoder–decoder architecture for the main vessel segmentation in coronary angiography. *Neural Netw*. (2020) 128:216–33. doi: 10.1016/j.neunet.2020.05.002

61. Ronneberger O, Fischer P, Brox T. U-net: convolutional networks for biomedical image segmentation. In: *Medical Image Computing and Computer-Assisted Intervention–MICCAI 2015: 18th International Conference, Munich, Germany, October 5-9, 2015, Proceedings, Part III 18*. Springer (2015). p. 234–41.

62. Kaba Ş., Haci H, Isin A, Ilhan A, Conkbayir C. The application of deep learning for the segmentation and classification of coronary arteries. *Diagnostics*. (2023) 13:2274. doi: 10.3390/diagnostics13132274

63. Yang S, Kweon J, Kim Y-H. Major vessel segmentation on x-ray coronary angiography using deep networks with a novel penalty loss function. (2019). Available online at: https://api.semanticscholar.org/CorpusID:119097475 (Accessed May 05, 2023).

64. Yang S, Kweon J, Roh J-H, Lee J-H, Kang H, Park L-J, et al. Deep learning segmentation of major vessels in x-ray coronary angiography. *Sci Rep*. (2019) 9:16897. doi: 10.1038/s41598-019-53254-7

65. Zhao C, Tang H, McGonigle D, He Z, Zhang C, Wang Y-P, et al. Development of an approach to extracting coronary arteries and detecting stenosis in invasive coronary angiograms. *J Med Imaging*. (2022) 9:044002. doi: 10.1117/1.JMI.9.4.044002

66. Ma Y, Hua Y, Deng H, Song T, Wang H, Xue Z, et al. Self-supervised vessel segmentation via adversarial learning. In: *Proceedings of the IEEE/CVF International Conference on Computer Vision* (2021). p. 7536–45.

67. Hamdi R, Kerkeni A, Bedoui MH, Ben Abdallah A. Res-GAN: residual generative adversarial network for coronary artery segmentation. In: *International Conference on Intelligent Data Engineering and Automated Learning*. Springer (2022). p. 391–8.

68. Huang J, Wu X, Qi H. Self-supervised segmentation using synthetic datasets via L-system. *Control Theory Technol*. (2023) 21:1–9. doi: 10.1007/s11768-023-00151-0

69. Zhang H, Zhang D, Gao Z, Zhang H. Joint segmentation and quantification of main coronary vessels using dual-branch multi-scale attention network. In: *Medical Image Computing and Computer Assisted Intervention–MICCAI 2021: 24th International Conference, Strasbourg, France, September 27–October 1, 2021, Proceedings, Part I 24*. Springer (2021). p. 369–78.

70. Tao X, Dang H, Zhou X, Xu X, Xiong D. A lightweight network for accurate coronary artery segmentation using x-ray angiograms. *Front Public Health*. (2022) 10:892418. doi: 10.3389/fpubh.2022.892418

71. Gao Y, Zhang L, Zhao J, Jiang Z. Improved U-Net with channel and spatial attention for coronary angiography segmentation. In: *2022 16th ICME International Conference on Complex Medical Engineering (CME)*. IEEE (2022). p. 123–6.

72. Mulay S, Ram K, Murugesan B, Sivaprakasam M. Style transfer based coronary artery segmentation in x-ray angiogram. In: *Proceedings of the IEEE/CVF International Conference on Computer Vision*. (2021). p. 3393–401

73. Park T, Khang S, Jeong H, Koo K, Lee J, Shin J, et al. Deep learning segmentation in 2D x-ray images and non-rigid registration in multi-modality images of coronary arteries. *Diagnostics*. (2022) 12:778. doi: 10.3390/diagnostics12040778

74. Gao Z, Wang L, Soroushmehr R, Wood A, Gryak J, Nallamothu B, et al. Vessel segmentation for x-ray coronary angiography using ensemble methods with deep learning and filter-based features. *BMC Med Imaging*. (2022) 22:10. doi: 10.1186/s12880-022-00734-4

75. Han T, Ai D, Wang Y, Bian Y, An R, Fan J, et al. Recursive centerline-and direction-aware joint learning network with ensemble strategy for vessel segmentation in x-ray angiography images. *Comput Methods Programs Biomed*. (2022) 220:106787. doi: 10.1016/j.cmpb.2022.106787

76. Park J, Kweon J, Kim YI, Back I, Chae J, Roh J-H, et al. Selective ensemble methods for deep learning segmentation of major vessels in invasive coronary angiography. *Med Phys*. (2023) 50:7822–39. doi: 10.1002/mp.16554

77. Shen Y, Chen Z, Tong J, Jiang N, Ning Y. DBCU-Net: deep learning approach for segmentation of coronary angiography images. *Int J Cardiovasc Imaging*. (2023) 39:1–9. doi: 10.1007/s10554-023-02849-3

78. He H, Banerjee A, Beetz M, Choudhury RP, Grau V. Semi-supervised coronary vessels segmentation from invasive coronary angiography with connectivity-preserving loss function. In: *2022 IEEE 19th International Symposium on Biomedical Imaging (ISBI)*. IEEE (2022). p. 1–5.

79. He H, Banerjee A, Choudhury RP, Grau V. Automated coronary vessels segmentation in x-ray angiography using graph attention network. In: *Statistical Atlases and Computational Models of the Heart. Regular and CMRxRecon Challenge Papers*. Cham, Switzerland: Springer Nature (2024). p. 209–19.

80. Shin SY, Lee S, Noh KJ, Yun ID, Lee KM. Extraction of coronary vessels in fluoroscopic x-ray sequences using vessel correspondence optimization. In: *Medical Image Computing and Computer-Assisted Intervention-MICCAI 2016: 19th International Conference, Athens, Greece, October 17–21, 2016, Proceedings, Part III 19*. Springer (2016). p. 308–16.

81. O'Brien JF, Ezquerra NF. Automated segmentation of coronary vessels in angiographic image sequences utilizing temporal, spatial, and structural constraints. In: Robb RA, editor. *Visualization in Biomedical Computing 1994*. SPIE (1994). Vol. 2359. p. 25–37.

82. M'hiri F, Duong L, Desrosiers C, Leye M, Miró J, Cheriet M. A graph-based approach for spatio-temporal segmentation of coronary arteries in x-ray angiographic sequences. *Comput Biol Med*. (2016) 79:45–58. doi: 10.1016/j.compbiomed.2016.10.001

83. Sonka M, Winniford MD, Collins SM. Robust simultaneous detection of coronary borders in complex images. *IEEE Trans Med Imaging*. (1995) 14:151–61. doi: 10.1109/42.370412

84. Xia S, Zhu H, Liu X, Gong M, Huang X, Xu L, et al. Vessel segmentation of x-ray coronary angiographic image sequence. *IEEE Trans Biomed Eng*. (2019) 67:1338–48. doi: 10.1109/TBME.2019.2936460

85. Wan T, Chen J, Zhang Z, Li D, Qin Z. Automatic vessel segmentation in x-ray angiogram using spatio-temporal fully-convolutional neural network. *Biomed Signal Process Control*. (2021) 68:102646. doi: 10.1016/j.bspc.2021.102646

86. Wang L, Liang D, Yin X, Qiu J, Yang Z, Xing J, et al. Coronary artery segmentation in angiographic videos utilizing spatial-temporal information. *BMC Med Imaging*. (2020) 20:1–10. doi: 10.1186/s12880-020-00509-9

87. Zhang D, Zhang H, Zhang H, Xu L, Zhang J, Gao Z. Distance transform learning for structural and functional analysis of coronary artery from dual-view angiography. *Future Gen Comput Syst*. (2023) 145:136–49. doi: 10.1016/j.future.2023.03.007

88. Liang D, Wang L, Han D, Qiu J, Yin X, Yang Z, et al. Semi 3D-TENet: semi 3D network based on temporal information extraction for coronary artery segmentation from angiography video. *Biomed Signal Process Control*. (2021) 69:102894. doi: 10.1016/j.bspc.2021.102894

89. Qin B, Mao H, Liu Y, Zhao J, Lv Y, Zhu Y, et al. Robust PCA unrolling network for super-resolution vessel extraction in x-ray coronary angiography. *IEEE Trans Med Imaging*. (2022) 41:3087–98. doi: 10.1109/TMI.2022.3177626

90. Qin B, Jin M, Ding S. Extracting heterogeneous vessels in x-ray coronary angiography via machine learning. In: El-Baz AS, editor. *Cardiovascular and Coronary Artery Imaging*. Elsevier (2022). p. 89–127.

91. Solanki R, Gosling R, Rammohan V, Pederzani G, Garg P, Heppenstall J, et al. The importance of three dimensional coronary artery reconstruction accuracy when computing virtual fractional flow reserve from invasive angiography. *Sci Rep*. (2021) 11:19694. doi: 10.1038/s41598-021-99065-7

92. Çimen S, Gooya A, Grass M, Frangi AF. Reconstruction of coronary arteries from x-ray angiography: a review. *Med Image Anal*. (2016) 32:46–68. doi: 10.1016/j.media.2016.02.007

93. Unberath M, Taubmann O, Hell M, Achenbach S, Maier A. Symmetry, outliers, and geodesics in coronary artery centerline reconstruction from rotational angiography. *Med Phys*. (2017) 44:5672–85. doi: 10.1002/mp.12512

94. Vukicevic AM, Çimen S, Jagic N, Jovicic G, Frangi AF, Filipovic N. Three-dimensional reconstruction and NURBS-based structured meshing of coronary arteries from the conventional x-ray angiography projection images. *Sci Rep*. (2018) 8:1711. doi: 10.1038/s41598-018-19440-9

95. Galassi F, Alkhalil M, Lee R, Martindale P, Kharbanda RK, Channon KM, et al. 3D reconstruction of coronary arteries from 2D angiographic projections using non-uniform rational basis splines (NURBS) for accurate modelling of coronary stenoses. *PLoS One*. (2018) 13:e0190650. doi: 10.1371/journal.pone.0190650

96. Banerjee A, Choudhury RP, Grau V. Optimized rigid motion correction from multiple non-simultaneous x-ray angiographic projections. In: Deka B, Maji P, Mitra S, Bhattacharyya DK, Bora PK, Pal SK, editors. *Pattern Recognition and Machine Intelligence*. Cham: Springer International Publishing (2019). p. 61–9.

97. Banerjee A, Kharbanda RK, Choudhury RP, Grau V. Automated motion correction and 3D vessel centerlines reconstruction from non-simultaneous angiographic projections. In: *Statistical Atlases and Computational Models of the*

Heart. Atrial Segmentation and LV Quantification Challenges Cham: Springer International Publishing (2019). p. 12–20.

98. Fang H, Zhu J, Ai D, Huang Y, Jiang Y, Song H, et al. Greedy soft matching for vascular tracking of coronary angiographic image sequences. *IEEE Trans Circuits Syst Video Technol*. (2019) 30:1466–80. doi: 10.1109/TCSVT.2019.2903883

99. Hwang M, Hwang S-B, Yu H, Kim J, Kim D, Hong W, et al. A simple method for automatic 3D reconstruction of coronary arteries from x-ray angiography. *Front Physiol*. (2021) 12:724216. doi: 10.3389/fphys.2021.724216

100. Tong J, Wang F, Li M, Xia S, Lin W. The optimization of parameters and matching point pairs in the 3D reconstruction of coronary artery. *Biomed Signal Process Control*. (2021) 67:102534. doi: 10.1016/j.bspc.2021.102534

101. Tong J, Xu S, Wang F, Qi P. 3D reconstruction with coronary artery based on curve descriptor and projection geometry-constrained vasculature matching. *Information*. (2022) 13:38. doi: 10.3390/info13010038

102. Xiao R, Yang J, Fan J, Ai D, Wang G, Wang Y. Shape context and projection geometry constrained vasculature matching for 3D reconstruction of coronary artery. *Neurocomputing*. (2016) 195:65–73. doi: 10.1016/j.neucom.2015.08.110

103. Zhu J, Li H, Ai D, Yang Q, Fan J, Huang Y, et al. Iterative closest graph matching for non-rigid 3D/2D coronary arteries registration. *Comput Methods Programs Biomed*. (2021) 199:105901. doi: 10.1016/j.cmpb.2020.105901

104. Law AK, Zhu H, Chan FH. 3D reconstruction of coronary artery using biplane angiography. In: *Proceedings of the 25th Annual International Conference of the IEEE Engineering in Medicine and Biology Society (IEEE Cat. No. 03CH37439)*. IEEE (2003). Vol. 1. p. 533–6.

105. Jandt U, Schäfer D, Grass M, Rasche V. Automatic generation of 3d coronary artery centerlines using rotational x-ray angiography. *Med Image Anal*. (2009) 13:846–58. doi: 10.1016/j.media.2009.07.010

106. Li J, Cohen LD. Reconstruction of 3D tubular structures from cone-beam projections. In: *2011 IEEE International Symposium on Biomedical Imaging: From Nano to Macro*. IEEE (2011). p. 1162–6.

107. Cong W, Yang J, Ai D, Chen Y, Liu Y, Wang Y. Quantitative analysis of deformable model-based 3D reconstruction of coronary artery from multiple angiograms. *IEEE Trans Biomed Eng*. (2015) 62:2079–90. doi: 10.1109/TBME.2015.2408633

108. Cong W, Yang J, Liu Y, Wang Y. Energy back-projective composition for 3D coronary artery reconstruction. In: *2013 35th Annual International Conference of the IEEE Engineering in Medicine and Biology Society (EMBC)*. IEEE (2013). p. 5151–4.

109. Yang J, Cong W, Chen Y, Fan J, Liu Y, Wang Y. External force back-projective composition and globally deformable optimization for 3D coronary artery reconstruction. *Phys Med Biol*. (2014) 59:975. doi: 10.1088/0031-9155/59/4/975

110. Cohen LD, Cohen I. Finite-element methods for active contour models and balloons for 2D and 3D images. *IEEE Trans Pattern Anal Mach Intell*. (1993) 15:1131–47. doi: 10.1109/34.244675

111. Xu C, Prince JL. Snakes, shapes, and gradient vector flow. *IEEE Trans Image Process*. (1998) 7:359–69. doi: 10.1109/83.661186

112. Xu C, Prince JL. Generalized gradient vector flow external forces for active contours. *Signal Process*. (1998) 71:131–9. doi: 10.1016/S0165-1684(98)00140-6

113. Liu X, Li S, Wang B, Xu L, Gao Z, Yang G. Motion estimation based on projective information disentanglement for 3D reconstruction of rotational coronary angiography. *Comput Biol Med*. (2023) 157:106743. doi: 10.1016/j.compbiomed.2023.106743

114. Taubmann O, Unberath M, Lauritsch G, Achenbach S, Maier A. Spatio-temporally regularized 4D cardiovascular C-arm CT reconstruction using a proximal algorithm. In: *2017 IEEE 14th International Symposium on Biomedical Imaging (ISBI 2017)*. IEEE (2017). p. 52–5.

115. Unberath M, Taubmann O, Aichert A, Achenbach S, Maier A. Prior-free respiratory motion estimation in rotational angiography. *IEEE Trans Med Imaging*. (2018) 37:1999–2009. doi: 10.1109/TMI.2018.2806310

116. Liu X, Hou F, Hao A, Qin H. A parallelized 4D reconstruction algorithm for vascular structures and motions based on energy optimization. *Vis Comput*. (2015) 31:1431–46. doi: 10.1007/s00371-014-1024-4

117. Royer-Rivard R, Girard F, Dahdah N, Cheriet F. End-to-end deep learning model for cardiac cycle synchronization from multi-view angiographic sequences. In: *2020 42nd Annual International Conference of the IEEE Engineering in Medicine & Biology Society (EMBC)*. IEEE (2020). p. 1190–3.

118. Song S, Du C, Liu X, Huang Y, Song H, Jiang Y, et al. Deep motion tracking from multiview angiographic image sequences for synchronization of cardiac phases. *Phys Med Biol*. (2019) 64:025018. doi: 10.1088/1361-6560/aafa06

119. Farhad A, Reza R, Azamossadat H, Ali G, Arash R, Mehrad A, et al. Artificial intelligence in estimating fractional flow reserve: a systematic literature review of techniques. *BMC Cardiovasc Disord*. (2023) 23:407. doi: 10.1186/s12872-023-03447-w

120. Hoque K, Ferdows M, Sawall S, Tzirtzilakis E, Xenos M. Hemodynamic characteristics expose the atherosclerotic severity in coronary main arteries: one-dimensional and three-dimensional approaches. *Phys Fluids*. (2021) 33:121907. doi: 10.1063/5.0069106

121. Hu X, Liu X, Wang H, Xu L, Wu P, Zhang W, et al. A novel physics-based model for fast computation of blood flow in coronary arteries. *Biomed Eng Online*. (2023) 22:56. doi: 10.1186/s12938-023-01121-y

122. Pfaller MR, Pham J, Verma A, Pegolotti L, Wilson NM, Parker DW, et al. Automated generation of 0D and 1D reduced-order models of patient-specific blood flow. *Int J Numer Method Biomed Eng*. (2022) 38:e3639. doi: 10.1002/cnm.3639

123. Yin M, Yazdani A, Karniadakis GE. One-dimensional modeling of fractional flow reserve in coronary artery disease: uncertainty quantification and Bayesian optimization. *Comput Methods Appl Mech Eng*. (2019) 353:66–85. doi: 10.1016/j.cma.2019.05.005

124. Sagawa K, Lie RK, Schaefer J. Translation of Otto frank's paper "die grundform des arteriellen pulses" Zeitschrift für Biologie 37: 483–526 (1899). *J Mol Cell Cardiol*. (1990) 22:253–4. doi: 10.1016/0022-2828(90)91459-K

125. Feng Y, Fu R, Li B, Li N, Yang H, Liu J, et al. Prediction of fractional flow reserve based on reduced-order cardiovascular model. *Comput Methods Appl Mech Eng*. (2022) 400:115473. doi: 10.1016/j.cma.2022.115473

126. Kim J, Jin D, Choi H, Kweon J, Yang DH, Kim Y-H. A zero-dimensional predictive model for the pressure drop in the stenotic coronary artery based on its geometric characteristics. *J Biomech*. (2020) 113:110076. doi: 10.1016/j.jbiomech.2020.110076

127. Blanco PJ, Bulant CA, Müller LO, Talou GM, Bezerra CG, Lemos PA, et al. Comparison of 1D and 3D models for the estimation of fractional flow reserve. *Sci Rep*. (2018) 8:17275. doi: 10.1038/s41598-018-35344-0

128. Grande Gutiérrez N, Sinno T, Diamond SL. A 1D –3D hybrid model of patient-specific coronary hemodynamics. *Cardiovasc Eng Technol*. (2022) 13:1–12. doi: 10.1007/s13239-021-00580-5

129. Pfaller MR, Pham J, Wilson NM, Parker DW, Marsden AL. On the periodicity of cardiovascular fluid dynamics simulations. *Ann Biomed Eng*. (2021) 49:3574–92. doi: 10.1007/s10439-021-02796-x

130. Deshpande S, Sosa RI, Bordas S, Lengiewicz J. Convolution, aggregation and attention based deep neural networks for accelerating simulations in mechanics. *Front Mater*. (2023) 10:1128954. doi: 10.3389/fmats.2023.1128954

131. Cai S, Mao Z, Wang Z, Yin M, Karniadakis GE. Physics-informed neural networks (PINNs) for fluid mechanics: a review. *Acta Mech Sin*. (2021) 37:1727–38. doi: 10.1007/s10409-021-01148-1

132. Mahmoudabadbozchelou M, Karniadakis GE, Jamali S. nn-PINNs: non-Newtonian physics-informed neural networks for complex fluid modeling. *Soft Matter*. (2022) 18:172–85. doi: 10.1039/D1SM01298C

133. Mao Z, Jagtap AD, Karniadakis GE. Physics-informed neural networks for high-speed flows. *Comput Methods Appl Mech Eng*. (2020) 360:112789. doi: 10.1016/j.cma.2019.112789

134. Rao C, Sun H, Liu Y. Physics-informed deep learning for incompressible laminar flows. *Theor Appl Mech Lett*. (2020) 10:207–12. doi: 10.1016/j.taml.2020.01.039

135. Deshpande S, Bordas S, Lengiewicz J. MAgNET: a graph U-Net architecture for mesh-based simulations. *arXiv* [Preprint]. *arXiv:2211.00713* (2022).

136. Deshpande S, Lengiewicz J, Bordas SP. Probabilistic deep learning for real-time large deformation simulations. *Comput Methods Appl Mech Eng*. (2022) 398:115307. doi: 10.1016/j.cma.2022.115307

137. Fossan FE, Müller LO, Sturdy J, Bråten AT, Jørgensen A, Wiseth R, et al. Machine learning augmented reduced-order models for FFR-prediction. *Comput Methods Appl Mech Eng*. (2021) 384:113892. doi: 10.1016/j.cma.2021.113892

138. Jaegle A, Borgeaud S, Alayrac J-B, Doersch C, Ionescu C, Ding D, et al. Perceiver IO: a general architecture for structured inputs & outputs. *arXiv* [Preprint]. *arXiv:2107.14795* (2021).

139. Montes de Oca Zapiain D, Stewart JA, Dingreville R. Accelerating phase-field-based microstructure evolution predictions via surrogate models trained by machine learning methods. *NPJ Comput Mater*. (2021) 7:3. doi: 10.1038/s41524-020-00471-8

140. Itu L, Rapaka S, Passerini T, Georgescu B, Schwemmer C, Schoebinger M, et al. A machine-learning approach for computation of fractional flow reserve from coronary computed tomography. *J Appl Physiol*. (2016) 121:42–52. doi: 10.1152/japplphysiol.00752.2015

141. Carson JM, Chakshu NK, Sazonov I, Nithiarasu P. Artificial intelligence approaches to predict coronary stenosis severity using non-invasive fractional flow reserve. *Proc Inst Mech Eng H*. (2020) 234:1337–50. doi: 10.1177/0954411920946526

142. Gao Z, Wang X, Sun S, Wu D, Bai J, Yin Y, et al. Learning physical properties in complex visual scenes: an intelligent machine for perceiving blood flow dynamics from static CT angiography imaging. *Neural Netw*. (2020) 123:82–93. doi: 10.1016/j.neunet.2019.11.017

143. Xie B, Liu X, Zhang H, Xu C, Zeng T, Yuan Y, et al. Conditional physics-informed graph neural network for fractional flow reserve assessment. In: *International Conference on Medical Image Computing and Computer-Assisted Intervention*. Springer (2023). p. 110–20.

144. Zhang D, Liu X, Xia J, Gao Z, Zhang H, de Albuquerque VHC. A physics-guided deep learning approach for functional assessment of cardiovascular disease

in IoT-based smart health. *IEEE Internet Things J.* (2023) 10:18505–16. doi: 10.1109/JIOT.2023.3240536

145. Morris PD, Ryan D, Morton AC, Lycett R, Lawford PV, Hose DR, et al. Virtual fractional flow reserve from coronary angiography: modeling the significance of coronary lesions: results from the VIRTU-1 (VIRTUal fractional flow reserve from coronary angiography) study. *JACC Cardiovasc Interv.* (2013) 6:149–57. doi: 10.1016/j.jcin.2012.08.024

146. Morris PD, Silva Soto DA, Feher JF, Rafiroiu D, Lungu A, Varma S, et al. Fast virtual fractional flow reserve based upon steady-state computational fluid dynamics analysis: results from the VIRTU-Fast study. *Basic Transl Sci.* (2017) 2:434–46. doi: 10.1016/j.jacbts.2017.04.003

147. Newman T, Borker R, Aubiniere-Robb L, Hendrickson J, Choudhury D, Halliday I, et al. Rapid virtual fractional flow reserve using 3D computational fluid dynamics. *Eur Heart J Digit Health.* (2023) 4:ztad028. doi: 10.1093/ehjdh/ztad028

148. Pederzani G, Czechowicz K, Ghorab N, Morris PD, Gunn JP, Narracott AJ, et al. The use of digital coronary phantoms for the validation of arterial geometry reconstruction and computation of virtual FFR. *Fluids.* (2022) 7:201. doi: 10.3390/fluids7060201

149. Masdjedi K, van Zandvoort LJ, Balbi MM, Nuis R-J, Wilschut J, Diletti R, et al. Validation of novel 3-dimensional quantitative coronary angiography based software to calculate fractional flow reserve post stenting. *Catheter Cardiovasc Interv.* (2021) 98:671–7. doi: 10.1002/ccd.29311

150. Papafaklis MI, Muramatsu T, Ishibashi Y, Lakkas LS, Nakatani S, Bourantas CV, et al. Fast virtual functional assessment of intermediate coronary lesions using routine angiographic data and blood flow simulation in humans: comparison with pressure wire-fractional flow reserve. *EuroIntervention.* (2014) 10:574–83. doi: 10.4244/EIJY14M07_01

151. Pellicano M, Lavi I, De Bruyne B, Vaknin-Assa H, Assali A, Valtzer O, et al. Validation study of image-based fractional flow reserve during coronary angiography. *Circ Cardiovasc Interv.* (2017) 10:e005259. doi: 10.1161/CIRCINTERVENTIONS.116.005259

152. Saveljic I, Djukic T, Nikolic D, Djorovic S, Filipovic N. Numerical simulation of fractional flow reserve in atherosclerotic coronary arteries. In: *2021 IEEE 21st International Conference on Bioinformatics and Bioengineering (BIBE).* IEEE (2021). p. 1–4.

153. Tar B, Jenei C, Dezsi CA, Bakk S, Beres Z, Santa J, et al. Less invasive fractional flow reserve measurement from 3-dimensional quantitative coronary angiography and classic fluid dynamic equations. *EuroIntervention.* (2018) 14:942–50. doi: 10.4244/EIJ-D-17-00859

154. Tu S, Barbato E, Köszegi Z, Yang J, Sun Z, Holm NR, et al. Fractional flow reserve calculation from 3-dimensional quantitative coronary angiography and TIMI frame count: a fast computer model to quantify the functional significance of moderately obstructed coronary arteries. *JACC Cardiovasc Interv.* (2014) 7:768–77. doi: 10.1016/j.jcin.2014.03.004

155. Tu S, Westra J, Yang J, von Birgelen C, Ferrara A, Pellicano M, et al. Diagnostic accuracy of fast computational approaches to derive fractional flow reserve from diagnostic coronary angiography: the international multicenter FAVOR pilot study. *Cardiovasc Interv.* (2016) 9:2024–35. doi: 10.1016/j.jcin.2016.07.013

156. Tufaro V, Torii R, Erdogan E, Kitslaar P, Koo B-K, Rakhit R, et al. An automated software for real-time quantification of wall shear stress distribution in quantitative coronary angiography data. *Int J Cardiol.* (2022) 357:14–9. doi: 10.1016/j.ijcard.2022.03.022

157. Zhao Q, Li C, Chu M, Gutiérrez-Chico JL, Tu S. Angiography-based coronary flow reserve: the feasibility of automatic computation by artificial intelligence. *Cardiol J.* (2023) 30(3):369–78. doi: 10.5603/CJ.a2021.0087

158. Kern MJ. Coronary physiology revisited: practical insights from the cardiac catheterization laboratory. *Circulation.* (2000) 101:1344–51. doi: 10.1161/01.CIR.101.11.1344

159. May AN, Kull A, Gunalingam B, Francis JL, Lau GT. The uptake of coronary fractional flow reserve in Australia in the past decade. *Med J Aust.* (2016) 205:127. doi: 10.5694/mja15.01225

160. Murphy J, Hansen P, Bhindi R, Figtree G, Nelson G, Ward M. Cost benefit for assessment of intermediate coronary stenosis with fractional flow reserve in public and private sectors in Australia. *Heart Lung Circ.* (2014) 23:807–10. doi: 10.1016/j.hlc.2014.03.027

161. Pijls NH, Sels J-WE. Functional measurement of coronary stenosis. *J Am Coll Cardiol.* (2012) 59:1045–57. doi: 10.1016/j.jacc.2011.09.077

162. Hill D, Bykowski A, Lim MJ. Fractional flow reserve. StatPearls [Internet]. (2018).

163. Baumgart D, Haude M, Liu F, Ge J, Goerge G, Erbel R. Current concepts of coronary flow reserve for clinical decision making during cardiac catheterization. *Am Heart J.* (1998) 136:136–49. doi: 10.1016/S0002-8703(98)70194-2

164. Baumgart D, Haude M, Goerge G, Ge J, Vetter S, Dagres N, et al. Improved assessment of coronary stenosis severity using the relative flow velocity reserve. *Circulation.* (1998) 98:40–6. doi: 10.1161/01.CIR.98.1.40

165. Gould KL, Kirkeeide RL, Buchi M. Coronary flow reserve as a physiologic measure of stenosis severity. *J Am Coll Cardiol.* (1990) 15:459–74. doi: 10.1016/S0735-1097(10)80078-6

166. Fearon WF, Kobayashi Y. Invasive assessment of the coronary microvasculature: the index of microcirculatory resistance. *Circ Cardiovasc Interv.* (2017) 10:e005361. doi: 10.1161/CIRCINTERVENTIONS.117.005361

167. Martínez GJ, Yong AS, Fearon WF, Ng MK. The index of microcirculatory resistance in the physiologic assessment of the coronary microcirculation. *Coron Artery Dis.* (2015) 26:e15–e26. doi: 10.1097/MCA.0000000000000213

168. Ng MK, Yong AS, Ho M, Shah MG, Chawantanpipat C, O'Connell R, et al. The index of microcirculatory resistance predicts myocardial infarction related to percutaneous coronary intervention. *Circ Cardiovasc Interv.* (2012) 5:515–22. doi: 10.1161/CIRCINTERVENTIONS.112.969048

169. Götberg M, Christiansen EH, Gudmundsdottir IJ, Sandhall L, Danielewicz M, Jakobsen L, et al. Instantaneous wave-free ratio vs. fractional flow reserve to guide PCI. *New Engl J Med.* (2017) 376:1813–23. doi: 10.1056/NEJMoa1616540

170. Petraco R, Al-Lamee R, Gotberg M, Sharp A, Hellig F, Nijjer SS, et al. Real-time use of instantaneous wave–free ratio: results of the advise in-practice: an international, multicenter evaluation of instantaneous wave–free ratio in clinical practice. *Am Heart J.* (2014) 168:739–48. doi: 10.1016/j.ahj.2014.06.022

171. Pisters R, Ilhan M, Veenstra L, Gho B, Stein M, Hoorntje J, et al. Instantaneous wave-free ratio and fractional flow reserve in clinical practice. *Neth Heart J.* (2018) 26:385–92. doi: 10.1007/s12471-018-1125-1

172. Kumar G, Desai R, Gore A, Rahim H, Maehara A, Matsumura M, et al. Real world validation of the nonhyperemic index of coronary artery stenosis severity—resting full-cycle ratio—re-validate. *Catheter Cardiovasc Interv.* (2020) 96:E53–8. doi: 10.1002/ccd.28523

173. Malmberg S, Lauermann J, Karlström P, Gulin D, Barmano N. Resting full-cycle ratio versus fractional flow reserve: a swedeheart-registry-based comparison of two physiological indexes for assessing coronary stenosis severity. *J Interv Cardiol.* (2023) 2023:6461691. doi: 10.1155/2023/6461691

174. Muroya T, Kawano H, Hata S, Shinboku H, Sonoda K, Kusumoto S, et al. Relationship between resting full-cycle ratio and fractional flow reserve in assessments of coronary stenosis severity. *Catheter Cardiovasc Interv.* (2020) 96:E432–8. doi: 10.1002/ccd.28835

175. Ono M, Kawashima H, Hara H, Gao C, Wang R, Kogame N, et al. Advances in IVUS/OCT and future clinical perspective of novel hybrid catheter system in coronary imaging. *Front Cardiovasc Med.* (2020) 7:119. doi: 10.3389/fcvm.2020.00119

176. Wu W, Oguz UM, Banga A, Zhao S, Thota AK, Gadamidi VK, et al. 3D reconstruction of coronary artery bifurcations from intravascular ultrasound and angiography. *Sci Rep.* (2023) 13:13031. doi: 10.1038/s41598-023-40257-8

177. Liang H, Zhang Q, Gao Y, Chen G, Bai Y, Zhang Y, et al. Diagnostic performance of angiography-derived fractional flow reserve analysis based on bifurcation fractal law for assessing hemodynamic significance of coronary stenosis. *Eur Radiol.* (2023) 33:1–10. doi: 10.1007/s00330-023-09682-1

178. Papamanolis L, Kim HJ, Jaquet C, Sinclair M, Schaap M, Danad I, et al. Myocardial perfusion simulation for coronary artery disease: a coupled patient-specific multiscale model. *Ann Biomed Eng.* (2021) 49:1432–47. doi: 10.1007/s10439-020-02681-z

179. Gamage PT, Dong P, Lee J, Gharaibeh Y, Zimin VN, Bezerra HG, et al. Fractional flow reserve (FFR) estimation from OCT-based CFD simulations: role of side branches. *Appl Sci.* (2022) 12:5573. doi: 10.3390/app12115573

180. Zhuk S, Smith O, Thondapu V, Halupka K, Moore S. Using contrast motion to generate patient-specific blood flow simulations during invasive coronary angiography. *J Biomech Eng.* (2020) 142:021001. doi: 10.1115/1.4044095

181. Khanmohammadi M, Engan K, Sæland C, Eftestøl T, Larsen AI. Automatic estimation of coronary blood flow velocity step 1 for developing a tool to diagnose patients with micro-vascular angina pectoris. *Front Cardiovasc Med.* (2019) 6:1. doi: 10.3389/fcvm.2019.00001

frontiers | Frontiers in Cardiovascular Medicine

TYPE Review
PUBLISHED 25 July 2024
DOI 10.3389/fcvm.2024.1392702

OPEN ACCESS

EDITED BY
Choon Hwai Yap,
Imperial College London, United Kingdom

REVIEWED BY
Giovanni Luigi De Maria,
Oxford University Hospitals NHS Trust, United Kingdom
Zsolt Kőszegi,
University of Debrecen, Hungary

*CORRESPONDENCE
Marco Zimarino
✉ m.zimarino@unich.it

RECEIVED 27 February 2024
ACCEPTED 15 July 2024
PUBLISHED 25 July 2024

CITATION
Bacigalupi E, Pizzicannella J, Rigatelli G, Scorpiglione L, Foglietta M, Rende G, Mantini C, Fiore FM, Pelliccia F and Zimarino M (2024) Biomechanical factors and atherosclerosis localization: insights and clinical applications. Front. Cardiovasc. Med. 11:1392702. doi: 10.3389/fcvm.2024.1392702

Biomechanical factors and atherosclerosis localization: insights and clinical applications

Elena Bacigalupi[1], Jacopo Pizzicannella[2], Gianluca Rigatelli[3], Luca Scorpiglione[1], Melissa Foglietta[1,4], Greta Rende[1], Cesare Mantini[1], Franco M. Fiore[5], Francesco Pelliccia[6] and Marco Zimarino[1,4]*

[1]Department of Neuroscience, Imaging and Clinical Sciences, "G. D'Annunzio" University of Chieti-Pescara, Chieti, Italy, [2]Department of Engineering and Geology, University "G. d' Annunzio" Chieti-Pescara, Pescara, Italy, [3]Cardiology Department, Ospedali Riuniti Padova Sud, Monselice, Italy, [4]Cardiology Department, SS. Annunziata Hospital, Chieti, Italy, [5]Division of Vascular Surgery, SS. Annunziata Hospital, Chieti, Italy, [6]Department of Cardiovascular Sciences, University Sapienza, Rome, Italy

Although the entire vascular bed is constantly exposed to the same risk factors, atherosclerosis manifests a distinct intra-individual pattern in localization and progression within the arterial vascular bed. Despite shared risk factors, the development of atherosclerotic plaques is influenced by physical principles, anatomic variations, metabolic functions, and genetic pathways. Biomechanical factors, particularly wall shear stress (WSS), play a crucial role in atherosclerosis and both low and high WSS are associated with plaque progression and heightened vulnerability. Low and oscillatory WSS contribute to plaque growth and arterial remodeling, while high WSS promotes vulnerable changes in obstructive coronary plaques. Axial plaque stress and plaque structural stress are proposed as biomechanical indicators of plaque vulnerability, representing hemodynamic stress on stenotic lesions and localized stress within growing plaques, respectively. Advancements in imaging and computational fluid dynamics techniques enable a comprehensive analysis of morphological and hemodynamic properties of atherosclerotic lesions and their role in plaque localization, evolution, and vulnerability. Understanding the impact of mechanical forces on blood vessels holds the potential for developing shear-regulated drugs, improving diagnostics, and informing clinical decision-making in coronary atherosclerosis management. Additionally, Computation Fluid Dynamic (CFD) finds clinical applications in comprehending stent-vessel dynamics, complexities of coronary bifurcations, and guiding assessments of coronary lesion severity. This review underscores the clinical significance of an integrated approach, concentrating on systemic, hemodynamic, and biomechanical factors in atherosclerosis and plaque vulnerability among patients with coronary artery disease.

KEYWORDS

biomechanical factors, wall shear stress, axial plaque stress, plaque structural stress, computational fluid dynamic

Abbreviations

APS, axial plaque stress; CFD, computational fluido-dynamic; FFR, fractional flow reserve; IST, intra-stent restenosis; IVUS, intravascular ultrasound; MB, main branch; OCT, optical coherence tomography; OSI, oscillatory shear index; PSS, plaque structural stress; QFR, quantitative flow ratio; RRT, relative residence time; SB, side branch; TAWSS, time-averaged wall shear stress; WSS, wall shear stress.

Key points

- Biomechanical factors are key players in coronary atherosclerosis and can be assessed *in vivo* through computational fluid dynamics techniques.
- Biomechanical factors contribute to valuable prognostic information beyond anatomical and physiological plaque characteristics in the localization and evolution of coronary atherosclerosis.
- Computational fluid dynamics offers clinical applications in the assessment of plaque vulnerability, coronary lesion severity, stent-vessel interactions, and coronary bifurcation complexities.

1 Introduction

Atherosclerosis, a chronic systemic disease marked by inflammation and fibro-proliferation, predominantly affects the intima of large and medium-sized elastic and muscular arteries (1). It is the leading cause of morbidity and mortality worldwide and presents its main clinical manifestation as ischemia, which can damage the heart, brain, or lower extremities. Despite uniform exposure to the same risk factors across the vascular bed, the formation and advancement of atheromatous lesions follow a unique pattern, frequently occurring in certain segments of the arterial system. This peculiar distribution might stem from a variable responsiveness to risk factors or differences in histopathology and blood flow, and has relevant clinical implications, as the prognosis of the disease varies according to localization (2).

The role of risk factors in atherosclerosis is complex, encompassing anatomical, physiological, and behavioral aspects. Conventional risk factors such as hypertension, hypercholesterolemia, tobacco smoking, diabetes mellitus, age, family history, and obesity, are well established (3). Recent evidence also highlight the significant role of inflammation and the immune system as key mechanism in the pathophysiology of cardiovascular disease (4).

In the context of atherosclerosis, biomechanical forces such as Wall Shear Stress (WSS), Axial Plaque Stress (APS), and Plaque Structural Stress (PSS) are pivotal in its localization and progression (5, 6). These forces, arising from blood flow dynamics, interact with the endothelial lining of blood vessels, influencing the formation, growth, and vulnerability of atherosclerotic plaques. The integration of advanced computational fluid dynamics (CFD) with imaging techniques like Coronary Computed Tomography (CT) and Intravascular Ultrasound (IVUS) has enabled a more detailed analysis of these biomechanical factors, providing new insights into their role in the localization and progression of coronary atherosclerosis.

This review explores the growing importance of biomechanical factors, focusing on recent discoveries related to WSS, APS, and PSS, along with the evolving role of CFD in the diagnosis and treatment of atherosclerosis.

2 Biomechanical factors: physiophatologic role and current evidence

The oscillatory nature of blood flow exerts mechanical stress on vascular tissues, significantly influencing vessel biology. In particular, blood flow generates circumferential, axial and shear stress in coronary vessels (Figure 1). Extensive research over the years has heightened our understanding of these forces and their critical role in the development and pathology of atherosclerotic plaques. Marked oscillations of blood pressure - as measured by blood pressure variability - are associated with both depressed left ventricular systolic function and target organ damage (7). Innovations in medical imaging and computational approaches have enabled more accurate *in vivo* assessments of these biomechanical stress, offering key insights into plaque localization and progression (8).

To analyze biomechanical factors in human coronary arteries, a combination of imaging techniques and CFD is needed. Imaging is essential for capturing the three-dimensional structure of the coronary artery. The geometrical data is then given to a CFD software program that compute the velocity and shear stress distribution. The most precise method involves using biplane ANGiography combined with intravascular UltraSound (ANGUS) (9). Alternatively, CT or MRI angiography can approximate the 3D orientation of IVUS images for those cases where biplane angiography is not feasible. In addition to structural information, CFD analysis necessitates further inputs, notably the flow rate through the coronary artery. This can be gauged through either invasive techniques, such as a coronary pressure/flow wire, or non-invasive methods, like monitoring blood pressure.

While CFD simulations compute WSS and APS based on the velocity of blood flow, calculating PSS involves a deeper understanding of the mechanical characteristics of plaque components. This includes the magnitude of forces applied to the plaque and the degree of resultant plaque deformation. To compute PSS, an engineering approach known as finite element analysis (FEA) is employed. FEA considers the dynamic forces acting on the plaque and reconstructs 2D/3D images using IVUS, VH-IVUS, or OCT, thereby estimating PSS and its fluctuation throughout the cardiac cycle. Alternatively, PSS can be calculated using fluid-structure interaction (FSI) simulations. This method aims to integrate both the cyclic fluid dynamics and structural mechanical forces to achieve a comprehensive solution (10). While FSI enables the quantification of both WSS and PSS within a single artery, the engineering processes involved are highly complex, which limits its current use in clinical settings.

2.1 Wall shear stress

WSS is the parallel frictional force exerted by blood flow on the endothelium of the arterial wall. It is expressed in units of force/unit area [N/m^2 or Pascal (Pa) or $dyne/cm^2$; 1 N/m^2 = 1 Pa = 10 $dyne/cm^2$]. In straight arterial segments, WSS is

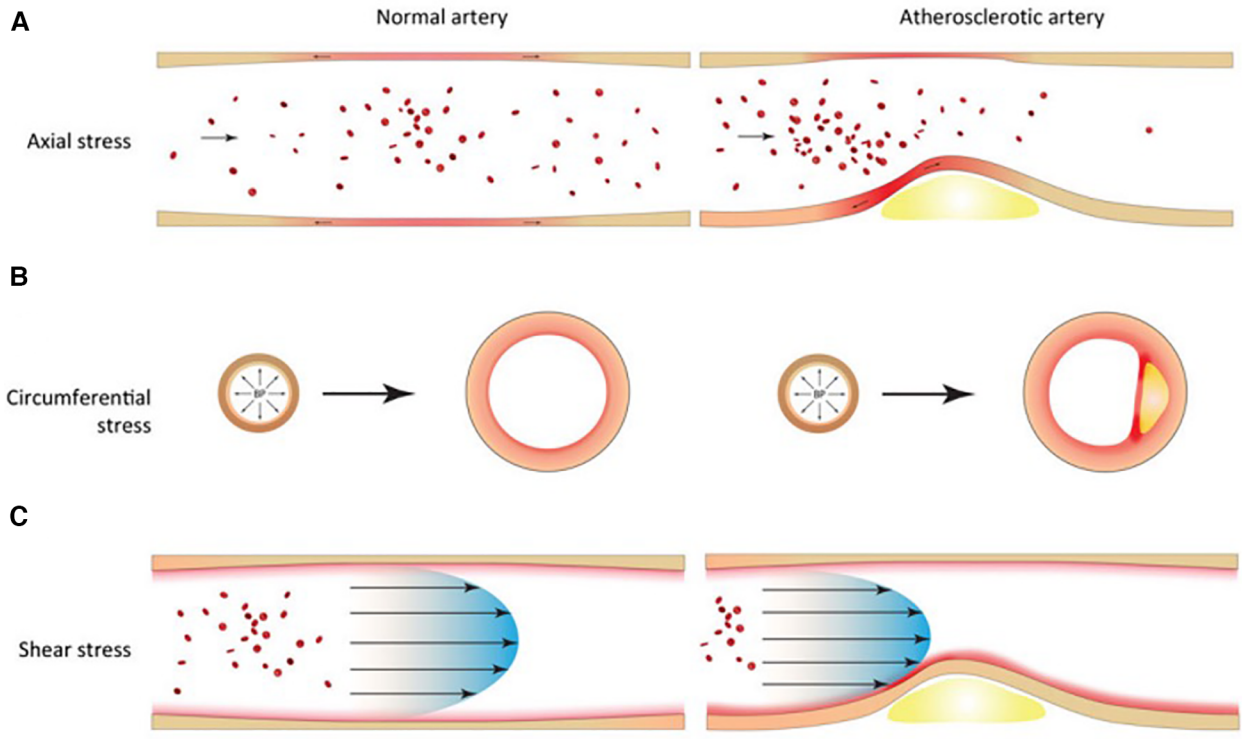

FIGURE 1
Biomechanical factors in normal and atherosclerotic vascular tissues. (A) Axial stress arises from longitudinal stretching of tethered blood vessels. (B) Circumferential stress arises from radial expansion and recoil over the cardiac cycle. (C) Shear stress arises from the frictional force of blood flowing against the vessel wall.

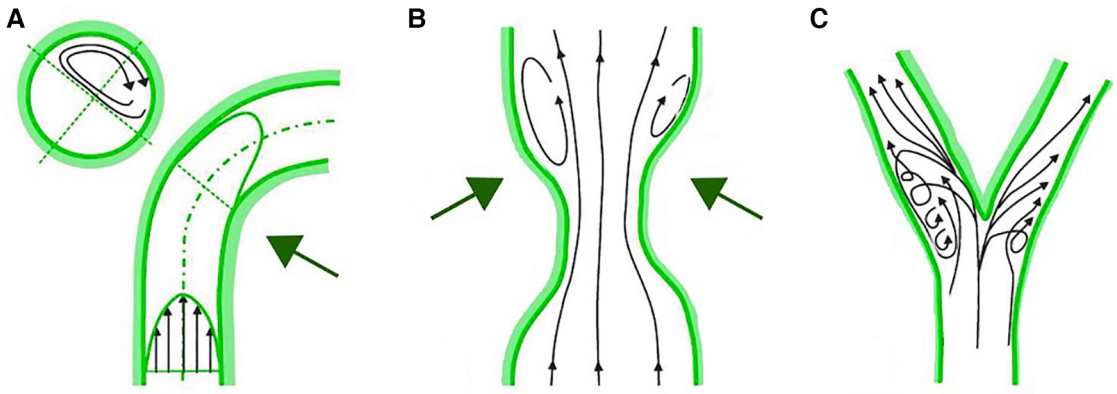

FIGURE 2
Complex flow patterns in coronary arteries. (A) Inner curvature of vessels. (B) Downstream part of stenosed segments. (C) Lateral wall of bifurcations.

pulsatile and unidirectional, fluctuating between 15 and 70 dyne/cm^2 over the cardiac cycle. The mechanotransduction of WSS via endothelial cell transmembrane proteins influences intracellular enzyme functions, gene expression, synthesis of proteins and micro-RNAs. These processes modulate endothelial cell structure and function, influencing the surrounding environment, and the balance between inhibition and promotion of atherosclerosis. WSS above 15 dyne/cm^2 promotes a quiescent, antiproliferative, antioxidant, and antithrombotic phenotype, alongside an atheroprotective gene expression profile. In critical geometrically irregular points of the coronary tree, complex flow dynamic patterns occur, with swirling flow, flow separation, and flow reversal that generates low and/or oscillatory WSS. These regions are the inner curvature of vessels, hips, or the lateral wall of bifurcations and the downstream part of stenosed segments (Figure 2). Low and oscillatory WSS (<10 dyne/cm^2) results in

inflammation and proatherogenic pathways of the endothelium. Low WSS decreases the production of fibrinolytics, vasodilators, and antioxidants and increases the expression of growth factors, oxidative elements, vasoconstrictors, acute inflammatory mediators and proteolytic enzymes. This sequence of endothelial dysfunction and acute inflammation can perpetuate injury that contributes to plaque growth and arterial remodeling. Notably, areas subjected to low WSS experience accelerated plaque progression, even in regions initially free of plaque (11).

The early stages of atherosclerosis feature positive remodeling of coronary vessels, which temporarily prevents narrowing due to plaque protrusion. However, segments exposed to low WSS remain susceptible to further atherogenesis, leading to a detrimental cycle of ongoing endothelial damage, plaque expansion, and deteriorating flow dynamics (12). This phenomenon continues until the plaque occupies a significant part of the vessel's area (around 40%), at which point luminal compensation fails. As a result, the plaques that protrudes into the lumen are exposed to higher WSS. This alteration in WSS magnitude and distribution creates a biomechanical environment that not only favors downstream plaque progression but also changes plaque vulnerability. Whereas higher WSS is typically considered atheroprotective in healthy vessels, its presence in arteries with protruding plaques can promote further vulnerable changes leading to thin-cap fibroatheroma (TCFA) morphology. This phenomenon involves an upregulation in nitric oxide production and the activation of metalloproteinases, which contribute to the regression of fibrous caps, thus destabilizing the plaques (13, 14). Even endothelial progenitor cells have been hypothesized to act as mediators in the link between traditional risk factors, WSS, and atherosclerosis, but evidence has been controversial (15).

Numerous studies support these pathophysiological evaluations, elucidating the role of WSS in the origin and progression of coronary atherosclerosis. The PREDICTION study, an IVUS-based CFD analysis, identified low WSS as a key factor in increasing plaque burden and reducing lumen area (16). Low WSS was also predictive of lesions requiring percutaneous intervention in a majority of asymptomatic chronic coronary syndrome (CCS) patients during the follow-up. Similarly, Bourantas and colleagues demonstrated that low WSS in non-culprit vessels of patients with myocardial infarction (MI) was an independent indicator of disease progression (17). Evidence underscores also the role of WSS in changing plaque vulnerability, leading to destabilization and rupture (18). In the EMERALD study, coronary computed tomographic angiography (CTA), documented that, in patients with acute coronary syndrome (ACS), culprit lesions were more likely to exhibit both adverse plaque characteristics (APC) - positive remodeling, low attenuation, and varied calcifications - and adverse hemodynamic characteristics (AHC), namely higher proximal WSS. Lesions exhibiting both APC and AHC were associated with a higher risk of subsequent acute events, compared with patient without APC/AHC and those with either APC or AHC (19). The prognostic role of WSS was also demonstrated in 441 patients with chronic coronary syndrome with significant lesions enrolled in the medical therapy arm of the FAME II trial (20). The authors found that higher WSS in the proximal segments of coronary lesions correlates with MI within 3 years. Similarly, Zuin et al. demonstrated that in angiographically non-significant left-main (LM) bifurcation disease, both higher proximal WSS of each branch and higher WSS of the entire lesion predicted the occurrence of bifurcation-located MI over the following 3 years (21). Parallel findings by Fukumoto et al. using IVUS (22) and Jin (23) in an OCT-based CFD study reinforced the link between higher WSS and plaque rupture locations.

2.2 Axial plaque stress

Axial stress comes from the longitudinal stretching of tethered blood vessels and represents the fluid stress aligned along the vessel's central axis throughout the cardiac cycle. Non-diseased arteries maintain minimal levels of axial stress. In atherosclerotic arteries with flow obstructions, the imbalance of external hemodynamic forces across lesions increases the axial stress and overall plaque strain. This axial stress is of a higher magnitude than WSS and may become concentrated at the upstream and downstream segments of a plaque. The increase of axial stress due to flow obstruction and subsequent pressure gradients may play a role in plaque rupture (24).

Choi and colleagues evaluated APS acting on stenotic lesions and its relationship with lesions' length and geometry (25). The authors divided lesions in upstream- and downstream-dominant according to the localization (upstream or downstream, respectively) of steeper radius change, where radius change refers to the difference between the lesion starting (or ending) point radius and the radius at the location of minimum lumen area. In addition, a negative correlation between APS and lesion length was found and APS was higher in the upstream segment of upstream-dominant lesions and in the downstream segment of downstream-dominant lesions. This offers insight into why short, focal lesions are more prone to rupture than long ones and elucidates the paradoxical phenomenon of downstream rupture. Furthermore, the EMERALD study found that axial stress had an incremental value for predicting ACS, resulting in higher APS in culprit compared to non-culprit lesions.

2.3 Plaque structural stress

Circumferential stress is generated through the radial dilation and contraction of arteries within the cardiac cycle. In healthy arteries, this force is uniformly distributed along the artery wall due to homogenous tissue composition. Plaque Structural Stress (PSS) is the circumferential stress located inside an atherosclerotic plaque as a consequence of vessel expansion induced by arterial pressure. The magnitude of PSS is influenced by factors such as plaque composition, architecture, and lumen geometry. In particular, PSS increases with increasing lumen area, eccentricity, and necrotic core, and decreases in the presence of dense calcium (26). In addition, there is a reciprocal relationship between plaque composition and morphology, the

thickness of fibrous cap (27), WSS, and PSS itself. Recently (28), both in areas of plaque progression and regression, higher PSS was associated with larger increases in necrotic core, leading to vulnerable phenotype. Indeed, PSS was higher in patients presenting with ACS vs. CCS (29), in peri-minimum lumen area (MLA) of plaques showing rupture vs. no rupture (30), and in non-culprit lesions leading to MACEs vs. no MACEs even with similar characteristics (31).

2.4 Radial wall strain

Radial wall strain (RWS) similarly reflects the interplay between cyclic pulsatile intravascular pressure and vessel wall tissue composition, resulting in higher values for vulnerable plaque components like lipids or macrophages, and lower values for fibrous tissue or calcium. Coronary strain can be measured using computational dynamic techniques with FEA from IVUS or OCT images. However, this requires intracoronary imaging devices and complex analytical processes. Recently, a novel artificial intelligence (AI) method was developed to calculate RWS from a single angiographic projection (RWS-Angio) and has been validated against corresponding intravascular images (32). This method provides a simplified and cost-effective tool for assessing plaque biomechanical characteristics, potentially accessible in all cath labs. Studies have demonstrated a strong correlation between RWS-Angio and intracoronary imaging features of plaque vulnerability in intermediate coronary stenosis (33). Additionally, RWS-Angio has shown increased and independent prognostic value in predicting target vessel failure (TVF), regardless of FFR values (34). Given the recent focus on the unfavorable clinical outcomes of non-flow limiting coronary plaques with high-risk characteristics (35) and the ongoing debate about the revascularization of such lesions (36), the ability to estimate RWS from a routine diagnostic coronary angiogram could provide significant prognostic value in managing intermediate coronary lesions and improving CAD treatment strategies.

3 Computational fluido dynamics models and clinical applications

3.1 Assessment of plaque vulnerability and rupture

The primary clinical outcome of atherosclerosis is ischemia, leading to significant damage in the heart, brain, or lower limbs. However, it is noteworthy that such lesions tend to manifest predominantly in specific regions of the arterial tree (37). CFD has been recently applied to the pathophysiology of atherosclerosis to understand the mechanisms underlying plaque progression. Over the years, both invasive and non-invasive imaging studies have consistently demonstrated that evaluating anatomical characteristics of plaque provides a more accurate prediction of cardiac event risks than merely assessing the extent of lumen obstruction (38, 39). Nevertheless, the evaluation of plaque vulnerability based solely on imaging features has its limitations. As the PROSPECT study showed (40), only a small proportion (<10%) of thin-cap fibroatheroma plaques progress to cause clinical events over 3 years; similarly, Motoyama et al. (41) documented that the majority (84%) of coronary high-risk plaques defined by CTA failed to cause any event. While these morphological characteristics are crucial indicators of vulnerable plaques, there is a need for additional markers to identify plaques that are likely to advance to clinical significance. As mentioned before, WSS, APS, PSS and RWS account for changes in plaque composition, leading to plaque vulnerability and rupture. Recent investigations have also delved into the phenomenon of cavitation, which physically occurs when fluid pressure in a particular area falls below the vapor pressure (42). CFD studies demonstrated that cavitation, triggered by both concentric and eccentric coronary artery stenosis, travels downstream, forming microbubbles that burst when fluid pressure dips below the vapor pressure in a local thermodynamic condition. This might damage endothelial surfaces, promoting thrombosis (43).

None of these biomechanical and anatomical factors alone can however explain the complex phenomenon of plaque rupture and acute thrombosis. They act as concurrent factors in the precipitation of atherosclerotic disease. Future prospective studies are warranted to understand whether the assessment of biomechanical factors acting on a coronary lesion can provide predictive value beyond anatomical and functional data and to explore its potential clinical application in guiding preventive and therapeutic measures.

3.2 Assessment of stent-vessel interaction

CFD is increasingly applied to assess how stent architecture influences coronary blood flow dynamics. Recent studies suggest that the geometry created by an implanted stent can alter local blood flow and wall shear stress (WSS) distribution. This alteration can predispose certain vessel wall areas to neointimal hyperplasia and restenosis (44), rather than promoting the typical shear stress-induced re-endothelialization (45). However, in such cases, the precise mechanism driving the excessive neointimal proliferation is still unclear.

When a stent, which is comparatively rigid, is implanted in a curved vessel like a coronary artery, it alters the segment's shape, essentially straightening it. This results in increased curvature at the stent's edges, creating zones of low WSS and potential flow reversal. Furthermore, the stent deployment - considering the applied pressure, the design of the stent, and strut dimensions - may result in the struts extending into the lumen, which modifies velocity and the distribution of shear stress, thereby creating zones of high and low WSS. Although *in vitro* studies have correlated these flow disturbances to increased platelet adhesion, there is a lack of studies evaluating clinical restenosis outcomes. Furthermore, post-stent implantation, if the diameter of the restored lumen within the stent surpasses that of the artery's proximal section, a sudden lumen expansion just downstream of the stent's leading edge occurs. Such flow patterns are comparable with low-WSS flow

recirculation documented downstream stenosis. LaDisa et al. (46, 47) demonstrated that low WSS occurs predominantly in the proximal and distal edges of the stent. Such low WSS regions are also notable behind struts, especially those protruding into the lumen at steep angles to the flow direction (48), and were associated with neo-atherosclerosis (49). Moreover, *in vitro* experiments exploring the impact of stent geometry on platelet adhesion and aggregation, found that localized platelet accumulation is influenced by flow convection, implying that vascular response to stent deployment can be somewhat governed by the hemodynamics associated with stent configuration (50).

CFD models show promise in understanding how stents interact with blood vessels. Optimizing stent design must account for the local flow patterns induced by the stent's deployment, to avoid the fluid dynamic conditions that can promote neointimal hyperplasia and subsequent restenosis.

3.3 Assessment of bifurcations

In bifurcations, the flow divides into two daughter branches and changes in direction. Consequently, the faster moving particles will impinge on the inner wall areas of the side branch (SB) proximal to the carina, while in the hips or lateral wall occurs low and oscillatory WSS with flow separation (Figure 3). This complex flow pattern is influenced by several factors, including the bifurcation angle, the size of the SB, and how the blood flow is distributed between the branches.

Coronary bifurcation revascularization poses challenges for interventionalists. Factors such as the dimensions of the SB, the extent of lesions, calcification levels, the morphology of the bifurcation carina, and the angles formed between the two branches demand careful consideration in treatment planning. Bifurcation stenting inevitably affects coronary flow patterns and induces geometric changes in both the main (MB) and SB. CFD was used to anticipate the results of complex bifurcation stenting and to understand how bifurcation rheology changes following stenting with various devices and techniques. Key hemodynamic parameters assessed at stented coronary bifurcations through CFD include WSS, time-averaged wall shear stress (TAWSS), oscillatory shear index (OSI), and relative residence time (RRT). TAWSS quantifies the mean WSS over a cardiac cycle, OSI reflects the variability of WSS, and RRT combines TAWSS and OSI to indicate the duration that blood particles remain near the vessel wall. Areas of low and oscillatory WSS with high OSI and RRT, such as the lateral wall of stented MB, are prone to intra-stent restenosis (ISR). Factors like the number and thickness of stent struts (51), the bifurcation angle, and any stent malapposition significantly affect the development of adverse hemodynamic conditions and can promote ISR and thrombus formation.

Thus, choosing the optimal stenting strategy, whether a provisional single-stent or a more complex two-stent approach, is of paramount importance. Single-stent technique tends to leave vulnerable areas opposite the flow divider (52), while dual-stent techniques can create secondary flow disturbances and low WSS due to strut apposition at the carina, strut layering and protrusion into the MB, which are associated with ISR or thrombosis. The

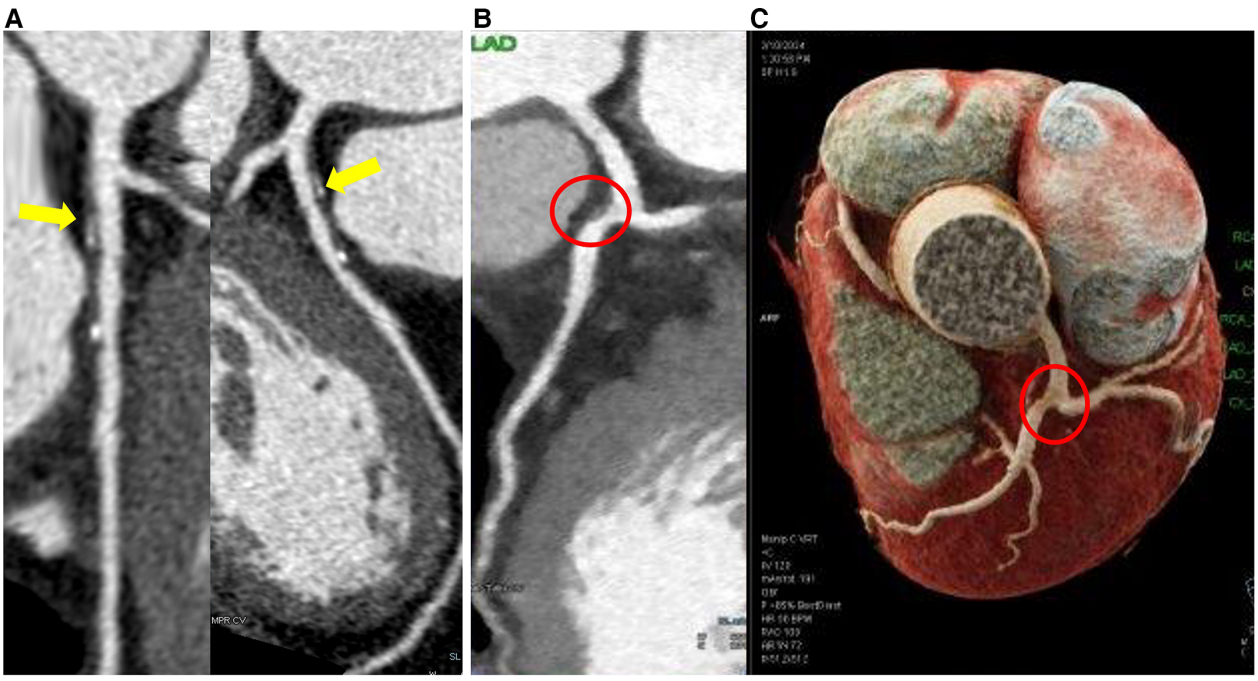

FIGURE 3
Coronary computed tomography angiography shows plaques located at the lateral wall of the bifurcation. (**A**) Eccentric partially calcified plaque in the left anterior descending coronary artery immediately downstream of the left main bifurcation. (**B**) Eccentric vulnerable plaque in lateral wall of left anterior descending coronary artery immediately downstream of the left main bifurcation (red circle) in 2D and 3D reconstruction (**C**).

best double stenting strategies with the most favorable fluid dynamics are under debate (53–55) and efficiency of single or double stenting depends also on bifurcation anatomical complexity. A recent OCT derived-CFD study evaluating RRT in complex left main bifurcation disease suggested for example that RRT is increased after cross-over stenting while is substantially unchanged after double stenting techniques (56). Anyway, when approaching a bifurcation stenting procedure, careful planning is crucial, as the deployment of unplanned bailout additional stents is associated with adverse events (57).

The application of CFD in this context may represent a powerful tool to guide both PCI strategies and the type and duration of antithrombotic therapy after bifurcation PCI (58) in order to predict adverse events and identify the optimal strategy to improve clinical outcomes.

3.4 Assessment of the functional severity of coronary lesion

In recent years, the practice of coronary revascularization has been revolutionized by physiology-guided approaches, leading to improved outcomes in the management of CAD, compared to revascularization based solely on angiographic data. While several non-hyperemic pressure ratios have been developed to expand the use of physiology beyond FFR and its adenosine-induced hyperemia issues, the integration of these methods into routine practice remains limited, due to prolonged procedural durations and risks associated with guidewire use (59, 60). Addressing these challenges, computational approaches have emerged with Quantitative Flow Ratio (QFR) as the most validated technique (61), based on a three-dimensional vessel reconstruction and estimation of its contrast media flow velocity. QFR employs three-dimensional quantitative coronary angiography (3D-QCA) in combination with CFD to calculate the functional impact of coronary stenosis. This angiography-based method offers an accurate alternative to estimate FFR, bypassing the need for coronary wiring or the induction of hyperemia. Strong agreement between QFR and traditional FFR measurements have been observed (62, 63), including post-PCI assessment (64, 65) and prognostication in patients with left main or multi-vessels disease (66). Furthermore, QFR technology can predict the post-PCI functional outcomes through virtual angioplasty. This "virtual angioplasty" could be pivotal in strategizing revascularization plans and potentially forecasting procedural outcomes. Recent investigations exploring the relationship between QFR-obtained "virtual angioplasty" and wire-based post-PCI functional evaluations gave conflicting results, especially in tandem and complex lesions (67–69).

4 Conclusion and future prospective

Biomechanical factors are fundamental in coronary atherosclerosis formation and progression and should be considered beyond anatomical and physiological plaque characteristics. The application of biomechanical models in patient studies is proving to be a game-changer, significantly deepening our understanding of how shear stress interacts with endothelial function and the pathogenesis of atherosclerosis. Moreover, CFD applications extend beyond plaque assessment, evaluating stent-vessel interactions, coronary bifurcation complexities, and coronary lesion severity.

The advancements in noninvasive imaging and the understanding of blood flow properties through CFD models will set the basis for a personalized approach. This will enable tailored, patient-specific, or even plaque-specific solutions to various issues. The assessment of plaque vulnerability and the risk of rupture, along with the consequent need for revascularization, through the evaluation of biomechanical factors beyond anatomical and physiological characteristics will be explored. Determining the optimal stent design that minimizes damage to the coronary wall becomes a feasible consideration. While numerous issues still require resolution before incorporating these techniques into clinical practice, the integration of noninvasive imaging and biomechanical modeling will support cardiologists in improving diagnosis and establishing optimal treatment strategies for cardiovascular disease.

Author contributions

EB: Writing – original draft, Writing – review & editing. JP: Writing – original draft, Writing – review & editing. GiR: Writing – original draft, Writing – review & editing. LS: Writing – original draft, Writing – review & editing. MF: Writing – original draft, Writing – review & editing. GrR: Writing – original draft, Writing – review & editing. CM: Writing – original draft, Writing – review & editing. FF: Writing – original draft, Writing – review & editing. FP: Writing – original draft, Writing – review & editing. MZ: Writing – original draft, Writing – review & editing.

Funding

The author(s) declare that no financial support was received for the research, authorship, and/or publication of this article.

Conflict of interest

The authors declare that the research was conducted in the absence of any commercial or financial relationships that could be construed as a potential conflict of interest.

Publisher's note

References

1. Libby P. Mechanisms of acute coronary syndromes and their implications for therapy. *N Engl J Med*. (2013) 368:2004–13. doi: 10.1056/NEJMra1216063

2. Possati G, Gaudino M, Alessandrini F, Zimarino M, Glieca F, Luciani N. Systematic clinical and angiographic follow-up of patients undergoing minimally invasive coronary artery bypass. *J Thorac Cardiovasc Surg*. (1998) 115:785–90. doi: 10.1016/S0022-5223(98)70356-3

3. Brunner H, Cockcroft JR, Deanfield J, Donald A, Ferrannini E, Halcox J, et al. Endothelial function and dysfunction. Part II: association with cardiovascular risk factors and diseases. A statement by the working group on endothelins and endothelial factors of the European Society of Hypertension*. *J Hypertens*. (2005) 23:233–46. doi: 10.1097/00004872-200502000-00001

4. Ross R. Atherosclerosis — an inflammatory disease. *N Engl J Med*. (1999) 340:115–26. doi: 10.1056/NEJM199901143400207

5. Wentzel JJ, Chatzizisis YS, Gijsen FJH, Giannoglou GD, Feldman CL, Stone PH. Endothelial shear stress in the evolution of coronary atherosclerotic plaque and vascular remodelling: current understanding and remaining questions. *Cardiovasc Res*. (2012) 96:234–43. doi: 10.1093/cvr/cvs217

6. Cameron JN, Mehta OH, Michail M, Chan J, Nicholls SJ, Bennett MR, et al. Exploring the relationship between biomechanical stresses and coronary atherosclerosis. *Atherosclerosis*. (2020) 302:43–51. doi: 10.1016/j.atherosclerosis.2020.04.011

7. Tatasciore A, Zimarino M, Tommasi R, Renda G, Schillaci G, Parati G, et al. Increased short-term blood pressure variability is associated with early left ventricular systolic dysfunction in newly diagnosed untreated hypertensive patients. *J Hypertens*. (2013) 31:1653. doi: 10.1097/HJH.0b013e328361e4a6

8. Thondapu V, Bourantas CV, Foin N, Jang I-K, Serruys PW, Barlis P. Biomechanical stress in coronary atherosclerosis: emerging insights from computational modelling. *Eur Heart J*. (2016) 38(2):ehv689. doi: 10.1093/eurheartj/ehv689

9. Krams R, Wentzel JJ, Oomen JAF, Vinke R, Schuurbiers JCH, De Feyter PJ, et al. Evaluation of endothelial shear stress and 3D geometry as factors determining the development of atherosclerosis and remodeling in human coronary arteries *in vivo*: combining 3D reconstruction from angiography and IVUS (ANGUS) with computational fluid dynamics. *ATVB*. (1997) 17:2061–5. doi: 10.1161/01.ATV.17.10.2061

10. Wang Q, Tang D, Wang L, Meahara A, Molony D, Samady H, et al. Multi-patient study for coronary vulnerable plaque model comparisons: 2D/3D and fluid–structure interaction simulations. *Biomech Model Mechanobiol*. (2021) 20:1383–97. doi: 10.1007/s10237-021-01450-8

11. Hartman EMJ, De Nisco G, Kok AM, Tomaniak M, Nous FMA, Korteland S-A, et al. Wall shear stress–related plaque growth of lipid-rich plaques in human coronary arteries: an near-infrared spectroscopy and optical coherence tomography study. *Cardiovasc Res*. (2023) 119:1021–9. doi: 10.1093/cvr/cvac178

12. Stone PH, Coskun AU, Kinlay S, Clark ME, Sonka M, Wahle A, et al. Effect of endothelial shear stress on the progression of coronary artery disease, vascular remodeling, and in-stent restenosis in humans: *in vivo* 6-month follow-up study. *Circulation*. (2003) 108:438–44. doi: 10.1161/01.CIR.0000080882.35274.AD

13. Gijsen FJH, Wentzel JJ, Thury A, Mastik F, Schaar JA, Schuurbiers JCH, et al. Strain distribution over plaques in human coronary arteries relates to shear stress. *Am J Physiol Heart Circ Physiol*. (2008) 295:H1608–14. doi: 10.1152/ajpheart.01081.2007

14. Samady H, Eshtehardi P, McDaniel MC, Suo J, Dhawan SS, Maynard C, et al. Coronary artery wall shear stress is associated with progression and transformation of atherosclerotic plaque and arterial remodeling in patients with coronary artery disease. *Circulation*. (2011) 124:779–88. doi: 10.1161/CIRCULATIONAHA.111.021824

15. Pelliccia F, Zimarino M, De Luca G, Viceconte N, Tanzilli G, De Caterina R. Endothelial progenitor cells in coronary artery disease: from bench to bedside. *Stem Cells Transl Med*. (2022) 11:451–60. doi: 10.1093/stcltm/szac010

16. Stone PH, Saito S, Takahashi S, Makita Y, Nakamura S, Kawasaki T, et al. Prediction of progression of coronary artery disease and clinical outcomes using vascular profiling of endothelial shear stress and arterial plaque characteristics: the PREDICTION study. *Circulation*. (2012) 126:172–81. doi: 10.1161/CIRCULATIONAHA.112.096438

17. Bourantas CV, Räber L, Sakellarios A, Ueki Y, Zanchin T, Koskinas KC, et al. Utility of multimodality intravascular imaging and the local hemodynamic forces to predict atherosclerotic disease progression. *JACC Cardiovasc Imaging*. (2020) 13:1021–32. doi: 10.1016/j.jcmg.2019.02.026

18. Russo G, Pedicino D, Chiastra C, Vinci R, Lodi Rizzini M, Genuardi L, et al. Coronary artery plaque rupture and erosion: role of wall shear stress profiling and biological patterns in acute coronary syndromes. *Int J Cardiol*. (2023) 370:356–65. doi: 10.1016/j.ijcard.2022.10.139

19. Lee JM, Choi G, Koo B-K, Hwang D, Park J, Zhang J, et al. Identification of high-risk plaques destined to cause acute coronary syndrome using coronary computed tomographic angiography and computational fluid dynamics. *JACC Cardiovasc Imaging*. (2019) 12:1032–43. doi: 10.1016/j.jcmg.2018.01.023

20. Kumar A, Thompson EW, Lefieux A, Molony DS, Davis EL, Chand N, et al. High coronary shear stress in patients with coronary artery disease predicts myocardial infarction. *J Am Coll Cardiol*. (2018) 72:1926–35. doi: 10.1016/j.jacc.2018.07.075

21. Zuin M, Rigatelli G, Vassilev D, Ronco F, Rigatelli A, Roncon L. Computational fluid dynamic-derived wall shear stress of non-significant left main bifurcation disease may predict acute vessel thrombosis at 3-year follow-up. *Heart Vessels*. (2020) 35:297–306. doi: 10.1007/s00380-019-01494-y

22. Fukumoto Y, Hiro T, Fujii T, Hashimoto G, Fujimura T, Yamada J, et al. Localized elevation of shear stress is related to coronary plaque rupture. *J Am Coll Cardiol*. (2008) 51:645–50. doi: 10.1016/j.jacc.2007.10.030

23. Jin C, Torii R, Ramasamy A, Tufaro V, Little CD, Konstantinou K, et al. Morphological and physiological characteristics of ruptured plaques in native arteries and neoatherosclerotic segments: an OCT-based and computational fluid dynamics study. *Front Cardiovasc Med*. (2022) 9:890799. doi: 10.3389/fcvm.2022.890799

24. Li Z-Y, Taviani V, Tang T, Sadat U, Young V, Patterson A, et al. The mechanical triggers of plaque rupture: shear stress vs pressure gradient. *BJR*. (2009) 82:S39–45. doi: 10.1259/bjr/15036781

25. Choi G, Lee JM, Kim H-J, Park J-B, Sankaran S, Otake H, et al. Coronary artery axial plaque stress and its relationship with lesion geometry. *JACC Cardiovasc Imaging*. (2015) 8:1156–66. doi: 10.1016/j.jcmg.2015.04.024

26. Costopoulos C, Huang Y, Brown AJ, Calvert PA, Hoole SP, West NEJ, et al. Plaque rupture in coronary atherosclerosis is associated with increased plaque structural stress. *JACC Cardiovasc Imaging*. (2017) 10:1472–83. doi: 10.1016/j.jcmg.2017.04.017

27. Tang D, Yang C, Kobayashi S, Ku DN. Effect of a lipid pool on stress/strain distributions in stenotic arteries: 3-D fluid-structure interactions (FSI) models. *J Biomech Eng*. (2004) 126:363–70. doi: 10.1115/1.1762898

28. Costopoulos C, Timmins LH, Huang Y, Hung OY, Molony DS, Brown AJ, et al. Impact of combined plaque structural stress and wall shear stress on coronary plaque progression, regression, and changes in composition. *Eur Heart J*. (2019) 40:1411–22. doi: 10.1093/eurheartj/ehz132

29. Teng Z, Brown AJ, Calvert PA, Parker RA, Obaid DR, Huang Y, et al. Coronary plaque structural stress is associated with plaque composition and subtype and higher in acute coronary syndrome: the BEACON I (biomechanical evaluation of atheromatous coronary arteries) study. *Circ Cardiovasc Imaging*. (2014) 7:461–70. doi: 10.1161/CIRCIMAGING.113.001526

30. Costopoulos C, Maehara A, Huang Y, Brown AJ, Gillard JH, Teng Z, et al. Heterogeneity of plaque structural stress is increased in plaques leading to MACE. *JACC Cardiovasc Imaging*. (2020) 13:1206–18. doi: 10.1016/j.jcmg.2019.05.024

31. Brown AJ, Teng Z, Calvert PA, Rajani NK, Hennessy O, Nerlekar N, et al. Plaque structural stress estimations improve prediction of future major adverse cardiovascular events after intracoronary imaging. *Circ Cardiovasc Imaging*. (2016) 9:e004172. doi: 10.1161/CIRCIMAGING.115.004172

32. Huang J, Tu S, Li C, Hong H, Wang Z, Chen L, et al. Radial wall strain assessment from AI-assisted angiography: feasibility and agreement with OCT as reference standard. *J Soc Cardiovasc Angiograph Interv*. (2023) 2:100570. doi: 10.1016/j.jscai.2022.100570

33. Hong H, Li C, Gutiérrez-Chico J, Wang Z, Huang J, Chu M, et al. Radial wall strain: a novel angiographic measure of plaque composition and vulnerability. *EuroIntervention*. (2022) 18(12):1001–10. doi: 10.4244/EIJ-D-22-00537

34. Yang S, Wang Z, Park S-H, Hong H, Li C, Liu X, et al. Relationship of coronary angiography-derived radial wall strain with functional significance, plaque morphology, and clinical outcomes. *JACC Cardiovasc Interv*. (2024) 17:46–56. doi: 10.1016/j.jcin.2023.10.003

35. Kedhi E, Berta B, Roleder T, Hermanides RS, Fabris E, IJsselmuiden AJJ, et al. Thin-cap fibroatheroma predicts clinical events in diabetic patients with normal fractional flow reserve: the COMBINE OCT–FFR trial. *Eur Heart J*. (2021) 42:4671–9. doi: 10.1093/eurheartj/ehab433

36. Park S-J, Ahn J-M, Kang D-Y, Yun S-C, Ahn Y-K, Kim W-J, et al. Preventive percutaneous coronary intervention versus optimal medical therapy alone for the treatment of vulnerable atherosclerotic coronary plaques (PREVENT): a multicentre, open-label, randomised controlled trial. *Lancet*. (2024) 403:1753–65. doi: 10.1016/S0140-6736(24)00413-6

37. Chen Q, Smith CY, Bailey KR, Wennberg PW, Kullo IJ. Disease location is associated with survival in patients with peripheral arterial disease. *J Am Heart Assoc*. (2013) 2:e000304. doi: 10.1161/JAHA.113.000304

38. Puchner SB, Liu T, Mayrhofer T, Truong QA, Lee H, Fleg JL, et al. High-risk plaque detected on coronary CT angiography predicts acute coronary syndromes independent of significant stenosis in acute chest pain. *J Am Coll Cardiol*. (2014) 64:684–92. doi: 10.1016/j.jacc.2014.05.039

39. Stone GW, Maehara A, Lansky AJ, De Bruyne B, Cristea E, Mintz GS, et al. A prospective natural-history study of coronary atherosclerosis. *N Engl J Med*. (2011) 364:226–35. doi: 10.1056/NEJMoa1002358

40. Stone PH, Maehara A, Coskun AU, Maynard CC, Zaromytidou M, Siasos G, et al. Role of low endothelial shear stress and plaque characteristics in the prediction of nonculprit major adverse cardiac events. *JACC Cardiovasc Imaging*. (2018) 11:462–71. doi: 10.1016/j.jcmg.2017.01.031

41. Motoyama S, Ito H, Sarai M, Kondo T, Kawai H, Nagahara Y, et al. Plaque characterization by coronary computed tomography angiography and the likelihood of acute coronary events in mid-term follow-up. *J Am Coll Cardiol*. (2015) 66:337–46. doi: 10.1016/j.jacc.2015.05.069

42. Rigatelli G, Zuin M, Bilato C, Nguyen T. Coronary artery cavitation as a trigger for atherosclerotic plaque progression: a simplified numerical and computational fluid dynamic demonstration. *Rev Cardiovasc Med*. (2022) 23:058. doi: 10.31083/j.rcm2302058

43. Rigatelli G, Zuin M, Ngo TT, Nguyen HT, Nanjundappa A, Talarico E, et al. Intracoronary cavitation as a cause of plaque rupture and thrombosis propagation in patients with acute myocardial infarction: a computational study. *J Transl Intern Med*. (2019) 7:69–75. doi: 10.2478/jtim-2019-0014

44. Pelliccia F, Zimarino M, Niccoli G, Morrone D, De Luca G, Miraldi F, et al. In-stent restenosis after percutaneous coronary intervention: emerging knowledge on biological pathways. *Eur Heart J Open*. (2023) 3:oead083. doi: 10.1093/ehjopen/oead083

45. Jenei C, Balogh E, Szabó GT, Dézsi CA, Kőszegi Z. Wall shear stress in the development of in-stent restenosis revisited. A critical review of clinical data on shear stress after intracoronary stent implantation. *Cardiol J*. (2016) 23:365–73. doi: 10.5603/CJ.a2016.0047

46. LaDisa JF Jr, Guler I, Olson LE, Hettrick DA, Kersten JR, Warltier DC, et al. Three-dimensional computational fluid dynamics modeling of alterations in coronary wall shear stress produced by stent implantation. *Ann Biomed Eng*. (2003) 31:972–80. doi: 10.1114/1.1588654

47. LaDisa JF, Olson LE, Douglas HA, Warltier DC, Kersten JR, Pagel PS. Alterations in regional vascular geometry produced by theoretical stent implantation influence distributions of wall shear stress: analysis of a curved coronary artery using 3D computational fluid dynamics modeling. *BioMed Eng OnLine*. (2006) 5:40. doi: 10.1186/1475-925X-5-40

48. Chen WX, Poon EKW, Hutchins N, Thondapu V, Barlis P, Ooi A. Computational fluid dynamics study of common stent models inside idealised curved coronary arteries. *Comput Methods Biomech Biomed Engin*. (2017) 20:671–81. doi: 10.1080/10255842.2017.1289374

49. Torii R, Stettler R, Räber L, Zhang Y-J, Karanasos A, Dijkstra J, et al. Implications of the local hemodynamic forces on the formation and destabilization of neoatherosclerotic lesions. *Int J Cardiol*. (2018) 272:7–12. doi: 10.1016/j.ijcard.2018.06.065

50. Duraiswamy N, Cesar JM, Schoephoerster RT, Moore JE Jr. Effects of stent geometry on local flow dynamics and resulting platelet deposition in an *in vitro* model. *Biorheology*. (2008) 45:547–61. doi: 10.3233/BIR-2008-0497

51. Wentzel J, Gijsen F, Schuurbiers JCH, van der Steen A, Serruys PW. The influence of shear stress on in-stent restenosis and thrombosis. EuroIntervention. Available online at: https://eurointervention.pcronline.com/article/the-influence-of-shear-stress-on-in-stent-restenosis-and-thrombosis (accessed January 7, 2024).

52. Tyczynski P, Ferrante G, Moreno-Ambroj C, Kukreja N, Barlis P, Pieri E, et al. Simple versus complex approaches to treating coronary bifurcation lesions: direct assessment of stent strut apposition by optical coherence tomography. *Rev Esp Cardiol (Engl Ed)*. (2010) 63:904–14. doi: 10.1016/S1885-5857(10)70184-5

53. Rigatelli G, Zuin M, Dell'Avvocata F, Vassilev D, Daggubati R, Nguyen T, et al. Evaluation of coronary flow conditions in complex coronary artery bifurcations stenting using computational fluid dynamics: impact of final proximal optimization technique on different double-stent techniques. *Cardiovasc Revasc Med*. (2017) 18:233–40. doi: 10.1016/j.carrev.2017.01.002

54. Brindise MC, Chiastra C, Burzotta F, Migliavacca F, Vlachos PP. Hemodynamics of stent implantation procedures in coronary bifurcations: an *in vitro* study. *Ann Biomed Eng*. (2017) 45:542–53. doi: 10.1007/s10439-016-1699-y

55. Katritsis DG, Theodorakakos A, Pantos I, Gavaises M, Karcanias N, Efstathopoulos EP. Flow patterns at stented coronary bifurcations: computational fluid dynamics analysis. *Circ Cardiovasc Interv*. (2012) 5:530–9. doi: 10.1161/CIRCINTERVENTIONS.112.968347

56. Rigatelli G, Zuin M, Marchese G, Rodino G, Hiso E, Mileva N, et al. Residence-time in complex left main bifurcation disease after stenting. *Cardiovasc Revasc Med*. (2023) 61:1–5. doi: 10.1016/j.carrev.2023.11.013

57. Zimarino M, Briguori C, Amat-Santos IJ, Radico F, Barbato E, Chieffo A, et al. Mid-term outcomes after percutaneous interventions in coronary bifurcations. *Int J Cardiol*. (2019) 283:78–83. doi: 10.1016/j.ijcard.2018.11.139

58. Zimarino M, Angiolillo D, Dangas G, Capodanno D, Barbato E, Hahn J-Y, et al. Antithrombotic therapy after percutaneous coronary intervention of bifurcation lesions. *EuroIntervention*. (2021) 17(1):59–66. doi: 10.4244/EIJ-D-20-00885

59. Toth GG, Toth B, Johnson NP, De Vroey F, Di Serafino L, Pyxaras S, et al. Revascularization decisions in patients with stable angina and intermediate lesions: results of the international survey on interventional strategy. *Circ Cardiovasc Interv*. (2014) 7:751–9. doi: 10.1161/CIRCINTERVENTIONS.114.001608

60. Härle T, Zeymer U, Hochadel M, Zahn R, Kerber S, Zrenner B, et al. Real-world use of fractional flow reserve in Germany: results of the prospective ALKK coronary angiography and PCI registry. *Clin Res Cardiol*. (2017) 106:140–50. doi: 10.1007/s00392-016-1034-5

61. Tu S, Westra J, Yang J, Von Birgelen C, Ferrara A, Pellicano M, et al. Diagnostic accuracy of fast computational approaches to derive fractional flow reserve from diagnostic coronary angiography. *JACC Cardiovasc Interv*. (2016) 9:2024–35. doi: 10.1016/j.jcin.2016.07.013

62. Westra J, Andersen BK, Campo G, Matsuo H, Koltowski L, Eftekhari A, et al. Diagnostic performance of in-procedure angiography-derived quantitative flow reserve compared to pressure-derived fractional flow reserve: the FAVOR II Europe-Japan study. *JAHA*. (2018) 7:e009603. doi: 10.1161/JAHA.118.009603

63. Cortés C, Carrasco-Moraleja M, Aparisi A, Rodriguez-Gabella T, Campo A, Gutiérrez H, et al. Quantitative flow ratio—meta-analysis and systematic review. *Cathet Cardio Intervent*. (2021) 97:807–14. doi: 10.1002/ccd.28857

64. Rimac G, Fearon WF, De Bruyne B, Ikeno F, Matsuo H, Piroth Z, et al. Clinical value of post–percutaneous coronary intervention fractional flow reserve value: a systematic review and meta-analysis. *Am Heart J*. (2017) 183:1–9. doi: 10.1016/j.ahj.2016.10.005

65. Azzalini L, Poletti E, Demir OM, Ancona MB, Mangieri A, Giannini F, et al. Impact of post-percutaneous coronary intervention fractional flow reserve measurement on procedural management and clinical outcomes: the REPEAT-FFR study. *J Invasive Cardiol*. (2019) 31:229–34.

66. Zhang R, Song C, Guan C, Liu Q, Wang C, Xie L, et al. Prognostic value of quantitative flow ratio based functional SYNTAX score in patients with left main or multivessel coronary artery disease. *Circ Cardiovasc Interv*. (2020) 13:e009155. doi: 10.1161/CIRCINTERVENTIONS.120.009155

67. Amat-Santos IJ, Marengo G, Sánchez-Luna JP, Cortés Villar C, Rivero Crespo F, Jiménez Díaz VA, et al. Validation of quantitative flow ratio-derived virtual angioplasty with post-angioplasty fractional flow reserve—the QIMERA-I study. *JCDD*. (2023) 11:14. doi: 10.3390/jcdd11010014

68. Van Diemen PA, De Winter RW, Schumacher SP, Bom MJ, Driessen RS, Everaars H, et al. Residual quantitative flow ratio to estimate post-percutaneous coronary intervention fractional flow reserve. *J Interv Cardiol*. (2021) 2021:1–11. doi: 10.1155/2021/4339451

69. Rubimbura V, Guillon B, Fournier S, Amabile N, Chi Pan C, Combaret N, et al. Quantitative flow ratio virtual stenting and post stenting correlations to post stenting fractional flow reserve measurements from the DOCTORS (does optical coherence tomography optimize results of stenting) study population. *Cathet Cardio Intervent*. (2020) 96:1145–53. doi: 10.1002/ccd.28615

frontiers | Frontiers in Cardiovascular Medicine

TYPE Original Research
PUBLISHED 07 November 2024
DOI 10.3389/fcvm.2024.1382585

OPEN ACCESS

EDITED BY
Viktor Kočka,
Charles University, Czechia

REVIEWED BY
Rafal Adam Januszek,
Andrzej Frycz Modrzewski Krakow University, Poland
Suvitesh Luthra,
University Hospital Southampton NHS Foundation Trust, United Kingdom

*CORRESPONDENCE
Isaac Pascual
✉ ipascua@live.com

†These authors have contributed equally to this work and share first authorship

RECEIVED 05 February 2024
ACCEPTED 21 October 2024
PUBLISHED 07 November 2024

CITATION
Alperi A, Almendárez M, Pascual I, Alvarez R, Betanzos JL, Hernández-Vaquero D, Ptaszynski R, Ortiz JF, Moris C and Avanzas P (2024) Sex related disparities after complex percutaneous coronary interventions. Front. Cardiovasc. Med. 11:1382585. doi: 10.3389/fcvm.2024.1382585

Sex related disparities after complex percutaneous coronary interventions

Alberto Alperi[1,2†], Marcel Almendárez[1,2,3†], Isaac Pascual[1,2,3*], Rut Alvarez[1], Jose Luis Betanzos[1], Daniel Hernández-Vaquero[1,2,3], Raul Ptaszynski[1,2], Juan Francisco Ortiz[1], Cesar Moris[1,2,3] and Pablo Avanzas[1,2,3,4]

[1]Department of Cardiology, Heart Area, Hospital Universitario Central de Asturias, Oviedo, Spain, [2]Department of Cardiology, Health Research Institute of Asturias (Instituto de Iinvestigación Sanitaria del Principado de Asturias), Oviedo, Spain, [3]Department of Medicine, Faculty of Medicine, University of Oviedo, Oviedo, Spain, [4]Department of Cardiology, Centro de Investigación en Red de Enfermedades Cardiovasculares (CIBERCV), Madrid, Spain

Introduction: Complex Percutaneous coronary intervention (PCI) for the treatment of ischemic heart disease has increased significantly. We aimed to evaluate sex-related differences in patients undergoing complex PCI.
Methods: single-center prospective observational study including patients undergoing complex PCI between 2017 and 2023. Baseline and procedural features, and mid-term outcomes were compared according to the gender distribution. The combined primary endpoint included stroke, myocardial infarction, need for a new coronary revascularization, and all-cause mortality. Propensity score (PS) matching with an inverse probability of treatment weight (IPW) approach was used to adjust for differences in baseline characteristics.
Results: 1,283 patients were included, 983 (76.6%) male and 300 (23.4%) female. Median follow-up was 2.4 (IQR: 1–3.8) years. There was a higher rate of no-reflow phenomenon (4% vs. 1.8%, $p = 0.03$) among female patients. In the overall cohort, female patients had a greater risk for the combined primary endpoint (HR 1.28, 95% CI: 1.02–1.59). In the matched cohort, female patients exhibited a higher risk for the combined primary endpoint (HR 1.23, 95% CI: 1.06–1.42), as well as for myocardial infarction (HR 1.34, 95% CI 1.03–1.75), and all-cause mortality (HR 1.21, 95% CI 1.02–1.45), and a trend towards a higher risk for the need of a new coronary revascularization (HR 1.22, 95% CI 0.92–1.61).
Conclusions: in a contemporary cohort of patients undergoing complex PCI procedures, female patients are associated with a higher risk of early complications.

KEYWORDS

coronary artery disease, percutaneous coronary intervention, complex PCI, myocardial infarction, sex-related differences inverse probability of treatment weight

Abbreviations
CI, confidence interval; HR, hazard ratio; IPW, inverse probability of treatment weight; LVEF, left ventricular ejection fraction; PCI, percutaneous coronary intervention; PS, propensity-score.

Introduction

Cardiovascular disease continues to be the leading cause of morbidity and mortality among Western countries, and an exponential growth in its incidence is expected over the following decades due to the aging population, the increased incidence of obesity and other metabolic disorders, and certain social conditions (1). Percutaneous coronary intervention (PCI) for treating ischemic heart disease has increased dramatically over the last decades due to its low invasiveness and improved clinical outcomes (2). However, certain features of the coronary lesions are known to represent a major challenge for the interventionalists and might impact early- and long-term cardiovascular outcomes. Nowadays, the widely known complex PCI and high-risk PCI procedures have gained relevance given their frequency in clinical practice, and this has been a matter of study in recent years (3, 4).

It is broadly known that females with cardiovascular disease exhibit differential clinical features than males. For instance, women with diabetes show a greater risk for cardiovascular complications than their male counterparts, probably related with inflammatory parameters and smaller coronary vessel size (5). Additionally, their clinical course differs from men in several cardiovascular pathologies (6–8).

Little is known so far about sex-related differences in patients undergoing complex PCI, but some reports suggest there might be relevant disparities. Prior studies on patients undergoing rotational atherectomy or chronic total occlusion PCI found that women more often experience coronary dissection, cardiac tamponade, and significant complications than men (9–11). Therefore, we aimed to evaluate differences in baseline clinical conditions and procedural features among patients undergoing complex PCI procedures according to their gender. Besides, we sought to evaluate a sex-related clinical impact beyond other clinical conditions in this specific setting.

Methods

Patient selection

This was a single-center, observational, and prospective study. All patients receiving a complex percutaneous coronary intervention in our center between 2017 and 2023 were prospectively included in a dedicated database. Baseline and procedural features were incorporated at the time of PCI, and in-hospital outcomes were added at the time of discharge. The treating physicians decided to undergo complex PCI after carefully considering all available alternatives. Patients were informed and consented to the procedure and data collection. The local Ethics Committee of the center approved data collection and reporting (2020.026).

Inclusion criteria

Complex PCI was defined when any of the following conditions were present (12): true bifurcation lesions according to the Medina classification (13) with a side-branch diameter of at least 2.5 mm; a chronic total occlusion; unprotected left main coronary artery disease; long coronary-artery lesions requiring at least 60 mm of stent length; multivessel PCI involving the 3 major epicardial coronary arteries being treated at the same time; a severely calcified lesion needing plaque modification with either rotational atherectomy or intravascular lithotripsy; PCI in a prior saphenous bypass graft; PCI in a single remaining patent vessel; or aorto-ostial lesions of a major epicardial coronary artery.

Exclusion criteria

For the purpose of homogeneity, those patients presenting with cardiogenic shock that needed emergent placement of a left ventricular assist device were excluded from the present analysis.

Therefore, emergent cases (ST-elevation myocardial infarction) were included if they fulfilled the criteria for complex PCI and did not require an acute ventricular assist device placement due to cardiogenic shock.

Follow-up

Clinical follow-up was performed 6 months after the intervention and yearly thereafter. All relevant clinical events were updated at every outpatient visit. In case of missing a clinical follow-up, telephonic contact and a review of the medical files were performed to ensure live status and to avoid missing any relevant clinical event for every patient. In our region, healthcare professionals have unrestricted access to the entire clinical history of the patient, hence minimizing the miss of any significant event.

Endpoints

The main combined primary endpoint included stroke, admission due to myocardial infarction, the need for a new coronary revascularization, and all-cause mortality.

Secondary endpoints were the individual components of the main primary endpoint.

Statistical analysis

Results are displayed as numbers (percentage) for categorical data and as mean (standard deviation) for continuous variables. Student's *t*-test was used to compare normally continuous variables and the Mann–Whitney *U*-test was used for continuous non-normally distributed variables. The chi squared and Fisher's exact tests were used to compare categorical variables. Two groups according to patient's gender (male and female) were used to evaluate baseline characteristics and outcomes.

Propensity score (PS) matching with an inverse probability of treatment weight (IPW) approach was used to adjust for

10.3389/fcvm.2024.1382585

differences in baseline characteristics and potential confounders. A PS was obtained for each patient to estimate the propensity toward belonging to a specific group (female vs. male). This was done by means of a multivariate logistic regression including the following covariates: age, diabetes mellitus, hypertension, chronic kidney disease, peripheral artery disease, history of stroke, left ventricular ejection fraction (LVEF), clinical presentation (stable coronary disease, unstable angina, non-ST elevation myocardial infarction or ST elevation myocardial infarction), PCI to a chronic total occlusion lesion, PCI to a true bifurcation lesion, PCI of an aorto-ostial lesion, PCI involving the left main coronary artery, severe calcification of the treated coronary vessel, and the use of an intra-aortic balloon pump during PCI. The propensity score calculation allowed case-weight estimation to predict the inverse probability of belonging to the female group among the study participants. The case weights balanced the cohorts for an IPW analysis that included all patients with available data for the variables included in the propensity model. The adequate balancing of covariate distribution between the matched groups was numerically assessed by means of standardized means differences after IPW-matching, and graphically assessed by means of the cumulative probability plots for raw and IPW-adjusted data (Supplementary Figure S1). Then, an inverse probability of treatment-weighted Cox regression was performed to determine the relation between gender and our primary and secondary endpoints. Survival-free curves for both groups are displayed using the Kaplan–Meier method. Data analyses were performed using STATA (v14.0; StataCorp), and p-values <0.05 were considered significant.

TABLE 1 Baseline characteristics according to gender in the overall cohort.

	Men (n = 983)	Women (n = 300)	p value
Age, years	69.6 ± 11.4	73.8 ± 11.1	0.001
Diabetes Mellitus	367 (33.3)	109 (36.3)	0.75
Hypertension	681 (69.3)	214 (71.3)	0.5
Dyslipidemia	621 (63.2)	185 (65.7)	0.64
Chronic kidney disease	182 (14.5)	54 (18.1)	0.85
Prior MI	42 (4.3)	10 (3.3)	0.62
Prior CABG	79 (8)	16 (5.3)	0.12
Peripheral artery disease	181 (18.4)	25 (8.3)	0.001
Prior Stroke	85 (8.6)	18 (6)	0.14
Presentation:			0.18
Stable CAD	375 (38.2)	94 (31.3)	
Unstable angina	152 (15.5)	53 (17.7)	
NSTEMI	274 (27.9)	89 (29.7)	
STEMI	182 (18.5)	64 (21.3)	
LVEF, %	50.9 ± 11.7	52.8 ± 11.5	0.02
Chronic total occlusion	159 (16.2)	42 (14)	0.36
Number of diseased vessels	1.62 ± 0.8	1.58 ± 0.8	0.43
Number of treated vessels	1.30 ± 0.6	1.31 ± 0.6	0.82
Left main PCI	379 (38.6)	132 (44)	0.09
Bypass graft PCI	24 (2.4)	8 (2.7)	0.83
3-vessel PCI	42 (4.3)	13 (4.3)	0.97
Aorto-ostial lesion PCI	213 (21.7)	85 (28.3)	0.02
Bifurcation lesion PCI	320 (30.7)	91 (30.3)	0.44
Euroscore 2	4.7 ± 3.1	4.9 ± 4.6	0.39

CABG, coronary artery bypass graft; CAD, coronary artery disease; LVEF, left ventricle ejection fraction; MI, myocardial infarction; NSTEMI, non-ST elevation myocardial infarction; PCI, percutaneous coronary intervention; STEMI, ST elevation myocardial infarction.

Results

A total of 1,283 patients were included, 983 (76.6%) male and 300 (23.4%) female. The main baseline characteristics of the study population are presented in Table 1. Female patients exhibited an older age at the time of PCI (73.8 ± 11.1 vs. 69.6 ± 11.4 years, $p < 0.001$), had a greater LVEF (52.8 ± 11% in females vs. 50.9 ± 11.7% in males, $p = 0.02$), and a trend towards a higher rate of left main PCI and a higher rate of aorto-ostial lesions (28.3% female vs. 21.7% male, $p = 0.02$). Male patients exhibited a higher burden of peripheral artery disease (18.4% male vs. 8.3% female, $p = 0.001$).

The main procedural features are displayed in Table 2. The main access was radial (61% in males and 55.5% in females).

TABLE 2 Procedural and in-hospital characteristics according to gender distribution in the overall cohort.

	Men (n = 983)	Women (n = 300)	p value
Access			0.17
Radial	596 (61)	166 (55.5)	
Femoral	371 (37.9)	131 (43.8)	
Double access	11 (1.1)	2 (0.7)	
Bifurcation strategy:			0.71
Provisional-stent	192 (62.9)	51 (60.7)	
Double-stent	113 (37.1)	33 (39.3)	
Severe angulation	74 (7.5)	19 (6.3)	0.49
Severe calcification	316 (32.2)	102 (34)	0.55
Use of cutting or scoring-balloon	135 (13.8)	33 (11)	0.21
Use of drug-coated balloon	217 (22.3)	43 (14.4)	0.003
Use of intracoronary lithotripsy	92 (9.4)	18 (6)	0.07
Use of rotablation	140 (14.2)	41 (13.7)	0.80
Intra-aortic balloon pump	107 (10.9)	43 (14.3)	0.11
Number of stents	2.17 ± 1.2	2.03 ± 1.2	0.08
Length of stent	53 ± 31	47.8 ± 28	0.01
Time of fluoroscopy	27.5 ± 89	22.7 ± 20	0.37
Dose of radiation	3,190 ± 3600	2,330 ± 1842	0.001
Contrast media used	191 ± 96	178 ± 88	0.06
Procedural complications			
Unsuccessful PCI	49 (4.9)	12 (4)	0.48
Vascular closure failure	10 (1)	2 (0.7)	0.58
Perforation	9 (0.9)	6 (2)	0.13
Dissection	39 (4)	13 (4.3)	0.78
Side branch closure	13 (1.3)	6 (2)	0.40
No-reflow	18 (1.8)	12 (4)	0.03
Procedural death	11 (1.1)	8 (2.7)	0.05
In hospital complications			
Vascular complication	30 (3)	13 (4.3)	0.28
Stroke/TIA	12 (1.2)	3 (1)	0.76
Contrast-induced nephropathy	98 (10)	33 (11)	0.61
In-hospital death	79 (8)	35 (11.7)	0.05
Length of hospitalization	7 ± 9.7	7.9 ± 12	0.19

PCI, percutaneous coronary intervention; TIA, transient ischemic attack.

The rates of true bifurcation lesions, severe lesion angulation, and severe calcification were comparable between genders, but there was a trend towards a greater use of intracoronary lithotripsy (9.4% vs. 6%, $p = 0.07$), and higher number of stents and stent length among male PCI recipients.

Procedural-related complications and in-hospital outcomes are summarized in Table 2. There were no significant differences between study groups in PCI failure (4.9% vs. 4%). However, there was a higher rate of no-reflow phenomenon (4% vs. 1.8%, $p = 0.03$) and a trend towards a higher risk of procedural mortality (2.7% vs. 1.1%, $p = 0.05$) among female patients. Similarly, differences in in-hospital complications were not statistically significant but for a trend towards a higher risk of in-hospital mortality for the female group.

Median follow-up was 2.4 (IQR: 1–3.8) years. Over that period, a total of 290 (22.6%) patients died (205 [20.8%] and 85 [28.3%] deaths among male and female patients, respectively), 14 (1.1%) patients had a stroke (8 [0.8%] and 6 [2%] strokes among male and female patients, respectively), 106 (8.3%) patients underwent new coronary revascularizations (81 [8.2%] and 25 [8.3%] new coronary revascularizations among male and female patients, respectively), and there were 116 (9.1%) admissions for acute myocardial infarction (87 [8.8%] and 29 [9.7%] among male and female patients, respectively).

In the univariate Cox regression analysis, several variables conferred a significantly higher risk for the primary combined endpoint (older age, diabetes, hypertension, chronic kidney disease, peripheral artery disease, number of diseased vessels, left main PCI, and true bifurcation lesions), whereas other were protective factors (higher LVEF and PCI of a total chronic occlusion). Besides, female gender was also associated with a higher risk for the combined endpoint (HR 1.32, 95% CI: 1.07–1.64). In the multivariate analysis, after adjustment for covariates, female gender was yet associated with a higher risk of death, stroke, myocardial infarction or new coronary revascularization (HR 1.28, 95% CI: 1.02–1.59) (Table 3). This higher risk for the combined endpoint was mainly based on all-cause mortality (HR 1.38, 95% CI: 1.07–1.77) and stroke rates (HR 2.57, 95% CI: 0.89–7.4), and no significant differences for myocardial infarction or new revascularization were observed for the overall unadjusted cohort (Table 4). Kaplan–Meier graphics for the primary and secondary endpoints are represented in Figures 1, 2, respectively.

IPW-adjusted cohort

After PS-IPW adjustment, baseline characteristics were well-balanced between study groups (Supplementary Tables S1 and S2 and Supplementary Figure S1).

In the IPW-adjusted cohort, there was a higher risk for the combined primary endpoint (HR 1.23, 95% CI: 1.06–1.42) among female patients (Table 4 and Figure 3).

Besides, female patients exhibited higher rates for admission due to myocardial infarction (HR 1.34, 95% CI: 1.03–1.75), a higher risk for

TABLE 3 Univariate and multivariate cox regression analysis for the primary combined endpoint of myocardial infarction, stroke, new coronary revascularization and all-cause mortality.

Variable	Univariate		Multivariate	
	HR (95% CI)	*p* value	HR (95% CI)	*p* value
Age, years	1.03 (1.02–1.04)	0.001	1.02 (1.01–1.03)	0.001
Diabetes Mellitus	1.82 (1.48–2.22)	0.001	1.67 (1.32–2.09)	0.001
Hypertension	1.32 (1.05–1.66)	0.02	1.02 (0.78–1.36)	0.83
Dyslipidemia	1.11 (0.90–1.37)	0.32		
Chronic kidney disease	2.2 (1.76–2.7)	0.001	1.26 (0.96–1.64)	0.09
Prior MI	1.39 (0.90–2.14)	0.13		
Prior CABG	1.19 (0.82–1.72)	0.35		
Peripheral artery disease	1.84 (1.44–2.36)	0.001	1.46 (1.09–1.94)	0.009
Prior Stroke	1.54 (1.1–2.14)	0.01	1.02 (0.71–1.49)	0.89
Presentation:				
Stable CAD (reference)				
Unstable angina	1.27 (0.92–1.77)	0.14	1.03 (0.73–1.48)	0.83
NSTEMI	1.85 (1.42–2.4)	0.001	1.27 (0.95–1.68)	0.10
STEMI	2.12 (1.61–2.79)	0.001	1.57 (1.13–2.17)	0.006
LVEF, %	0.96 (0.95–0.97)	0.001	0.97 (0.96–0.98)	0.001
Chronic total occlusion	0.35 (0.26–0.52)	0.001	0.64 (0.42–0.98)	0.04
Number of diseased vessels	1.43 (1.27–1.61)	0.001	1.27 (1.11–1.44)	0.001
Left main PCI	1.74 (1.42–2.12)	0.001	1.09 (0.83–1.44)	0.53
Bypass graft PCI	1.99 (1.21–3.29)	0.007	2.01 (1.16–3.45)	0.02
3-vessel PCI	1.37 (0.89–2.11)	0.15		
Aorto-ostial lesion PCI	1.21 (0.97–1.53)	0.09	1.12 (0.87–1.44)	0.39
Bifurcation lesion PCI	1.59 (1.29–1.96)	0.001	1.33 (1.01–1.74)	0.03
Gender (female vs. male)	1.32 (1.07–1.64)	0.01	1.28 (1.02–1.59)	0.04

CABG, coronary artery bypass graft; CAD, coronary artery disease; CI, confidence interval; HR, hazard ratio; LVEF, left ventricle ejection fraction; MI, myocardial infarction; NSTEMI, non-ST elevation myocardial infarction; PCI, percutaneous coronary intervention; STEMI, ST elevation myocardial infarction.

all-cause mortality (HR 1.21, 95% CI: 1.02–1.45), and a trend towards a higher risk for the need of a new coronary revascularization (HR 1.22, 95% CI: 0.92–1.61) (Table 4 and Figure 4).

Discussion

The main findings of our investigation are summarized as follows: (i) female patients undergoing complex PCI exhibited differential features compared to their male counterparts, like a higher rate of left main PCI, aorto-ostial lesion PCI, and a higher risk for non-reflow phenomenon. (ii) female gender was independently associated with a higher risk for the combined primary endpoint (stroke, myocardial infarction, new coronary revascularization, and all-cause mortality) over follow-up, and those results remain concordant after adjustment for baseline covariates; (iii) in the adjusted cohort, female patients exhibited a higher risk for myocardial infarction and a trend towards a higher risk for new coronary revascularization over follow-up.

TABLE 4 Survival analysis for the primary and secondary endpoints according to gender in the overall and IPW-adjusted populations.

Overall cohort		
Endpoint	HR (95% CI)	*p* value
Combined primary endpoint	1.32 (1.07–1.64)	0.01
Stroke	2.57 (0.89–7.4)	0.08
New revascularization	1.06 (0.68–1.67)	0.79
Myocardial infarction	1.13 (0.75–1.73)	0.55
All-cause mortality	1.38 (1.07–1.77)	0.01
IPW-adjusted cohort		
Endpoint	HR (95% CI)	*p* value
Combined primary endpoint	1.23 (1.06–1.42)	0.01
Stroke	1.71 (0.77–3.84)	0.19
New revascularization	1.22 (0.92–1.61)	0.17
Myocardial infarction	1.34 (1.03–1.75)	0.03
All-cause mortality	1.21 (1.02–1.45)	0.03

CI, confidence interval; HR, hazard ratio; IPW, inverse probability of treatment weight.

Sex-related differences in baseline and procedural characteristics

Although cardiovascular disease develops 5 to 10 years later in women than in men, this is yet the leading cause of death in women older than 65 years. In line with prior data, the higher age of women presenting with ischemic heart disease was also manifest in our patient cohort. Despite this age difference, male patients carried a slightly higher cardiovascular disease burden in our patient population, with a significantly higher rate of peripheral artery disease and comparable rates of diabetes, hypertension, and chronic kidney disease.

Coronary artery disease could be underrecognized among female patients, given the disparities in clinical presentation (frequent association of atypical symptoms) and the perception that women are invariably more protected against cardiovascular disease due to inherent endocrine characteristics (e.g., estrogen-

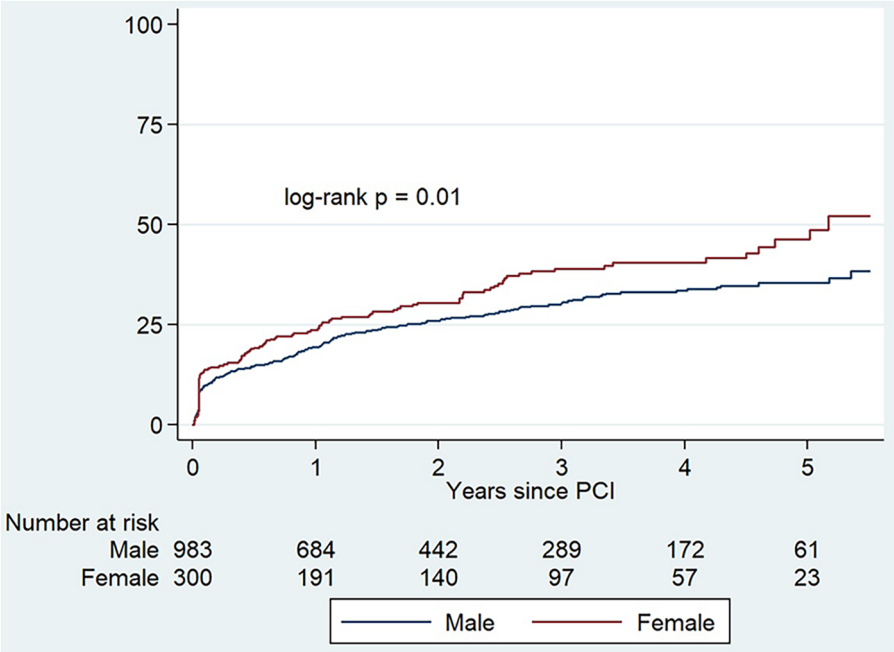

FIGURE 1
Kaplan–Meier cumulative incidence estimates for the combined primary endpoint (stroke, new coronary revascularization, myocardial infarction or all-cause mortality) in the overall cohort of patients.

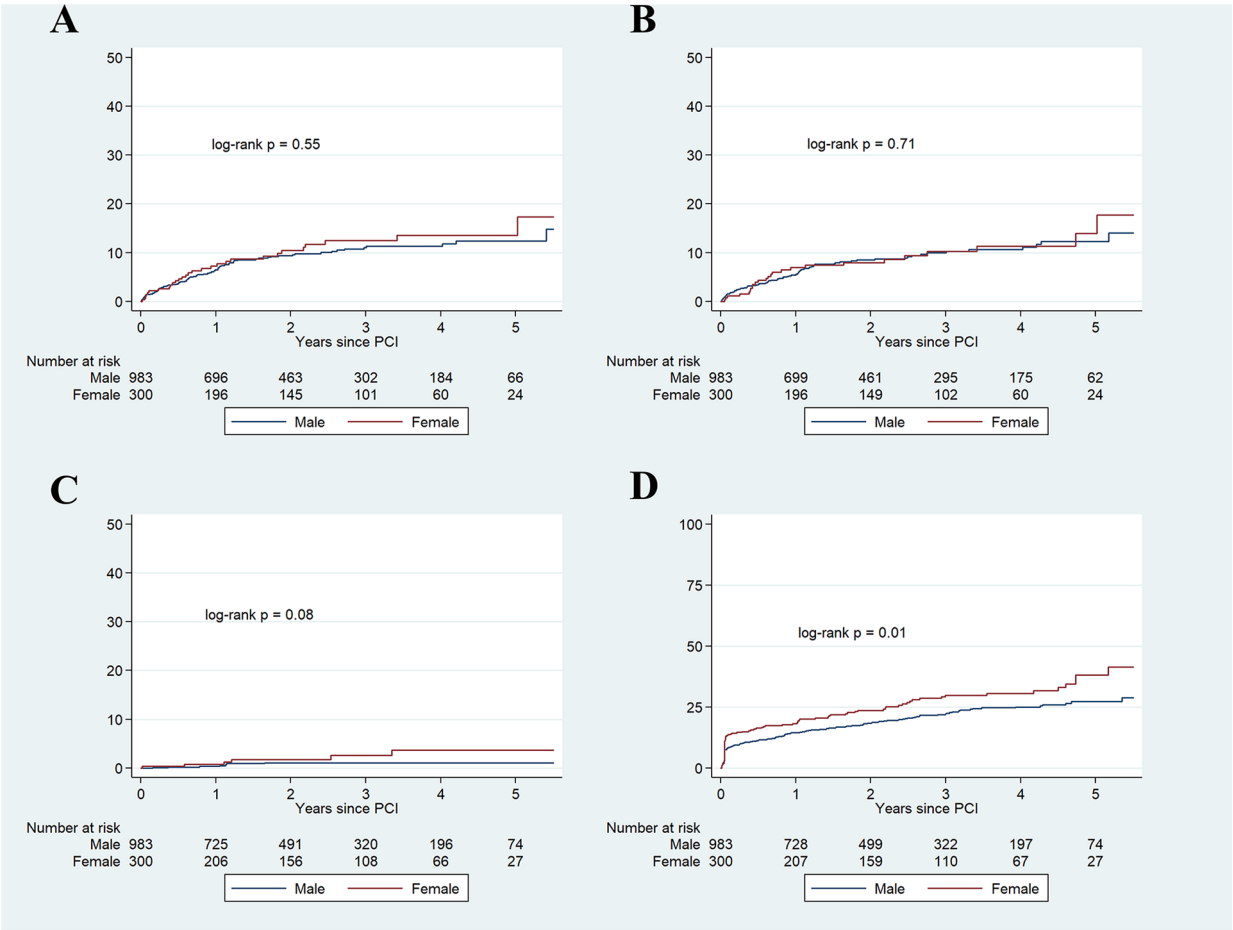

FIGURE 2
Kaplan–Meier cumulative incidence estimates for myocardial infarction (A), new coronary revascularization (B), stroke (C), and all-cause mortality (D).

dependent vasodilatation of the endothelial wall). These facts could lead to a delayed diagnosis among women, causing a more advanced coronary disease at presentation and ultimately impacting prognosis.

Notably, there was a lower use of contemporary techniques for the management of complex coronary lesions in women than in men in our cohort. As a matter of fact, despite similar rates of severe lesion calcification, the use of intravascular lithotripsy and cutting/scoring-balloon was numerically lower among female patients. These data are in line with prior reports in which ischemic stress testing and invasive procedures for the diagnosis and management of ischemic heart disease were underused in women (14). However, it should be noted that coronary anatomy and pathophysiology vary significantly between genders. Women tend to present with a smaller vessel size, less collateral flow, lower coronary flow reserve, greater vascular stiffness, and more tortuous anatomies (15). Hence, whether the disparities observed in PCI technical aspects are driven by pathophysiological and anatomical features between men and women remains widely unknown. Nevertheless, in our cohort, there was a higher risk for no-reflow in women even after adjustment by baseline characteristics, which may underline the more complex vessel and endothelial regulation associated with the female gender (7). This fact might also play a role in the higher rate of complications observed in women undergoing rotational and orbital atherectomy (9, 10, 16, 17). It could be a factor underlying the numerically higher rate of early mortality (both procedural and in-hospital) observed in our investigation.

In the setting of left-main PCI, women have frequently been underrepresented in clinical trials. For instance, in the SYNTAX trial, women with unprotected left main disease accounted for only 10.3% of participants. Besides, women within the PCI group had a higher adjusted 4-year mortality rate than men (18). Noteworthy, there were both a higher rate of left main PCI and of aorto-ostial lesions among women in our patient population. Considering that women develop ischemic heart disease at an older age than men and that cardiac surgical risk increases steadily with age, those facts might translate into a greater proportion of women with left main disease undergoing PCI rather than surgery. Hence, aorto-ostial lesions involving the left main ostium were probably more frequently managed percutaneously among the female subgroup. Besides, bifurcation

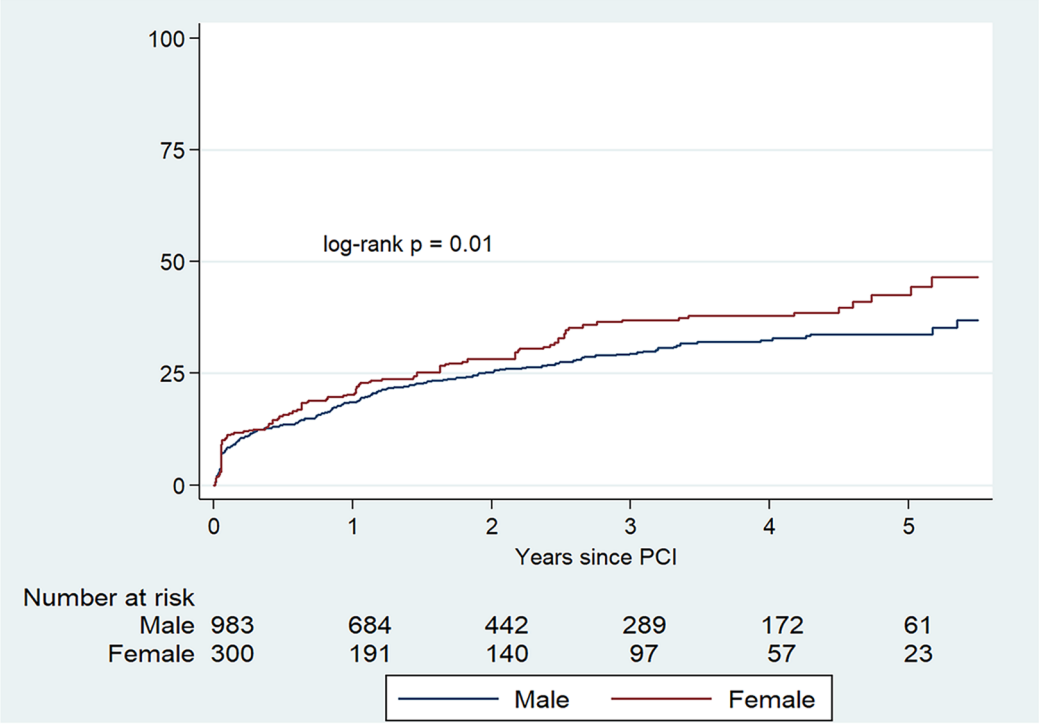

FIGURE 3
Kaplan–Meier cumulative incidence estimates for the combined primary endpoint (stroke, new coronary revascularization, myocardial infarction or all-cause mortality) in the IPW-adjusted cohort.

involvement within the left main was probably less frequent in women, rarely needing two-stent strategies in such a relevant anatomic position. It should be also mentioned that ostial lesions (more frequent among women) are characterized by being more calcific and rigid, often associating a recoil phenomenon after stent placement, altogether increasing PCI complexity (19).

Noteworthy, women presented more frequently exhibiting an acute myocardial infarction. This issue might be related to differences in clinical presentation, as women more frequently experienced atypical symptoms such as weakness, palpitations, or lightheadedness, hence delaying the diagnosis of ischemic heart disease until most severe settings (STEMI) developed.

Sex-related differences for the study endpoints

Although riskier baseline conditions may partially account for poorer outcomes among the female group of patients, the concordant results in both the multivariate analysis and the IPW-adjusted cohort emphasize the differential clinical evolution for both genders beyond baseline features. In the context of an all-comer PCI study, it has already been reported that women carried a higher early and mid-term risk for major cardiovascular outcomes than men (20). The main reasons postulated behind this finding were the low inclusion of women in randomized trials, resulting in device-based techniques being optimized for men, as well as the greater rates of in-stent restenosis and lesion progression linked to the small diameter of target vessels. These facts could be even more accentuated in our patient population, given the greater complexity of the coronary anatomy compared to prior reports on all-comer PCI procedures. Consequently, the relevance of any technical aspect potentially impacting clinical outcomes (e.g., rigorous lesion preparation and optimal treatment of smaller vessels) increases in parallel with coronary lesion complexity.

As mentioned above, the well-known delay between symptom onset and diagnosis of ischemic heart disease in the female gender could also be a potential source for unequal clinical findings (21). Since the time between ischemic symptoms onset and reperfusion are key prognostic factors both in ST elevation and non-ST elevation myocardial infarction, a delayed presentation in women in our cohort could partially explain their poorer prognosis. Unfortunately, we do not have systematic data for all patients on the time interval between anginal symptoms onset and the time of PCI, so this matter still needs further investigation.

In light of our results, further investigations purposely designed to assess the net benefit of complex PCI procedures among women are needed, along with studies that implement strategies to mitigate the residual risk that female patients face after a PCI procedure beyond any disparities in baseline conditions.

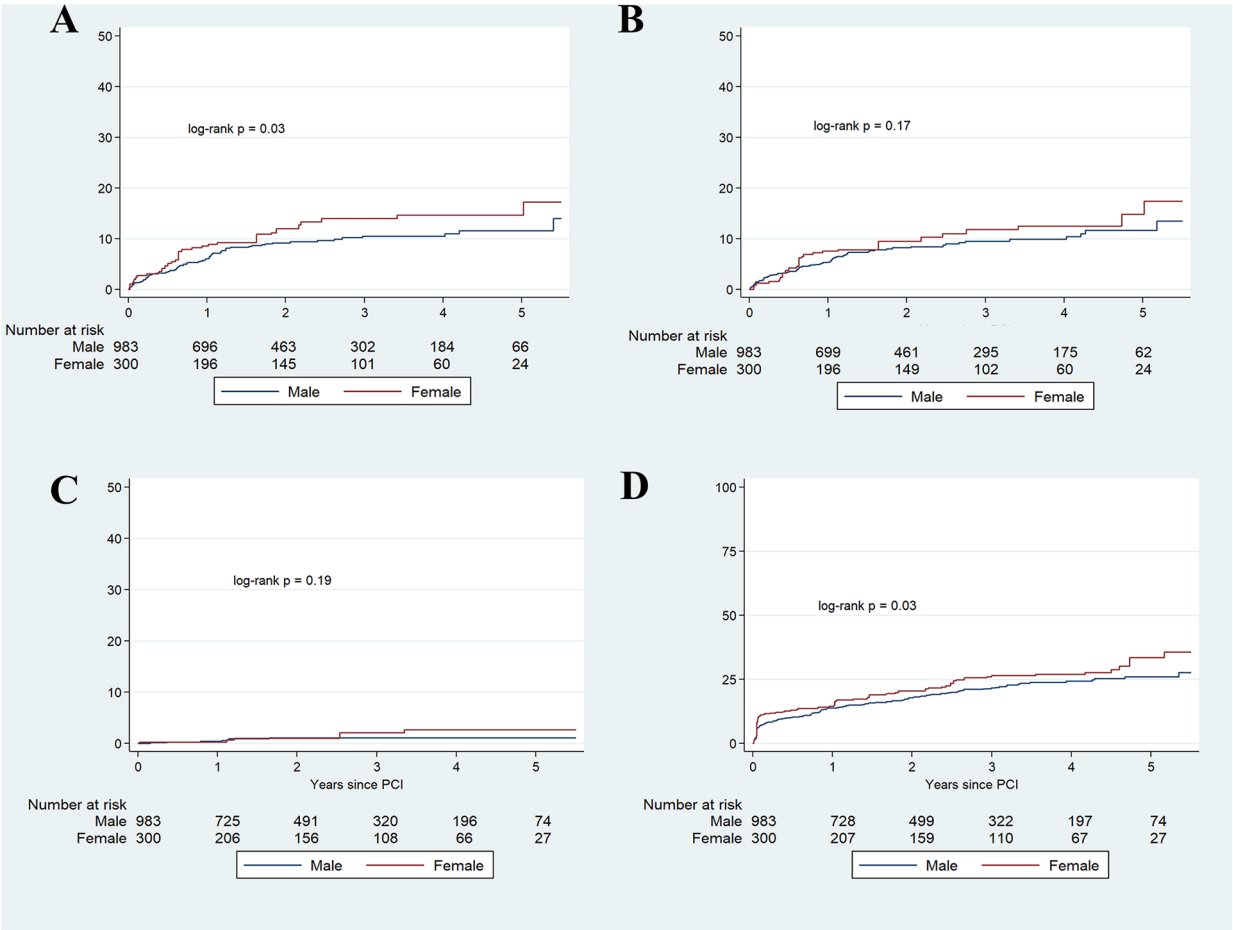

FIGURE 4
Kaplan–Meier cumulative incidence estimates for myocardial infarction (A), new coronary revascularization (B), stroke (C), and all-cause mortality (D) in the IPW-adjusted cohort.

Limitations

This study presents several limitations. Firstly, its observational nature is more prone to bias than randomized studies. Secondly, despite the good comparability between groups after IPW adjustment, the presence of unnoticed unbalanced confounders could not be discarded. Thirdly, some variables that might be of relevance were not assessed in our database, such as the SYNTAX score. Social biases in the access to medical care cannot be fully excluded, but its impact might be marginal considering that the study was developed in a region where universal health-care coverage without risking financial hardship has been implemented for a long period of time. Finally, recent trials have demonstrated better clinical outcomes in complex PCI settings such as bifurcation lesions with the guidance of intravascular imaging (22, 23), but we did not use systematic intracoronary imaging in our series. Future studies should further explore this issue.

In conclusion, in a contemporary cohort of patients undergoing complex PCI procedures, female patients are associated with a higher risk of early complications and receive less frequently state-of-the-art intravascular techniques despite similar complexity. Additionally, after adjustment for baseline features, women exhibited a higher risk for all-cause mortality, myocardial infarction, and for the combined primary endpoint of stroke, coronary revascularization, myocardial infarction, and all-cause mortality at mid-term follow-up.

Data availability statement

The raw data supporting the conclusions of this article will be made available by the authors, without undue reservation.

Ethics statement

The studies involving humans were approved by Institutional Review Board of Hospital Universitario Central de Asturias. The studies were conducted in accordance with the local legislation and institutional requirements. The participants provided their written informed consent to participate in this study.

Author contributions

AA: Data curation, Formal Analysis, Investigation, Methodology, Validation, Visualization, Writing – original draft, Writing – review & editing. MA: Data curation, Investigation, Writing – original draft, Writing – review & editing. IP: Conceptualization, Validation, Visualization, Writing – original draft, Writing – review & editing. RA: Writing – original draft, Writing – review & editing. JB: Writing – original draft, Writing – review & editing. DH-V: Writing – original draft, Writing – review & editing. RP: Writing – original draft, Writing – review & editing. JO: Writing – original draft, Writing – review & editing. CM: Writing – original draft, Writing – review & editing. PA: Writing – original draft, Writing – review & editing.

Funding

The author(s) declare that no financial support was received for the research, authorship, and/or publication of this article.

Conflict of interest

The authors declare that the research was conducted in the absence of any commercial or financial relationships that could be construed as a potential conflict of interest.

Publisher's note

Supplementary material

The Supplementary Material for this article can be found online at: https://www.frontiersin.org/articles/10.3389/fcvm.2024.1382585/full#supplementary-material

References

1. Powell-Wiley TM, Baumer Y, Baah FO, Baez AS, Farmer N, Mahlobo CT, et al. Social determinants of cardiovascular disease. *Circ Res.* (2022) 130:782–99. doi: 10.1161/CIRCRESAHA.121.319811

2. Inohara T, Kohsaka S, Spertus JA, Masoudi FA, Rumsfeld JS, Kennedy KF, et al. Comparative trends in percutaneous coronary intervention in Japan and the United States, 2013 to 2017. *J Am Coll Cardiol.* (2020) 76:1328–40. doi: 10.1016/j.jacc.2020.07.037

3. Protty M, Sharp ASP, Gallagher S, Farooq V, Spratt JC, Ludman P, et al. Defining percutaneous coronary intervention complexity and risk: an analysis of the United Kingdom BCIS database 2006–2016. *JACC Cardiovasc Interv.* (2022) 15:39–49. doi: 10.1016/j.jcin.2021.09.039

4. Hanna JM, Wang SY, Kochar A, Park DY, Damluji AA, Henry GA, et al. Complex percutaneous coronary intervention outcomes in older adults. *J Am Heart Assoc.* (2023) 12(19):e029057. doi: 10.1161/JAHA.122.029057

5. Gao Z, Chen Z, Sun A, Deng X. Gender differences in cardiovascular disease. *Med Nov Technol Devices.* (2019) 4:100025. doi: 10.1016/j.medntd.2019.100025

6. Sambola A, Del Blanco BG, Kunadian V, Vogel B, Chieffo A, Vidal M, et al. Sex-based differences in percutaneous coronary intervention outcomes in patients with ischemic heart disease. *Eur Cardiol Rev.* (2023) 18:e06. doi: 10.15420/ecr.2022.24

7. Maas AHEM, Appelman YEA. Gender differences in coronary heart disease. *Neth Heart J.* (2010) 18:598–603. doi: 10.1007/S12471-010-0841-Y

8. Pawlik A, Januszek R, Ruzsa Z, Óriás V, Kleczyński P, Wojtasik-Bakalarz J, et al. Gender differences and long-term clinical outcomes in patients with chronic total occlusions of infrainguinal lower limb arteries treated from retrograde access with peripheral vascular interventions. *Adv Med Sci.* (2020) 65:197–201. doi: 10.1016/J.ADVMS.2020.01.004

9. Ford TJ, Khan A, Docherty KF, Jackson A, Morrow A, Sidik N, et al. Sex differences in procedural and clinical outcomes following rotational atherectomy. *Catheter Cardiovasc Interv.* (2020) 95:232–41. doi: 10.1002/ccd.28373

10. Sabatowski K, Malinowski KP, Siudak Z, Reczuch K, Dobrzycki S, Lesiak M, et al. Sex-related differences and rotational atherectomy: analysis of 5 177 percutaneous coronary interventions based on a large national registry from 2014 to 2020. *Kardiol Pol.* (2021) 79:1320–7. doi: 10.33963/KP.A2021.0131

11. Siudak Z, Bryniarski L, Malinowski KP, Wańha W, Wojakowski W, Surowiec S, et al. Procedural outcomes in patients treated with percutaneous coronary interventions within chronic total occlusions stratified by gender. *J Clin Med.* (2022) 11:1419. doi: 10.3390/JCM11051419

12. Giustino G, Chieffo A, Palmerini T, Valgimigli M, Feres F, Abizaid A, et al. Efficacy and safety of dual antiplatelet therapy after Complex PCI. *J Am Coll Cardiol.* (2016) 68:1851–64. doi: 10.1016/J.JACC.2016.07.760

13. Medina A, de Lezo JS, Pan M. A new classification of coronary bifurcation lesions. *Rev Esp Cardiol.* (2006) 59:183. doi: 10.1016/S1885-5857(06)60130-8

14. Daly CA, Clemens F, Lopez Sendon JL, Tavazzi L, Boersma E, Danchin N, et al. The clinical characteristics and investigations planned in patients with stable angina presenting to cardiologists in Europe: from the euro heart survey of stable angina. *Eur Heart J.* (2005) 26:996–1010. doi: 10.1093/EURHEARTJ/EHI171

15. Shaw LJ, Bugiardini R, Merz CNB. Women and ischemic heart disease: evolving knowledge. *J Am Coll Cardiol.* (2009) 54:1561–75. doi: 10.1016/J.JACC.2009.04.098

16. Kim CY, Lee AC, Wiedenbeck TL, Lee MS, Chambers JW. Gender differences in acute and 30-day outcomes after orbital atherectomy treatment of *de novo*, severely calcified coronary lesions. *Catheter Cardiovasc Interv.* (2016) 87:671–7. doi: 10.1002/CCD.26163

17. Januszek R, Pawlik A, Staszczak B, Jędrychowska M, Bartuś J, Legutko J, et al. Age and gender differences in clinical outcomes of patients with heavy-calcified coronary artery lesions treated percutaneously with rotational atherectomy. *Adv Clin Exp Med.* (2020) 29:225–33. doi: 10.17219/ACEM/110314

18. Thuijs DJFM, Kappetein AP, Serruys PW, Mohr FW, Morice MC, Mack MJ, et al. Percutaneous coronary intervention versus coronary artery bypass grafting in patients with three-vessel or left main coronary artery disease: 10-year follow-up of the multicentre randomised controlled SYNTAX trial. *Lancet.* (2019) 394:1325–34. doi: 10.1016/S0140-6736(19)31997-X

19. Jaffe R, Halon DA, Shiran A, Rubinshtein R. Percutaneous treatment of aorto-ostial coronary lesions: current challenges and future directions. *Int J Cardiol.* (2015) 186:61–6. doi: 10.1016/j.ijcard.2015.03.161

20. Kosmidou I, Leon MB, Zhang Y, Serruys PW, von Birgelen C, Smits PC, et al. Long-term outcomes in women and men following percutaneous coronary intervention. *J Am Coll Cardiol.* (2020) 75:1631–40. doi: 10.1016/j.jacc.2020.01.056

21. Lawesson SS, Isaksson RM, Ericsson M, Ängerud K, Thylén I. Gender disparities in first medical contact and delay in ST-elevation myocardial infarction: a prospective multicentre Swedish survey study. *BMJ Open.* (2018) 8:e020211. doi: 10.1136/BMJOPEN-2017-020211

22. Holm NR, Andreasen LN, Neghabat O, Laanmets P, Kumsars I, Bennett J, et al. OCT Or angiography guidance for PCI in complex bifurcation lesions. *N Engl J Med.* (2023) 389:1477–87. doi: 10.1056/nejmoa2307770

23. Lee JM, Choi KH, Bin SY, Lee J-Y, Lee S-J, Lee SY, et al. Intravascular imaging–guided or angiography-guided complex PCI. *N Engl J Med.* (2023) 388:1668–79. doi: 10.1056/nejmoa2216607

Frontiers in
Cardiovascular Medicine

Innovations and improvements in cardiovascular treatment and practice

Focuses on research that challenges the status quo of cardiovascular care, or facilitates the translation of advances into new therapies and diagnostic tools.

Discover the latest Research Topics

See more →

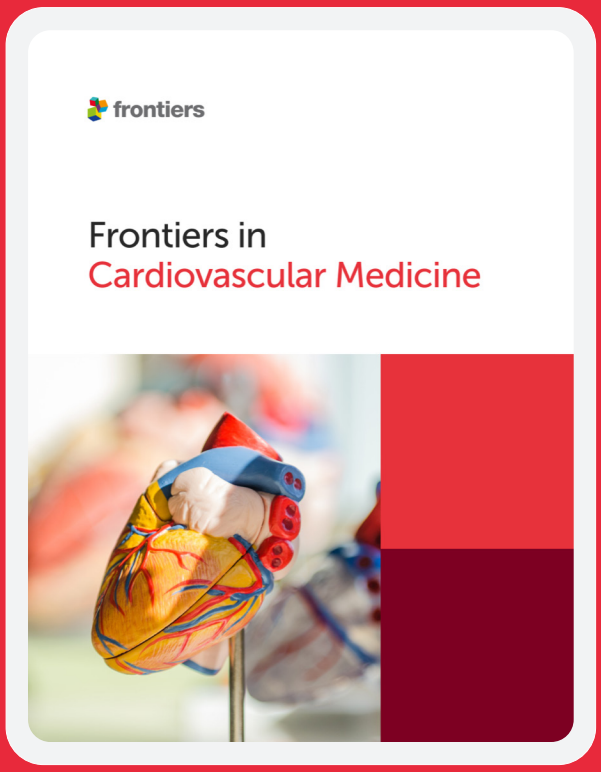

Frontiers

Avenue du Tribunal-Fédéral 34
1005 Lausanne, Switzerland
frontiersin.org

Contact us

+41 (0)21 510 17 00
frontiersin.org/about/contact